UNIVERSITY OF OKLAHOMA

GRADUATE COLLEGE

PHYSICO-CHEMICAL BEHAVIORS OF SHALE/FLUID/SOLUTE INTERACTION IN GEO-ENVIRONMENTAL AND GEO-ENGINEERING APPLICATIONS

A DISSERTATION

SUBMITTED TO THE GRADUATE FACULTY

in partial fulfillment of the requirements for the

degree of

Doctor of Philosophy

By

YASSER MOSAAD AHMED MOHAMED
Norman, Oklahoma
2007

PHYSICO-CHEMICAL BEHAVIORS OF SHALE/FLUID/SOLUTE INTERACTION
IN GEO-ENVIRONMENTAL AND GEO-ENGINEERING APPLICATIONS

A DISSERTATION APPROVED FOR THE
SCHOOL OF GEOLOGY AND GEOPHYSICS

By

James M. Forgotson, Chair

Thomas A. Dewers, Chair

Roger M. Slatt

Richard D. Elmore

Michael J. Soreghan

Musharraf Zaman

This dissertation is dedicated with love and gratitude to my family. A warm dedication goes to my father and my mother for supporting my interest and education. A special dedication goes to my lovely wife and my beautiful children, El-Shymaa, Ammar and Zeyad for their love, understanding, patience, and encouragements during this work.

Acknowledgements

My deep and heartfelt gratitude is due to **GOD Almighty** for his care, provisions, and absolute love towards me.

I would like to acknowledge the **Embassy of the Arab Republic of Egypt, Cultural and Educational Bureau** for the opportunity given to me to pursue this Ph.D. degree, with financial support throughout this venture.

I would like to express my deepest gratitude to **Dr. Thomas Dewers,** Professor of Environmental Geology, School of Geology and Geophysics, University of Oklahoma, for initiating the present point of study, kind assistance during laboratory work, valuable suggestions and discussions during the progress of this work, and for his great help in reading the manuscript. His unlimited encouragement and incredible help in so many different ways can never be repaid.

Special thanks are due to **Dr. James M. Forgotson,** Kerr McGee Professor of Petroleum Geology, School of Geology and Geophysics, University of Oklahoma, for accepting a position as my co-chair, his invaluable contribution to this work, and for his great help in reading the manuscript. He is always available when I need his help. His expertise in several areas and scientific-orientation were decisive for my growth.

Thanks are also due to **Dr. Roger M. Slatt, Dr. Douglas R. Elmore, and Dr. Michael J. Soreghan**, School of Geology and Geophysics, and also **Dr. Musharraf Zaman,** School of Civil Engineering and Environmental Science, University of Oklahoma, for accepting to serve as members of my doctoral advisory committee and for revising this document. Important technical concepts were acquired during courses taken with them, as well as in informal conversations that, in one way or another, contributed somehow to successful completion of this dissertation.

Special thanks to **Dr. Evgueni M. Chesnokov and Dr. Raymon L. Brown,** Institute for Theoretical Geophysics, University of Oklahoma, for their helpful discussions and for funding me throughout the last seven months. In addition, I must thank **Devon Energy** specially **Mike Ammerman** for supporting me during these seven months. Additionally, thanks go to the Friday Seminar held by the Institute for Theoretical Geophysics.

I would like to extend my appreciation to those who helped me throughout my study, particularly the staff of the School of Geology and Geophysics especially **Robert Turner** for his readiness to assist me in the XRD lab. Also, I would like to thank **Dr. Preston Larson** from the Noble Electron Microscopy Laboratory, Department of Botany and Microbiology, University of Oklahoma, for his SEM assistance and available discussions. In addition, **John Brumley** and **Dr. Gene Scott** from Poromechanics Institute, University of Oklahoma, are thanked for generous loan of equipment and their time and talent in helping get the experiments up and running. In addition, the partial funding from the National Science Foundation and the Poromechanics Institute is gratefully acknowledged.

I would like to thank all of my fellow graduate students and friends who have contributed to the completion of this work, among them **Dr. Ahmed Alahdal** and **Dr. Nikolay Dyaur.**

Finally, a special note of gratitude goes to those who helped me throughout my study especially my professors and friends in the Geology Department, Tanta University, Egypt, for their encouragements to achieve the success of this study in one way or another.

Contents

List of Figures

List of Tables

Abstract

Artificial dewatering of shales is a method to eliminate shale related problems such as wellbore stability, swelling, and soil instability that produces landslides. In this dissertation, the semi-permeable membrane behavior of shale, permitting osmotic flux of fluid to the partial exclusion of ions, has been studied as a means to dewater shales exposed to chemical solutions with ion activities less than that of the in situ shale pore fluid.

This dissertation examines the rich and complex physical-mechanical behaviors exhibited by shales when exposed to differing solutions over time, temperature, chemical, and stress conditions. Using several unique experimental designs and numerical modeling, this study advances the level of understanding of time dependent shale behavior arising from changes in clay mineral structure and crystalline phase.

The flux of water and ions over time due to semi-permeable membrane properties of shale and very fine-grained material has been numerically modeled. The purposes of this model are to predict the flux of fluid and ions through natural geological fine-grained and clay-rich materials over time and to predict the effect of this flux on long-term shale membrane behaviors. The required input parameters for the model, including water activity of both interfacial chemical fluid and the pore-fluid of the membrane, membrane properties (reflection coefficient, porosity, hydraulic conductivity, mineral compressibility, diffusion processes), and temperature and pressure conditions, were determined by laboratory work on Pierre Shale using High-Temperature High-Pressure (HTHP) Shale Apparatus. Results of this model reveal that, due to the flux of solute through the semi-permeable membrane, the shale's pore fluid activity will reduce

through time, leading to a reduction in the ideality of the membrane. Given enough time (depending on the activity of the chemical used and the membrane thickness and permeability), the chemical and hydraulic difference across the membrane will disappear, leading to a diminishing of the osmotic fluid flux. This model can help in correlating and representing the semi-permeable membrane behavior of fine-grained and clay-rocks, and enhance understanding of the relevant processes. The implications for geo-environmental exploitation of the membrane properties of shales are discussed in light of these results.

Three different nitrate fluids ($NaNO_3$, KNO_3 and $Ca(NO_3)_2$) with different concentrations were used in a laboratory study of the membrane behavior of Pierre Shale. Clay mineral content, permeability, and grain-size distribution of the shale were investigated as the primary factors controlling the osmotic flow through the shale. In addition, the impact of chemical fluids on the shale's parameters and components were investigated.

During laboratory studies, Pierre Shale acted as a non-ideal, semi-permeable membrane with a maximum short term membrane efficiency of 13 % for 0.25 molal sodium nitrate ($NaNO_3$) and decreased to a minimum 1 % for 2 molal calcium nitrate ($Ca(NO_3)_2$) for the solutions examined. Membrane efficiency was found to decrease with increasing nitrate fluid concentration. This decrease is greater using calcium nitrate solutions. Osmotic pressure changes over time in the experiments are due to a reduction in the concentration difference across shale membranes through diffusion or reducing Na-smectite mineral content by progressive illitization.

Depending on the type and concentration of the fluids used, the initial (871 nDarcy on an average) permeability of studied samples was changed after three days.

Sodium nitrate solutions had the greatest effect on reducing permeability values. Potassium nitrates increased the permeability to 2612 nDarcy with 2 molal concentration. 0.5 and 1 molal calcium nitrate produced higher permeability values compared to the same concentrations of other nitrate fluids. Also, the osmotic pressure that was produced from those two $Ca(NO_3)_2$ concentrations showed oscillatory transients phenomena. Both the osmotic tests and subsequent permeability tests showed a strong inverse relationship between osmotic pressure and permeability.

Diffusion of ions through the Pierre Shale was investigated using the same nitrate fluids for up to 40 days. During the diffusion test, many ions are adsorbed through clay minerals structure. This ability illustrated the same trends as the membrane efficiency tests. The ions' diffusion over long-term tests led to a decrease of the membrane ideality with time because of changes that occurred within the original clay minerals' structure and pore fluid activity. Concurrently to these diffusion tests, swelling stress measurements were taken using specially designed Hydrostatic Triaxial Apparatus. These measurements, involving replacement of pore fluid with nitrate fluids, showed a strong relationship between swelling, diffusion, permeability and osmotic pressure, where swelling reduces the ability of both fluid and ions to move through shale, leading to develop high osmotic pressure. The swelling stress of shale is dependent on chemical type and elapsed time. KNO_3 solutions produced very little swelling stress, while $NaNO_3$ solution produced the maximum swelling stress. Swelling stress showed transient, oscillatory behavior over the time with all nitrate fluids. Intensity and frequency of these phenomena is dependant on the type of pore fluid solute. These phenomena may lead to

episodic changes in shale permeability resulting from opening tensile fractures in the shale because of increasing the fluid pressure in pores and micro-cracks.

The impacts of nitrate fluids on Pierre Shale mineralogical and textural characteristics were studied over time as functions of temperature, effective pressure, and pore fluid chemistry. Experiments were run with concentration ranging from zero molal (distilled water) to two molal calcium, sodium, and potassium nitrate solutions at temperatures from room temperature up to 150 degrees Celsius, and pressure from one atmosphere pressure up to 3000 psi confining pressure, and were measured throughout one year. For the same reasons, Na, Ca and K carbonates with different concentrations were also preformed but only at room conditions. These studies indicated the susceptibility of clay minerals to alteration, as they are affected easily by any change in pore fluid chemistry, even at normal temperature conditions. XRD and SEM studies for treated samples recorded new phases of clay minerals from room temperature, up to 150 °C. Experiments using sodium and calcium solutions developed an authigenic smectite phase. In the presence of K ions, smectite showed a progressive transformation to smectite-illite and/or illite at temperature less than 150 °C. This was controlled by K concentration, temperature and test duration. SEM recorded an amorphous silica phase especially at 150 °C and four months duration, resulting from destruction of smectite and illite structures. The only changes in grain-size distribution during these experiments were recorded within the 1-4 μm range for sampled performed under room temperatures and within 1-7 μm for that done under HTHP conditions, with about 0.5 to 1.5 % increase in each of these grain-size fractions.

Chapter 1

Introduction

1.1. General overview

Shales, the most abundant sedimentary rock, are often described as a fine-grained, highly compacted, and partially dehydrated rock (Tourtelot, 1960). However, some authors prefer to restrict the usage of the term shale to fine-grained rocks that show lamination (Bates and Jackson, 1987 and O'Brien and Slatt, 1990). In this study, the term "shale" will be used for all sedimentary rocks composed mainly of mud-size particles. Shales are composed primarily of clay minerals, and fine grain-size quartz, and feldspars, with minor amounts of carbonate minerals, sulfides, iron oxides, and some amount of organic carbon (Boggs, 1995).

Because of weathering interaction between primary rocks and aqueous solutions, the primary rock components are broken and dissolved (incongruently) to produce clays minerals and fine-grained particles. These products are predominantly transported to depositional basins by water, but sometimes wind and ice can play important roles. Clays and fine-grained particles can accumulate under any environmental conditions in which fine sediments are abundant and water energy is sufficiently low to allow the settling of suspended fine materials. Marine environments adjacent to major continents, where the seafloor lies below wave base of storms, are the primary environment for accumulation of fine-grained sediment. In addition, these sediments can accumulate in lakes, quiescent parts of rivers, and in lagoonal, tidal-flat and deltaic environments (Potter et al., 1980). As the sediments are buried, the pressure and temperature increases, leading to compaction and

mineralogical transformation of both clay minerals and fine-grained particles. The results of all of the above processes are shales which have distinct layers, a high clay content, and very low permeability (Folk, 1974).

According to Mitchell (1993) particles, matrix and pore space are the basic elements of shales microstructure (Fig. 1-1).

1-*Particles* include individual particles of sand, silt and clay platelets;

2- Matrix is a distinct agglomeration of one or more elementary particles, usually clays, that has a specific mechanical function and;

3-Pore spaces include both the intramatrix pores, which usually filled by free water (moisture content), and interlamellar pores which are contain water that is adsorbed on to the clay mineral layers and, influences ions exchange that produces swelling of the shale.

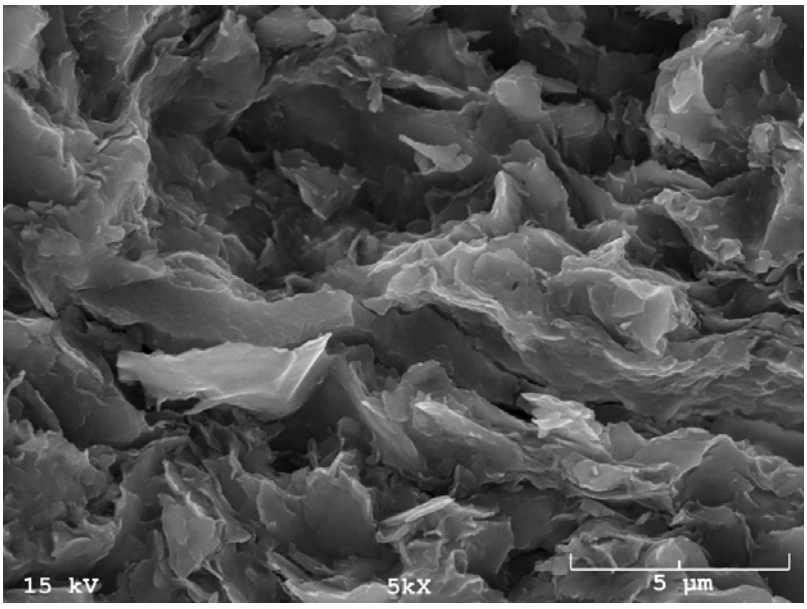

Figure (1-1): Microstructure of shale *(Pierre Shale).*

According to Manohar (1999), clay mineral content and low permeability due to poor pore connectivity are the most distinguishing features of shale. These features

make shale vulnerable to phenomena such as hydration, swelling, shrinkage, strength reduction, and failure when exposed to water and ions. The ability of shale to absorb water or ions depends on the amount and type of clay minerals.

1.2. Physico-chemical behaviors of shale

To understand the physico-chemical behaviors of shale, let us assume a buried shale system, as in Figure (1-2). According to Van Oort (2003), forces that act on shale within this system can be subdivided into three types including:

1- **In-situ stresses** include both vertical and horizontal stresses. Vertical stress is the result of the overburden weight and is equal to

$$\sigma_i = \rho_s g h$$

where ρ_s is the overburden rock density, g is gravity acceleration, and h is the overburden thickness (usually the vertical stress gradient is 1 *psi/ft*). Horizontal stress is the result of the tectonic activity of the area or the horizontal expansion of the surrounding rocks.

2- **The pore pressure,** in normal-pressured areas, is the weight of the water column above the shale system and is equal to

$$P_{pore} = \rho_w g h_w$$

where ρ_w is the saturated water density and h_w is the water column thickness (usually pore pressure gradient is 0.45 *psi/ft*).

3- **Inter-granular contact points stresses,** acts primarily in the clay fabric and includes: Van Der Waals attraction; electrostatic bond repulsion; short-range repulsive and attractive forces that are derived from hydration/salvation of clay

surfaces and the ions that are present in interlayer spacing (adsorbed or free). Together these forces usually form the "hydration stress/pressure", “disjoining pressure”, or "swelling stress/pressure", as they are responsible for the characteristic swelling behavior of clays and shales.

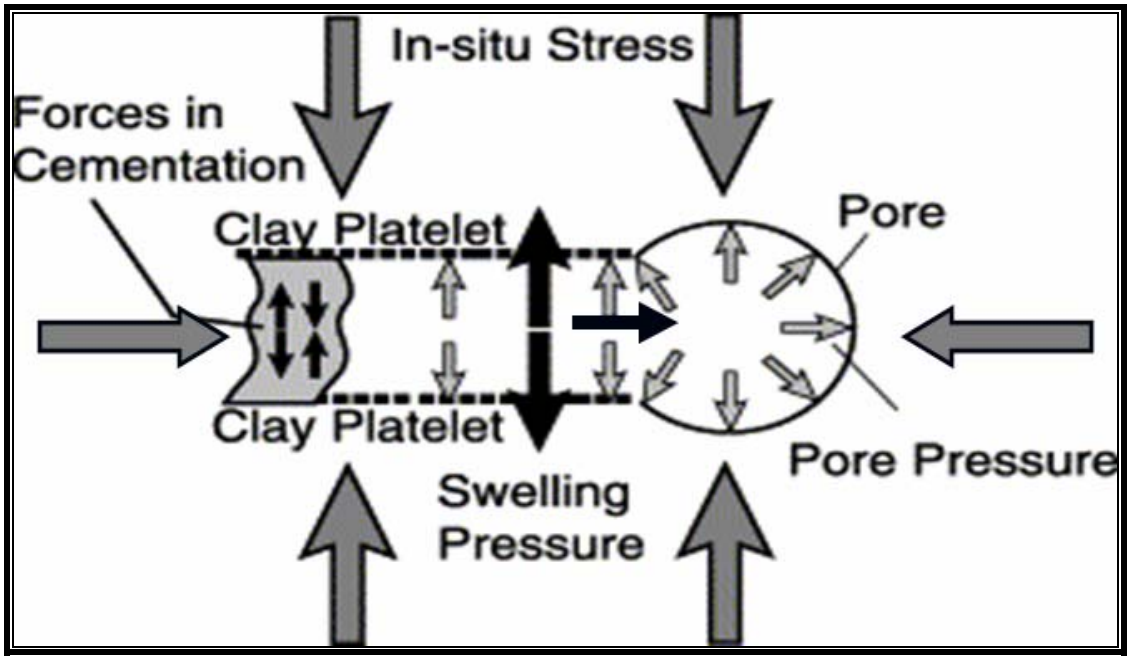

Fig (1-2): A schematic diagram representing the natural forces acting on a shale system (Source: Van Oort, 2003).

According to Terzaghi (1943), the effective stress of the above system will be equal to

$$\sigma_i^{eff} = \sigma_i - P_{pore} - P_{swelling}$$

where σ are the in-situ formation stresses, P_{pore} is the pore pressure and, $P_{swelling}$ is the swelling pressure. The failure envelope, which reflects the shale’s strength according to Jaeger and Cook (1979) is

$$\tau = \sigma \tan\phi + C$$

where τ is the shear stress, ϕ is the friction angle, and C is cohesion. During the balance condition, in-situ stresses, pore pressure, hydration stress and the cohesion cementation force are all balanced and do not overcome the shale strength. If this balance were disrupted by any change, as if fluid were induced to the system, the shale would become unstable; this in turn will lead to failure. This might happen if pore pressure increases, which reduces the effective stress, or there is an increase in the swelling pressure due to unfavorable ions exchange at the clay minerals, which also reduces the effective stress, or by chemical alteration and reduction of cementation bonds (cohesion), which leads to a reduction in the shale strength and hence the failure envelope. The opposite is true also; a more stable situation may arise when pore pressure or hydration stress is reduced, or if chemical alteration strengthens the shale.

The situation is more complex than mentioned above because of many other factors, such as the friction angle, horizontal stresses, abnormal pore pressure and so on. However, the present study is focused on the reduction of both pore and swelling pressures using different chemical fluids. Accordingly, it is worthwhile to understand how much damage might occur for the shale system as the results of forces imbalance produced by shale fluid interface. The following paragraphs address two main shale related problems.

The swelling of shales and clay rich rocks and soils may cause serious damage to fabricated structures, which may cost millions of dollars to rebuild. Damage ranges from the minor cracking of pavements or interior finishes in buildings, which are very common, to the irreparable displacement of footings and

superstructure elements (Ruwaih, 1987 and Dhowain et al., 1990). Many researchers such as Morgenstern and Balasubramonian (1980) and Huang et al. (1993), Mitchell (1993) concluded that swelling is largely due to water migration into the rock matrix and a decrease in the mechanical interaction of the particles caused by a release of the confining pressure. However, factors such as clay mineral type, clay content surface charges, and pore fluid chemistry greatly influence the swelling of fine-grained rocks. Therefore, these factors could be the key to answering the question of why the fluid migrates into the rock matrix. The mechanisms controlling these reactions are very complex and are not fully understood. These reactions result from the affinity of shale to absorb water into their structure, leading to an increase of the fluid volume within the shale structure, manifesting itself as an increase in volume, or swelling at the macroscopic level. Swelling deformation is much greater than elastic deformation and therefore cannot be predicted using classic elastic deformation theory.

Borehole instability in shale intervals is one of the major problems encountered during the drilling of wells for oil and natural gas, with an estimated cost reaching to more than hundreds of millions of dollars each year in remedial works (Dzialowski et al., 1993). This will be happen when the effective stresses on the wellbore wall exceeds the strength of the shale rock.

To overcome these problems, many theoretical and experimental studies have focused on different factors, such as strength and anisotropy of the rock, mechanical failure mechanisms, and physico-chemical interactions between fluids and formation. One of the suggested solutions was the dewatering of the shale formation to reduce the pore pressure. The questions are, how can this be done efficiently and what are

the consequences of this pore pressure and chemistry change on the swelling pressure and shale components. It is widely known that the fine pore sizes and negative surface clay charges associated with the clay crystal structures, make shale act as semi-permeable membrane (Mitchell, 1993). Hence, the flow of water out of shale because of chemical potential differences is similar to the osmotic flow of water through a semi-permeable membrane. The driving force involved is the chemical potential gradient across the membrane, which is related to the difference in solute concentration (or, in the thermodynamic sense, the water chemical potential or "activity"). With an imposed gradient in water activity, an osmotic outflow of pore fluid from the formation will reduce the pore pressure in the formation. If the osmotic outflow is greater than the flow caused by the hydraulic gradient, there will be a net flow of water out of the formation, into the wellbore. This will result in lowering the pore pressure below the in-situ value and the dehydration of the shale formation (Mody and Hale, 1993, and Yu et al., 2003).

However, because of the wide range of pore sizes in the shale, it exhibits a non-ideal semi-permeable membrane (i.e. for the ideal semi-permeable membrane, all solutes are reflected by the membrane and only water molecules can pass through the membrane). The solutes transferred across the membrane system will reduce the chemical potential or water activity of the pore fluid. This will gradually reduce the chemical potential difference between the chemical fluid and the shale (Fritz, 1986). Until now, experimental data on the semi-permeable behavior of naturally occurring shales and clay-rich materials are rare and limited, especially at elevated temperatures and pressures relevant to sedimentary basin diagenesis.

1.3. Objectives and strategy

As mentioned above, understanding the shale-fluid interaction is a key point in eliminating many of shale's related problems, such as wellbore stability, swelling, landslides, and soil stability problems. Therefore, this study focuses on two main objectives:

1- to study membrane behavior of shale and clay-rich rocks related to shale-fluid interaction phenomena and,

2- to investigate the impacts of fluid chemistry on shale behaviors and components.

To accomplish the first objective, an integrative numerical modeling and experimental approach was adapted. Many laboratory investigations were performed under different pressure and temperature conditions. Three different fluid chemistries were used on Pierre Shale using a High Temperature High Pressure (HTHP) Shale Apparatus and Atomic Absorption Spectrophotometer to study osmotic flow and solute diffusion behaviors.

To reach the second objective, a number of laboratory experiments were performed using Pierre Shale samples with focusing on the impact of the chemicals used on permeability, swelling stress, clay mineral phase changes, and grain-size distribution variations. The HTHP Shale Apparatus was used for permeability studies, the HP triaxial apparatus was used for swelling stress, XRD and SEM were used for clay minerals studies, and a Laser Grain-Size Analyzer was used for grain-size studies.

1.4. Thesis overview

The current dissertation is divided into two parts and appendices:

Part One is essentially designed for theoretical background and modeling works. A summary of the literature review of shale, clay minerals, shale-fluid interactions and the membrane behavior of shale is addressed in Chapter 2. Some important definitions, concepts, and formulae are also reviewed with an emphasis on certain controversies in the literature. Chapter 3 presents a numerical model for membrane phenomena of shale and clay-rich rocks. The numerical solution of this model for shale's standard parameters is also presented.

Part Two is dedicated to experimental work, results and discussions. This part includes Chapters 4 through 8.

-Chapter 4 describes in detail the solid starting materials and the different chemical fluids used in laboratory studies. A more detailed characterization of different methodologies and tools used in the current study is also presented in this chapter.

- Chapter 5 presents the osmotic membrane behavior of Pierre Shale with different nitrate fluids and the impact of these chemicals on shale permeability. The tests designs and procedures, sample preparation and interpretations of osmotic and permeability results are included in this chapter.
- Chapter 6 introduces diffusion of both fluid and solute behaviors of shales with fluids. In addition, this chapter describes the impact of these different nitrate fluids on the swelling pressure of Pierre Shale at high-pressure conditions (1000 psi confining pressure). The tests designs and procedures, samples preparation and interpretations of diffusion and swelling tests, results and discussions are also included in this chapter.

- Chapter 7 addresses the impact of different fluids on clay minerals and grain-size distribution of Pierre Shale samples under different pressure and temperature conditions. The tests conditions and designs as well as the results and interpretationsare presented also in this chapter.

-Finally, Chapter 8 summarizes the results obtained, the new interaction mechanisms observed, and presents the conclusions of this study.

Four Appendices have been included to help readers understand some of the shale-fluid interaction mechanisms and certain details of the laboratory work that was done during this study. Appendix A presents the numerical solution for osmotic flow and ions flux through shales models. Appendix B describes the permeability measurements and modeling for shale and very low permeability rocks. Appendix C contains a table of nomenclature and units conversion used in the dissertation. Appendix D is a CD with worksheets for the raw-data for different experiments.

Chapter 2
Literature Review

This chapter introduces a short, but comprehensive, review of clay minerals, shale-fluid interactions, and semi-permeable membrane behaviors of shale. This review is divided into three parts. The first and second parts are focused on clay minerals and their fluid interaction mechanisms respectively, as these are responsible for most problems encountered in shale and clay-rich rocks. The third part reviews the coupled flow due to shale-fluid interface with a focus on the chemical osmosis phenomena of shale. Additionally, it includes a discussion on some applications and the impact of osmotic flow in natural systems.

2.1. Clay mineral overview

2.1.1. Background

Clay minerals, the most common in shales and the main cause of shale problems, refer to a group of hydrous alumina-silicates with predominately clay-sized particles. The term clay mineral is used for a class of layer or phyllosilicate minerals with dimensions less than four μm (Grim, 1953). These minerals are often formed because of interaction of aqueous solutions with the mechanically broken preexisting primary rocks minerals. Dissolution and re-crystallization are the processes by which clay minerals are formed and transformed. In sedimentary contexts, clay minerals may be derived from clays formed in other environments (*detrital clay*), or formed in-situ (*authigenic clay*) by direct precipitation from solution (*neoformation process*) or by transformation of some precursor minerals, usually preexisting clay minerals or by

re-crystallization of amorphous materials originated from volcanic activities (Millot, 1970; Velde, 1995 and Diek et al., 1996).

Among the clay minerals, there is variation in chemical and physical properties due to structural difference, but mostly they have platy morphology and perfect basal cleavage (001 plane). The fine-grained minerals (< 4 μm) and sheet-like shape of clays not only gives them the ability to be suspended and transported for a long distance by a moving fluid, but also gives them special properties such as a large surface area which is dominant in controlling the rates of clay chemical-fluids interactions. In addition, the sheet-like shape of clay minerals allow them to compact under the effects of overburden pressure more than other minerals (Chamley, 1989).

2.1.2. Structure of clay minerals

All phyllosilicate minerals, including clay minerals, are constructed from combinations of two simple structural units. The first unit is called an octahedron unit, and it is built from a sheet of closely packed oxygen or hydroxyl atoms bounded with aluminum, iron, or magnesium (divalent ions) atoms in six-fold coordination. The other unit is called a tetrahedron in which a silica atom is equidistant from four oxygens or hydroxyls, if hydroxyls are needed to balance the structure. These units are assembled in sheets with a general formula $(Si_2O_5)^{-2}_n$ for the tetrahedron and $(Al_2(OH)_6)_n$ or (Fe or $Mg)_3$ $(OH)_6)_n$ for the octahedron sheet (Grim, 1953 and Weaver, 1989). The difference among clay minerals results from the differences in the stacking of these sheets and the manner in which the two-or three-sheet plates are successively held together. Within the same clay mineral group, difference within the crystal structure of the tetrahedron and/or octahedron units are due to the presence of

Al^{3+} instead of Si^{4+} in the tetrahedron sheet and/or Mg^{2+} or Fe^{2+} instead of Al^{+3} in the octahedron sheet. This substitution is called *isomorphic substitution,* and because of it most clay surfaces have a net negative surface charge under natural conditions (Brindley and Brown, 1980; Reynolds, 1980).

According to Velde (1995), swelling properties and repeating of the crystallographic basic units of the layer structures are two different, elementary properties of clay minerals resulting from the structural differences that they possess. The repetition of layer structures gives rise to the availability of many types of clays, and each exhibits a different response upon interaction with fluids of different compositions.

2.1.3. Common clay minerals

More than 35 clay mineral groups are based on the different structures among the clay minerals. In this chapter, kaolinite, smectite, illite, chlorite and mixed layer, which are the most relevant clay minerals causing shale-related problems, will be briefly described (Fig. 2-1).

1-Kaolinite ($Al_4Si_4O_{20}(OH)_8$) is composed of one silicon tetrahedron sheet and one octahedron aluminum sheet (1:1 layer) sharing the same oxygen atoms by covalent bonds (Grim, 1953). Therefore, forces such as hydrodynamic, capillary, electrical, and salvation are unable to separate these strongly bonded two sheets. In addition, when kaolinite is immersed in water, the strength of these covalent bonds prevents any penetration of water molecules between its layers. Thus, kaolinite is classified as a non-swelling clay mineral (Dixon, 1990).

2-Smectite ($Al_4Si_8O_{20}(OH)_4.xH_2O$) is composed of one octahedron aluminum sheet sandwiched between two silicon tetrahedron sheets (2:1 layer). In this type of arrangement, the oxygen atoms of each sheet are adjacent to corresponding oxygen atoms of the neighboring sheet, leading to a very weak bond and an excellent cleavage between them. An important feature of the smectite structural arrangement is that water and polar molecules can enter between the unit layers causing the lattice to expand in the c-axis direction. The c-axis dimension of smectite varies from 9.6 A° if there are no polar molecules, to complete separation in some extreme cases if polar molecules are present (Bailey, 1980; Grim, 1953), but generally it is 14 A°.

3-Illite ($K_2Al_6Si_6O_{20}(OH)_4$) is similar to smectite in its basic unit structure (2:1 layer) (Fig. 2-1), except some of the silicon atoms are replaced by aluminums, leading to a charge deficiency which is balanced by potassium ions positioned between the unit layers. The c-axis dimension of illite is ≈ 10 A° (Grim, 1968). The structure of illite differs from that of smectite in several other important ways such as; the charge deficiency due to substitutions per unit layer is about 1.3 to 1.5 for illite as compared with about 0.5 to 0.9 for smectite. In addition, the seat of this charge in illite is largely in the silica sheet, close to the surface of the unit layers, however, in smectite it is frequently in the octahedral sheet at the center of the unit layer. The balancing cation between illite unit layers is mainly potassium, which is much bigger in ionic radius compared to sodium, the balancing cation between smectite unit layers. For illite, the polar ions cannot enter between its structure units to cause expansion and the interlayer balancing cations are not exchangeable. All of these differences make illite's structure relatively fixed in position (Mackenzie, 1959).

4-Chlorite ($Mg_{10}Al_4Si_6O_{20}(OH)_{16}$) generally is composed of alternate mica-like and brucite-like layers (Bailey and Robinson, 1951). Mica-like layers are 2:1 structure with the general composition $(Si.Al)_8(Mg.Fe)_6O_{20}(OH)_4$ (Fig. 2-1). The brucite-like layer has the general composition $(Mg.Al)_6(OH)_{12}$. The mica-like layers are unbalanced by the substitution of Al^{3+} for Si^{4+}, and this charge deficiency is balanced by the excess charge in the brucite sheet, which comes from substations of Al^{3+} or Fe^{3+} by Mg^{2+}. Depending on the amount of substitutions within mica and brucite layers, and the orientation of these layers, various members of the chlorite group exist (Grim, 1962).

5-Mixed layers clays are the kinds of clay minerals in which different clays' layer types alternate with each other in regular, segregated, or random ways (Reynolds and Hower, 1970; MacEwan and Ruiz-Amil, 1975; Reynolds, 1980; and Wilson, 1987). They are intermediate products of reactions involving pure end-member clays in natural environments ranging from surface to low-grade metamorphic and hydrothermal conditions (Srodon, 1999).

Solid-state transformation and dissolution/recrystallization are the two suggested mechanisms responsible for the formation of different mixed-layer clays. Mixed-layer clays can form by weathering that involves the removal or uptake of cations (e.g. K), hydrothermal alteration, or removal of hydroxide interlayers, and, in some cases, may represent an intermediate stage in the formation of swelling minerals from non-swelling minerals or visa versa (MacEwan and Ruiz-Amil, 1975; Reynolds, 1988).

The current study will focus on a smectite/illite mixed layer (S/I), which is the intermediate product of a reaction involving pure smectite transforming to illite. It is widely agreed that smectite transformation to illite, naturally or experimentally, is through a smectite/illite mixed layer. Details of the illitization of smectite will be discussed in chapter 7.

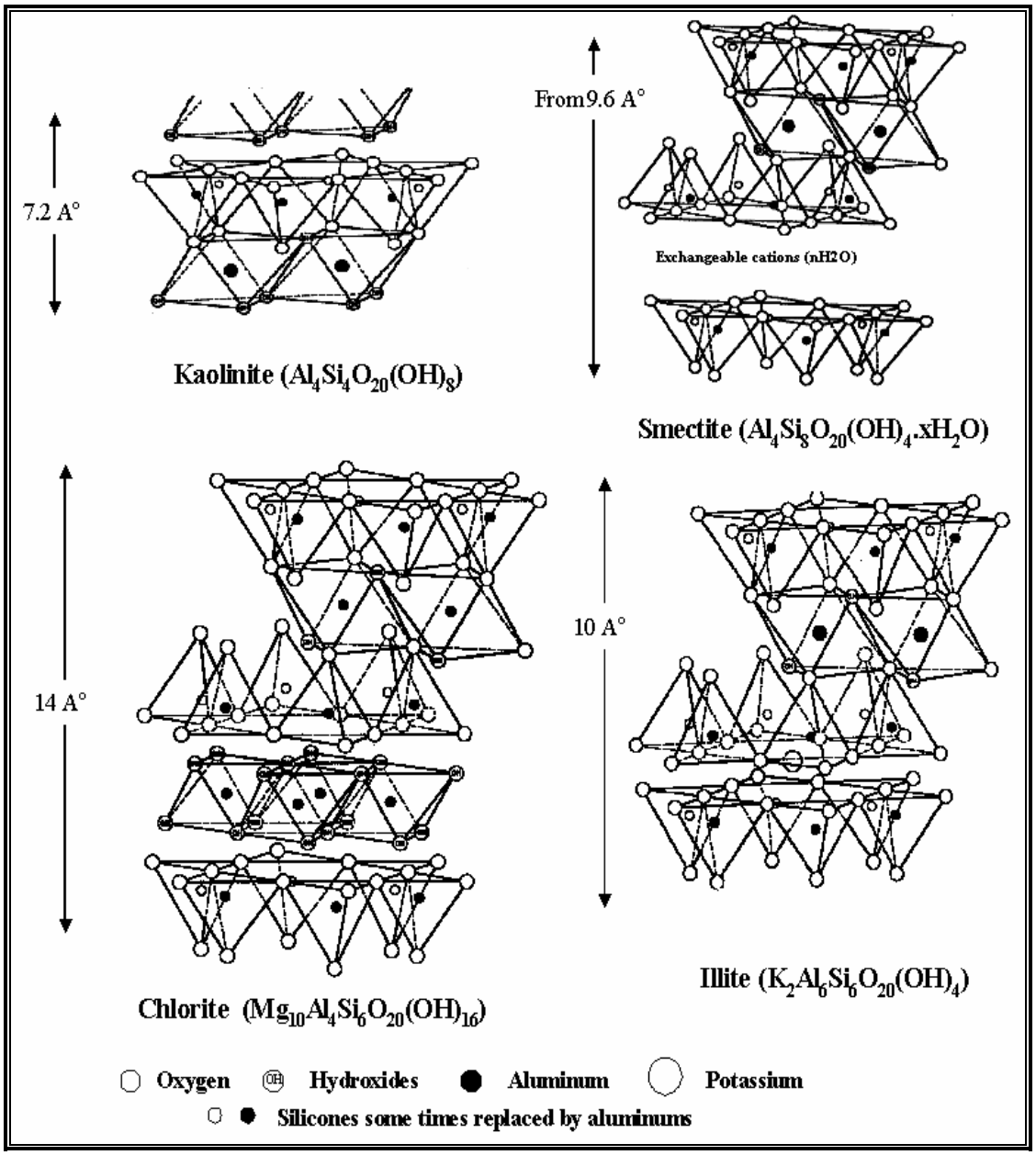

Figure (2-1): Diagrammatic sketch of common clay minerals structures (Source: Grim, 1968).

2.1.4. Clay-water interface

Because of their fine-grained size and a sheet-like shape, clay minerals have a large ratio of surface area as compared to volume. Also, because of the isomorphous substitution, they have layer charges usually on (001) surfaces. Moreover, commonly clays have charges on their edges due to broken bonds.

Water in shales can be divided into free water that fills the intramatrix pore, and the bound water that fills the interlamellar pore within expandable clay minerals. The latter is largely responsible for many of the properties clay minerals and clay-size materials, such as plasticity, compaction, suspension capability, cations-exchange, and cation holding. In general, the amount of clay water (free and bound) depends on the clay type, texture fabric, type and amount of interlayer cations, temperature, and pressure.

To compensate for the net negative charges of clay platelets and to attain electrical neutrality, positively charged cations such as Na^{+}, K^{+}, Mg^{2+}, and Ca^{2+} are adsorbed electro-statically around the surface of the clay platelets. Usually cations are attracted to (001) surfaces, and anions to edges.

In the dried state, the adsorbed cations adhere strongly to the platelets of the clay to maintain electrical neutrality, and the ion concentration gives the system minimum energy (Hillel, 1980).

Upon wetting the clay system with pure water, the adsorbed cations dissociate and move away from the clay surface due to the cation's thermal motion, which moves them towards the state of maximum entropy or disorder (i.e. the Second Law of Thermodynamics). This will result in the same ionic concentration everywhere in

the interlamellar pore space. Another reason for this dissociation is due to the water's dielectric constant caused by its dipolar nature. Low (1961) suggested several possible mechanisms by which water displaces the adsorbed cations and interacts with the clay surface (hydration). Among these is the ability of water to form hydrogen bonds with the negatively charged surfaces via the silicate oxygen. In addition, the ability of water to hydrate the cations themselves or through hydration by osmosis as the result of an increase of the concentration of cations at the clay surface, allows the water molecules to diffuse toward the clay surface in order to equalize this cation concentration.

The combined effect of the negatively charged clay platelet and the adsorbed and/or hydrated cations on and around the clay surface produce what is known as the diffuse double layer. Gouy (1910) and Chapman (1913) described the charge distribution of the clay surface and the cations in the interlamellar pore fluid (Fig. 2-2). As seen in the ions' concentration is a function of distance from the clay platelet surface. The concentration of cations decreases with this distance, but the anions' concentration increases.

From Low (1961), the cations in the double layer are subject to two opposing forces. Electrostatic forces attract the cations towards the charged clay surface; diffusion moves them away from the surface. Anions are repelled by the clay surface. Diffusion from the equilibrium solution towards the surface counteracts the electric repulsion of anions. Mitchell (1993) concluded that the double layer is influenced by the ions' valence and temperature. In addition, he said that when compaction produces overlap of the double layers of adjacent clay platelets, the clay could act as a

semi-permeable membrane. Allowing the clay to adsorb water extends the double layer and results in swelling deformation and an increase in swelling pressure. The amount of swelling is dependent upon the potential extent of the double layer, which is dependent upon clay mineral type, exchangeable cation valence, cation type and concentration.

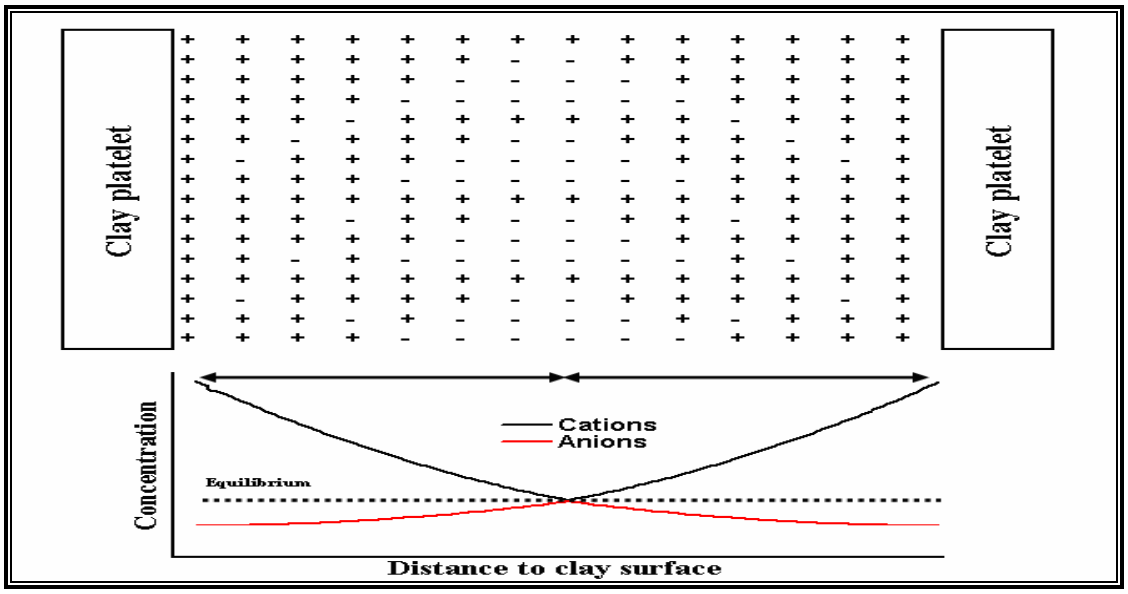

Figure (2-2): Distribution of cations and anions adjacent to clay platelets according to the diffuse double layer theory (modified after Mitchell (1993)).

When clay minerals, especially expandable ones (rich in Na^{+}), are in contact with a solution rich in cations (K^{+}, Ca^{2+}, Mg^{2+}), cations may be exchanged by broken bonds or by lattice substitutions. The exchangeable cations are held around the edges of the flakes of elongated units when bonds are broken or are held mostly on the basal plane surfaces in the case of lattice substitutions. When the amount of adsorbed water is barely able to develop plasticity, the adsorbed cations are held directly in contact with the clay mineral surface. However, given the electrostatic properties of water, the exchangeable cations may be at greater distances from the clay mineral surfaces, and may be separated from them by water molecules. The exchangeable cations

neutralize the layer's charge, influence the position of water molecules, and physically influence the intermolecular forces between the clay surfaces (Low, 1961). Over a long time, cation exchange can result in clay mineral transformations (Srodon et al., 2000).

2.2. Driving forces and fluxes through shales

By the principles of irreversible thermodynamics (DeGroot and Mazur, 1962), fluxes in fine grain-materials, including shales, that do not result in a change of state of these materials, are related linearly to their corresponding driving force (Mitchell, 1993) by the following equation:

$$J_i = L_{ii} X_i \tag{2-1}$$

where J_i is the flux of fluid solvent, electrons, solutes or heat,

L_{ii} is the conductivity coefficient of this flux, and

X_i is the corresponding driving force.

Because hydraulic and chemical potentials are the two most important driving forces governing fluxes in shales (Mody and Hale, 1993), the above relation can be written for water flux under the hydraulic driving force as the following:

$$Q_h = K_h I \tag{2-2}$$

This form is referred to as Darcy's law, where

Q_h is the flux of water

K_h is the hydraulic conductivity, and

I is the hydraulic pressure gradient

One or more driving forces can induce fluxes or flows of different types. According to Katchalsky and Curran (1965) and Mitchell (1993), this type of flow is called a coupled flow (table 2-1). This means a gradient of one type can cause the flow of another type. Thus, Equation (2-1) becomes the following:

$$J_i = \sum_{j=1}^{n} L_{ij} X_j \qquad (2\text{-}3)$$

where J_i is the flux of the type i,

L_{ij} is the coupling coefficient, and

X_j is the driving force of type j.

Accordingly, many equations for the description of coupled flows can be derived for the different driving forces (Alexander, 1990; Groenevelt and Bolt, 1969; Van Oort, 2003; Van Oort et al., 1996; Yeung and Mitchell, 1993).

Table (2-1): Driving force and corresponding flow phenomena (Alexander, 1990; Mitchell, 1993).

Flow	Gradient			
	Hydraulic	Temperature	Electrical	Chemical
Fluid	Hydraulic flow Dacy's law	Thermo-osmosis	Electro-osmosis	Chemical osmosis
Heat	Convective heat flow	Thermal conduction Fourier's law	Peltier effect	Dufour effect
Current	Streaming current	Seebeck effect	Electric current Ohm's law	Diffusion and membrane potentials
Ion	Streaming current	Soret effect	Electro-phoresis	Diffusion Ficks' law

Shaded cells are flows that considered in the current study.

In any sedimentary rock, including shales, flow induced by the hydraulic potential is always considered to follow Darcy's law (equation 2-2). Appendix B presented models and the methods used to measure the flow under the hydraulic potential through shale and fine-grained rocks. On the other hand, non-hydraulically

driven fluid flow is generally denoted as osmosis. When clay-rich rock is in contact with chemical fluids, and has a different chemical gradient than that of the shale pore fluid, osmotic flow is induced, causing movement of fluids and solutes in or out of the formation, depending on the activity difference between the formation fluid and the chemical fluid. The following paragraphs will focus on an evaluation of the chemical potential as a driving force in shale rocks.

2.3. Chemical osmosis

Chemical osmosis refers to the flow of water induced by a chemical potential difference across a semi-permeable membrane. This type of flow is usually called osmotic flow.

2.3.1. Osmotic flow

When two water (or other solvent) reservoirs are separated by a semi-permeable membrane (Fig. 2-3), water will flow from the side of lower solute concentration to the side of higher solute concentration. At the same time, the membrane will prevent the movement of solute molecules through it. In fact, the solute movement is wholly determined by fluctuations of thermal collisions with nearby solvent molecules. This means that the chemical gradient will transfer momentum to the membrane wall and, therefore, generate pressure on it and block solute movement. In addition, as the velocity is the same as that of a free molecule, the pressure will be the same as the pressure of an ideal gas of the same molecular concentration. Hence, the osmotic pressure is given by the Van't Hoff equation (Van't Hoff, 1887):

$$\Delta \pi = \frac{RT}{V_w} \ln \frac{a_{salt}}{a_{fresh}} \qquad (2\text{-}4)$$

where $\Delta\pi$ is the osmotic pressure difference across a membrane,

R is the gas constant,

T is the absolute temperature,

V_w is the mean partial molar volume of water, and

a is the activity of the water.

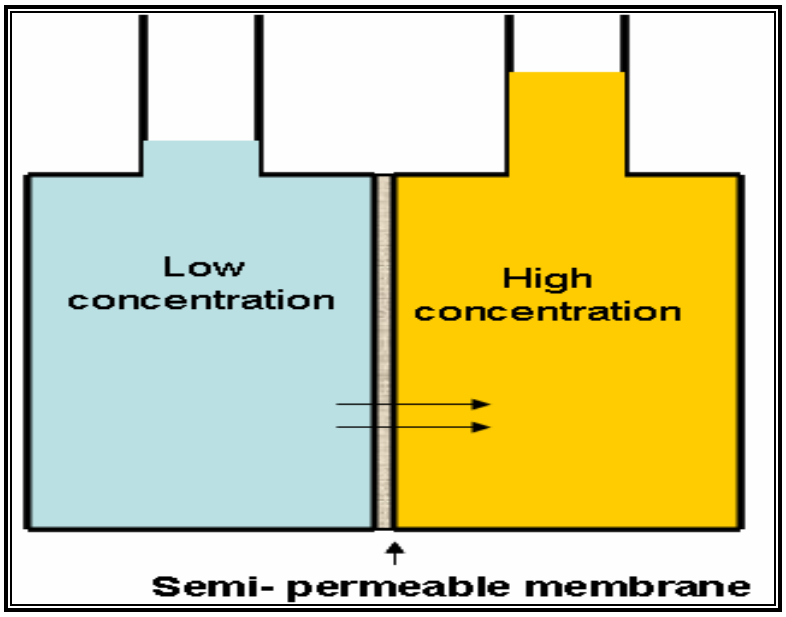

Figure (2-3): Osmotic flow due to change in two fluids' activities.

According to Robinson and Stokes (1959), the actual driving force is not the concentration gradient of the salt, but the chemical potential gradient of the water across the membrane, which can be calculated from:

$$\mu_w = \mu_w^0 + RT \ln a_w \qquad (2\text{-}5)$$

where a_w = unity at infinite dilute with T and P at standard defined conditions.

At low concentration, the activity of water can be expressed as a linear function with concentration (Alexander, 1990):

$$a_w = 1 - 0.017\nu m \tag{2-6}$$

where ν is an integer representing the number of ions in which the electrolyte dissociates, and

m is the concentration of solute in molality.

2.3.2. Reverse osmosis

Reverse osmosis refers to the flow of water due to hydraulic potential in the presence of a chemical gradient. It occurs when the osmotic flow stops, or is even reversed by applying external pressure on the side of the higher concentration. Thus, during reverse osmosis water flows across the membrane from the higher concentration to the lower concentration side, but the solute is still blocked by the membrane's effect. Reverse osmosis was a target for investigation of semi-permeable membrane properties of shale and natural clays by many researchers such as Demir (1988); Ishiguro et al. (1995); and Al-Bazali (2005). In industrial applications, reverse osmosis is used for desalination or the removal of inorganic and organic solutes from surface water and ground water (Ebrahim and Abdel-Jawad, 1994; Kastelan-Kunst et al., 1997; Merten, 1966).

2.3.3. Shale as a semi-permeable membrane

The fine pore's sizes and negative charges on the clay minerals' surfaces make shales exhibit the behavior of semi-permeable membranes. This will happen when the double layers of the adjacent clay particles overlap and both cations and

anions are excluded from the pores (Mitchell, 1993), but water and some smaller charged solutes are freely admitted to the membrane. For an ideal semi-permeable membrane, the membrane reflects all solutes and only water molecules can pass through the membrane. However, because of the wide range of the pore sizes of most shale, shale exhibits a non-ideal, semi-permeable membrane, admitting solutes of many different sizes to varying degrees. The difference between ideal and non-ideal membranes is presented in Figure (2-4). The solutes transferred across the membrane system over the time will reduce the chemical potential (water activity) of the pore fluid. In addition, diffusion of the solutes because of the imposed chemical gradient will occur. The non-ideality of a membrane is generally expressed in terms of a reflection coefficient (σ) (also referred to as membrane efficiency), which is defined as the ratio of the real developed pressure due to the natural membrane and the ideal osmotic pressure which is calculated from equation (2-4).

$$\sigma = \left[\frac{\delta P}{\Delta \pi} \right] \tag{2-7}$$

where δP is the change in the pressure head due to the osmotic flow behavior of shale, and Δπ is the calculated pressure for the ideal membrane.

Membrane efficiency is the measure of how well shales can block the ions from moving through the membrane. If the membrane efficiency is equal to one, the shale will completely prevent ions' movement. In this case, shale would be a perfect membrane. However, if the shale lets ions pass freely, the membrane efficiency will approach zero and the shale is called a non-selective membrane (Al-Bazali, 2005).

There are hosts of factors influencing the ideality of natural shale semi-permeable membranes, among them, the types of clay, their cation exchange

capacities, grain size distribution, porosity, permeability, degree of compaction and concentration of exchangeable cations in the equilibrium solution (Alexander, 1990; Whitworth, 1993). Although considerable work has been done to understand the membrane efficiency of shales, this idea has not been fully explored.

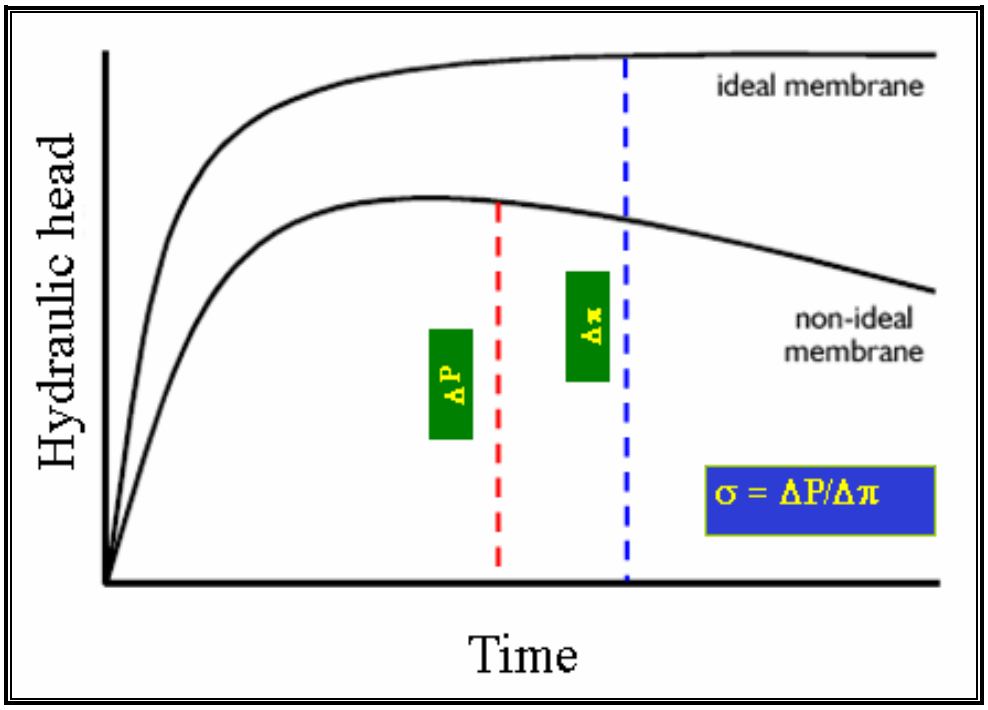

Figure (2-4): Hydraulic head across an ideal and non-ideal semi-permeable membrane (Source: Katchalsky and Curran, 1965).

2.3.4. Effect of time on shale's chemical osmotic behavior

Because of the movement of the solutes through the shale's semi-permeable membrane, the shale's pore fluid activity will be reduced as a function of time, leading to a reduction in the ideality of the membrane. Demir (1988) and Whitworth and Fritz (1994) observed a reduction in osmotic pressure that originated from samples with initially non-ideal behaviors over the time. Therefore, the researchers stated that natural semi-permeable materials go through a life cycle starting as a high membrane efficiency that is reduced by the effects of solute diffusion through the

membrane, which is time dependent. The life cycle will end when the pore water concentration in the membrane is sufficiently high that the hydraulic gradient is essentially absent. Given enough time, the chemical and hydraulic difference across the membrane will disappear.

2.3.5. Application of shale's membrane behavior

It is believed that controlling water and ion transfer into and out of shale can help to stabilize shale formations. Both osmotic forces and concentration gradients can drive the movement of water molecules and ions. Thus, if we create an imbalance of water activity between the shale pore fluid and the induced water (e.g. by borehole and drilling fluid), the water and solutes will move into or out of the shale because of this water activity imbalance (Mody and Hale, 1993).

Many researchers such as Chenevert (1970), Mody and Hale (1993), Van Oort et al. (1996), Yu et al. (2003) and Al-Bazali (2005) found that dehydration of shale formations around boreholes could lead to an increase in the shale strength and thus avoid wellbore failure. It was suggested that using a drilling fluid with water activity lower than that of the shale pore fluid would generate an osmotic pressure that produces a flow of water out of the shale and into the wellbore. Conversely, in order to build an effective osmotic pressure gradient in the wellbore, shale and drilling fluid must produce a high osmotic pressure gradient in the wellbore and exhibit high membrane efficiency, which is a function of both the shale formation and the drilling fluid. Therefore, it is very important to know the shale membrane efficiency and its pore fluid composition in order to design a drilling fluid that will produce a highly

effective osmotic pressure gradient when interacting with the shale formations (Al-Bazali, 2005).

2.3.6. Geological significance of osmotic flow through shale.

Many researchers such as Berry (1969), Hanshaw and Hill (1969), Marine and Fritz (1981), Graf (1983), Neuzil (1998), Neuzil (2000) and Cey et al. (2001) indicated that coupled flows are not only important on a laboratory scale, but also take place on a field scale. Marine and Fritz (1981) suggested that high salinity aquifer waters in oil fields (oil field brines) may have developed by osmosis. According to Wood (1976), Graf (1983), and Horseman et al. (1996), the abnormally high hydraulic heads of aquifers that cannot be explained with the assumptions of standard hydrogeological models may be explainable by chemical osmosis. Hanshaw and Zen (1965) suggested that osmotic pressure gradients could be responsible for anomalous high pressures in shale beds, which can lead to the development of an over thrust faulting of the shale. In the coastal area of the Netherlands, clay layers often separate aquifers of different chemical composition and water transport between these aquifers because of osmotic gradients was suggested by Loch and Keijzer (1996). The only in-situ measurements of osmotic flow in shale formations were done by Neuzil, (2000). He concluded that a long-term (7 years) in-situ field experiment on Pierre Shale shows water transport between boreholes in relation with an applied chemical gradient.

Chapter 3

Numerical Modeling of Flux of Fluid and Ions through Shale Semi-Permeable Membranes

Several models have been published during the last few decades for the prediction of the water flow in a natural system under chemical gradient based on the framework of irreversible thermodynamics. However, the ions' flux through these systems was neglected by most of these researchers. The flux of fluid and ions due to the semi-permeable membrane behavior of very fine-grained material has been numerically modeled in one spatial dimension and time in this study. The purpose of this model is to predict not only the fluid flow through natural geological semi-permeable membrane materials, but also the ions' flux through them as a time dependent factor and the effect of this flux on the materials' membrane's reflection coefficient. The required input parameters for the model include water activity of both chemical fluids and the pore-fluid of the membrane, and membrane properties: reflection coefficient, porosity, hydraulic conductivity, mineral compressibility, diffusion processes, and temperature and pressure conditions. These parameters are determined by laboratory work done on Pierre Shale using the HTHP Shale Apparatus as described in Chapters 5 and 6. The following sections present the equations, assumptions, and techniques used in model development. Appendix A presents the numerical solution of the model using the Mathematica Software Program™. Predictions about the flux of the fluid and ions through in-situ Pierre

Shale will be dependent on model parameterization using our lab results and the studies of Neuzil (2000) as discussed in the end of this chapter.

3.1. Osmotic fluxes through shale system

The flux or flow through fine grain-materials including shales can be related linearly to its corresponding driving force and is controlled by Equation (2-1) (Mitchell, 1993):

$$J_i = L_{ii} X_i$$

where J_i is the flux of the fluid, electrons, solutes or heat,

L_{ii} is the conductivity coefficient of this flux, and

X_i is the corresponding driving force.

This equation was written for water flux under the hydraulic driving force as Equation (2-2):

$$Q_h = K_h I$$

This is Darcy's law where

Q_h is the flux of water,

K_h is the hydraulic conductivity, and

I is the hydraulic pressure gradient.

In any fine-grained material, including shale, flow induced by the hydraulic potential is always considered to follow Darcy's Law. On the other hand, non-hydraulically driven fluid flow is generally denoted as osmosis, when clay-rich rock is in contact with fluids and possesses a chemical gradient different from that of its pore fluid, osmotic flow is induced. The result of this induces osmotic flow is the

movement of fluid and solute into or out of the formation, depending on the difference of activity between the formation pore fluid and the chemical fluid. In this system, water will flow from the side of lower solute concentration to the side of higher solute concentration. At the same time, the membrane will prevent the movement of solute molecules through it depending upon its ideality. In the ideal semi-permeable membrane, the induced osmotic pressure is given by the Van't Hoff equation (Van't Hoff, 1887):

$$\Delta \pi = \frac{RT}{V_w} \ln \frac{a_{salt}}{a_{fresh}}$$

where $\Delta\pi$ is the osmotic pressure difference across a membrane,

R is the gas constant,

T is the absolute temperature,

V_w is the mean partial molar volume of water, and

a is the activity of the water.

As mentioned before, the actual driving force is the chemical potential gradient of water across the membrane often expressed by the term of water activity:

$$\mu_w = \mu_w^0 + RT \ln a_w$$

where a_w = unity at infinite dilute when T and P are at standard conditions.

At low concentration, the activity of water can be expressed as a liner function with concentration (Alexander, 1990):

$$a_w = 1 - 0.017 \nu m$$

where ν is an integer representing the number of ions in which the electrolyte dissociates, and

m is the concentration of solute in molality (mol/kg).

Distilled water was used as shale pore fluid (with activity = 1) and nitrates solution as the high concentration solution with activity following the Alexander (1990) Equation (Fig . 3-1), allowing the Van't Hoff equation to be simplified as:

$$\pi = -\frac{RT}{V_w}\ln a_w \qquad (3\text{-}1)$$

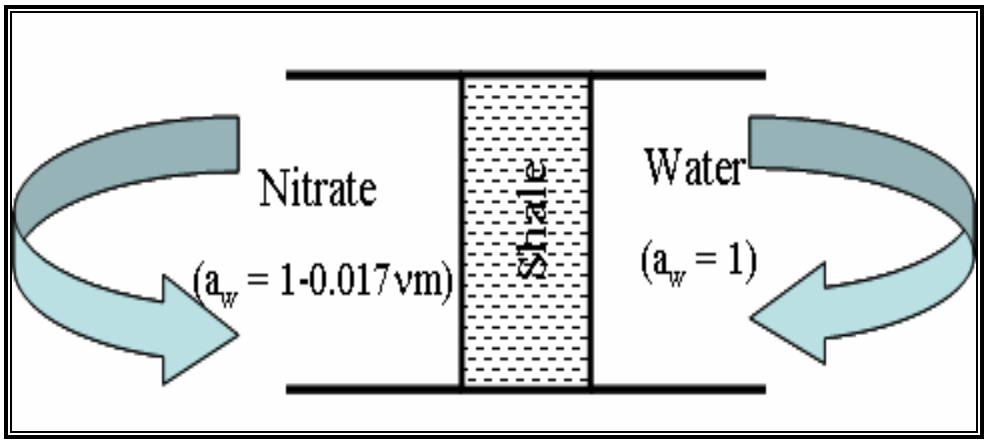

Figure (3-1): Schematic diagram for our shale/fluids system.

Using chain rule derivation, Equation (3-1) will become:

$$\nabla\pi = -\frac{RT}{V_w}.\frac{1}{a_w}\nabla a_w \qquad (3\text{-}2)$$

Replacing the solution activity a_w by its value as in the Alexander (1990) equation, the following Equation will be obtained:

$$\nabla\pi = 0.017\nu\frac{RT}{V_w a_w}\nabla m \qquad (3\text{-}3)$$

An ideal membrane completely restricts the passage of a solute through its structure. In natural systems semi-permeable membranes are seldom ideal, as most membranes do not restrict the passage of all solutes present in the solvent as they pass through the membrane due to heterogeneity, microfractures, or other factors. In

addition, a diffusion of solutes as a result of chemical gradient occurs (Fritz, 1986; Katchalsky and Curran, 1965). The non-ideality of a membrane is expressed as the reflection coefficient σ (membrane efficiency) which is defined as the ratio of the actually developed hydraulic pressure over the ideal calculated osmotic pressure (Equation 2-7).

$$\sigma = \left[\frac{\delta P}{\Delta \pi} \right]$$

where δP is the change in the pressure head resulting from the osmotic flow behavior of shale, and Δπ is the calculated pressure for the ideal membrane.

Keijer (2000) stated that many models have been published over the years illustrating predications of the reflection coefficient in natural systems based on the framework of irreversible thermodynamics as formulated by Katchalsky and Curran (1965). Throughout this chapter, the reflection coefficient model represented in Equation (2-7) will be used.

The total flow into or out of shale, J_v, is driven by differences in hydraulic pressure and chemical potential and can be described by irreversible thermodynamics, Katchalsky and Curran (1965), Fritz (1986) and Van Oort et al. (1996):

$$J_v = L_p(\Delta P - \sigma \Delta \pi_0) \qquad (3\text{-}4)$$

where J_v is the volume flux of the solution ($m.s^{-1}$),

L_p is the hydraulic permeability coefficient in ($m^3.N^{-1}.s^{-1}$),

ΔP is the hydraulic gradient across the membrane (Pa), and

$\Delta \pi_0$ is the osmotic pressure difference across the membrane in the equilibrium solution.

According to Fritz (1986), L_p is the measure of the mechanical filtration capacity of a membrane and is related to the fluid discharge through a membrane in response to a pressure difference. That means this coefficient is unequal to the typical hydraulic conductivity, which is usually denoted as K_h ($m.s^{-1}$) as it also includes the effect of membrane thickness. The hydraulic permeability coefficient and hydraulic conductivity can be related to each other according to (Fritz, 1986) as :

$$L_p = \frac{K_h}{\rho g x} \tag{3-5}$$

where ρ is fluid density (kg. m^{-3}),

g is the gravitational constant (9.8066 $m.s^{-2}$), and

x is the thickness of membrane (m).

Also, according to Fetter (1994) the hydraulic conductivity is equal to:

$$K_h = \frac{k\rho g}{\eta} \tag{3-6}$$

where k is the permeability coefficient, and

η is fluid viscosity (for water it equals to 10^{-9} MPa^{-5}).

From equations (3-5) and (3-6), L_p can be written as:

$$L_p = \frac{k}{\eta x} \tag{3-7}$$

which is in agreement with Van Oort et al. (1996). The volume flux of solution (Equation 3-4) at any point in x direction of the membrane can be given from:

$$\bar{J}_v = -\frac{k}{\eta}\nabla P + \frac{\sigma k}{\eta}\nabla \pi \tag{3-8}$$

This equation was also given by Neuzil (2000) for $\bar{q}$. Replacing $\nabla\pi$ by its value as in Equation (3-3) $\bar{J}_v$ became:

$$\bar{J}_v = -\frac{k}{\eta}\nabla P + 0.017\nu\frac{\sigma k}{\eta}\frac{RT}{V_w a_w}\nabla m \qquad (3\text{-}9)$$

To simplify Equation (3-9) let us use ϑ as constant $= \frac{RT}{V_w a_w}\, 0.017\nu$. Then it will be:

$$\bar{J}_v = -\frac{k}{\eta}\nabla P + \vartheta\frac{\sigma k}{\eta}\nabla m$$

Since m is concentration by molality (mol.kg$^{-1)}$, it can be replaced by c, which is solute concentration across the membrane (mol.m^{-3}):

$$\bar{J}_v = -\frac{k}{\eta}\nabla P + \vartheta\frac{\sigma k}{\eta}\nabla c \qquad (3\text{-}10)$$

For the solute flux equation, Fritz (1986) and Whitworth and Fritz (1994)'s derivation series was used:

$$J_s = c(1-\sigma)J_v + \omega\Delta\pi \qquad (3\text{-}11)$$

where J_s is flux of solute (mol.m^{-2}.s^{-1}) with time,

ω is solute permeability coefficient (mol.N^{-1}.s^{-1}) and is equal to:

$$\omega = \frac{D}{RTx\xi}$$

where D is the diffusion coefficient (m^{2}s^{-1}),

ξ is the tortuosity of the membrane (the ratio between the actual effective distance of flow and macroscopic distance of the membrane)

That means ω is a function in (D) and in the same way $\Delta\pi$ is a function in concentration (c). Thus, $\omega\Delta\pi$ = DΔc and Equation (3-11) can be written as:

$$J_s = c(1-\sigma)J_v + D\Delta c \tag{3-12}$$

From the Second Law of Thermodynamics (the mass conservation law), the change in the concentration of fluid overtime through the membrane can be written as:

$$\frac{\delta(c\phi)}{\delta t}$$

where ϕ is the active porosity.

The whole amount is equal to $-\nabla J_s$, so:

$$\frac{\delta c\phi}{\delta t} = -\nabla\left[-c(1-\sigma)J_v - D\nabla c\right] = D\nabla^2 c + c\nabla J_v(1-\sigma) \tag{3-13}$$

Assuming ϕ is a constant in space and time,

$$\frac{\delta c}{\delta t} = D\overline{\nabla}^2 c - \frac{(1-\sigma)}{\phi} c\overline{\nabla} J_v - \frac{(1-\sigma)}{\phi} J_v \overline{\nabla} c \tag{3-14}$$

If we insert J_v from Equation (3-10), then:

$$\frac{\delta c}{\delta t} = D\overline{\nabla}^2 c - \frac{(1-\sigma)}{\phi} c\overline{\nabla}\{-\frac{k}{\eta}\overline{\nabla}P + \vartheta\frac{\sigma k}{\eta}\overline{\nabla}c\} - \frac{(1-\sigma)}{\phi}\{-\frac{k}{\eta}\overline{\nabla}P + \vartheta\frac{\sigma k}{\eta}\overline{\nabla}c\}\overline{\nabla}c$$

$$\frac{\delta c}{\delta t} = D\overline{\nabla}^2 c + \frac{(1-\sigma)}{\phi}\frac{k}{\eta}c\overline{\nabla}^2 P - \frac{(1-\sigma)}{\phi}\vartheta\frac{\sigma k}{\eta}c\overline{\nabla}^2 c + \frac{(1-\sigma)}{\phi}\frac{k}{\eta}\overline{\nabla}P\overline{\nabla}c - \frac{(1-\sigma)}{\phi}\vartheta\frac{\sigma k}{\eta}\overline{\nabla}^2 c$$

$$\frac{\delta c}{\delta t} = \left[D - \frac{(1-\sigma)}{\phi}\vartheta\frac{\sigma k}{\eta}c\right]\overline{\nabla}^2 c + \left[\frac{(1-\sigma)}{\phi}\frac{k}{\eta}c\right]\overline{\nabla}^2 P - \frac{(1-\sigma)}{\phi}\overline{\nabla}c\left[-\frac{k}{\eta}\overline{\nabla}P + \vartheta\frac{\sigma k}{\eta}\overline{\nabla}c\right] \tag{3-15}$$

If we take $f_1 = \left[D - \frac{(1-\sigma)}{\phi}\vartheta\frac{\sigma k}{\eta}c\right]$, $f_2 = \left[\frac{(1-\sigma)}{\phi}\frac{k}{\eta}c\right]$ and $f_3 = \frac{(1-\sigma)}{\phi}\left[-\frac{k}{\eta}\overline{\nabla}P + \vartheta\frac{\sigma k}{\eta}\overline{\nabla}c\right]$, the equation will be:

$$\frac{\delta c}{\delta t} = f_1\overline{\nabla}^2 c + f_2\overline{\nabla}^2 P - f_3\overline{\nabla}c \tag{3-16}$$

To derive an equation for the fluid pressure across the membrane, drawing from the mass conservation law, the change in fluid density overtime can be written a:

$$\frac{\delta \rho \phi}{\delta t}$$

which is equal to $-\overline{\nabla}(\rho q)$ where q is the amount of fluid flux per unit time, since $\rho = \rho_0(1 + \beta(P - P_0))$. At $\overline{\nabla} p = 0$ ρ_0, β *and* ϕ are constant:

$$\phi \rho_0 \beta \frac{\delta P}{\delta t} = -\rho \overline{\nabla} q$$

$$\frac{\delta P}{\delta t} = \frac{-\rho}{\phi \rho_0 \beta} \left[\overline{\nabla} q \right] \qquad (3\text{-}17)$$

Since $\bar{\nabla} q$ is same as $\bar{\nabla} J_v$ (Neuzil, 2000), Equation (3-17) can be written as:

$$\frac{\delta P}{\delta t} = \frac{-\rho}{\phi \rho_0 \beta} \left[\overline{\nabla} \{ -\frac{k}{\eta} \overline{\nabla} P + \vartheta \frac{\sigma k}{\eta} \overline{\nabla} c \} \right]$$

which can be simplified as:

$$\frac{\delta P}{\delta t} = \frac{k}{\phi \beta \eta} \overline{\nabla}^2 P - \vartheta \frac{\sigma k}{\phi \beta \eta} \overline{\nabla}^2 c \qquad (3\text{-}18)$$

where β is the compressibility of the water (mPa^{-1}) = 4.59 X 10^{-4} mPa^{-1}.

3.2. Model numerical solution

Appendix A presents a numerical solution for the above models depending on shale parameters that are obtained from laboratory experiments in this dissertation. The shale parameters include permeability (κ), porosity (ϕ), membrane efficiency (σ), cross sectional area (a), and thickness of the study sample (x). The fluid parameters include chemical concentration (c), the constant (ϑ) which is solution activity factor, diffusion coefficient (D) (using Neuzil (2000) data), fluid

compressibility (β), the fluid viscosity (η) and the volume of the chemical reservoir (vol). The initial pressure across the samples was assumed to be seven MPa at a fixed temperature (25 °C). Since the temperature is stable, D, β and η are used as constant parameters as 1.0 X 10^{-12} m^2s^{-1} for D, 4.59 X 10^{-4} MPa^{-1} for β and = 1.0 X10^{-9} MPa^{-5} for η. Also, the volume of the chemical reservoir is used as a fixed parameter (10^{-6} m^3). The other parameters are used as variables to study the effect of these parameters on osmotic pressure and the ions' flux through the study samples.

3.2.1. Osmotic pressure

This model describes the distribution of the pressure induced by the chemical gradient inside the membrane itself along the three dimensions of pressure, time, and thickness (Appendix A). This model can be applied to any shale formation with a chemical gradient between its pore fluid and the induced fluid if we can constrain certain parameters. For example, when a chemical gradient is created between a wellbore and shale formation, the current model (if transformed into radial coordinates) can predict the distribution of the induced osmotic pressure inside the borehole. This model provide solution for the relation between osmotic pressure and both the rock parameters and the chemical solution characteristics.

The magnitude of the osmotic pressure depends on membrane efficiency, and both solution type and concentration. Osmotic pressure increases with increasing membrane efficiency and solution concentration (Fig 3-2 and 3-3). Since the solution activity is dependent on its type and concentration (see Chapter 4), ϑ (the activity dependant constant) needs to be modified to fit each of the three nitrate solutions used in the laboratory work during the current study. The osmotic pressure magnitude is

increased in the following order K < Na < Ca (Fig. 3-4). This means the osmotic pressure decreases with increasing nitrate fluid activity that follows the order K > Na > Ca (see Chapter 4). This also is indicated from the increase of osmotic pressure with increasing concentration, which has an opposite relationship with the activity.

The rate of osmotic pressure (how fast the induced pressures reach the maximum and then the steady state) is dependent on the permeability of the rock and the membrane thickness (sample thickness). Figure (3-4) shows the relationship between osmotic pressure and time with different rock permeability and indicates that the rate of osmotic pressure increases with increased permeability. This rate decreased with an increase in the sample thickness, as indicated from Figure (3-5).

Porosity has a very limited effect on either magnitude or the rate of osmotic pressure (Fig. 3-7). Permeability which depends mainly on the connected pore space (effective porosity) is the main factor that affects the passing of the solution through materials. The porosity that was used here is the total porosity.

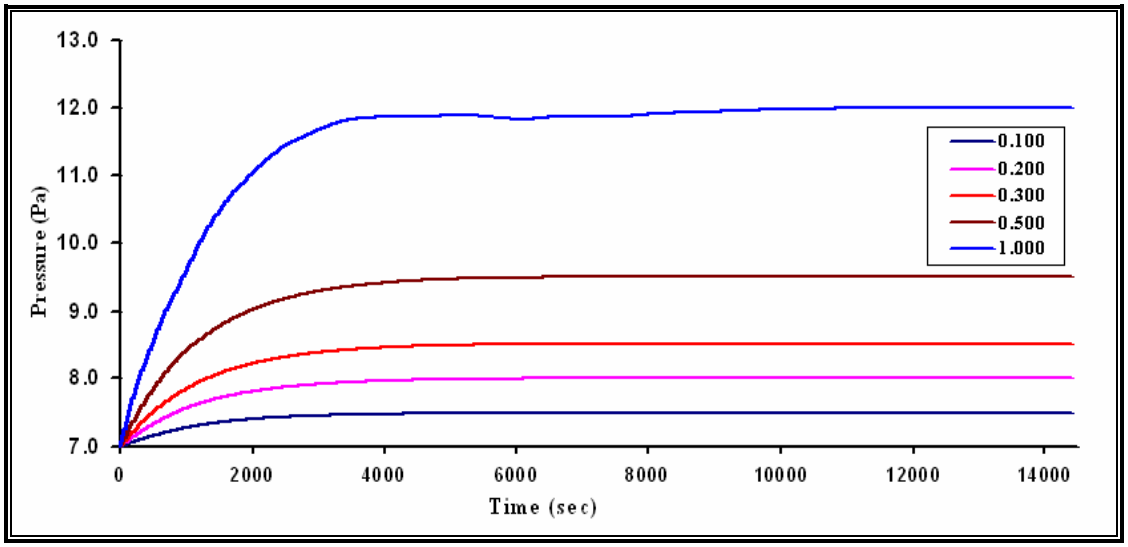

Figure (3-2): Numerical representation of the relationship between osmotic pressure and time for a different membrane efficiency (1 mole KNO_3, 3 mm thick, 7 Pa initial pressures, 25 n Darcy permeability and 2 % porosity).

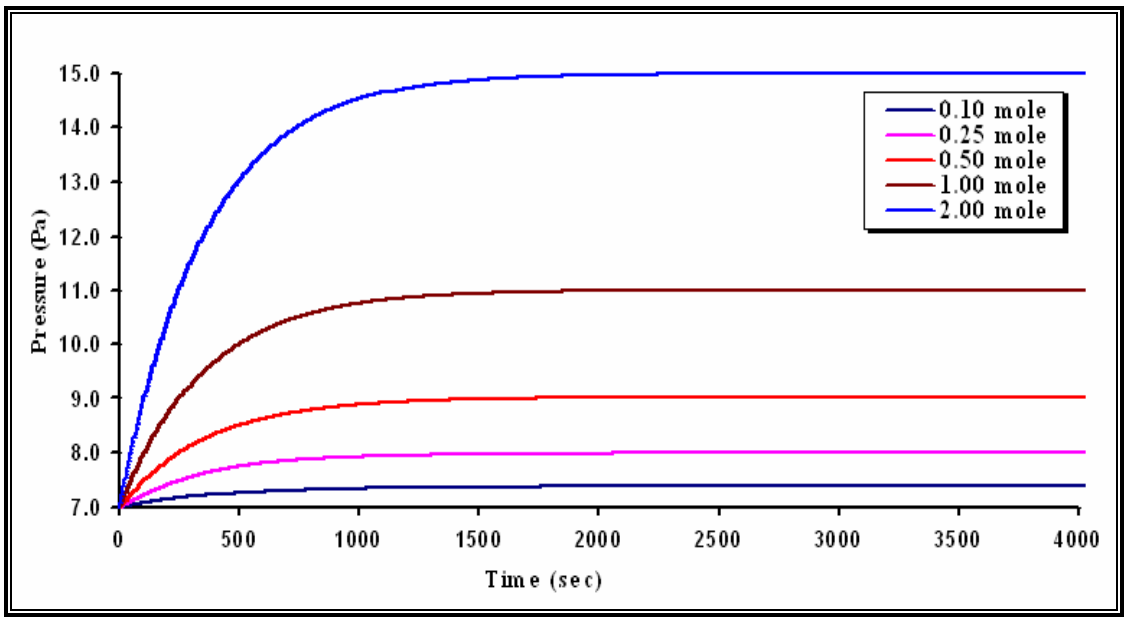

Figure (3-3): Numerical representation of the relationship between osmotic pressure and time for different KNO_3 concentrations (0.8 membrane efficiency, 3 mm thick, 7 Pa initial pressure, 25 n Darcy permeability and 2 % porosity samples).

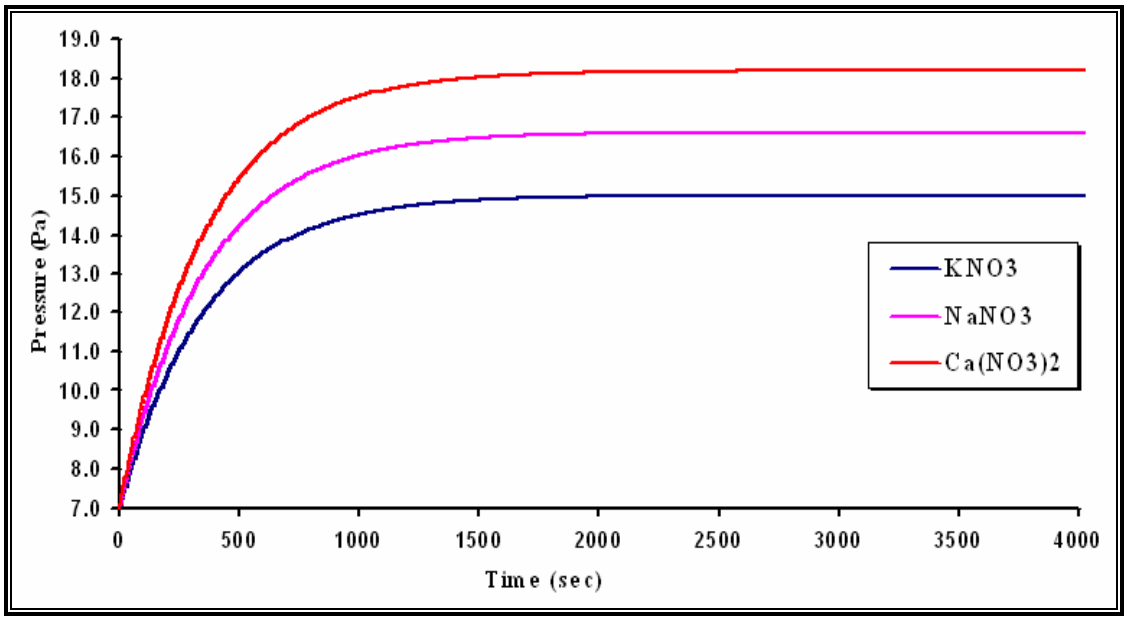

Figure (3-4): Numerical representation of the relationship between osmotic pressure and time for three nitrate solutions (2 mole concentration, 0.8 membrane efficiency, 3 mm thick, 7 Pa initial pressure, 25 n Darcy permeability and 2 % porosity).

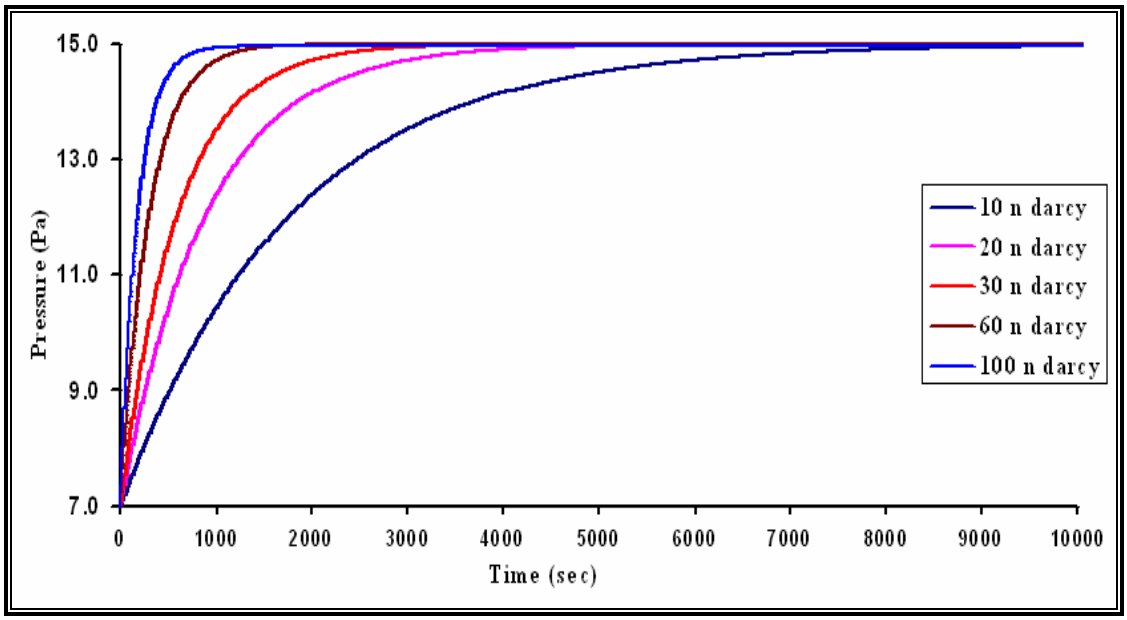

Figure (3-5): Numerical representation of the relationship between osmotic pressure and time for different permeability (0.8 membrane efficiency samples, 1 mole KNO_3, 3 mm thick, 7 Pa initial pressure and 2 % porosity samples).

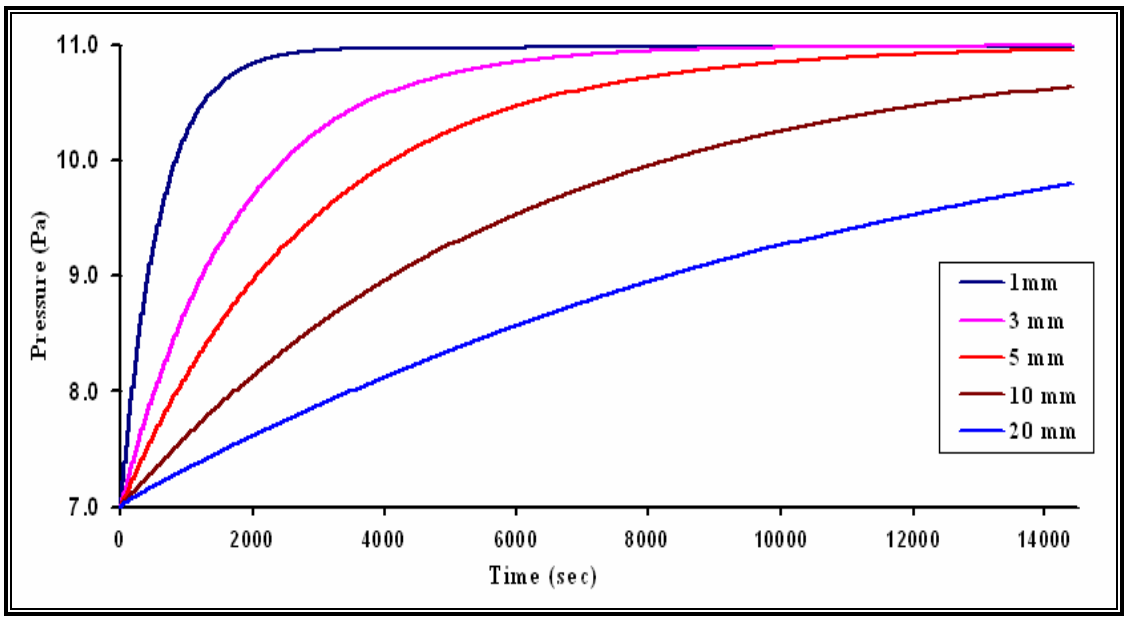

Figure (3-6): Numerical representation of the relationship between osmotic pressure and time for different membrane thickness (0.8 membrane efficiency samples, 1 mole KNO_3, 7 Pa initial pressures, 25 n Darcy permeability and 2 % porosity).

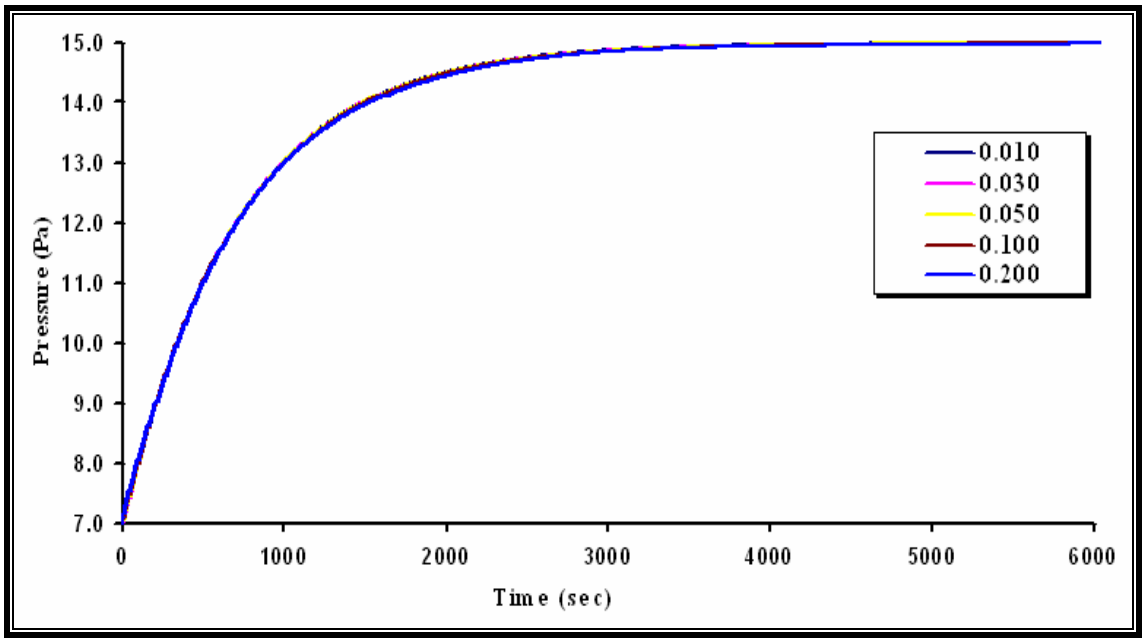

Figure (3-7): Numerical representation of the relationship between osmotic pressure and time for different porosity rocks (0.8 membrane efficiency, 1 mole KNO_3, 7 Pa initial pressure, 25 n Darcy permeability).

3.2.2 Ion flux

In addition to showing the pressure distribution through the study sample, this model provides us with ion spatial distribution over time. The ion flux, which was studied as the change in fluid concentration inside the sample, was affected mainly by diffusional transport, which is a time dependant factor. According to this model and laboratory tests (chapter 5) the membrane effect at different positions will lead to membrane change with time. Because the concentrations on both sides are stable, the rate of gained ions inside the sample will be equal to the rate of losing them through the membrane to the distilled water reservoir. In a close system, the movement of the membrane position and the concentration change on both sides will continue until the two concentrations become nearly equal. At this moment, there will be no chemical gradient to produce any osmotic pressure.

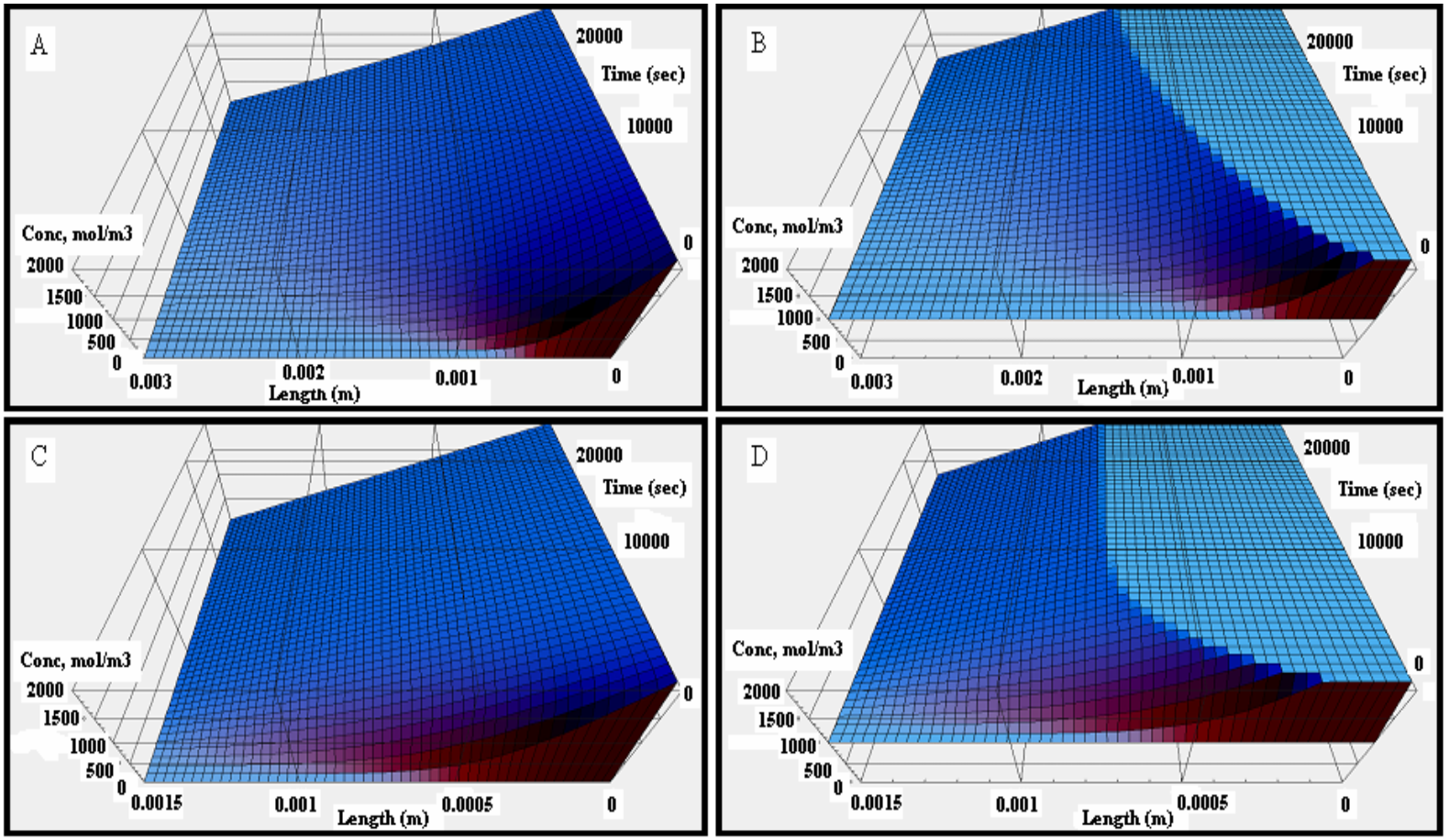

Figure (3-8): Numerical representation of distribution of fluid concentration through the sample over the time (0.8 membrane efficiency, 2-mole KNO_3, 7 Pa initial pressures, 25 n Darcy permeability and 2 % porosity).
A & B) 3 mm thickness samples and C&D) 1.5 mm samples.
A&C) 0 concentration on the low concentration side and B&D) 1 mole concentration on low concentration side.

There are many parameters which also effect the ions' flux through shales, such as ion exchange capacity and the ability of clay minerals to hold ions in its lattice structure (Chapter 6), which can be expressed as membrane efficiency. In addition, rock permeability and porosity also influence ion transport through the shale. The solution of the current model with different membrane efficiencies, permeabilities and porosities showed little effect on the ion flux through the simulated shale (Appendix A).

3.3. Conclusions

The study of this model reveals that, due to the flux of solutes through the semi-permeable membrane, shale's pore fluid activity will reduce with time, leading to a reduction in the ideality of the membrane. Thus, virtually all osmotic flows in shales are transient phenomena. Given enough time, the chemical and hydraulic difference across the membrane will disappear, leading to a diminishing of the fluid osmotic flow. This model can help in correlating and representing clay-rich rock's semi-permeable membrane behavior, and in enhanced understanding of the relevant processes.

Chapter 4

Methodology and Initial Materials

To study membrane behavior and investigate the impacts of fluid chemistry on behavior and structures of shales in the laboratory, many experiments were performed under different pressure and temperature conditions using a High Temperature High Pressure (HTHP) Shale Apparatus, HP Triaxial Apparatus, Atomic Absorption, XRD, SEM and Coulter Grain-Size Analyzer. These experiments were run with three different nitrate solutions with Pierre Shale. This chapter briefly describes the tools and methodology that were used throughout this study. The sample descriptions, bulk properties and the mineralogical characterizations will be given and evaluated. In addition, a short description of the chemical fluids that were used and their properties that may affect behavior and structures of shales will be reviewed.

4.1. Research tools and methodology

4.1.1. Physico-chemical properties of shale studies

Permeability, osmotic membrane, and ion diffusion properties of shale samples were studied at high-pressure conditions (up to 3000 psi) using the ***High Temperature High Pressure (HTHP) Shale Apparatus*** (Fig. 4-1). This system is composed of three hydrostatic cells (Cell No. I, Cell No. II, and Cell No. III) that can be pressurized up to 10,000 psi. Each of the three cells is connected to a common servo-control confining pressure system and common upstream pore pressure system. The pore pressures in the downstream phases are independently controlled and

different types of chemically reactive fluids can be flushed across the thin shale disk samples (3-10 mm thick and 25 mm diameter) during testing. In addition, each cell contains an internal thermocouple to monitor sample temperature. The data from each cell (confining pressure, upstream pressure, downstream pressure and temperature) is recorded every second using two types of data acquisition systems (Data Acq DI-710™ for pressure and Data Acq DI-1000™ for temperature) with the help of WinDaq Lite Data Acq DI-710™ and WinDaq Lite Data Acq DI-1000TC™ software provided with the data acquisition systems.

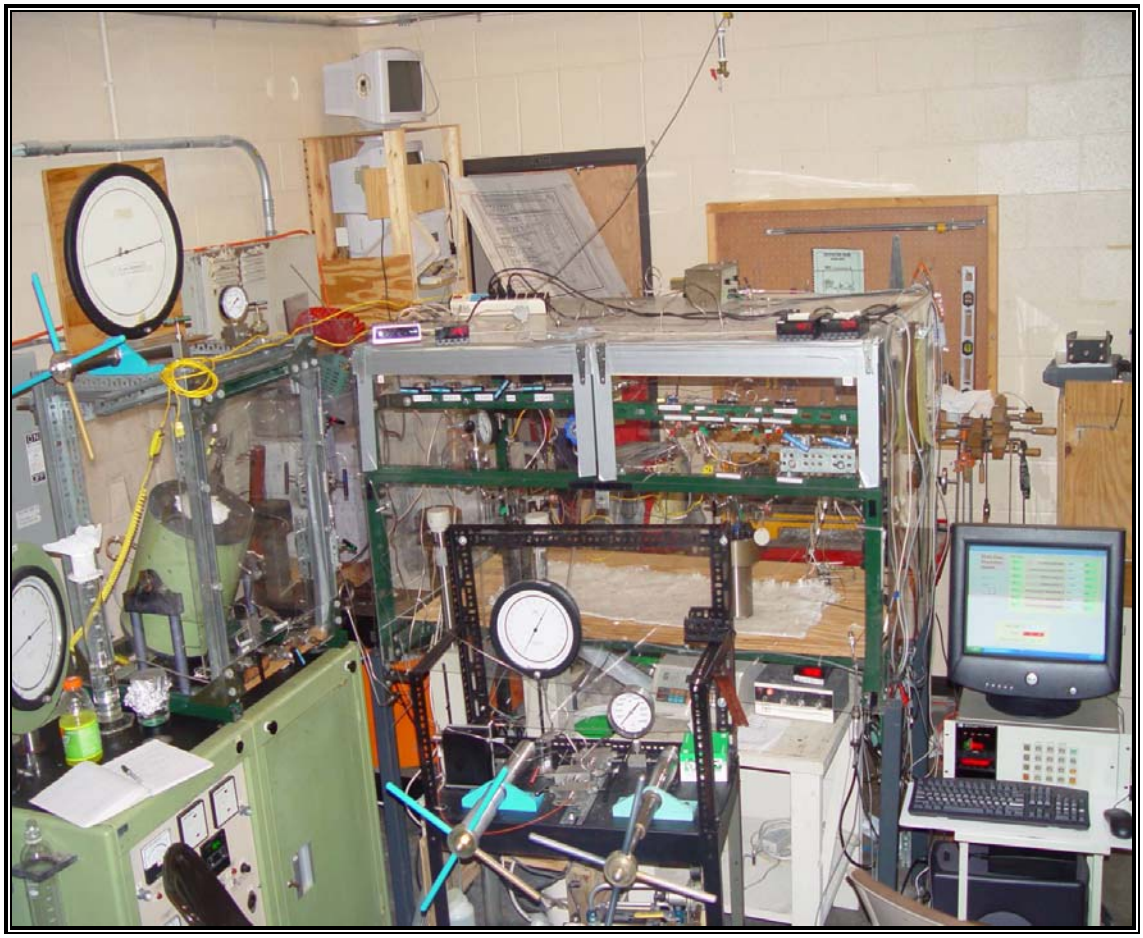

Figure (4-1): HTHP Hydrostatic Shale Testing Apparatus.

Each cell was utilized for different experimental purposes. Cell No. I was housed in a high temperature furnace and accordingly was used to examine illitization of smectite at high temperature, Cell No. II was used for solute diffusion experiments, and Cell No. III was used for room temperature shale membrane efficiency and pressure transient decay permeability measurement experiments. The internal design and the test procedures for each cell will be discussed later according to its purposes.

4.1.2 Swelling stress measurements

Measuring of the swelling stress and pressure that result from fluid and ion fluxes through shale membranes at the same pressure conditions of membrane studies are done with specially designed ***High-Pressure (HP) Triaxial Cell*** (Fig. 4-2). HP triaxial cell is composed of a triaxial pressure vessel and loading frame, connected to servo-controlled confining pressure and upstream pore pressure systems. The pore pressures in the downstream phases are independently controlled, and different types of chemically reactive fluids can be flushed across the relatively thick shale disk samples (10-20 mm thick and 25 mm diameter) such as in HTHP cells. Any change in stress due to swelling of shale is recorded through a stress transducer (SEDEME Sam 10000^{TM}). The stress transducer and the pressure outlets are connected to a computer through a four-channel data acquisition system (Data Acq DI-710^{TM}). The data are monitored and recorded using PC in the same way as in the HTHP Shale Apparatus. Vertical movement of the cell position is measured by a LVDT (with accuracy 0.001 mm) that is calibrated and attached to the cell and connected to a computer through the aforementioned data acquisition system. A thermocouple is also fixed in the

interior of the cell in a small well to record its temperature, which is recorded manually. Details of the HP Triaxial Cell design, the way it works, and the procedures will be discussed in Chapter 6.

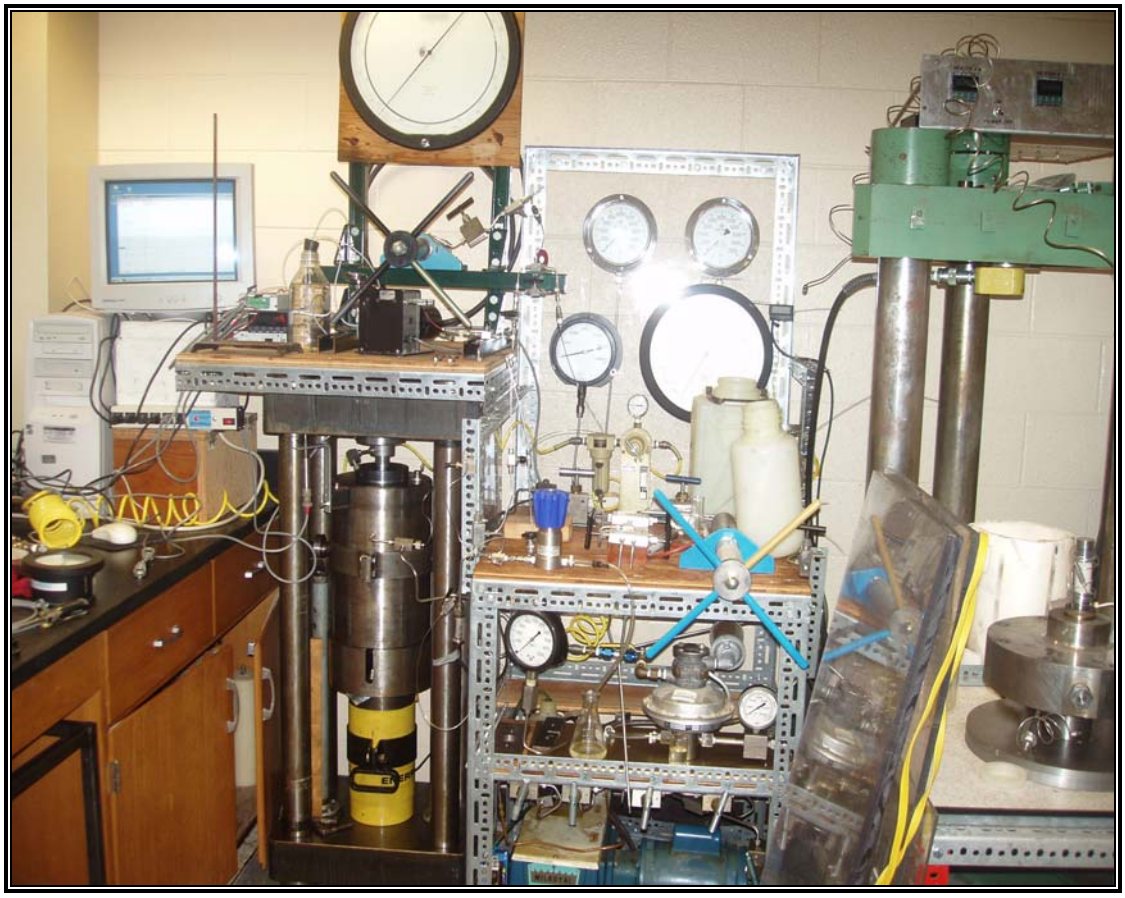

Figure (4-2): HP Triaxial Testing Apparatus.

4.1.3. Mineralogical studies

The mineralogy of clay and non-clay minerals was identified by the X-Ray Diffraction (XRD) technique and supplemented by Scanning Electron Microscope (SEM) observations for close inspection.

4.1.3.1. X-ray diffraction analysis (XRD)

With its limitations, XRD is considered the most widely used method to characterize the composition of fine-grained rocks because it can yield the relative

amount of each major mineral present. Mineralogical studies of our samples were carried out using XRD technique without addition of any chemicals, using the scheme proposed by Millot (1970) for oriented samples. To confirm the presence of smectite, the samples were subjected to ethylene glycol vapor for one hour in a desiccator at 90 °C (Bradley, 1945 and Brunton, 1955). Some samples were heated at 550 °C for two hours in a muffle furnace to confirm the presence of kaolinite. Samples were scanned on a Rigaku Geigerflux™ XRD diffractometer (Fig. 4-3) and the patterns were run in the range from 4-70 2θ. Automated operations were performed by MDI datascan software.

Figure (4-3): Rigaku Geigerflux XRD diffractometer with a computer.

Semiquantitative estimation of the clay minerals is based on peak area and for non-clay minerals on peak height (Pierce and Siegel, 1969) and with the assistance of MDI JADE™ minerals database. The crystallinity index of smectite, illite and kaolinite was also determined using peak height to half-peak width (Biscaye, 1965).

4.1.3.2. Scanning electron microscope (SEM) and energy dispersive X-ray spectrometer (EDX)

For close observations of clay minerals and their structures, a Scanning Electron Microscope (SEM) was used. SEM is an instrument that provides relatively high spatial resolution for surface and near surface information from bulk samples. Simply, instead of using light as in a petrographic microscope, electrons are ejected from filaments, accelerated, and focused into a small probe that is scanned over the surface sample. This high-energy electron beam behaves as a wave and interacts with samples in many ways to produce different signals that can be analyzed by various types of detectors and spectrometers, making the electron microscopes versatile instruments for three-dimensional images of minerals structures and for other solid materials (Everhart and Hayes, 1972). Interaction of the primary electron beam with the sample produces various forms of radiation, such as secondary electrons (SE), characteristic X-rays, auger electrons, backscatter electrons and background X-rays. All of these reactions occur at the same time and can be observed and analyzed. The SEM used in the current study uses the secondary electron micrograph (SEM micrograph) for three-dimensional topographic images, backscatter electrons for two-dimensional images, and the characteristic X-ray EDX spectrum for semi-quantitative elemental analysis. The rest of the radiation is dissipated into heat or lost in the walls of the SEM sample chamber.

Tiny pieces gently broken from shale samples (~ 2 by 5 by 5 mm) were attached to SEM specimen plugs by carbon tape and dried for an hour and coated first by Carbon (C) and then by Gold (Au)-Palladium (Pd). These thin coatings (200 °A

thick) applied in a Kinney evaporative coater were required to obtain a clear image. Then the sample was examined by JSM-880 SEM with EDX system (Fig. 4-4, *computer screen has a pyrite crystals*) under different magnifications from X500 to X100,000. Welton (1984) atlas was used to assist in interpretation of the samples' images.

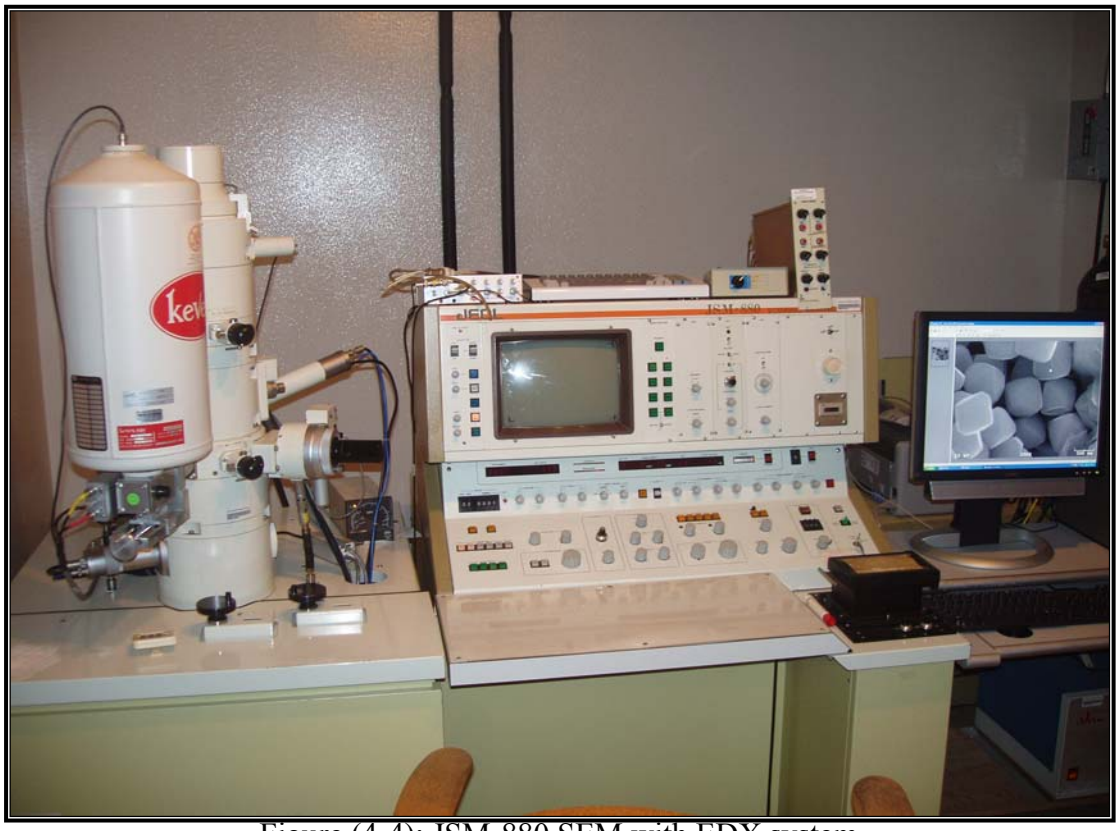

Figure (4-4): JSM-880 SEM with EDX system.

4.1.4. Grain-size analysis

Because the grain-sizes of the studied shale samples are mostly less than 64 μm in diameter, a ***Laser Particle Size Analyzer Technique*** was used to determine the particle size distribution of natural and chemically treated shale samples. The laser diffraction technique is based on the principle that particles of a given size will diffract light through a given angle. In the present study a Beckman Coulter LS 230

Laser Particle Size Analyzer (Fig. 4-5) which has a particle detection resolution range of 0.04 – 2000 μm was used. The LS 230 Particle Size Analyzer is composed of an array of 126 optical detectors; uses reverse Fourier lens optics incorporated in a binocular lens system and is based on either Fraunhofer or Mie theories of light scattering. This enables the optimization of light scattering across the widest dynamic range in a single scan and typically less than 1 percent reproducible. The LS 230 also utilizes an enhanced laser diffraction analyzer, comprised of six additional detectors, to enhance submicron particle characterization by using a polarization intensity differential scattering technique (PIDS), which dramatically increases the sub-micron resolution of particle-size distribution analysis.

For size measurement, it was essential to disperse the particles with a chemical surfactant. In the present study sodium hexametaphosphate (4g/1L) ($NaPO_3$) was used as dispersing agent (ASTM-D422, 1990). To aid in particle dispersion, the samples were later placed in an ultrasonic water bath and then ultrasonicated for 1 hour. The samples were allowed to sit overnight to insure that they were thoroughly dispersed before analyzing. Then samples were placed into a small volume cell containing a stirrer. A parallel beam of monochromatic light is passed through the chamber where the samples are in suspension. The diffracted light is then focused onto the ring detector, which senses the angular distribution of scattered light intensity. The instrument measured the diffraction and polarization intensity differential scattering patterns and then subsequently calculated the particle size distribution of the study samples. The particle size distribution could be displayed and analyzed graphically using a personal computer and particle-size analysis software

provided with the LS 230. The data was tabulated and graphed according to Bowles (1992).

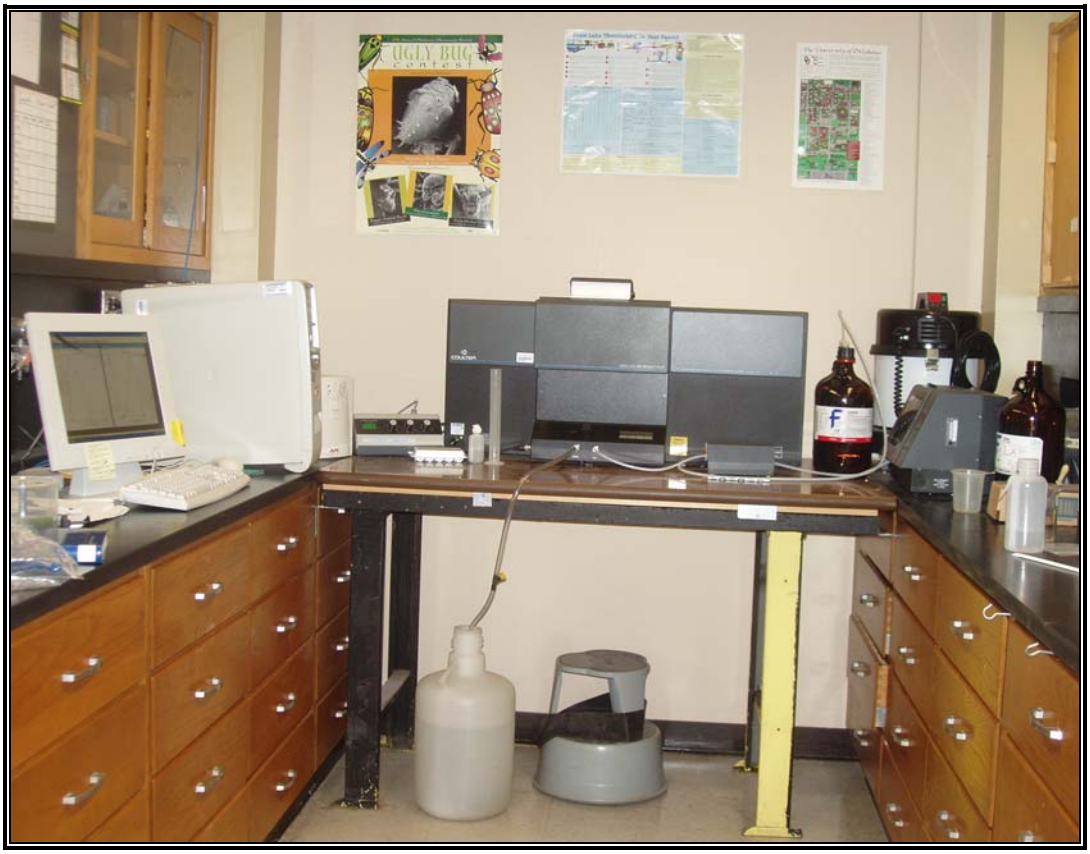

Figure (4-5): Beckman Coulter LS 230 Laser Particle Size Analyzer.

4.1.5. Chemical analysis

During the diffusion studies, the chemical concentration of K, Na and Ca in the downstream and upstream reservoirs was determined using a flame ***Atomic-Absorption Spectroscopy (AAS)*** (Fig. 4-6). AAS uses the absorption of light to measure the concentrations of metals in liquid samples. In their elemental form, metals will absorb ultraviolet light when they are excited by heat. Gas-phase atoms of each metal have a characteristic wavelength that will be absorbed. Since the studied samples are liquids, the technique used a flame to atomize the sample by vaporizing

it. The AAS instrument looks for a particular metal by focusing a beam of ultraviolet light at a specific wavelength through a flame and into a detector. If that metal is present in the sample, it will absorb some of the light, thus reducing its intensity. The instrument measures the change in intensity. A computer data system converts the change in intensity into an absorbance. As concentration goes up, absorbance goes up. The calibration curve for each cation was constructed by running standards of various concentrations of this cation on the AAS using its special lamp and wavelength and observing the absorbance at each concentration. From this curve a calibration equation was obtained. Then the studied samples were run on AAS using the cation lamp and the wavelength. By applying the absorbance of each sample on the calibration equation, the concentration of the studied cation was obtained.

Figure (4-6): Flame Atomic-Absorption Spectrometer (AAS).

4.2. Initial materials

4.2.1. Pierre Shale sample

Pierre Shale offers an almost ideal shale rock to investigate the high temperature high-pressure membrane efficiency, diffusion properties and swelling. In addition, the Pierre Shale contains the three common clay minerals (smectite, illite, and kaolinite) which make it a representative example. The Pierre Shale sample, obtained from TerraTek (Pierre Shale type 1) was used throughout the current study. The following few paragraphs present a detailed description of this Pierre Shale sample.

Pierre Shale occurs in South Dakota, Colorado, Minnesota, New Mexico, Wyoming, and Nebraska as division of Upper Cretaceous marine rocks and is well known by its richness of marine fossils such as *Ammonites* that were deposited along the western margin of the Western Interior Seaway. It was named for exposures studied near old Fort Pierre, SD. The Pierre Shale consists of about 600 m (2,000 feet) of dark gray shale, some sandstone, and many layers of bentonite.

The TerraTek Drilling Research Laboratory in Salt Lake City, Utah, cored the studied sample at an angle 60° to the bedding planes, in western Colorado at a depth of 25 ft (Fig 4-7).

The studied sample is dark gray in color and its moisture content is 5.2 %; its average bulk density is 2.44 g/cc and its cation exchange capacity is 11.0 meg/100g. Mineralogical composition, crystallinity index of clay minerals and grain-size distribution of the natural Pierre Shale sample are presented in table (4-1) and figure (4-8).

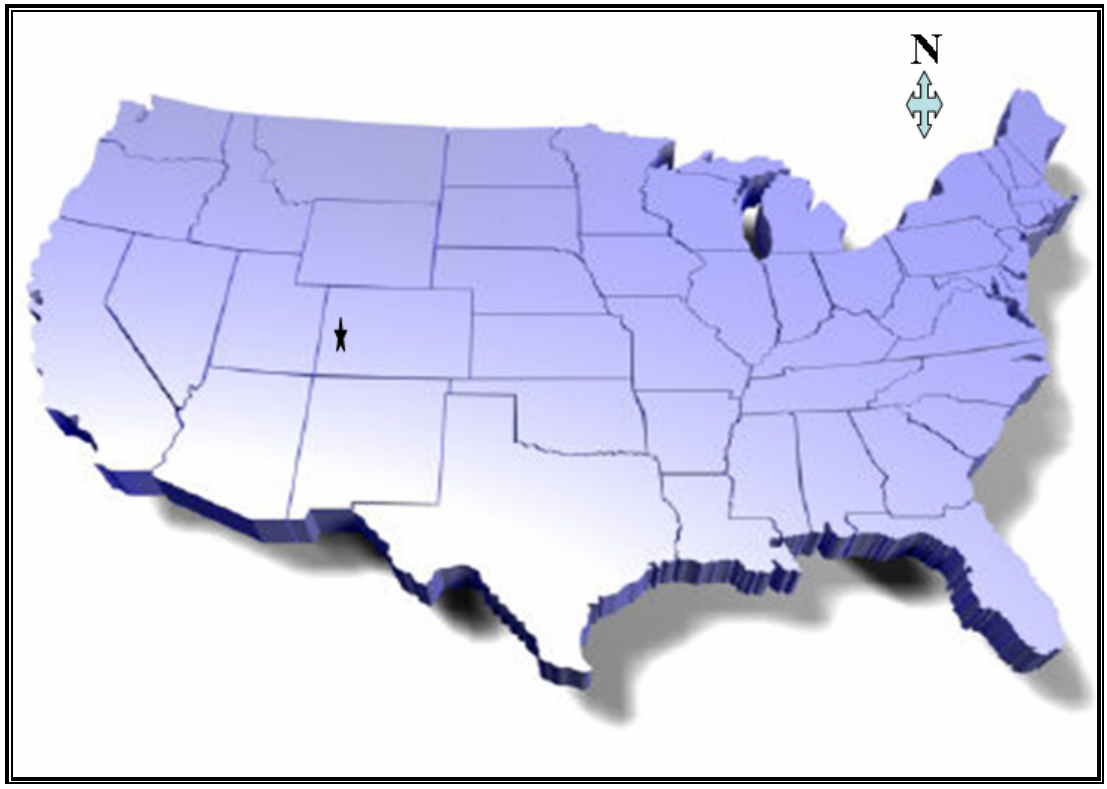

Figure (4-7): Location map of the studied sample.

Table (4-1): Grain-size, Mineralogical composition, CEC, M.C and BD of Pierre Shale sample.

Mineral composition						Grain size			CEC meg/ 100g	MC %	BD (g/cc)
Smectite	illite	kaolinite	quartz	plagioclase	Pyrite & oxides	Sand	Silt	Clay			
20.0	10.0	12.0	42.0	9.0	7.0	1.6	40.3	58.1	11.0	5.2	2.44

XRD error bar is ± 5 %

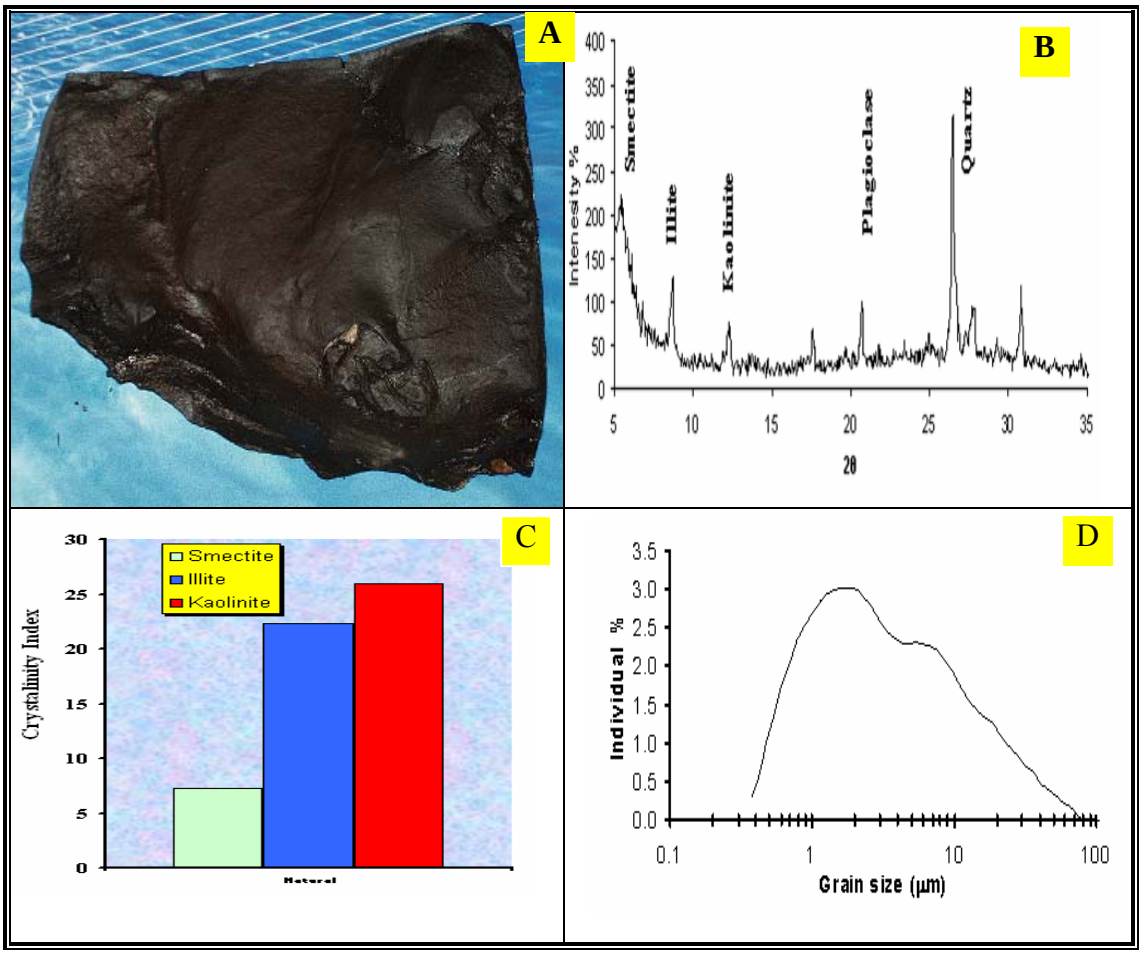

Figure (4-8): Pierre Shale sample:
A) Picture of a piece of it after storage under mineral oil to prevent shale-air contact effects;
B) XRD pattern of Pierre shale bulk sample;
C) Crystallinity index of the clay minerals content, and
D) Grain-size distribution pattern.

SEM and EDX analyses were done on a natural Pierre Shale sample. In addition to the clay minerals structures usually found, such as the honeycomb structure of smectite, closed-up kaolinite books and illite and quartz overgrowth dust lines (Fig. 4-9), Pierre Shale contained pyrite framboid structures (Fig. 4-10). These framboids are spheroidal aggregates of pyritic micro crystallites (~0.5 µm). Framboids are common in recent marine sediments and black shales (Sawlowicz, 1992). Pyrite framboids are considered as early diagenetic components in

sedimentary rocks (Berner, 1970; Love and Amstutz, 1966), but also they can form during late diagenesis by the pyritization of biotite or magnetite (Menon, 1967 and Canfield and Berner, 1987). Different genetic origins for pyrite framboids were discussed during the last few decades ranging from a purely inorganic origin (Berner, 1969; Farrand, 1970; Sunagawa et al., 1971) to a direct or indirect biogenic origin (Vallentyne, 1963 and Kalliokoski and Cathles, 1969). However, until now the mechanism of framboid formation remains unsolved.

4.2.2. Chemicals used

It is known that chloride solutions are corrosive to steel and iron alloy high-pressure laboratory equipment. As the aim of this study was to examine effects of differing exchangeable cations on shale properties, it was decided to use nitrate salts, in lieu of the more geologically common chloride salts, to make pore solutions for the experimental aspects of this study. Thus, reagent grade sodium nitrate ($NaNO_3$), potassium nitrate (KNO_3) and calcium nitrate ($Ca(NO_3)_2$) crystals were used to prepare 12 different aqueous solutions. These solutions were prepared by dissolution of 0.25, 0.50, 1.00 and 2.00 mole of each salt in one liter of distillated water at room temperature. The different thermodynamic properties of these aqueous electrolyte solutions are discussed by El-Guendouzi and Marouani (2003). The activity of these solutions is the most important properties controlling the results of the current study. Table (4-2) and Figure (4-11) show that the water activity is progressively lower in the order $a_{w(KNO3)} > a_{w(NaNO3)} > a_{w(Ca(NO3)2)}$ within the concentration range used in the current study. Also this figure indicated that, the activity of water is a perfect liner function with concentration.

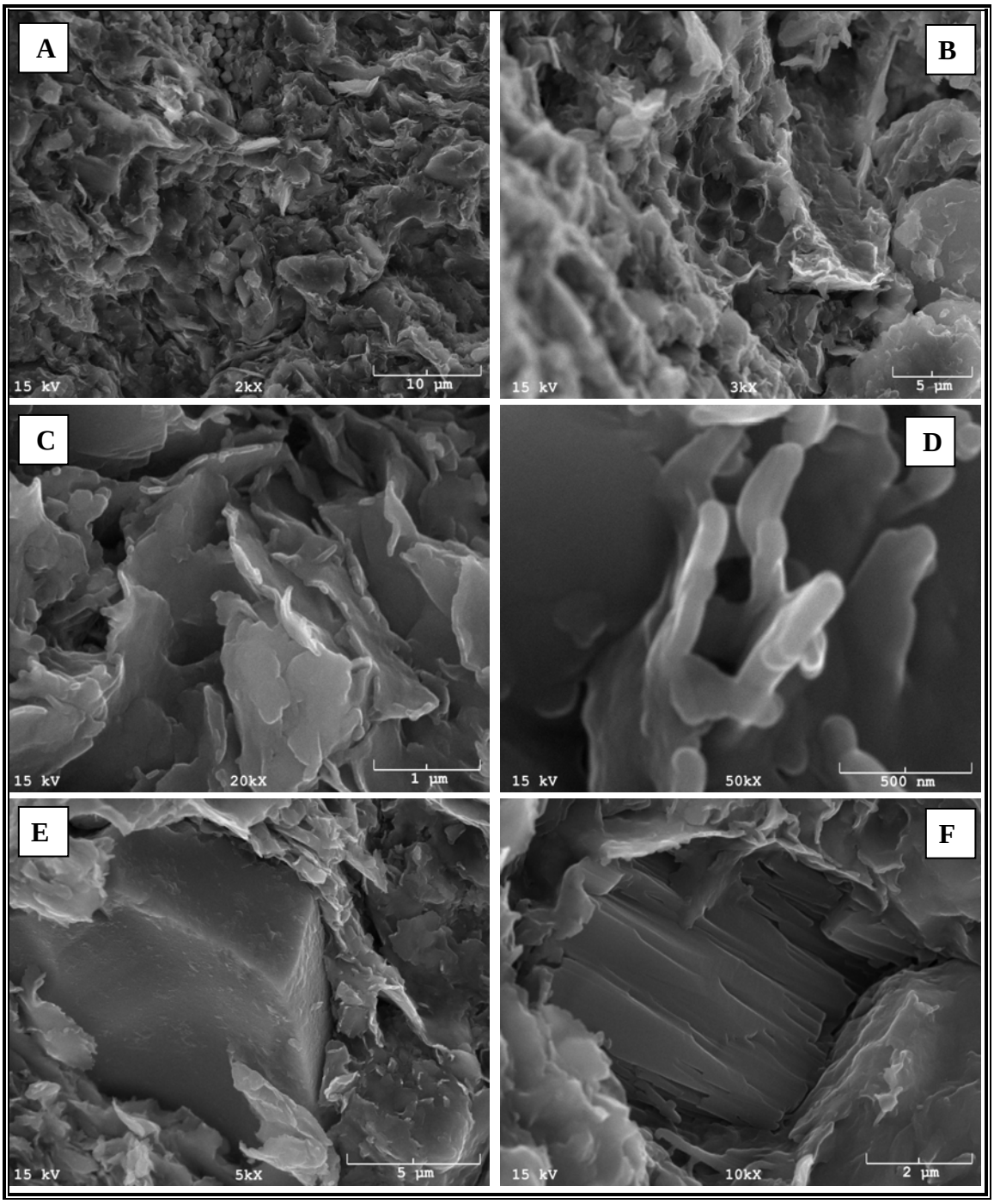

Figure (4-9): SEM photographs show some of Pierre Shale features:

A) General view for Pierre Shale
B) Webby or highly-crenulated smectite (honeycomb structure)
C) Thin illitic dust line (illitic clay ribbons) coated flaky smectite
D) Close-up view of the dust lines (illite and quartz overgrowth)
E) Detrital quartz grain surrounded by clay minerals (mostly smectite)
F) Fluted and partly resorbed detrital plagioclase feldspar.

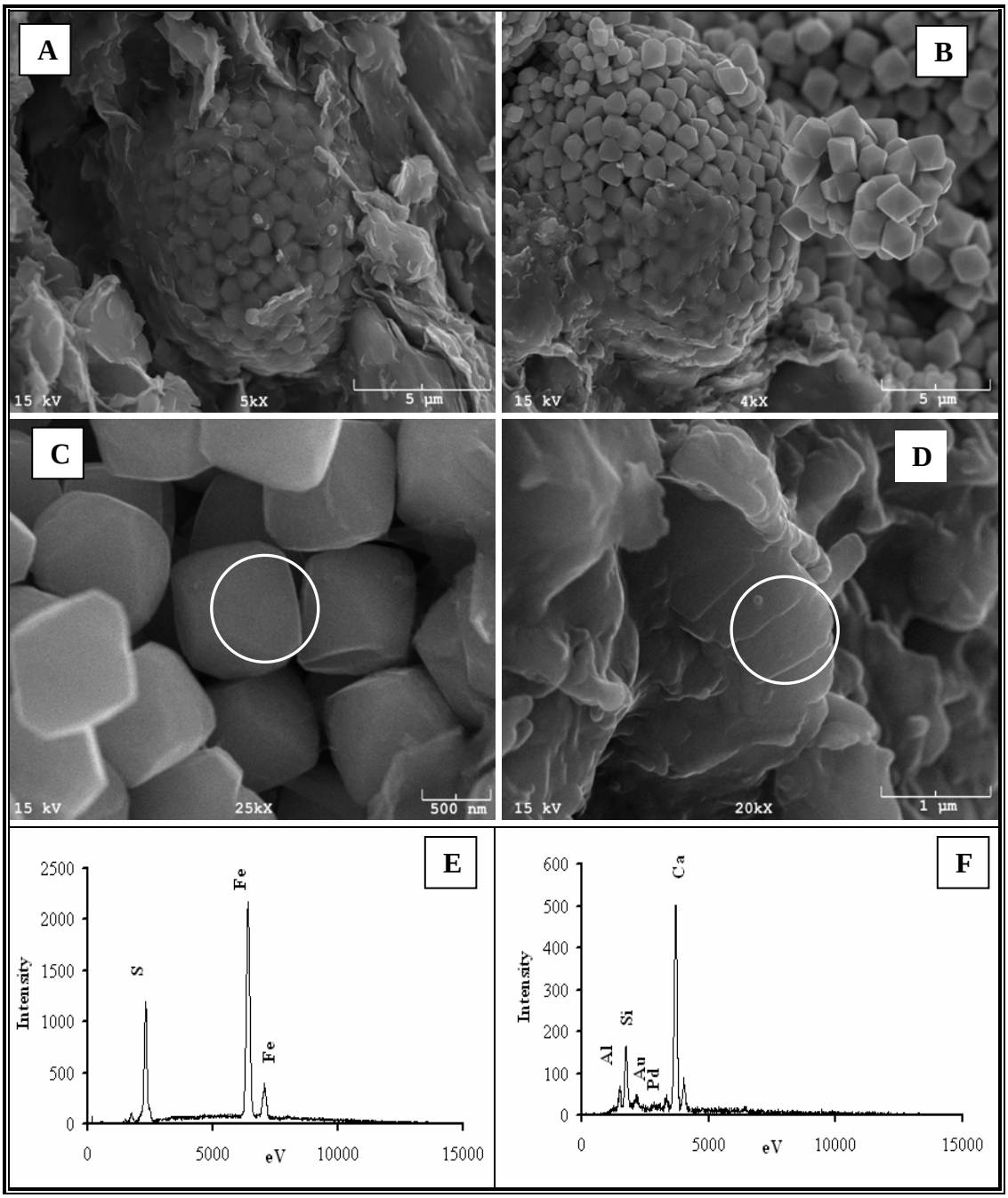

Figure (4-10): SEM photographs show some of Pierre Shale pyrite framboids and their euhedral:

A) Clay coated pyrite framboids

B) Close-up view of a pyrite framboid's crystals (~ 0.5 µm)

C) Well octahedron pyrite crystals form the framboids

D) Mollusc shell

E) EDX analysis for a pyrite crystal

F) EDX analysis the Mollusc shell.

This is in agreement with Alexander's (1990) equation which is written as:

$$a_w = 1 - 0.017\nu m \qquad (3\text{-}5)$$

where ν is an integer representing the number of ions in which the electrolyte dissociates, and

m is the concentration of solute in molality (mol/kg.).

Van't Hoff equation (equation 2-4) (Van't Hoff, 1887) is used to determine the osmotic pressure of an ideal semi-permeable membrane located between distilled water with activity equal of 1 and any of the above 12 solutions. The results are represented in Table (4-2) and Figure (4-11).

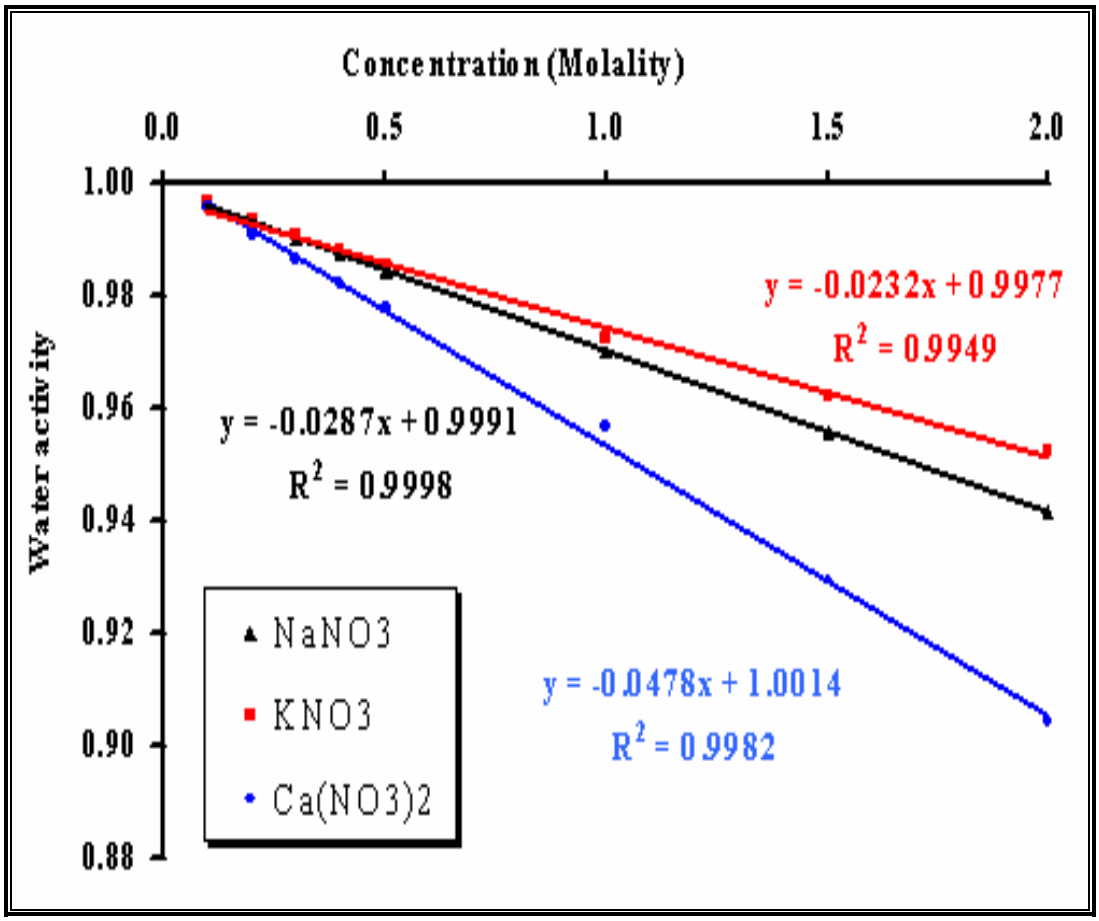

Fig (4-11): The relation between the water activity and concentration of nitrate solutions (data from El-Guendouzi and Marouani, 2003).

Table (4-2): Water activates of aqueous solutions of nitrates at 25 ºC (after El-Guendouzi and Marouani, 2003) and calculated osmotic pressure.

Molality	$NaNO_3$	KNO_3	$Ca(NO_3)_2$	$NaNO_3$	KNO_3	$Ca(NO_3)_2$
0.10	0.44	0.44	0.60	63.84	63.84	87.11
0.20	0.87	0.83	1.19	125.96	120.12	172.67
0.25	1.07	1.10	1.37	155.14	159.03	198.02
0.30	1.27	1.22	1.78	184.37	176.57	258.61
0.40	1.68	1.59	2.35	242.96	231.22	341.00
0.50	2.08	1.96	2.95	301.72	284.07	427.69
1.00	4.06	3.70	5.91	588.31	536.61	856.99
1.50	6.01	5.12	9.72	871.13	742.25	1409.99
2.00	7.96	6.44	13.40	1154.05	933.87	1942.94

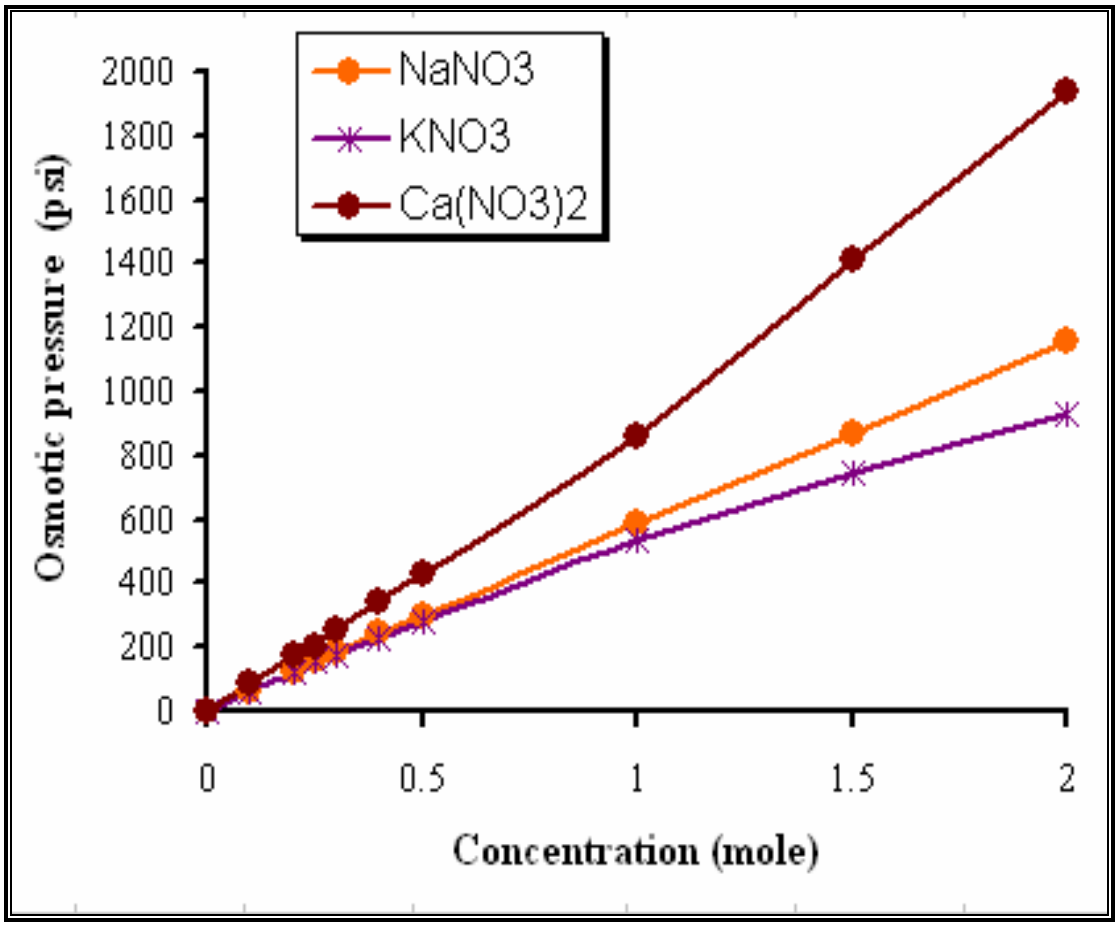

Fig (4-12): The relation between the concentration and the osmotic pressure resulting from ideal membrane.

Another 12 carbonate solutions were used to study the impact of the aqueous solutions on shale clay minerals components and grain-size distribution at room temperature. Sodium carbonate (Na_2CO_3), potassium carbonate (K_2CO_3), and calcium carbonate ($CaCO_3$) solid crystals were used to prepare these solutions at 0.25, 0.50, 1.00 and 2.00 molal concentration.

Chapter 5

Evaluation of Pierre Shale Osmotic and Hydraulic Flows

The flow in shales that does not change their state is related linearly to its corresponding driving force (Mitchell, 1993). According to Mody and Hale (1993), the most important two driving forces acting on shale are the hydraulic and chemical potentials.

Osmotic flow can be used as a means of driving water in or out of a shale formation during drilling depending on the difference between activity of shale pore fluid and the drilling fluid. When the water activity of shale is higher than that of drilling fluid the water will flow from the shale causing dehydration (Al-Bazali, 2005). However, when the activity of drilling fluid is higher than that of shale, mud filtrate moves into shale (Ewy and Stankovich, 2000). Zhang et al. (2004) state that the actual osmotic potential generated between shales and typical drilling fluid is usually less than the osmotic potential because shales generally have a wide range of pore sizes. Thus, the concept of membrane efficiency was introduced which describes the extent to which a shale departs from ideal membrane behavior. The membrane efficiency of shale is a complex material property, depending on pore size and distribution, clay mineralogy, degree of swelling, and fluid chemistry.

If the driving force is only hydraulic gradient without the importance of chemical potential, the flow will only be the hydraulic flow. The ability of rock to transport fluid under a hydraulic gradient is called permeability. Many geologic processes, mining, construction projects, and other geo-engineering projects that

involved flow of fluid through a porous medium are affected not only by the mechanical properties of solid rock but also by rock permeability.

When a chemical gradient is applied, movement of ions and cations and the flux of water through shale will interrupt the shale system (Fig. 1-2). This interruption will cause short-term (within 3 days) and long-term (more than a month) changes in shale properties, such as swelling potential and permeability. This chapter is designed to evaluate the osmotic flow through Pierre Shale with three different nitrate fluids (K, Na and Ca) of different concentrations (0.25, 0.5, 1.0 and 2 mole), and evaluate the impact of these fluids on shale permeability after a 3 day, osmotic test period.

To measure Pierre Shale permeability and osmotic potential, Cell no. III of HTHP Shale Apparatus was used. The sample preparation, cell no. III internal design and the test procedures are described in the following paragraphs.

5.1. Sample preparation and tests procedures

5.1.1. Sample preparation

For osmotic, permeability, diffusion, and HTHP clay minerals transformation studies, 25 mm diameter cylindrical disk samples were prepared (Fig. 5-1). First, shale was stored under oil to prevent exposure to air. Using a small piece, disk samples are prepared by grinding on sandpaper. The piece is moved slowly by hand in circular motion on sandpaper using progressively finer grain sizes from 100 to 220 grif. The grinding processes are gradually continued until the proper dimension of sample is obtained. Each disk sample is prepared just before being placed into the test machine to prevent sample-air reactions. Coring machines or any chemicals were not

used during in sample preparations to eliminate unwanted heat or chemical effects. Only hands and sandpaper were used to prepare the samples. Because of the difficulty in preparing samples, only samples cut with the cylinder axis perpendicular to the bedding planes were prepared.

Figure (5-1): Disk sample (25 mm diameter and 3 mm thick) for osmotic and permeability test.

5.1.2. Test procedures

Figure (5-2) shows a diagrammatic sketch for the internal and external design of cell no. III, that was used for osmotic and permeability measurements. It is a hydrostatic cell with the ability to hold both confining pressure and pore pressures in the upstream and downstream reservoirs up to 10,000 psi at temperatures to 300 degrees C.

The prepared sample was placed between the two porous 316 stainless steel frits (25 mm in diameter and 1.59 mm thick, 2 μm porosity and 10 mL/min water flow). On some experiments, the downstream side used two frits instead of one to increase the downstream reservoir volume. The frits and the sample are sandwiched

between two 316 steel end caps with the same diameter. Each cap has two fluid entry holes to enable flow across the frit/sample interface. This system is jacketed using a butyl rubber jacket and is sealed to the end caps at the two ends using hose clamps. During the tightening processes the system is exposed to ~ 10 psi unconfined uniaxial compressive stress to eliminate space between the sample and the frits or frits and caps. Then, the upper side cap is connected to two upstream pore pressure capillary tubes through the cap holes via high pressure cone-in-cone fittings, and in the same way, the downside cap is connected to the two downstream pressure capillary tubes.

To prevent any confining pressure leaking, after the system is placed in the pressure cell, the cell is closed and the 8 head bolts are tightened using an adjustable torque wrench to 30 ft-lbs in increments of 5 ft-lbs. After that, pore pressure tubing is connected to the appropriate valves and fittings, and the cell is connected to the confining pressure pump. Themocouple outlets and pressure transducers are connected to a computer via two types of data acquisition systems, one for confining and pore pressures and the other for temperature (Fig 5-2).

Both confining pressure (Pc) and pore pressure (Pp) are gradually increased using 50 psi increments using mineral oil to apply the confined pressure and distilled water to obtain pore pressures. Either Eldex^{TM} high-pressure liquid chromatography (HPLC) pumps or ISCO HPLC pumps were used for fluid pressuring and metering. To prevent leaking through the sample jacket, a 100 psi difference is kept between the confining pressure and the pore pressures during pressurizing. When the pressures reach 600 psi Pc and 500 psi Pp, all valves are closed and the sample is left for 24 hours to be sure it is completely saturated with distilled water. During this step, the

computer record is made for all condition parameters (temperature and pressures) by the data acquisition systems at a frequency of 1 Hz. After 24 hours, measuring the hydraulic or osmotic flow through the sample can be initiated according to the following procedures.

5.1.2.1. Osmotic flow

For osmotic pressure measurements, distilled water is gradually flushed from the "upstream" side and is replaced by a nitrate solution at a near constant 500 psi pressure (note that the use of "upstream" and "downstream" in this context refers to the direction of non-osmotic flux and is purely by convention). A backpressure regulator or an ISCO pump were used to maintain upstream pressure constant while replacing solutions. When the upstream side fluid is fully replaced by nitrate solution (at least four residence times equal to the upstream reservoir volume divided by the volume flow rate) pressures are readjusted to equal 500 psi for both upper and downstream sides and 600 psi for the confining pressure. Then all the pressure valves are closed to isolate the sample from the external plumbing. The pressure and temperature data acquisition systems record the pressures and temperature once per second.

At this point in the experiment, the sample is subjected only to a chemical gradient created from the difference in activity between the upstream nitrate fluid and downstream distilled water reservoirs on either side of the shale disc. Any subsequent flow through the sample will be only osmotically driven and will induce a pressure change between upstream and downstream reservoirs that is recorded for 72 hours.

These data are processed using WinDAQ® Recording and Playback software. Mathematica and Excel software are also used to process and graph the data.

Usually, graphs were constructed for each experiment, such as that given in Figure (5-3). In this case, we isolated both upstream and downstream reservoirs from any outside influence, and the upstream reservoir is approximately twice in volume of the downstream reservoir. The downstream reservoir pressure (with distilled water) is declining, but the upstream reservoir pressure (with nitrate solution) increases. The maximum difference between them is the osmotic pressure. This configuration is referred to as "model 1" configuration.

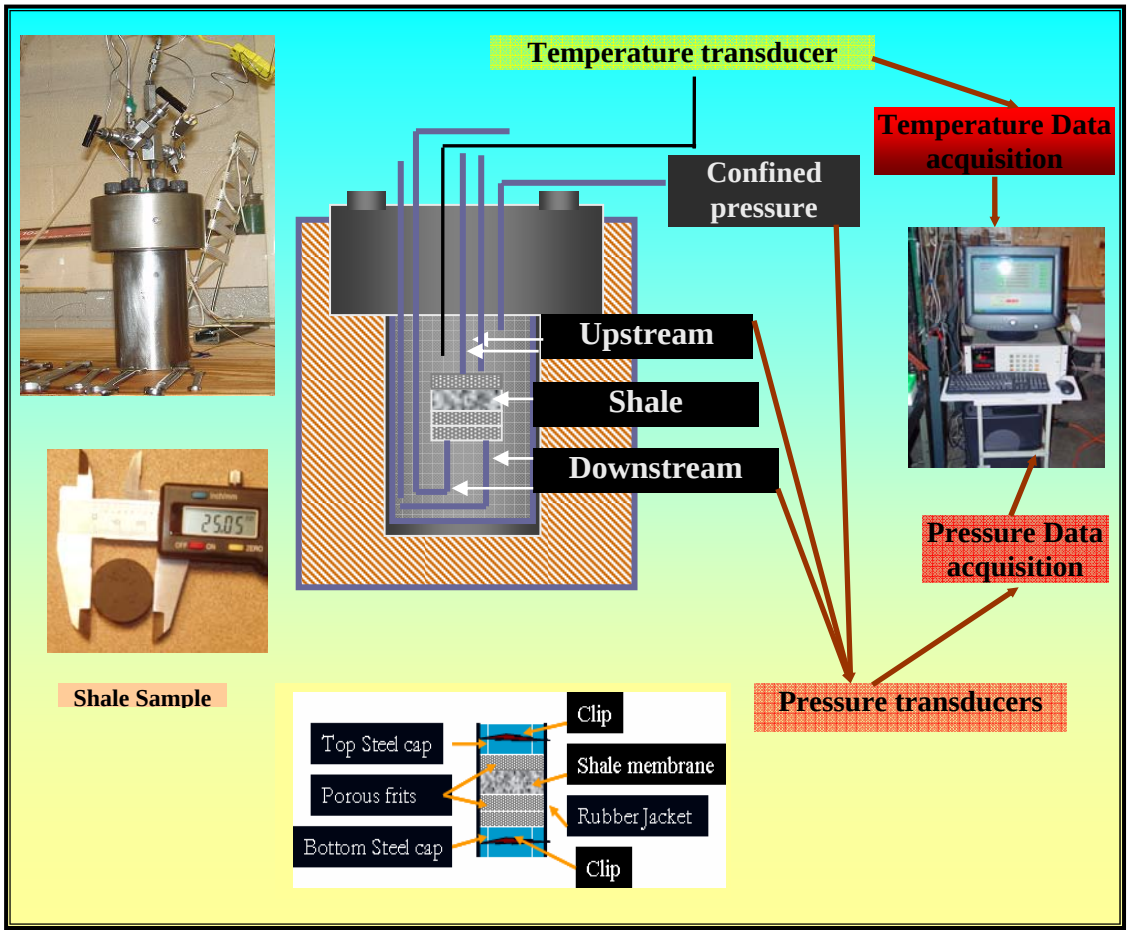

Figure (5-2): Schematic diagram for Cell no III internal design.

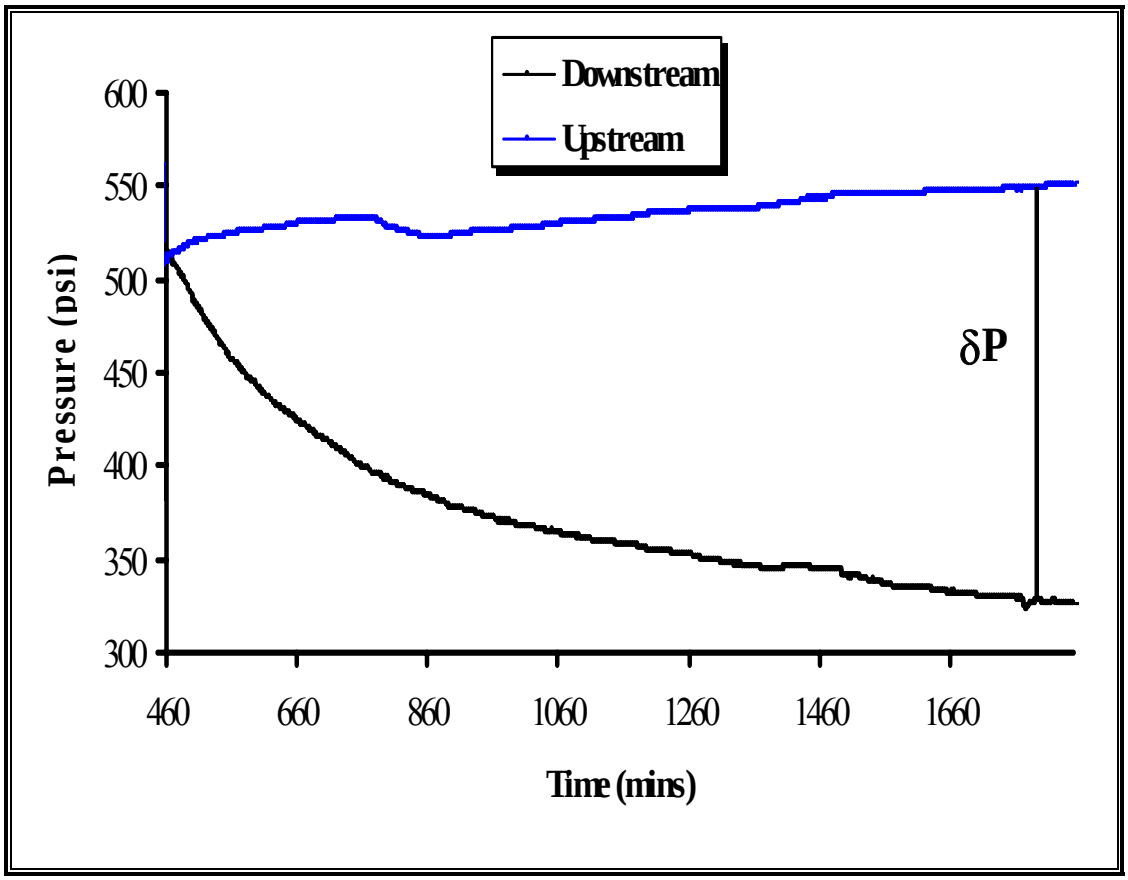

Figure (5-3): Up- and downstream reservoirs pressure behaviors; 1 molal KNO_3 was applied to the upstream reservoir (model 1 configuration).

In some experiments, instead of isolating the downstream side by closing its valve, we adjust its pressure at 500 psi using an ISCO pump act to "servo-control" the downstream pressure, i.e. keep it constant with time. In this case the downstream pressure becomes stable at 500 psi while the upstream one will increase over time in response to the osmotic flux (Fig. 5-4). The maximum difference between the pressures in the two reservoirs is the osmotic pressure, referred to as "model 2" configuration. To study the effect of concentration on the membrane efficiency, the same sample was used for the same cation different concentrations.

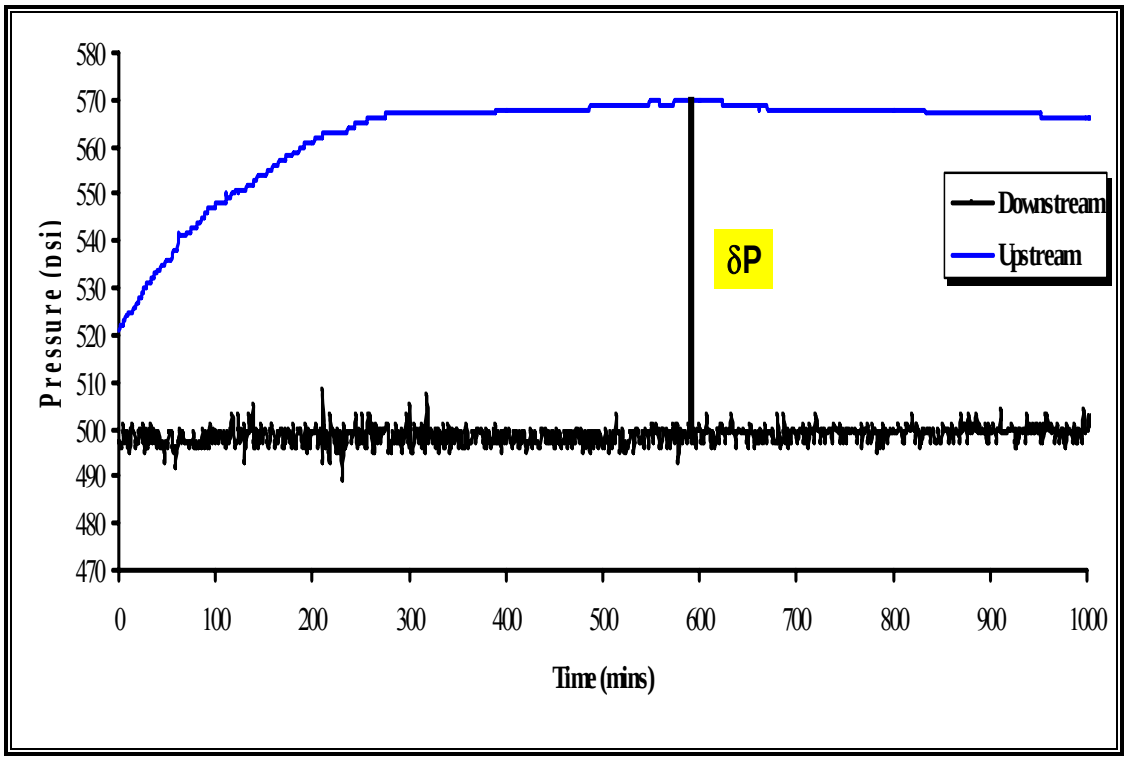

Figure (5-4): Up- and downstream reservoir pressure behaviors with time following application of 0.5 molal KNO_3 in upstream reservoir (model 2 configuration).

Membrane efficiency, which is defined as the ratio of the osmotic pressure produced by the natural shale membrane to the ideal one is obtained from the following equation

$$\sigma = \left[\frac{\delta P}{\Delta \pi} \right]$$

where δP is pressure difference shown in Figures 5-3 and 5-4 for each of the model configurations. Δπ is the osmotic potential for the chemical fluid used to obtain δP. Van't Hoff's equation (Van't Hoff, 1887) was used to determine Δπ for the different chemical fluids when these fluids are placed on one side of a membrane and distilled water with activity equal to the unit is placed on the other side of the membrane. The

results of $\Delta\pi$ were presented and graphed in a previous chapter (see Table (4-2) and Fig. (4-12)).

5.1.2.2. Hydraulic flow

To evaluate the permeability changes due to the reaction of minerals in the Pierre Shale with the solutions used for the osmotic flow test, permeability measurements are done for pristine unreacted samples and directly after osmotic pressure tests (3 days after using chemical fluid on the upstream side).

It is not practical to determine permeability for low permeability rocks such as shale using steady state methods. Such rocks require adequately long times to establish steady state flow. The current study focuses on the impact of nitrate fluids on permeability during short term experiments (three days) using the transient method suggested by Brace et al. (1968). This method depends on measuring the decay of small changes in pressure imposed at one end of the sample instead of measuring the flow rate or velocity of fluid through the sample (Appendix B). To measure the pressure decays for natural or treated samples, distilled water was used on the upstream hold at 500 psi. The downstream pressure was maintained at 500 psi and the confining pressure at 600 psi. The sample was maintained under these conditions for 24 hours. After that, the confining pressure was increased to 700 psi and the upstream pressure increased to 600 psi and the downstream pressure was adjusted to 500 psi. Then all valves were closed to isolate the sample from outside effects.

Because of the pressure differences between upstream and downstream reservoirs, a hydraulic gradient forces the fluid to move through the sample. Recording and evaluating the effect of this movement on pore pressure provides data

to calculate permeability. The computer records the pressures and temperature from different outlets every second, the same way as in the osmotic test. After at least 24 hours to register a sufficient pressure change the recorded data are processed and graphed by the same way as in the osmotic test.

The curves in Figure (5-6) show the upstream pressure declining with time while the downstream pressure is increasing until the pressure in both sides becomes stable, the final pressure. If we ignore the effect of temperature change (which is very small for our Lab), the change in upstream pressure relative to final pressure (δP_t) overtime is given by Brace et al.'s (1968) equation (described in Appendix B):

$$\delta P_t = \Delta P[(V_2 / V_1) + V_2]e^{-\alpha t}$$

where V_1 is the volume of upstream reservoir,

V_2 is the volume of downstream reservoir,

t is the time and

ΔP is the initial pressure difference between the upstream and the final pressure or $\delta P_t = P_u - P_{final}$ at time zero.

δP_t is the pressure difference with time (Fig. 5-5) and it is equal to:

$$\delta P_t = P_u - P_{final}$$

where P_u is the upstream pressure, and

P_{final} is the final pressure when the sample reaches the stable state (Fig. 5-6)., and

α is a constant equal to

$$\alpha = -\frac{kA}{\mu\beta L}\left[\frac{V_2 + V_1}{V_1 V_2}\right]$$

where k is rock permeability,

A is the sample cross-section area (4.91 cm^2),

L is the sample width (0.3 cm),

μ is the fluid viscosity, μ = 1 psi sec at 25 C°, and

β is the fluid compressibility, 2 X 10^{-6} psi^{-1}.

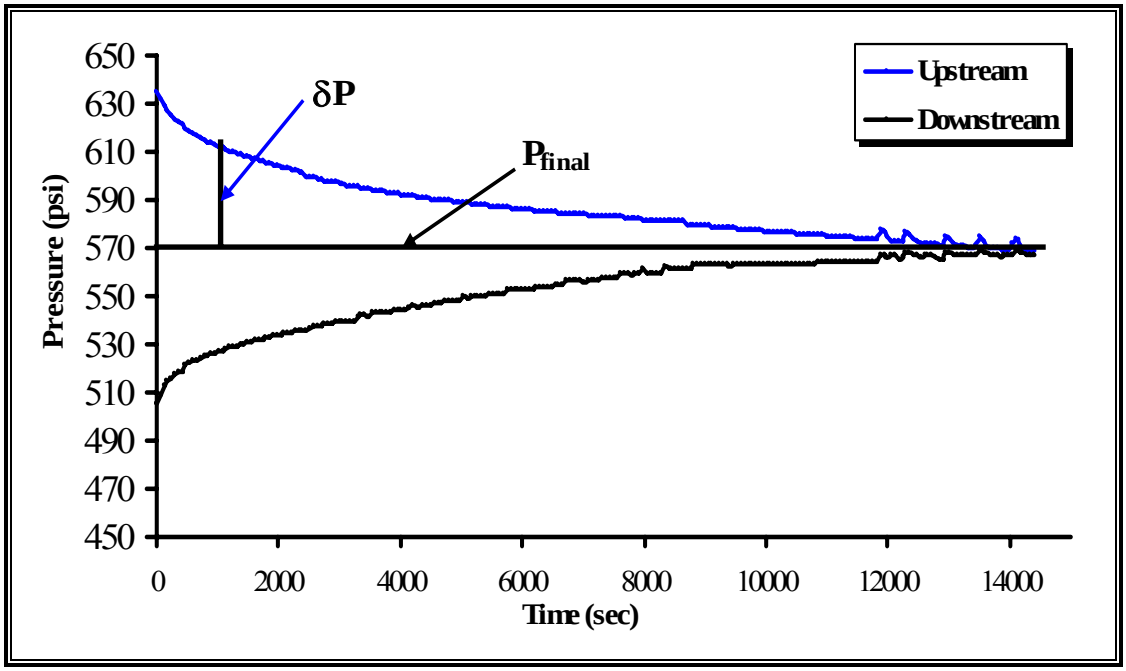

Figure (5-5): Upstream and downstream pressures decay when a hydraulic gradient was applied during a permeability measurement test.

However, the reservoirs' volumes may change from sample to sample but ΔP , V_1 and V_2 are constant for the same sample, so that:

$$\Delta P[(V_2 / V_1) + V_2] = C$$

So Brace's equation is simplified to be

$$\delta P_t = Ce^{-\alpha t}$$

By taking the natural logarithm of the above equation we will get

$$Ln\delta P_t = LnC + (-\alpha)t$$

Plotting $Ln\delta P_t$ verses time (t) as in Figure (5-6), $-\alpha$ is the slope of the best fit line. By substituting all parameters in the α equation, the permeability will be obtained.

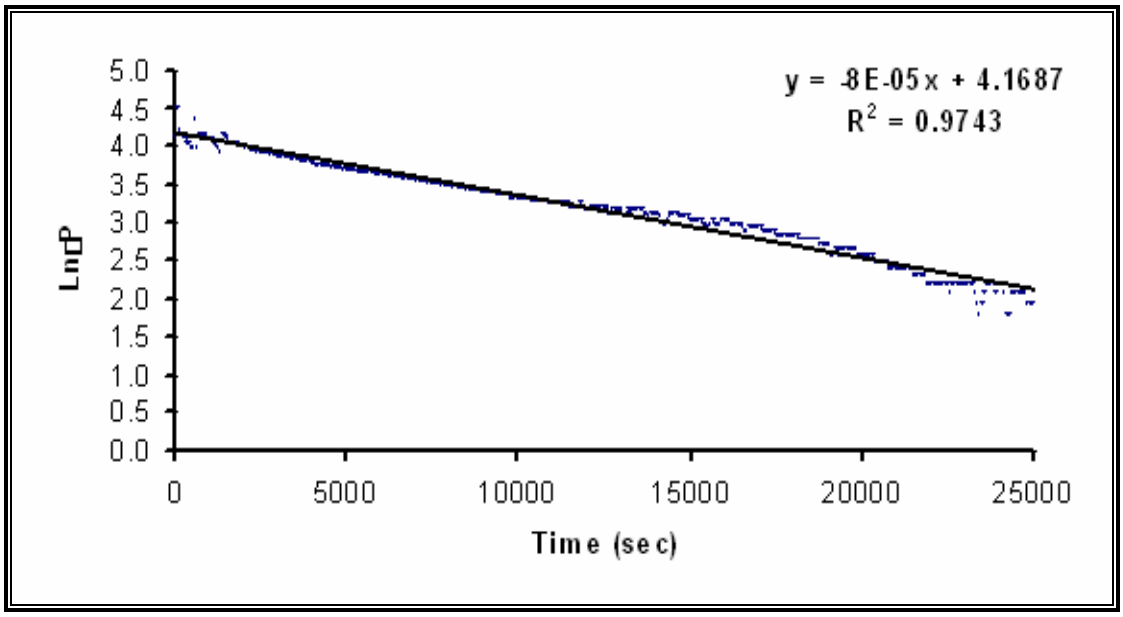

Figure (5-6): Ln δP_t verses time, with slope equal to $-\alpha$ (In this case α = 0.00008).
Dots are the measured data and the line is the best fit line

In some experiments, instead of isolating all the system from outside effect by closing all valves, the downstream pressure was held constant at 500 psi using an ISCO pump. In this case the upstream pressure will decrease but the downstream side will be constant (Fig. 5-7). This configuration is similar to an experimental design used by Al-Bazali (2005) (described in Appendix B) which depends on this following equation:

$$Ln\frac{\delta P_t}{\delta P_0} = \alpha t$$

where δP_t is $P_u - P_0$ with time, and δP_0 is δP_t at time zero.

In this case, α is equal to $\frac{-Ak}{\mu\beta VL}$ where V is the volume of the upstream reservoir.

$$Ln\delta P_t = Ln\delta P_0 + \alpha t$$

The slope of the best-fit line equals to - α of $Ln\delta P_t$ verses time plot (Fig. 5-8) and from it, k can be calculated.

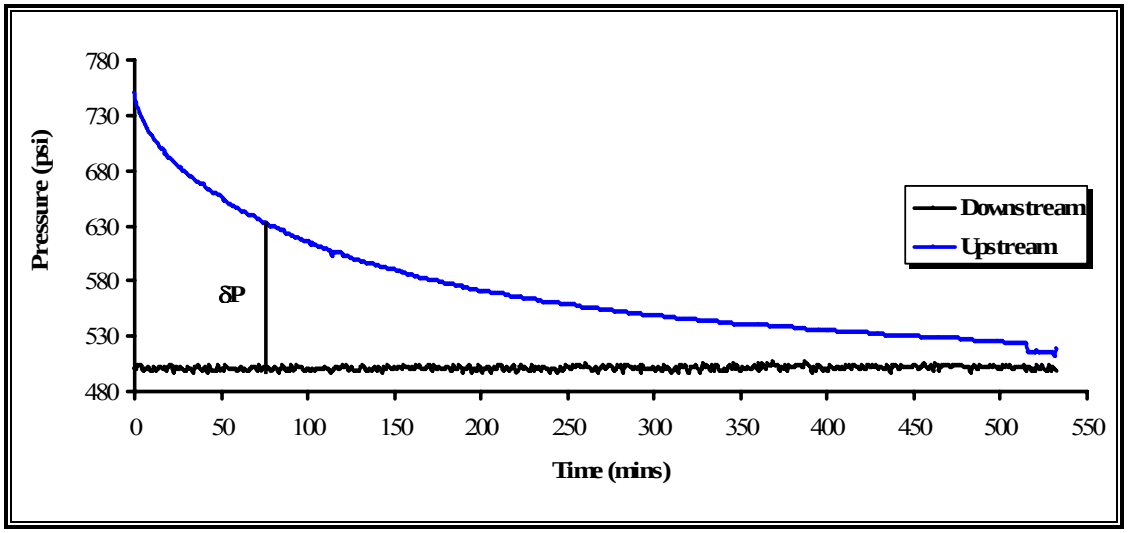

Figure (5-7): Measure the pressure decay for upstream (Model 2 configuration).

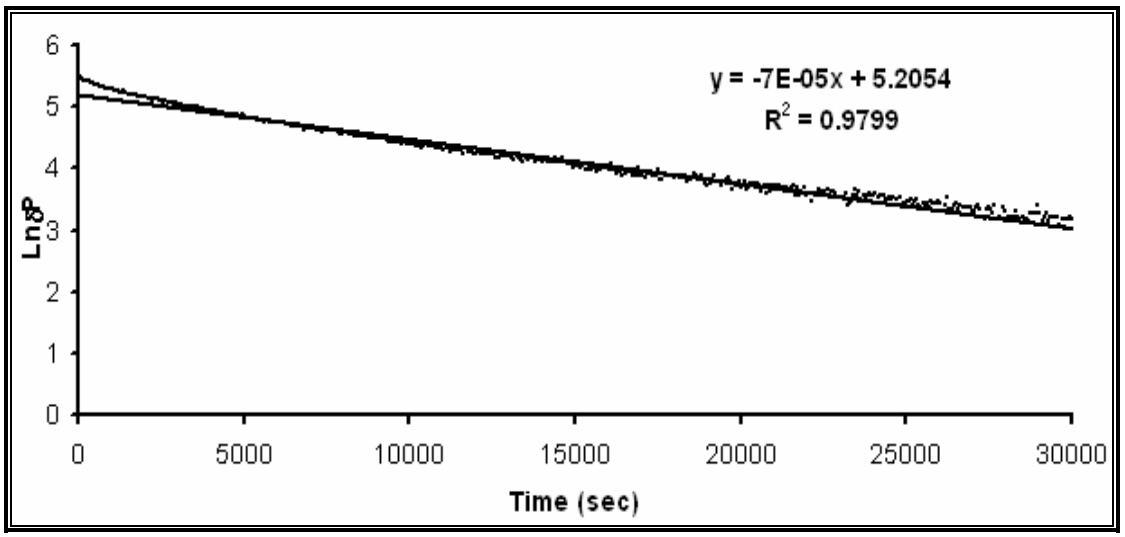

Figure (5-8): $Ln\,\delta P_t$ verses time, slope equal to α (In this case α = 0.00007).
Dots are the measured data and the line is the best fit line

Both of these models were used during the current study. Model 2 is preferred because only the volume of the upstream reservoir is required and it is not necessary to wait for the P_{final} as in first model, which requires a lot of time and sometimes cannot be achieved on a practical time scale.

5.2. Results and discussion

The results of osmotic pressure and osmotic efficiency of Pierre Shale using three different nitrate fluids are presented. Also, the impact of each of these nitrate fluids on permeability after three days (osmotic pressure test duration) is discussed.

5.2.1. Osmotic flow

Due to the application of a chemical gradient over the study samples, osmotic pressure developed for each of the nitrate solutions. That means Pierre Shale acts as a semi-permeable membrane. However the magnitudes of this osmotic pressure (the maximum developed pressure, presented in table 5-1) are small compared to the osmotic pressures that were calculated for ideal membranes (Chapter 4). This means Pierre Shale acts as a non-ideal, semi-permeable membrane. The magnitude of the developed osmotic pressures depends not only on type and concentration of the nitrate fluid, but also on time.

Sodium nitrate fluids ($NaNO_3$) developed higher osmotic pressures (Fig 5-9), but for an ideal membrane sodium nitrate should produce lower osmotic pressure than the other nitrates (Fig 4-12) depending on their activity. Potassium nitrates (KNO_3) produced lower osmotic pressures with lower concentrations (0.25 and 0.5 molal) (Fig. 5-9), but with higher concentrations, potassium nitrates achieve similar results

as Na- and Ca- nitrates. Calcium nitrates, which should develop the higher osmotic pressure under ideal membrane behavior (Fig. 4-12), produced lowest osmotic pressures at higher concentrations (1 and 2 moles) (Fig. 5-9).

The developed osmotic pressures in Pierre Shale samples increased monotonically with increasing nitrate concentration as predicted following an ideal membrane behavior (Figure 4-12) but with a much lower magnitude than in the ideal membrane. This rule has only one exception for 2 molal $Ca(NO_3)_2$ (21 psi for 1 molal and 17 psi for 2 molal, which are experimentally indistinguishable) (Table 5-1). The maximum osmotic pressure was 49 psi and developed by 2 molal $NaNO_3$ while the maximum one that would develop for ideal membrane was 1,943 psi by 2 molal $Ca(NO_3)_2$. Two molal KNO_3 developed 30 psi osmotic pressure while it should develop 934 psi under ideal membrane behavior.

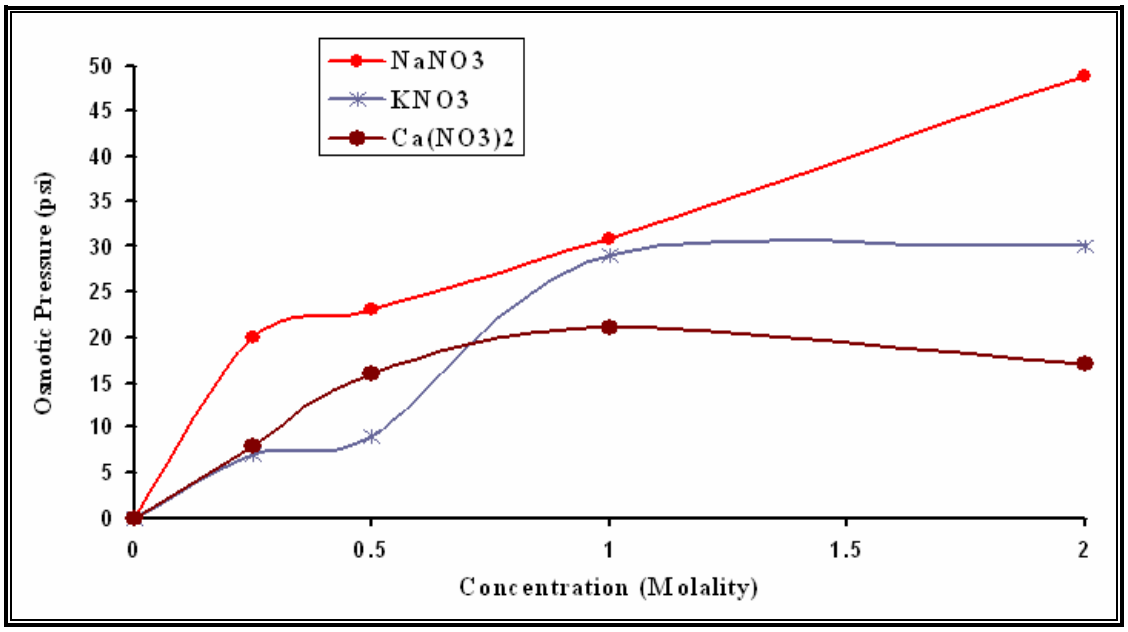

Figure (5-9): Relationship between osmotic pressure and concentration of different nitrate fluids. Standard error in pressure measurements is about +/- 4 psi.

Time plays an important role in the development of Pierre Shale osmotic pressure. The maximum pressure (δP) usually developed within 15 hours from the beginning of the test. After that, the osmotic pressure decreases with time (Fig. 5-10). This decrease may be the result of destruction of the membrane by slow cation transport by diffusion leading to decreased pore fluid activity. Another reason may be the loss of clay platelets surface charge by ionic exchange that serves as the driving force for the osmotic flow. The last reason is indicated from osmotic pressure magnitudes that were described in the pervious paragraph. $NaNO_3$ fluids developed maximum osmotic pressures because the ionic exchange in this case will lead to produce more driving force for the osmotic flow compared to Ca- or K-rich smectites.

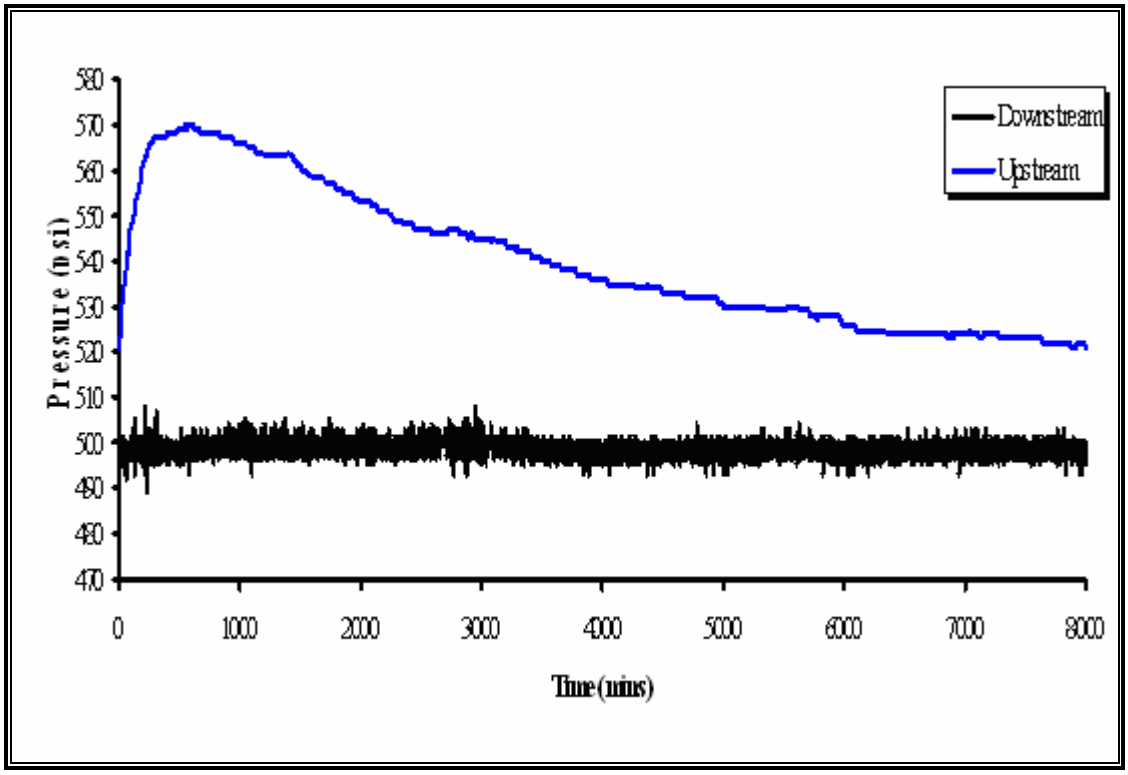

Figure (5-10): Osmotic pressure behavior over long experimental times (1 molal KNO_3).

The type of nitrate salt and its concentration influences the time needed to develop maximum osmotic pressure. It was a simple matter to determine the time

required to develop maximum osmotic pressure developed by $NaNO_3$ and KNO_3 especially with higher concentrations, but it is difficult to determine for $Ca(NO_3)_2$ because of its more complex behaviors. The maximum osmotic pressure time showed no consistent trend with concentration of $NaNO_3$ and $Ca(NO_3)_2$ solutions. For 0.25, 0.5 and 1 molal $NaNO_3$, the maximum osmotic pressure time is increased from 724 minutes for 0.25 moles to become 994 minutes for 1 molal. Then it decreases to 600 minutes at 2 molal concentration. The maximum osmotic pressure time decreases from 1,094 minutes to 547 minutes when $Ca(NO_3)_2$ concentration changes from 0.25 to 0.5 molal, then it increases with increasing concentration to reach 984 minutes with 2 molal (Table 5-1). This time showed a consistent monotonic trend with KNO_3, increasing from 994 minutes with 0.25 molal to its maximum for this study of 1471 minutes with 2 molal solution.

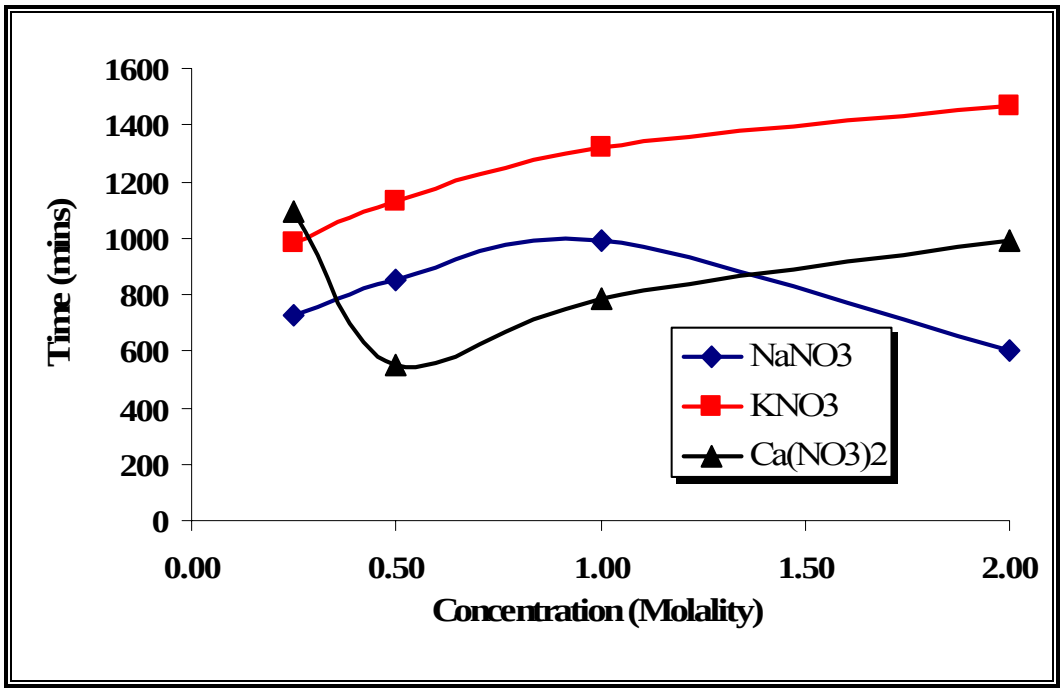

Figure (5-11): Time-to-develop maximum osmotic pressures for different nitrate solutions.

The osmotic pressure of $Ca(NO_3)_2$ showed oscillatory transient phenomena with time (Fig. 5-12). This is first time such behavior has been reported. This phenomenon may be the result of a changing membrane position with time because $Ca(NO_3)_2$ has the highest ionic strength. The high ionic strength of $Ca(NO_3)_2$ quickly produces high osmotic pressure (16 and 21 psi for 0.5 and 1 molal respectively) leading to a rapid increase of stress on the membrane located inside the sample and close to the upstream reservoir. With increasing stress, the membrane is destroyed by opening micro-fractures-like pores or grain boundaries that already exist in the membrane's area. This leads to movement of the fluid from the high concentration side to the low concentration side, creating a new sector inside the sample with a high concentration of fluid. The increased void space will lead to a dropping of pore pressure. The chemical gradient between this sector and the rest of the sample will create another membrane relatively farther from the upstream reservoir, and this membrane will be destroyed in the same way. Creating and destroying the membranes will be repeated with time until all pore fluid becomes chemically equal. With time the location of the membrane becomes far from the upstream reservoir. Creating the membrane produces a pressure peak while the membrane destruction produces the valleys of the oscillations of figure (5-12). Opening the micro-fractures should increase the permeability of the study samples, which will be discussed latter in this chapter.

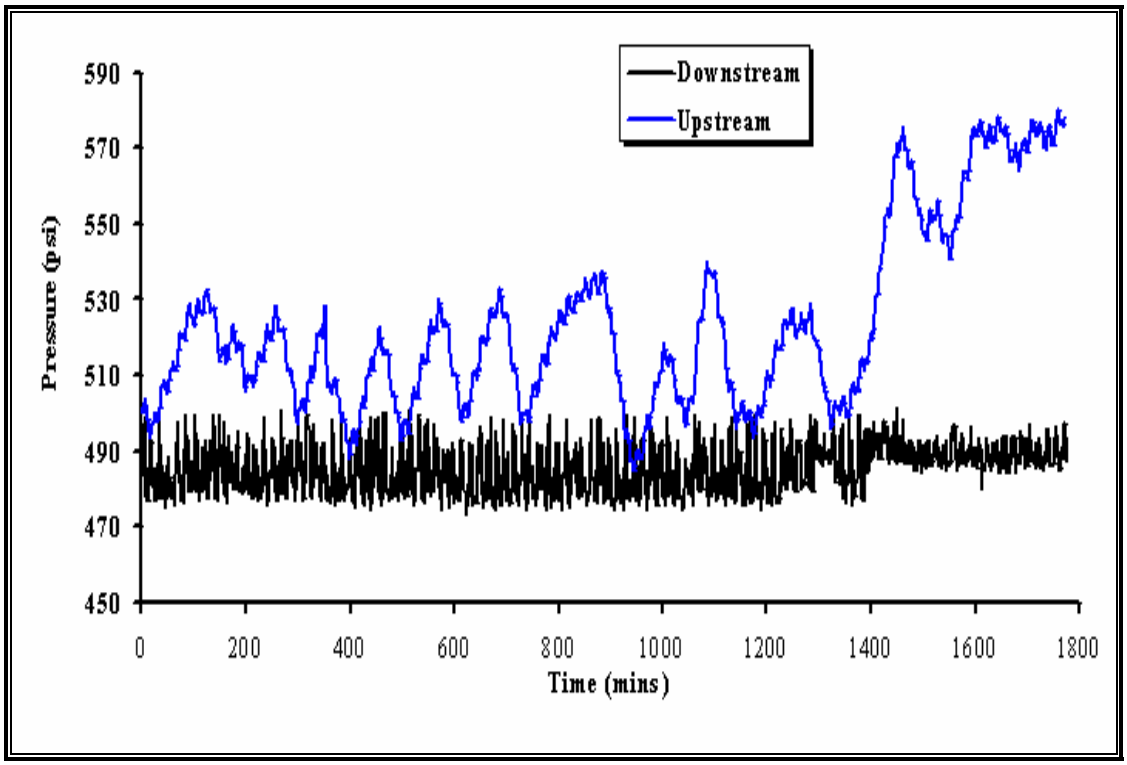

Figure (5-12): Oscillatory transient behavior of $Ca(NO_3)_2$ osmotic pressure. *(1 molal $Ca(NO_3)_2$)*

The ideality of the Pierre Shale membrane is recorded as membrane efficiency (σ) (Table 5-1). The membrane efficiency usually decreases with increasing concentration except for KNO_3 solutions, which show some increase with 1 molal concentration in comparison to the 0.5 molal solution (Fig. 5-13). $NaNO_3$ solutions showed the maximum membrane efficiency; $Ca(NO_3)_2$ showed the minimum. The maximum membrane efficiency recorded with 0.25 mole $NaNO_3$ was (0.13); the minimum recorded with 2 moles $Ca(NO_3)_2$ was (0.01). Decrease of membrane efficiency (the ratio between the measured osmotic pressure and the ideal osmotic pressure) with concentration because the rate of osmotic pressure increase is much less than the rate of increase for an ideal membrane.

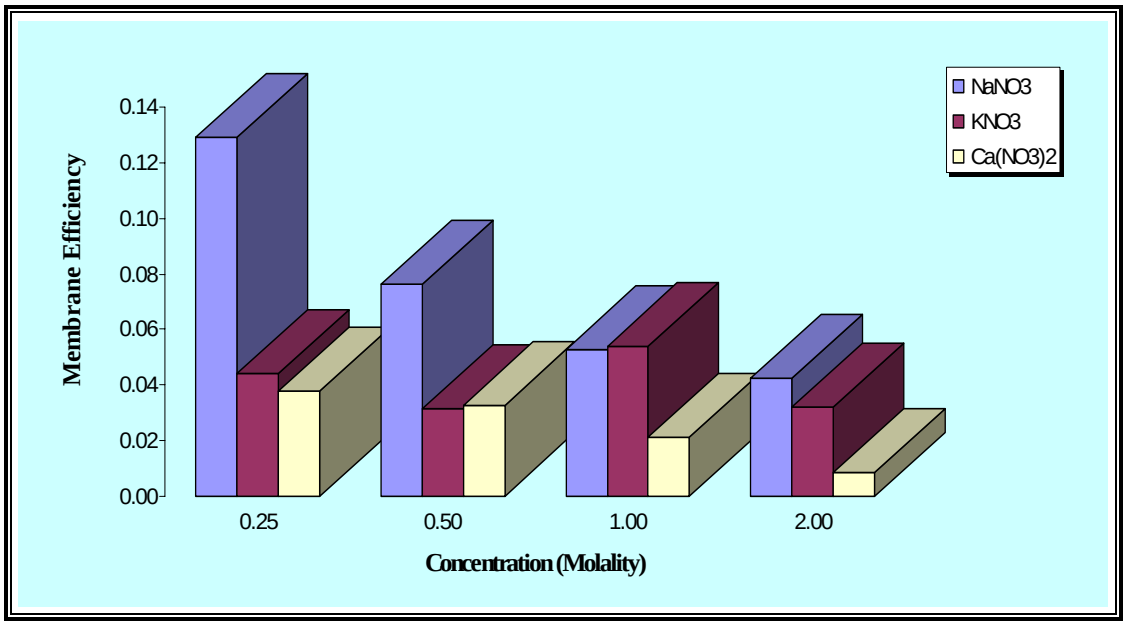

Figure (5-13): Membrane efficiency for different nitrate solutions.

Table (5-1): Osmotic pressure, time of maximum osmotic pressure, and membrane efficiency for different nitrate solutions (± 4 psi for δπ and 1 % for σ).

Concentration (Molality)	$NaNO_3$			KNO_3			$Ca(NO_3)_2$		
	δπ (psi)	σ	Time	δπ (psi)	σ	Time	δπ (psi)	σ	Time
0.25	20	0.13	726	7	0.04	983	8	0.04	1094
0.5	23	0.08	849	9	0.03	1130	16	0.03	548
1	31	0.05	994	29	0.05	1320	21	0.02	783
2	49	0.04	600	30	0.03	1471	17	0.01	992

"Time" equals time to achieve the maximum osmotic pressure (minutes)

5.2.2. Permeability

To study the short term (three-day) impact of nitrate fluids on the hydraulic conductivity of Pierre Shale, permeability studies were carried out for samples before and after three days exposure on the upstream side to nitrate fluids (osmotic pressure test duration). The results of these studies are presented in table (5-2). These results show that permeability is affected by nitrate fluids. The impact of nitrate fluids on permeability depends on the type of nitrate cation and the concentration of it in the

solution (Fig. 5-14). Usually the lower concentrations improve the permeability by increasing it while the higher concentrations reduce it except for KNO_3 fluids. The highest permeability values were produced by KNO_3 while the lowest values were produced by $NaNO_3$ (table 5-2 and Fig. 5-14).

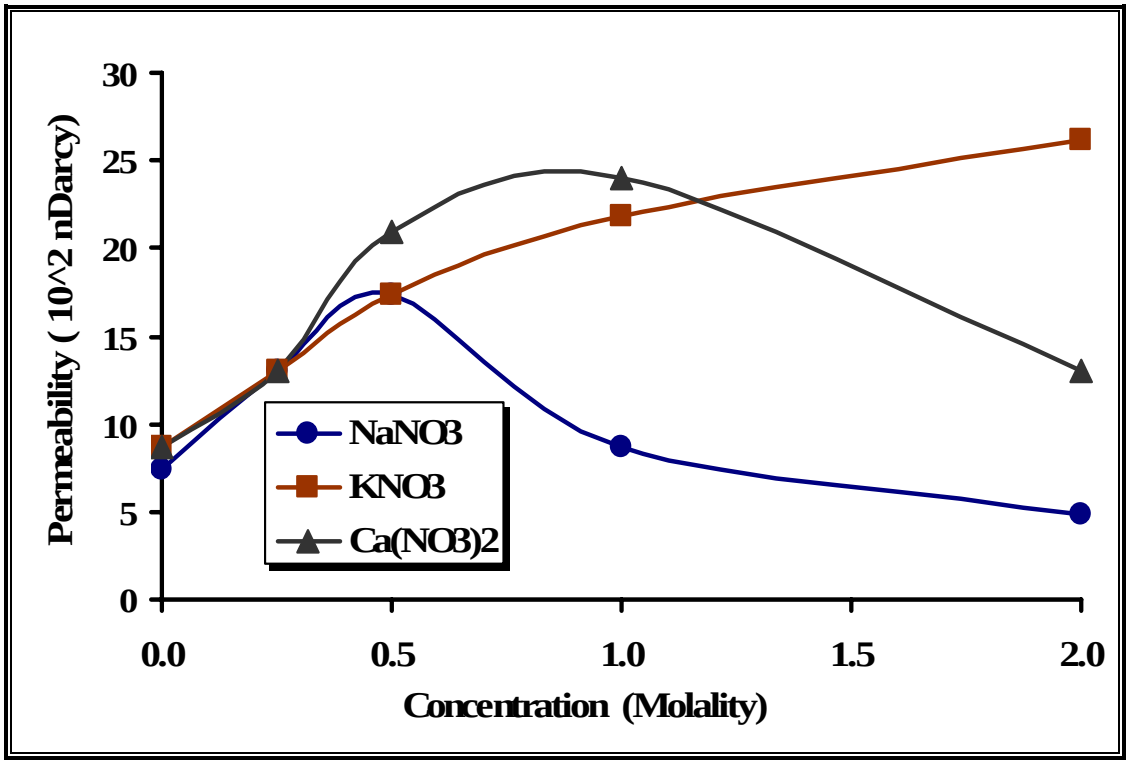

Figure (5-14): Permeability for different nitrate solutions.
(Uncertainty in permeability measurements is approximately ± 140 nDarcy based on three duplicate experiments).

Table (5-2): Permeability of Pierre Shale after three days exposure to different nitrates fluids in osmotic studies.

Concentration (Molality)	Permeability (100 nDarcy)		
	$NaNO_3$	KNO_3	$Ca(NO_3)_2$
0.00	7.40	8.71	8.71
0.25	13.06	13.06	13.06
0.50	17.41	17.41	20.98
1.00	8.71	21.77	23.95
2.00	4.79	26.12	13.06

Low concentrations (0.25 and 0.5 molal) of sodium nitrate solutions increased the permeability. It increased from 740 nDarcy for the unreacted samples to 1,714 nDarcy after exposure to 0.5 molal Na nitrate for three days. The higher Na nitrate concentrations reduced the permeability to the minimum recorded permeability value observed in the current study, which was 479 nDarcy for a sample treated by 2 molal $NaNO_3$ (Fig. 5-15). Higher concentrations of sodium nitrate produced more Na-enriched smectite which has more swelling potential leading to close the connected pores. The low concentrations did not produce swelling of this extent during this short period. This result agrees with the previous osmotic pressure studies that showed the high concentration $NaNO_3$ fluids develop the highest osmotic pressure. Over longer periods, it is likely that all $NaNO_3$ concentrations will reduce the permeability values (see chapter 7).

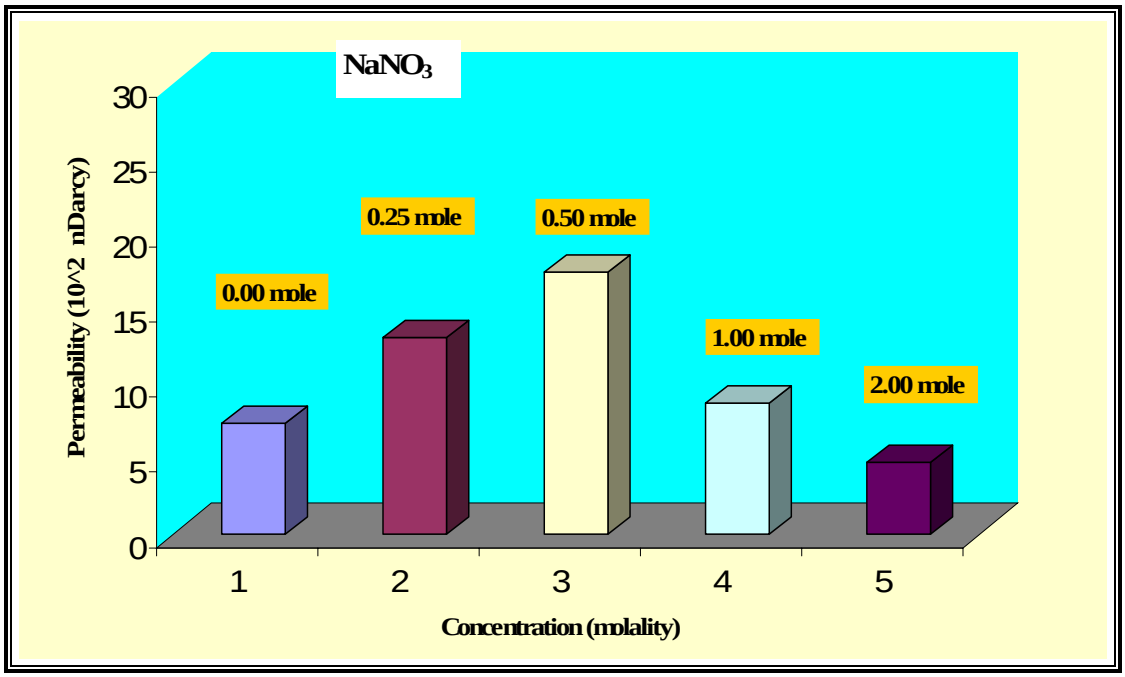

Figure (5-15): The recorded permeability after three days using $NaNO_3$ fluids for osmotic studies.

On the other hand, all concentrations of potassium nitrate fluids produced an increase in permeability. The value of permeability increased from 871 nDarcy for a natural sample to a maximum permeability recorded during the current study of 2,612 nDarcy for a 2 mole KNO_3 treated sample (Fig. 5-16). This trend also agrees with the osmotic pressure studies that showed KNO_3 fluids produced the lowest osmotic pressure. That means the osmotic pressure decreases are correlative with permeability increases. These results likely can be explained in terms of reducing the amount of Na-smectite by K-Na ionic exchange. Na-smectite is a swelling and positively charged mineral. Reducing it means reducing both swelling and positively charged components. Less swelling means an increase in permeability. Reducing the positive charges reduces the driving force for osmotic flow, which leads to reducing osmotic pressure. When KNO_3 was used, these effects will be continuing over the long term because more K-rich clay mineral (i.e. illite) will be produced.

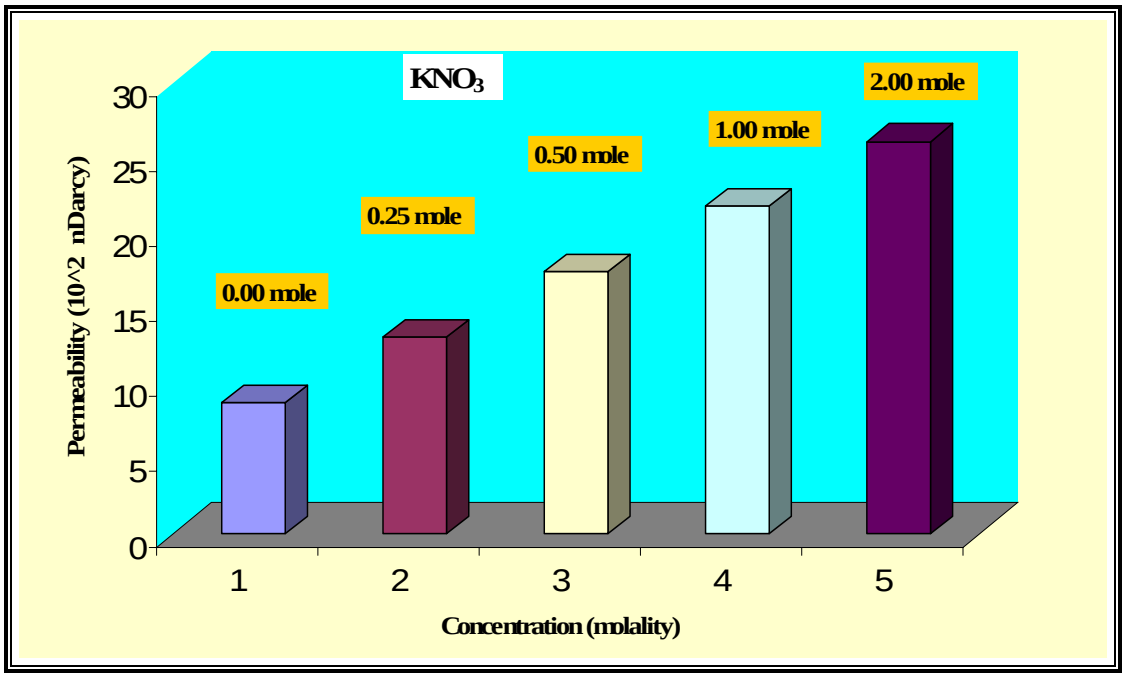

Figure (5-16): The recorded permeability after three days using KNO_3 fluids for osmotic studies.

Low concentrations of calcium nitrate up to 1 molal increased permeability values from 871 nDarcy for unreacted natural sample to 2,395 nDarcy for 1 molal $Ca(NO_3)_2$. Then, the permeability decreased to become 1,306 nDarcy at 2 molal $Ca(NO_3)_2$ (Fig. 5-17). 0.5 molal and 1 molal $Ca(NO_3)_2$ developed higher permeability values than the same concentrations of Na and K nitrates. This may be a result of opening micro-fractures and pores responsible for the oscillatory transient phenomena recorded during the osmotic pressure studies of $Ca(NO_3)_2$ at these concentrations.

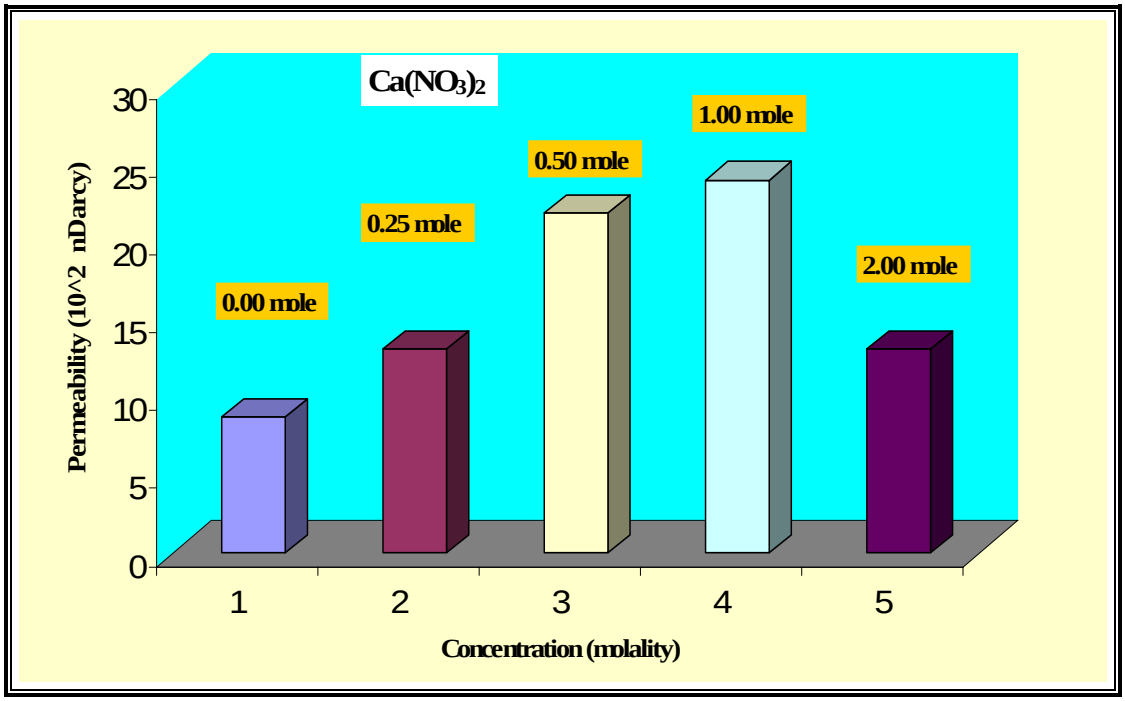

Figure (5-15): The recorded permeability after three days using $Ca(NO_3)_2$ fluids for osmotic studies.

5.3. Conclusions

The study of Pierre Shale osmotic flow using three different nitrate solutions and their effect on permeability indicate that:

1- Pierre Shale is a very low permeable rock, averaging 871 nDarcy.

2- Pierre Shale acts as a non-ideal, semi-permeable membrane with membrane efficiency of 13 % for 0.25 molal $NaNO_3$ and decreases to 1 % for 2 molal $Ca(NO_3)_2$.

3- Membrane efficiency decreases with increasing nitrate fluid concentration; this decrease is more dramatic for the calcium nitrate solutions.

4- Osmotic pressure changes with time in the experiments were caused by the reduction of the concentration difference across the sample through diffusion or the reduction of Na-smectite mineral content by K-Na ionic exchange leading to K-rich clay minerals.

5- Low concentration solutions increased the permeability value; higher concentrations reduce it (except for KNO_3 solutions).

6- Sodium nitrate solutions develop the lowest permeability values. Potassium nitrates solutions develop the highest values.

7- 0.5 and 1 molal calcium nitrate fluids produced high permeability values as compared to the same concentrations of other nitrate fluids. Also, the osmotic pressure that was produced from those two $Ca(NO_3)_2$ concentrations showed oscillatory pore pressure behavior, which has never been described before in the literature.

8- Good inverse correlation exists between osmotic pressure and the developed permeability. Samples that have the highest osmotic pressure have the lowest permeability values. Samples that have the lowest osmotic pressure have the highest permeability values.

Depending on the nature of the geo-engineering project K- or Na- bearing solutions can be used to change the osmotic and permeability behaviors of shale rocks. Potassium will produce a relatively low osmotic pressure but will increase the permeability which can be used in oil production, especially with drilling mud to avoid wellbore instability. It can also increase permeability of reservoirs containing Na-smectite. Sodium solutions will produce more osmotic pressure but will reduce the permeability which can be used for nuclear waste disposal projects to reduce permeability of the formation and produce more Na-smectite that is characterized by good adsorption and fixation capacities, which are essential for preventing migration of radionuclides.

Chapter 6

Evaluation of Diffusion and Swelling Stress of Pierre Shale

According to laboratory studies done in the last chapter, Pierre Shale acted as a non-ideal, semi-permeable membrane. The semi-permeable membrane will allow water to flow from the low concentration side to the high concentration side while the non-ideal behavior of the membrane will permit a partial flow of cations and anions from the high concentration side to the low concentration side by diffusion. Chapter 5 indicated that the flux of water and solutes through shale would affect the permeability within only 3 days (time of osmotic test). The current chapter is designed to evaluate the flux of cations (K, Na and Ca) through a Pierre Shale membrane over a longer time scale (more than one month). In addition, the affect of solution flux through a membrane on swelling behavior of Pierre Shale was studied by measuring the swelling stress under confining pressure conditions that are used in osmotic flow tests but for a longer test period. Cell No. II in the HTHP Shale Apparatus was used for diffusion studies, and a specially designed triaxial cell was used for the swelling stress studies.

This chapter provides an overview of both the cation flux through shale and the swelling behaviors of shale. The internal design of cell no II and the triaxial cell, which are used for diffusion and swelling tests respectively, is explained. Sample preparation and test procedures are described. Results and discussions for both the diffusion and swelling tests are given. The chapter closes with a summary of results and conclusions for these two shale phenomena.

6.1. General background

When a semi-permeable membrane separates two aqueous solutions of different activities, an electrical potential will develop because of the difference in ionic mobility. Generally, smaller ions have higher mobility than larger ones, and the mono-valent ions have higher mobility than multivalent ions. Difference in ionic mobility can be attributed to the hydration shell for each ion. For example, sodium ions have a smaller hydrated ion size than nitrate ions. Thus, sodium ions move faster than nitrate and, as a result, a diffusion potential develops (Chenevert, 1990).

The magnitude of this diffusion potential depends on the difference between the transport number of cations and anions and the ratio of the ionic activities on both sides of membrane:

$$D = (t^+ - t^-)\frac{RT}{F}\ln\frac{a_{fresh}}{a_{salt}} \qquad (6\text{-}1)$$

where D is the diffusion potential,

$(t^+ - t^-)$ are the transport numbers of the cation and anion respectively,

R is the universal gas constant,

T is the absolute temperature,

F is the faraday constant, and

a is the ionic activity.

If the membrane blocks the passage of the anions, the charge transport is produced only by the cations. In this case, the membrane is called an ion-selective membrane. A special form for equation (6-1) gives the maximum possible diffusion potential by

a perfect ion-selective membrane, when the anion transport number is zero and the cation transport number is one.

$$D = \frac{RT}{F} \ln \frac{a_{fresh}}{a_{salt}} \qquad (6\text{-}2)$$

Negative charges on the shale component (clay minerals and possibly organic matter) increase the movement of positive ions and restrict the movement of negatively charged ions (Loma et al., 2000). Passing and restricting the movement of anions produces a modified diffusion potential. Therefore, shales are considered a cation-selective membrane. The very low (nDarcy scale) permeability of the Pierre Shale still permits Darcy flow, which means some of the cations, and anions, will move in permeable channels without any selectivity. Because clay structures have the ability to hold some of the positively charged ions, shale membrane has a leaky ion-selectivity (Loma et al., 2000).

The current study measured the transportation of positive ions by diffusion through Pierre Shale using the same conditions that were used to measure the osmotic flow. This provided a correlation with the membrane efficiency of shale (σ) because the diffusion potential measures the ability of a membrane to restrict cation movement relative to an ideal membrane that prevents movement of all ions.

Cations held by clay structure cause an ion-exchange between clay interlayer ions and the induced fluid ions which plays an important role in affecting not only the rate of transport of ions but also the mechanical and swelling properties of shale (Sherwood, 1995). The ability of clay to adsorb water in its structure affects the rate of fluid transportation and both mechanical and swelling properties of shale. Generally, the ability of clay to hold ions or adsorb water in its structure is controlled

by how the clay interlayer ionic surface sites are occupied. This ability increases with increasing the Na/K ratio and becomes minimal when this ratio approaches zero. In other words, Na-smectite has the ability to adsorb water and hold ions on its structure. Illite, which is K-rich, does not have this ability, or at least possesses less of it. The presence of Ca instead of Na in smectite's interlayer reduces this ability but does not stop it. The fine grain-size of the clay produces a huge surface area that enhances both water adsorption and ion exchange rates that increase the swelling potential of shale.

Swelling deformation of shale at the shale/fluid interface is one of the most important topics in geo-engineering and environmental work. As water migrates to the clay structure, leading to swelling, the mechanical interactions of particles decrease by a release of confining pressures. Shales, depending on amount of Na-smectite, have an affinity to adsorb water into their structure, leading to an increase in fluid volume within the clay structure which produces swelling observable at the macroscopic level (Mitchell, 1993). This swelling deformation is often greater than the elastic deformation, and therefore cannot be predicted using classical elastic or plastic deformation theory. Damages to structures, slope instability and wellbore instability are some of the results of such deformation. The USA Department of Housing and Urban Development estimated an average annual loss due to swelling and shrinking phenomena of clay-rich materials at $9 billion in 1981.

Many studies have shown that shale swelling occurs when the adsorbed water in the shale (due to osmotic pressure) has a lower activity than an external test fluid. Accordingly, there are two categories of swelling:

1- The inner-crystalline swelling (hydration swelling) is a process whereby the exchangeable cations in the interlayer and at the surface of clay minerals build one to four hydration shells.
2- The intra-crystalline swelling (osmotic swelling) results from the difference in the ion concentrations close to the clay mineral surfaces and ion in the pore fluid. The ionic composition influences the extent of swelling, produced by the different hydration energies of the cations, which depends on ionic size and valence.

Furthermore, the swelling behavior of clay-rich soils and rocks depends strongly on the type and quantity of clay minerals they contain and on the content of other minerals which show swelling behavior. The fabric and density of clays determines the time dependent swelling behavior (Barbour and Fredlund, 1989).

It is important to note that the osmotic pressure responsible for swelling is at the mineral, or microscopic, scale. The osmotic pressure measurement described in chapter 5 is at the whole sample, or macroscopic, scale. The osmotic pressure at the mineral scale is produced by the chemical potential difference between a clay mineral interlayer fluid and the pore fluid. The sample scale osmotic pressure is a result of the chemical gradient between the pore's fluid and the downstream reservoir fluid in the lab test (or drilling fluid in the borehole example). That means when the sample scale osmotic pressure changes the pore fluid chemistry, the mineral scale osmotic pressure will change the clay structure via a volumetric change. If this change is a volumetric increase, it will produce swelling, but if this change causes a volumetric reduction in the clay interlayers it will cause the clay structure to shrink. The change in clay interlayer volume most probably, and according to the Gouy-Chapman theory, is due

to the change in thickness of the double layer. As mentioned in chapter 2, the double layer is sensitive to variations in electrolyte concentration, cation valence, the dielectric constant of the solution, and temperature (Mitchell, 1993). The thickness of the double layer can be calculated according to (Mitchell, 1993):

$$m = \left[\frac{\varepsilon_0 \varepsilon b T}{2 n_0^2 e^2 v} \right]^{0.5} \tag{6-3}$$

where m is the thickness of the double layer in m,

ε_0 is the permittivity of a vacuum,

ε is the dielectric constant of water,

b is the Boltzmann's constant,

T is the absolute temperature,

n_0 is the electrolyte concentration in ions per m^3, and

v is the valence of the cation.

It is clear from this equation that the thickness of the double layer is dependent on the electrolyte concentration. In contact with ionized water and in the absence of pressure, the double layers will swell to complete separation. However, the presence of a pressure overlap (due to a normal load across the layers) will cause the double layer to be truncated.

Swelling potential of clay-rich materials can be obtained from studying physical properties such as activity, specific surface area, and cation exchange capacity (CEC). Under fluid saturated conditions, not all shale components are effected equally by the fluid flow because most of shale pores are isolated. These

non-homogenous clay fluid reactions lead to unpredicted swelling deformation, which makes modeling of shale swelling potential or pressure very difficult, particularly for clays that have experienced desiccations. Thus, sample preparation and history can play a large role in subsequent experimental behavior.

Applying a load to a clay specimen squeezes out a certain amount of pore fluid (Bolt, 1956). According to diffuse double layer theory, the water is continuously displaced until the osmotic pressure of the clay-fluid system is equal to the ultimate loading pressure. This is consistent with the application of the osmotic pressure equation (Van't Hoff's equation), for approximating the swelling pressure that develops in clay minerals (Warkentin and Bozozuk, 1961; Kemper and Rollis, 1966; Kemper and Van Schaik, 1966; El-Swaify and Henderson, 1967; Olson and Mesri, 1970; Mitchell et al., 1973; Barbour and Fredlund, 1989; Chenevert, 1990; Chenevert and Osisanya, 1992; Osisanya and Chenevert, 1996). The simple model for this approximation was introduced by Barbour and Fredlund (1989) where the volume change due to swelling is equal to

$$\varepsilon = m_v \Delta\sigma_e + m_\pi \Delta\pi \qquad (6\text{–}4)$$

where m_v is coefficient of volume change with respect to effective stress σ_e, and m_π is the coefficient of volume change with respect to osmotic pressure $\Delta\pi$.

The large volumetric expansions or swelling reported in the literature that can not be attributed to osmotic flow makes some researchers believe that capillary pressure is the main driving mechanism for shale swelling (Forsans and Schmitt, 1994; Carminati et al., 1997), and may be due to dehydration of desiccated clays.

While the effect of water flux on shale swelling and failure has gained considerable interest, the flux of ions has been generally ignored. Kemper and Van Schaik (1966), Chenevert (1990), and Loma et al. (2000) concluded that the flux of ions into shale could have a detrimental impact on shale strength. Al-Bazali (2005) concluded that the invasion of ions into the shales might change the pore fluid composition and the mechanical properties of the shale such as cohesion, degradation, matrix expansion and swelling. He also said osmosis and ion diffusion operate simultaneously during the interaction of shales with drilling fluids. The first is dominant in high concentration solutions; and ion diffusion is dominant in dilute solutions.

The activity of solutions is the main factor that affects the double layer thickness. When we induce fluid into the clay system, we knew the activity of this fluid; however, the activity of the smectite interlayer fluid is unknown. This depends on the ability of interlayer cations to move and react. This ability is the difference between Na-smectite that has Na within its interlayer position and illite that has K in its interlayer position (chapter 2, Fig. (2-1)). Na has a small ionic radius and low charge compared to K. Thus, Na is easy to move creating charge unbalance in smectite, which will regain balance by attracting bigger molecules such as water and/or a large ionic charge such as K if it is available. Water molecules can enter the interlayer position causing swelling, but the charge unbalance remains. This charge unbalance and the attraction of water molecules will continue until the loading pressure is equal to these swelling forces. When a large ion with a high positive charge like K enters the interlayer position, the attraction force between the layers and

K will squeeze the water out of the clay interlayer position. This is why the K fluids are used to minimize the smectite swelling.

6.2. Sample preparation and tests procedures

6.2.1. Samples preparation

For diffusion and swelling studies cylindrical disks were prepared, as described in the previous chapter. For the diffusion test, 25 mm diameters by 5 mm thick disk samples were used. To measure swelling pressure relatively thick samples were used: 25 mm diameter by 10 mm thick. The samples with cylindrical axis perpendicular to bedding planes were prepared by the same way presented in Chapter 5.

6.2.2. Test procedures

6.2.2.1. Diffusion test

Cell no. II from HTHP Shale Apparatus was used to study the ion diffusion through Pierre Shale. Figure (6-2) shows a diagrammatic sketch for the internal and external design of this cell. Cell no. II is a hydrostatic cell with the same capability as Cell no. III that used for osmotic pressure studies. The prepared sample is emplaced in its position inside the confining cell as previously described in Chapter 5. In this cell, the upstream and downstream sides are connected to two big reservoirs (500 ml). After the system set up is complete, confining pressure is gradually increased using mineral oil until it reaches 100 psi to prevent leaking through the sample jacket. Then, to maintain a constant concentration in each reservoir, fluid is continually circulated upstream and downstream at normal pressure using a two-way peristaltic pump.

At the beginning of the procedures for measuring diffusion, both upstream and downstream fluids are distilled water. Then the confining pressure valve is closed,

and the sample is left for 24 hours to be sure it is completely saturated by distilled water. At this stage distilled water is cycling in both upstream and downstream sides at the same rate. After 24 hours, the downstream reservoir is replaced by the nitrate solution and cycled in the same way and at the same rate as the upstream side reservoir, which is kept full with distilled water. Fluid samples from the two reservoirs are taken by syringes at planned intervals. Each diffusion experiment is run for more than 30 days. During this time, ~ 3 ml solution samples were taken from each reservoir every three days. Samples were stored in marked bottles at 4 °C. At the end of the test, all samples were analyzed for the concentration of K, Na or Ca using flame Atomic-Absorption Spectroscopy as described in Chapter 4. Results of the chemical analyses of the upstream and downstream solutions through time were graphed using Excel software.

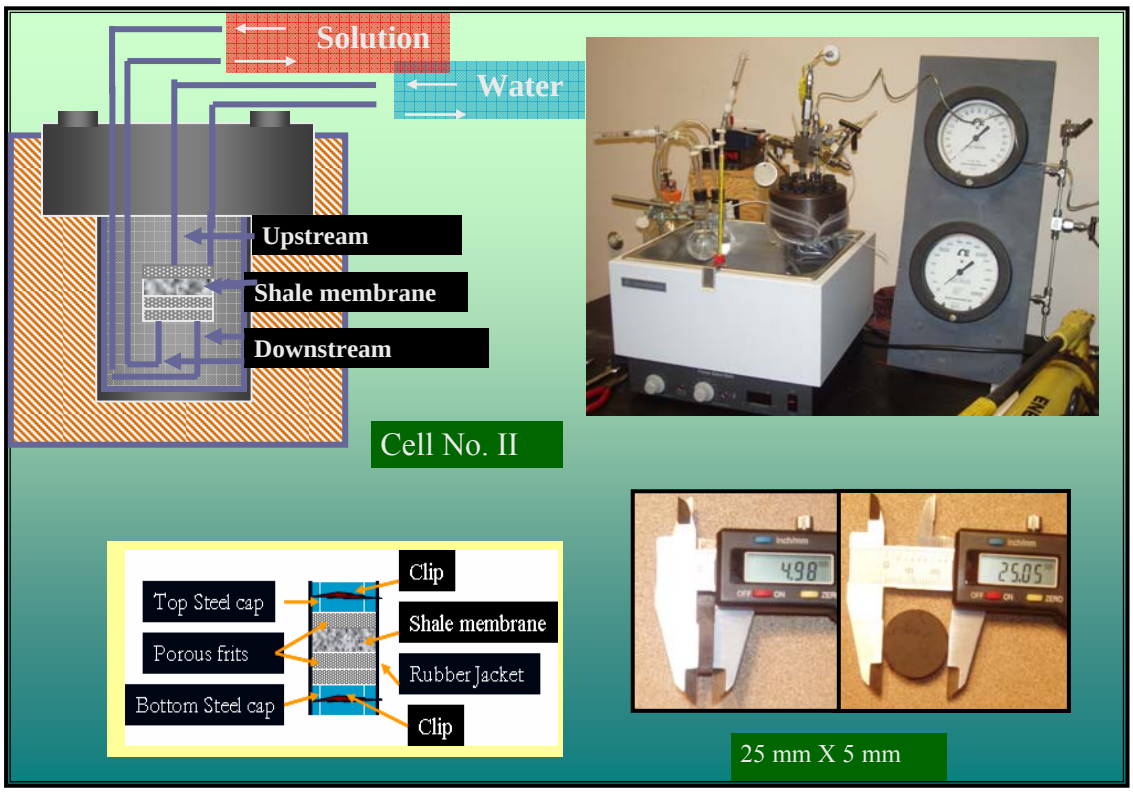

Figure (6-1): Schematic diagram for Cell no II.

6.2.2.2. Swelling stress measurement

Several test procedures exist for determining the swelling pressure of clay-rich materials. The most common of these procedures are:

1- Free swell Oedometer Test, which is performed under a given, but small load followed by compression of the samples to their original volume.

2- Loaded swell Oedometer test, in which the sample is allowed to swell under different loading forces.

3- Constant volume Oedometer test, in which the sample swelling is restricted by maintaining a constant volume through increasing the loading forces.

In all of these tests, the swelling pressure is determined as the load or pressure required to bring the sample back to its original volume. All of these swelling tests were conducted under low pressure conditions (~ 20 psi), which does not represent a deeply buried shale formation system.

This study used a specially designed triaxial cell to determine the swelling pressure in a manner similar to the constant volume Oedometer Test and similar to the equipment used by Steiger (1993) and Bilir et al. (2004). Figure (6-2) represents the external and the internal design of the triaxial cell used to measure the swelling stress under high pressure conditions. The concept is that when the vertical and horizontal deformation of the sample is restricted, the swelling of Na-smectite during water uptake will fill most of the voids, preventing a further increase in the volume of smectite, and the resulting force exerted on a piston by the sample is measured by a load cell external to the triaxial cell.

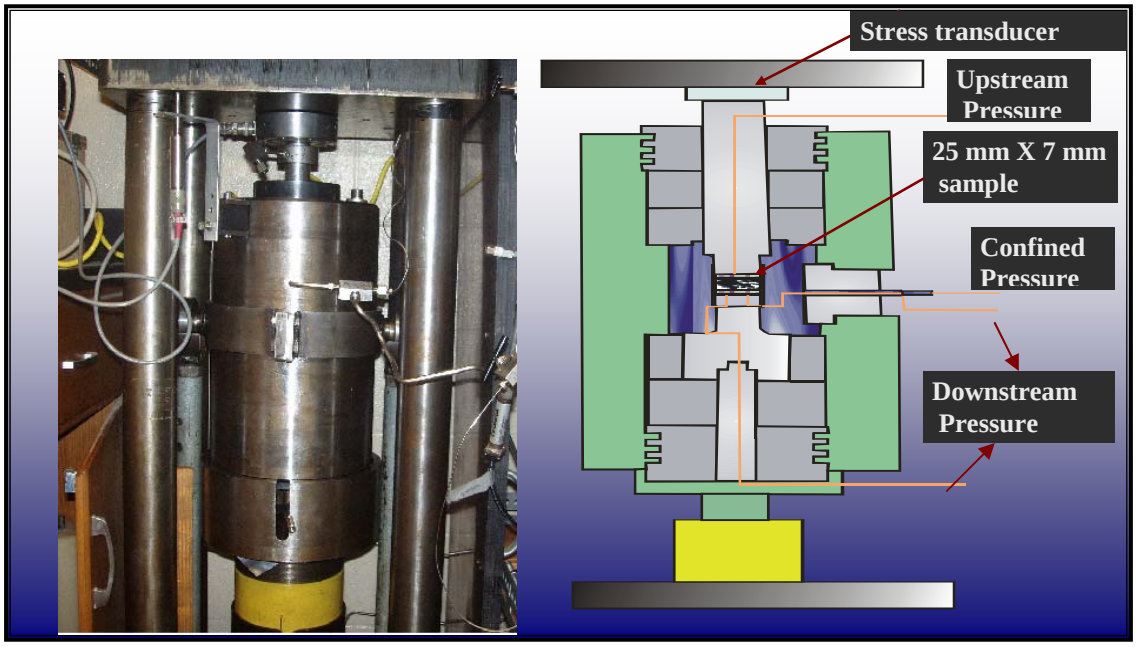

Figure (6-2): Schematic diagram for Triaxial Cell.

Figure (6-3) shows the forces that act on the sample inside the triaxial cell. In this case, the horizontal swelling deformation is restricted by applying enough confining pressure (1000 psi) and no space for vertical displacement, restricted by an axial load equivalent to stress of 750 psi acting on the one inch diameter piston. The samples used in this study were prepared perpendicular to the bedding plane, so most of the clay minerals are oriented with the 001 direction perpendicular to the piston (Fig. 6-3) which means most of the swelling should be in the vertical direction (σ_1 direction). The expansion of the sample in the vertical direction applies more force to the loading piston that transforms the force to the load cell where the change in σ_1 is recorded as swelling load. This is converted to swelling pressure by dividing the load over the cross section area of the sample.

The triaxial cell has the ability to hold and regulate both confining pressure and pore pressures (upstream and downstream) up to 10,000 psi, and has three pore

fluid access ports. Figure (6-4) shows the whole system design. The prepared sample was placed between two porous 316 stainless steel frits (25 mm in diameter). The two frits and the sample are sandwiched by two top steel end-pieces (25 mm in diameter). The upper end piece has two holes to allow communication between the test fluids and the shale samples. This end piece is connected vertically to the piston that is free to move in a vertical direction. The piston is connected to the load cell, which transmits stress data to the computer through aforementioned data acquisition system.

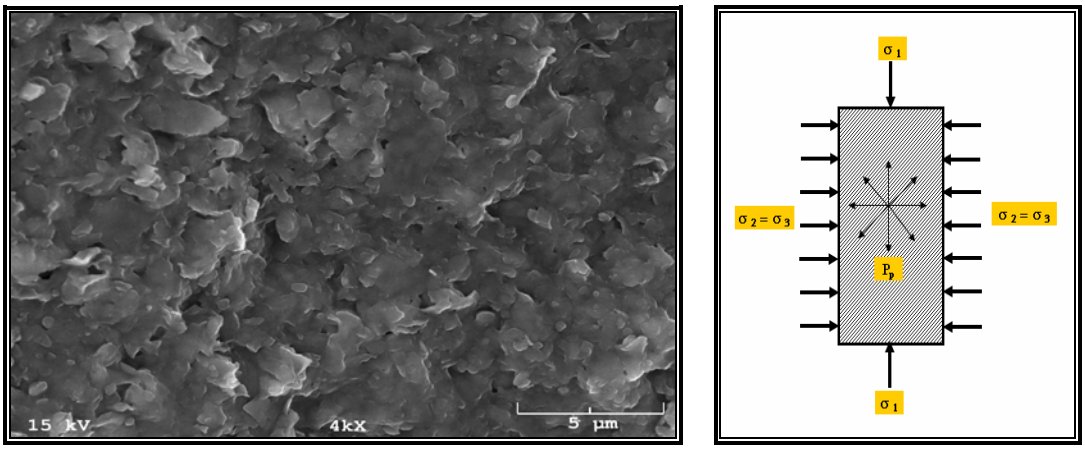

Figure (6-3): Left panel: The clay alignment parallel to bedding, looking down the 001 axis of most clay particles oriented in plane of image; Right panel: Schematic of forces acting on a sample restricting swelling in a vertical direction. In triaxial loading configuration, $\sigma_1 < \sigma_2 = \sigma_3$.

The bottom end piece has only one hole that is connected to the downstream pressure. This cap is located on the base of the cell and is not allowed to move (Fig. 6-4). Sample, frits, and end pieces are jacketed using PTFE Teflon jackets that are heat-shrunk around the sample system. This system is tightened by two compression seals to prevent leakage. During tightening the system is exposed to 10 psi unconfined uniaxial pressure to be sure there is minimal space between sample and frits or frits and end pieces. Then, the upper end piece is connected to the upstream

pressure tubes that pass through the two end piece holes. The downstream end piece is connected to the downstream pressure tubing that passes through a hole in the end piece. Then this system is placed into the triaxial confining cell with the upper end piece connected to the vertical piston and the bottom end piece connected to the cell base. The whole system is aligned in a vertical position. Then the cell is closed and the upper and lower closures tightened. The three capillary tubes leading to the end pieces are connected to the external pumping and the thermocouple is connected to the data acquisition system. The upstream pore pressure lines are connected to a large fluid reservoir (500 ml). The downstream line is connected to an ELDEX^{TM} HPLC pump (Fig. 6-4).

After the system is connected, the confining pressure is gradually increased until it reaches 250 psi. Then the upstream fluid is cycled at 50 psi and the downstream pressure and the vertical stress are increased to 50 psi. The three pressure outlets and the vertical stress are increased by 50 psi steps until the planned pressure is reached. When the confining pressure reaches 1,000 psi, upstream pore pressure 750 psi, downstream pore pressure 750 psi, all valves are closed except the upstream pressure valve through which the upstream fluid is continuously cycled at a constant pressure is (750 psi) using a Back Pressure Regulator.

The computer records any change in the axial load and vertical position of the cell through a LVDT attached to the cell. The data obtained by this system over a period of more than 30 days was used to analyze the swelling stress behaviors of shale samples used in this study.

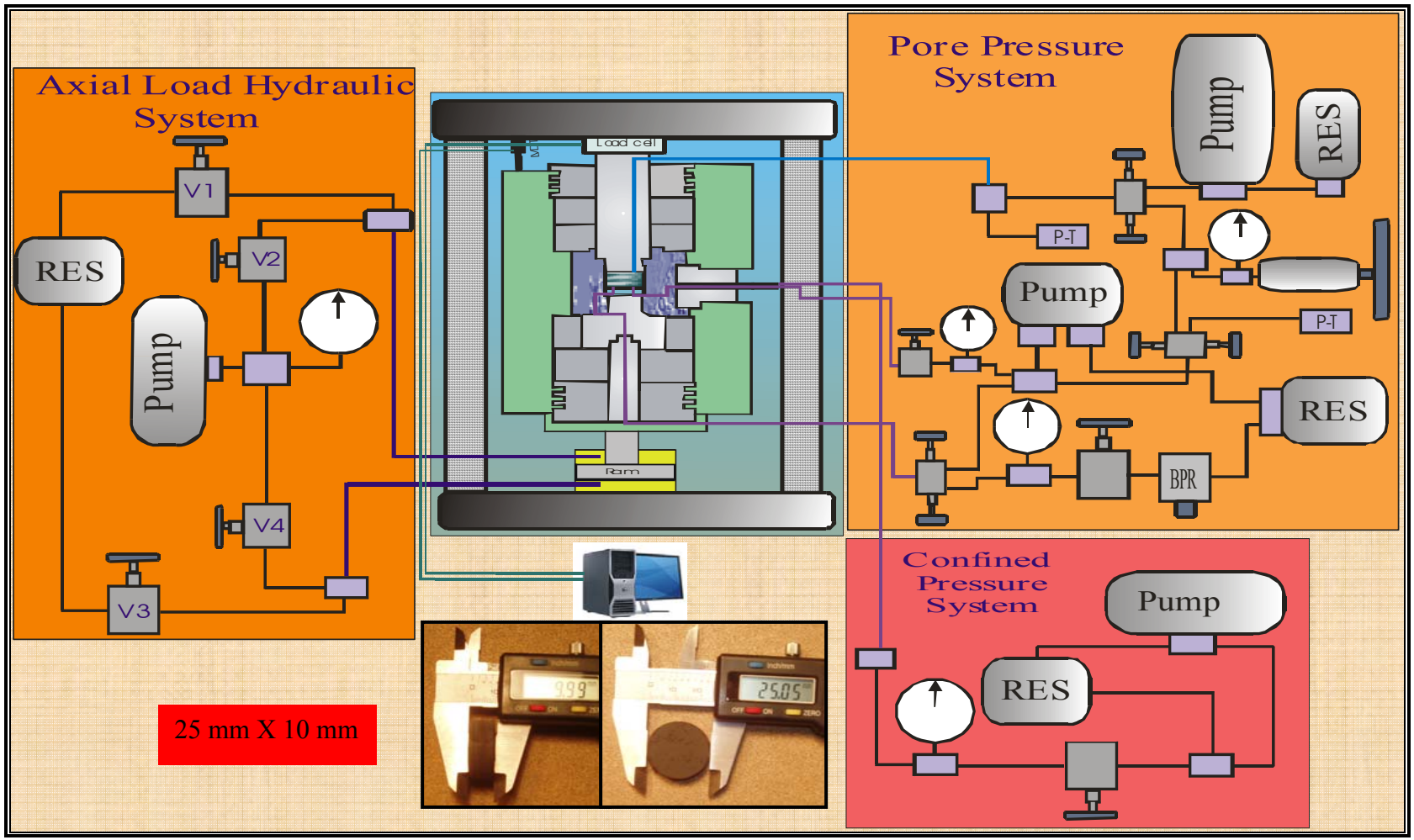

Figure (6-4): Schematic diagram for the Triaxial system design.

6.3. Results and discussions

6.3.1. Diffusion test results

Prior to the diffusion experiments, all the samples were saturated by distilled water during the first 24 hours. After the saturation period, the diffusion experiments were started. The solutions containing nitrate replaced the water from the downstream side. Every 3 days periodic sampling was carried out by collecting samples from the upstream and downstream reservoirs. For all the experiments, the diffusion path was dominantly perpendicular to the bedding. A flame Atomic-Absorption Spectroscopy was used for measurement of Na, K, and Ca concentrations in the upstream and downstream reservoirs. The experimental conditions that were explained before are more or less similar to the concentration model that was described in Chapter 3. A practical way to apply this model is as follows. Consider the coupled solute and water flux depicted schematically in figure 6-5. If we choose reservoir 1 as the nitrate containing reservoir, the concentration of nitrate, C_1, will decrease with diffusional flux through the membrane. The concentration of nitrate in reservoir 2, C_2, will initially be zero, but will increase in accordance with the loss of nitrate in reservoir 1. Because of the membrane properties of Pierre Shale, fluid will flow across the membrane from reservoir 2 to reservoir 1. This change in water content between the two reservoirs will also influence the concentrations, diluting C_1 and concentrating C_2, and result in volume changes as well.

The experimental results of studied samples are represented in Table (6-1). These results indicated that the effective flux of cations into the upstream side or out

from downstream is unequal, that is, a greater decrease in concentration is evident in the upstream reservoir than is gained in the downstream reservoir.

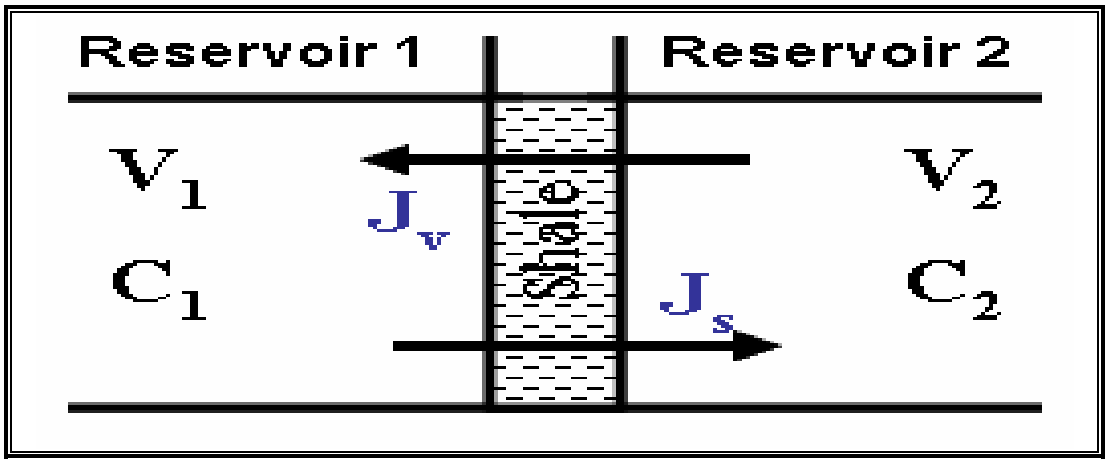

Figure (6-5): Schematic of experimental design for diffusion flux experiments, consisting of two reservoirs separated by a thin shale membrane.

Table (6-1): Cation concentration in upstream and downstream reservoirs with time for different nitrate solution (± 10 %).

Time (days)	Concentration (mg/L)					
	$NaNO_3$		$Ca(NO_3)_2$		KNO_3	
	Upstream	Downstream	Upstream	Downstream	Upstream	Downstream
0	3.22	46172.72	0.00	48295.18	0.00	48326.04
3			28.57	46282.34		
5	161.83	40344.25			32.14	45091.6
8	581.16	38877.81	89.29	44083.27	85.71	41418.07
12	530.99	38354.64	146.43	42217.05	139.29	41758.7
14			250.00	41383.73		
15	635.42	38260.09			217.86	41831.42
18			325.00	39951.21		
19	791.19	37159.13			317.86	38830.07
23	987.73	35923.34				
25			607.14	39381.01	539.29	39714.75
26	1152.73	34325.21				
28			750.00	39176.67		
29					703.57	38982.00
31			857.14	37093.11		
33					842.86	36704.80
36	1420.53	30304.17				
38			1214.29	36474.98		
40					1057.14	37286.05

Figures (6-6 a, b and c) show the difference between the rate of increasing concentration in the water reservoir and, the rate of decreasing concentration in the nitrate reservoir. The rate of decrease in the high concentration side is much greater than the rate of increases in the low concentration side. The difference between the two rates reached its maximum with $NaNO_3$. The rate of decrease in the concentration from the higher concentration side is greater than the rate of increase in the low concentration side by 15.2 times. The difference between the two rates is 11.3 times with KNO_3 solutions, and 13.5 times with $Ca(NO_3)_2$ solutions.

To analyze these changes, the variant of the model given in Chapter 3 was applied following the coupled solute-water flux model given first by Kedem and Katchalsky (1958). Consider that the number of moles of cation in each reservoir of Figure 6-5 can be given by

$$n_1 = c_1 V_1;\ n_2 = c_2 V_2 \qquad 6\text{-}1$$

where n_1 is the number of moles of cation in reservoir 1, and similarly for n_2. The flux of solute and water across the membrane can be expressed as:

$$\frac{\partial n_1}{\partial t} = -J_s A; \qquad \frac{\partial n_2}{\partial t} = J_s A \qquad 6\text{-}2$$

$$\frac{\partial V_1}{\partial t} = -J_v A; \qquad \frac{\partial V_2}{\partial t} = J_v A \qquad 6\text{-}3$$

where J_s and J_v are the solute and fluid flux respectively, and retain their meaning from Chapter 3. A is the cross section area of the shale membrane. This formulation assumes an infinitely thin membrane. In each reservoir, the change in concentration due to the coupled solute-water fluxes can be written as:

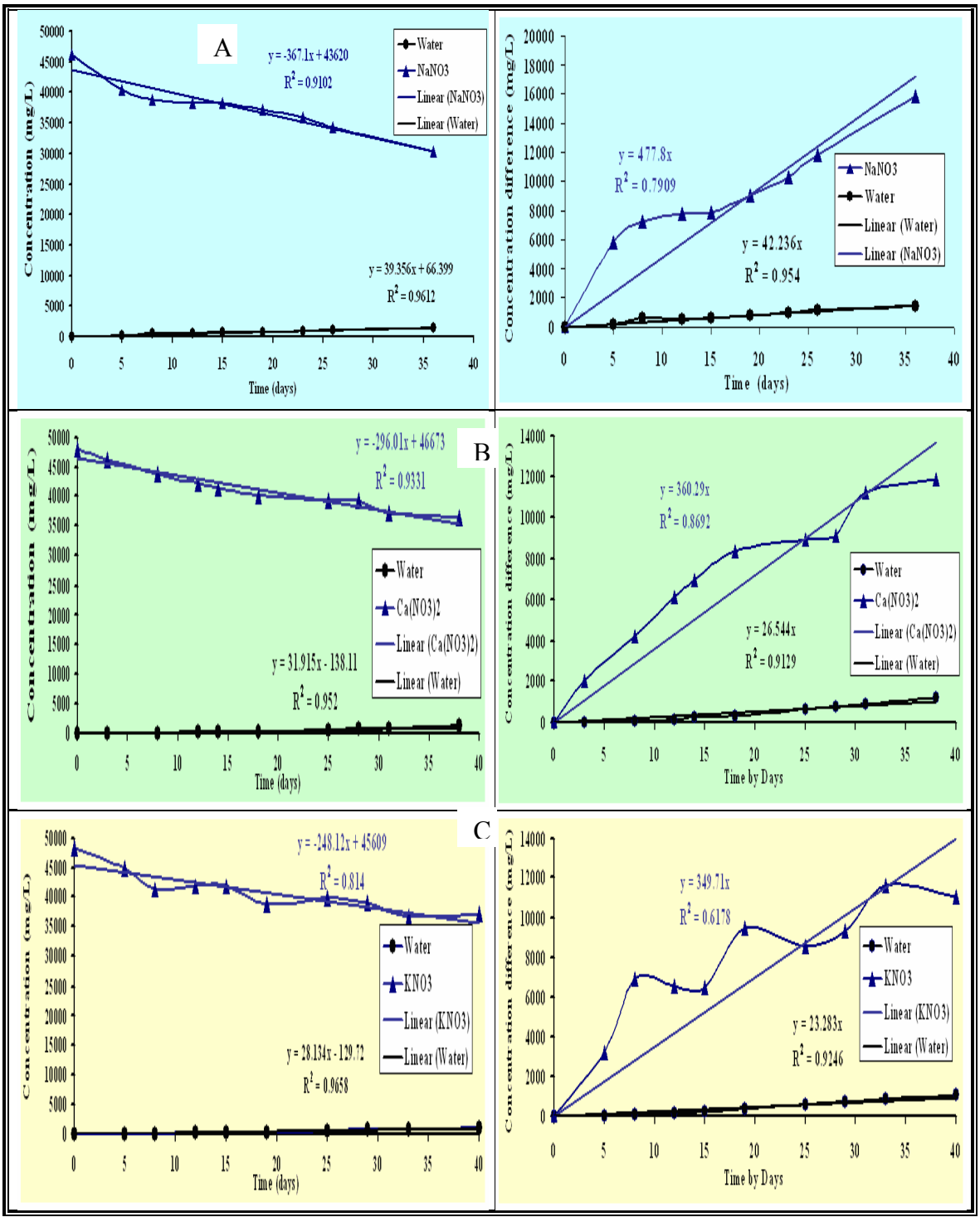

Figure (6-6): Relationship between the concentrations of the two reservoirs overtime

A) Na concentrations at both reservoirs,
B) Ca concentration of both reservoirs, and
C) K concentration of both reservoirs.

$$\frac{dc_i}{dt} = \frac{1}{V}\frac{\partial n_i}{\partial t}\Big|_V - \frac{n_i}{V^2}\frac{\partial V}{\partial t} \qquad 6\text{-}4$$

From Figure 6-6, the changes of concentration with time in each reservoir are well represented by linear functions with constant slopes. Setting the left-hand side of equation 6-4, and substituting equations 6-1 through 6-3 yields two closed equations (one for each reservoir) for J_s and J_v. Assuming, for the early times in the diffusion experiments where changes in concentration are linear, that each flux can be considered constant permits solving these two equations for J_s and J_v.

In the case of Na diffusion, the rate of change of $NaNO_3$ in reservoir 1 is -367.1 mg/l-day (with $R^2 = 0.95$), and that in reservoir 2 is + 42.2 mg/l-day. With this, the solute and fluid fluxes are found to be

$J_s = 5.06 \times 10^{-5}$ mol/cm^2-day

$J_v = -0.72$ cm^3/cm^2-day (the "Darcy velocity") 6-5

Using the form of the solute flux and parameters given in equation 3-12 and in Appendix A, one can calculate a diffusion coefficient for Na cation in Pierre Shale of

$D = 5.4 \times 10^{-11}$ m^2/s

which is close to the value of 1-3 x 10^{-11} m^2/s reported for Pierre Shale in the field experiment by Neuzil (2000).

Similarly, using the form of J_v given by equation 3-10 in Chapter 3 and parameters given in Appendix A, one can calculate the product of the reflection coefficient and permeability from the experimentally determined value in equation 6-5:

$\sigma k = 1.9 \times 10^{-19}$ m^2

With a reflection coefficient of 0.08 from Table 5-1 in Chapter 5, the permeability of Pierre Shale to sodium nitrate solutions is 2370 nDarcys, which is close to the value of 1740 nDarcys found using pressure decay method in Chapter 5 and reported in Table 5-2. Similar results can be determined from the calcium and potassium diffusion experimental results plotted in Figure 6-6.

6.3.2. Swelling stress studies

Prior to the swelling stress experiments, all the samples were exposed to chemical gradients that were created by using distilled water in the downstream reservoir and nitrate solution in the upstream reservoir. This situation was performed for more than one month at 750 psi pore pressures, 1000 psi confined pressure and at room temperature.

According to different swelling theories, vertical swelling pressures should be similar to Figure (6-7), and the swelling pressure will be the maximum swelling pressure. According to this sketch, after the swelling increases during the transient stage, it reaches a maximum and remains constant during the steady state stage. In the experimental test and during the early stage (8 days for $NaNO_3$ and 4 days for $Ca(NO_3)_2$) the recorded vertical swelling stress showed the same behavior. However, with increasing time the swelling stress recorded during the experiments on Pierre Shale shows an oscillatory phenomenon with all nitrate solutions. The intensity and frequency of the oscillations depends on the type of nitrate fluid and the curing time (Figs 6-8).

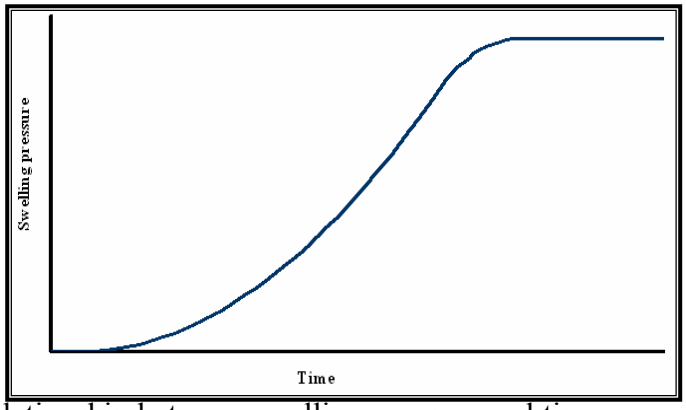

Figure (6-7): Relationship between swelling pressure and time, according to swelling theory and early stage of the experimental.

By carefully studying swelling pressure (Fig. 6-8 and 6-9), calculated from the sum of the load increments divided by the cross-sectional area of the sample, the following results were found that:

1- The swelling pressure depends on chemical type and time

2-The studied samples showed some fluctuations (regardless the O-ring fraction which is minimum) with intensity and frequency depending on the type of the chemicals.

3-The lowest swelling pressure is produced by K-nitrate, and the highest one is produced by Na nitrate. Ca nitrate behaved between Na and K (Fig. 6-8 and 6-9). This study shows the effect of the ionic exchange between the induced chemical and clay structures. Na will produce Na-smectite, which has a high swelling potential. K produces lesser ion exchange, possibly producing illite or illite/smectite mixed layer, which does not have moderate or non-swelling potential.

4-The swelling pressure was about 180 psi for 0.5 mole $NaNO_3$, less than 24 psi for the same KNO_3 concentration, and 92 psi for 0.5 mole $Ca(NO_3)_2$.

5-The pore-pressure is an important swelling factor. Swelling pressure decreases with increasing pore pressure.

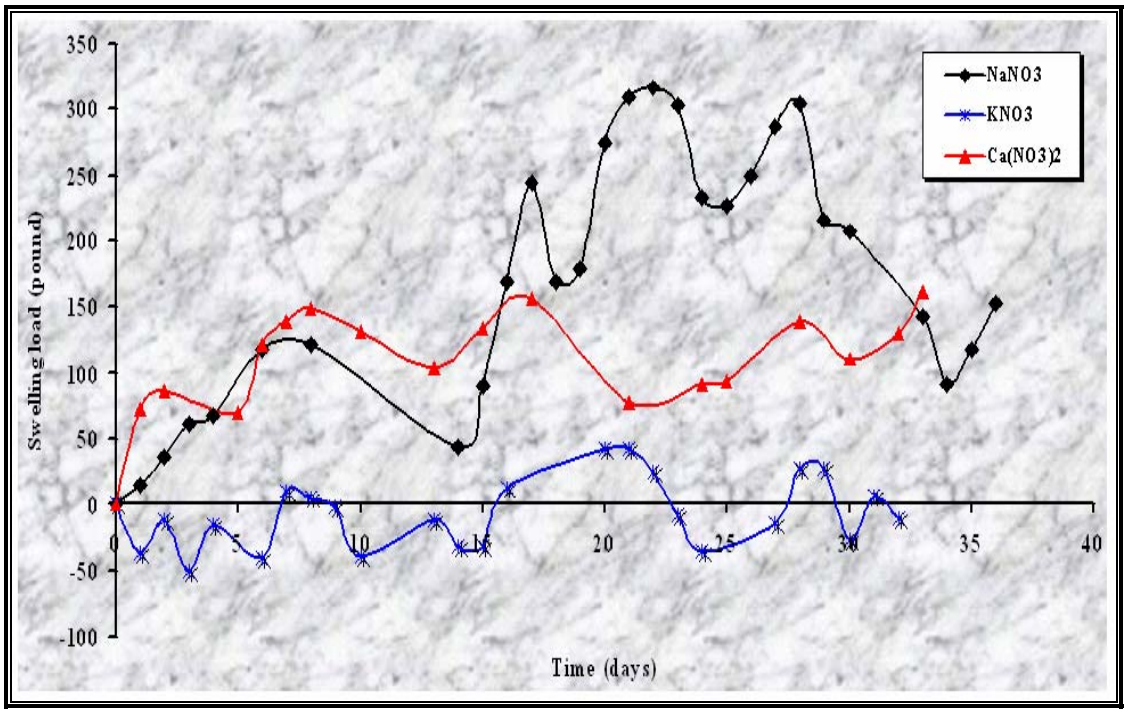

Figure (6-8): Swelling load-time relationship for 0.5 molal concentration.

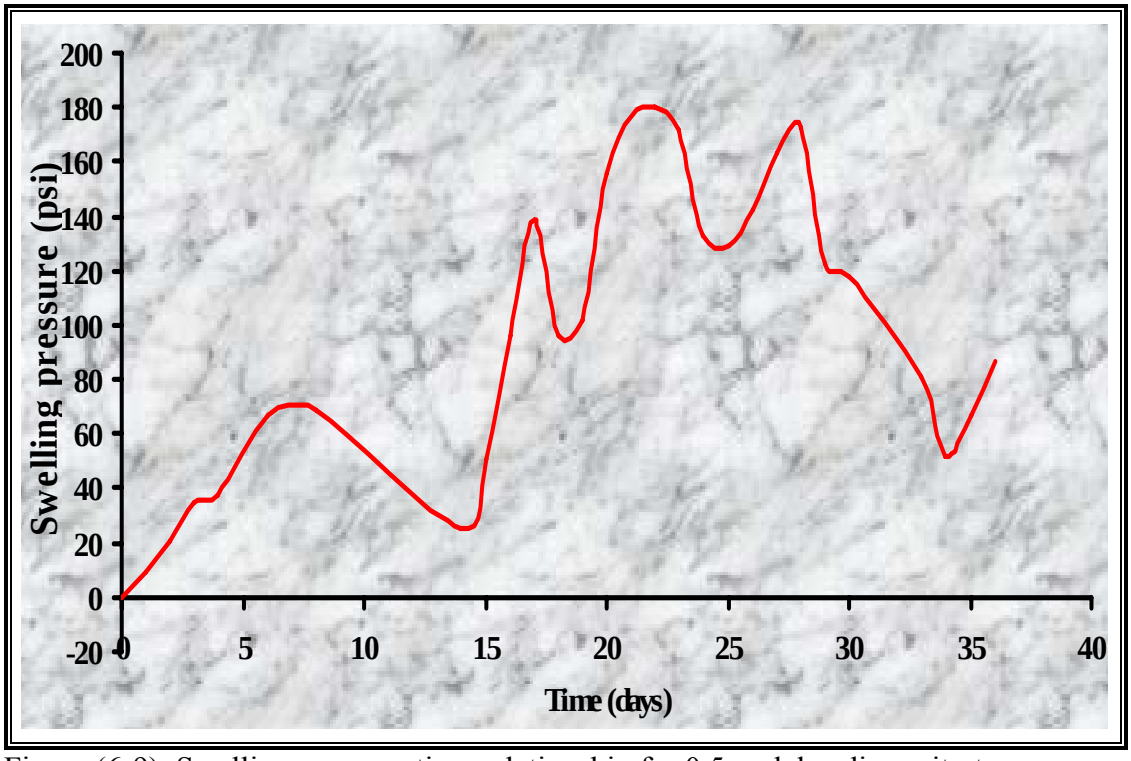

Figure (6-9): Swelling pressure-time relationship for 0.5 molal sodium nitrate.

Since all samples showed fluctuations in swelling pressure with time, this study presents an explanation of this phenomenon that may occur when any fluid is induced to any type of shale.

The permeability of Pierre Shale is very low (nDarcy scale), the pores are unconnected, and study samples are relatively thick (10 mm). All of these create compartmentalized pore pressure zones inside the sample (Fig. 6-10) when pore pressure is increased from one side. These zones are dependent on the applied pore pressure and connectivity of the pores. The micro-scale pores make the connectivity between these zones time dependent. Swelling of clay minerals is also time dependent. When the water and/or cations start moving through the sample under osmotic pressure, the water enters the first zone leading to changes in the pore fluid chemistry in this zone. Due to its effect, Na-clay minerals start to react with this water causing swelling. The test conditions in this study restrict the vertical and horizontal deformation of the sample causing the swelling of smectite to fill most of the voids (Fig. 6-11). When the voids are filled, the volume of smectite cannot increase and the pressure that is caused by the swelling is measured as the swelling pressure.

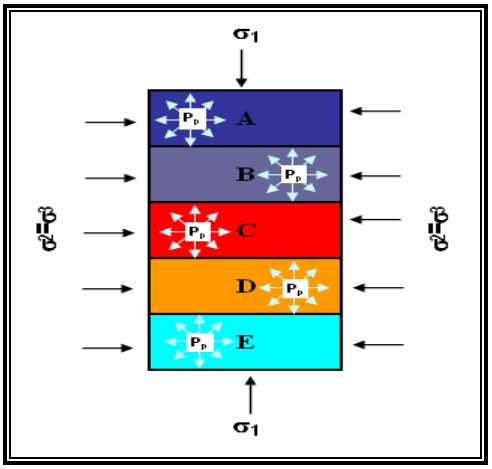

Figure (6-10): Schematic diagram for stresses and pore pressure zones distribution inside the study sample (each zone has its own pore pressure).

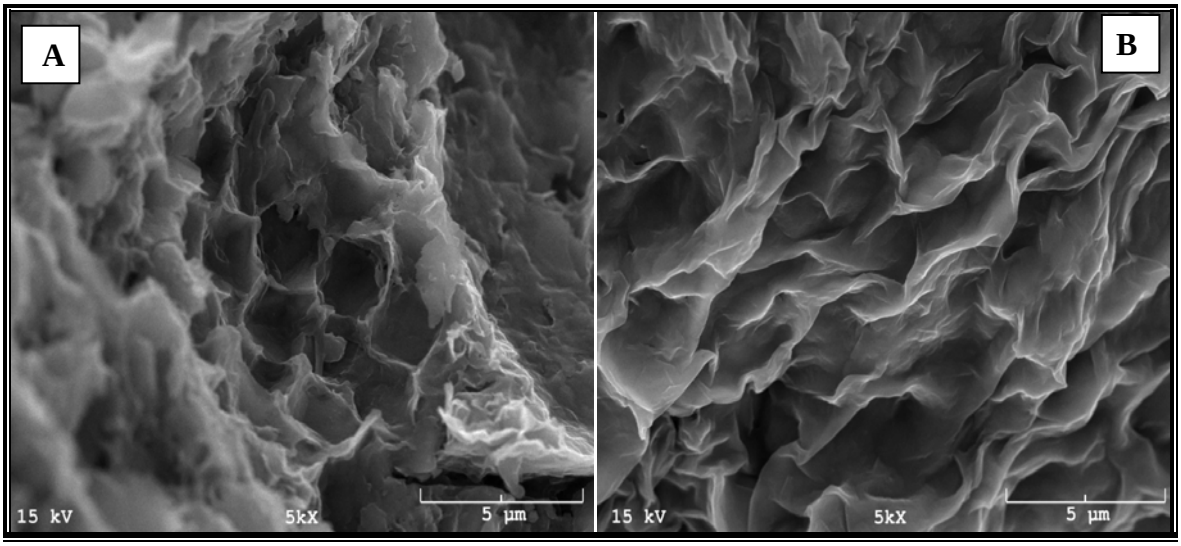

Figure (6-11): SEM photographs show the difference between natural and swelling smectite
A) Honeycomb structure of smectite found in Pierre Shale
B) Na-smectite after exposure to water for 6 months at normal room conditions.
Note the reduction of pores and increase in smectite platelets volume

Filling the pores with swelling material (Fig. 6-11b) increases the pore pressure inside the first zone (Fig 6-10). When the pore pressure increases, the initial stress circle will shift toward the failure envelop on the Mohr circle (Fig. 6-12). When the circle reaches the failure envelop, this zone starts failing by opening pre-existing micro-fractures or tensile fractures as shown in Figure (6-13 a and b). These micro-fractures allow water to move to the next zone. At this point, the recorded swelling stress will decrease. When the clay minerals in the next zone start swelling, the recorded swelling stress will increase again until this zone fails in a similar manner causing another reduction in swelling stress. Also, this zone failure will lead to the movement of water into the other zones. Similar phenomena were recorded during osmotic pressure tests using $Ca(NO_3)_2$ solutions, with an increase in permeability associated with this phenomena occurring within three days. This is why these

phenomena may be shown when introducing fluid into shale rock under pressure. This explanation is in agreement with Griffith (1920) theory for tensile fracture.

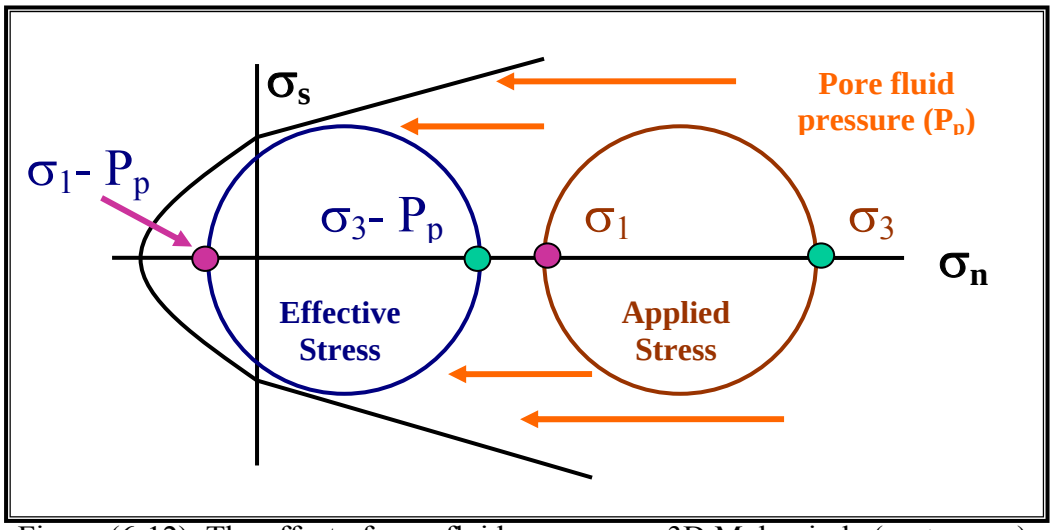

Figure (6-12): The effect of pore fluid pressure on 3D Mohr circle ($\sigma_1 < \sigma_2 = \sigma_3$).

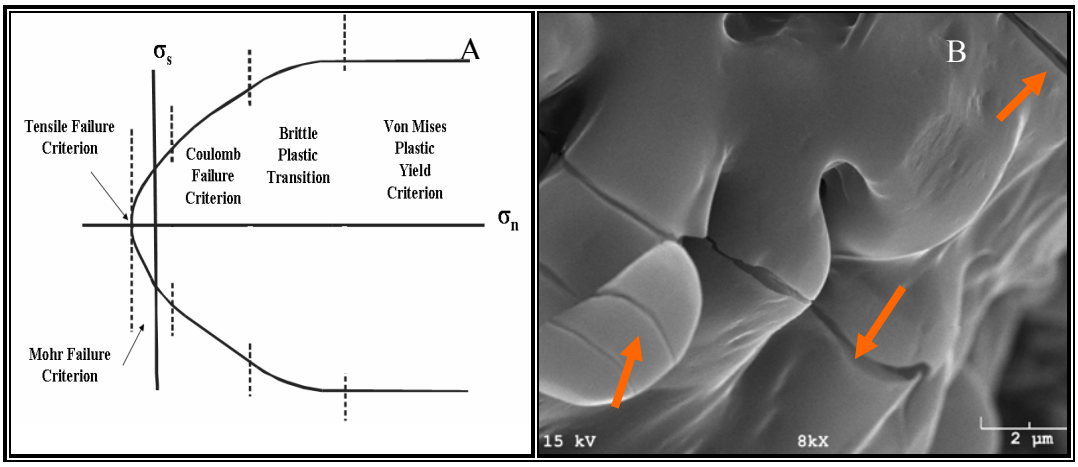

Figure (6- 13): Tensile failure envelope and the micro-fractures.
A) Composite failure envelope (Van der Pluijm and Marshak, 1997).
B) SEM image for the initial micro fractures (red arrows) that can open by increasing the pore pressure (Na smectite treated by water for 6 months at normal room conditions).

6.4. Conclusions and suggestions

The following conclusions are from studying the results of the diffusion and swelling behaviors of Pierre Shale;

1- A good relationship exists between swelling, diffusion, permeability and osmotic pressure where swelling reduces the ability of both fluid and cations to move through shale leading to higher osmotic pressure.

2- Meaningful results comparable to other methods and field experiments can be performed using the method applied here. Diffusion of cations through Pierre Shale is approximately 10^{-11} m^2/s. Darcy flux through Pierre shale induced by modest chemical gradients can reach ~ 1 cm/day.

3- Swelling of shale is dependent on chemical type and time

4- Very little swelling pressure is measured with KNO_3 solutions, with $NaNO_3$ solutions producing larger and measurable swelling stresses.

5- Swelling pressure showed oscillatory phenomena with all nitrate fluids. Intensity and frequency of this phenomenon is dependent on the type of solute. This phenomenon may lead to increase the shale permeability. This phenomenon likely created tensile fracturing in a rock cylinder by increasing the fluid pressure in pores and cracks.

The excluded ions through shale membrane, makes certain shales useful in water purification as also suggested by Ebrahim and Abdel-Jawad (1994). By assuming shale formation located between two different salinity reservoirs as in Figure (6-14). The higher salinity reservoir has a water table higher than the low salinity reservoir and the hydraulic gradient between the two reservoirs is greater than the induced osmotic pressure. In this case, the water molecules will move from a high salinity reservoir to a low salinity one under the effect of hydraulic gradient according to Darcy's Law but ions will be excluded by clay layers. That means the fresh water

reservoir will be recharged by fresh water through shale formation. If this situation is created e.g. by inducing the sea water to a high TDS reservoir to create a hydraulic gradient greater than the osmotic pressure, the low TDS reservoir will be recharged with low-cost fresh water. This process could help provide fresh water especially in water drought areas such as Egypt.

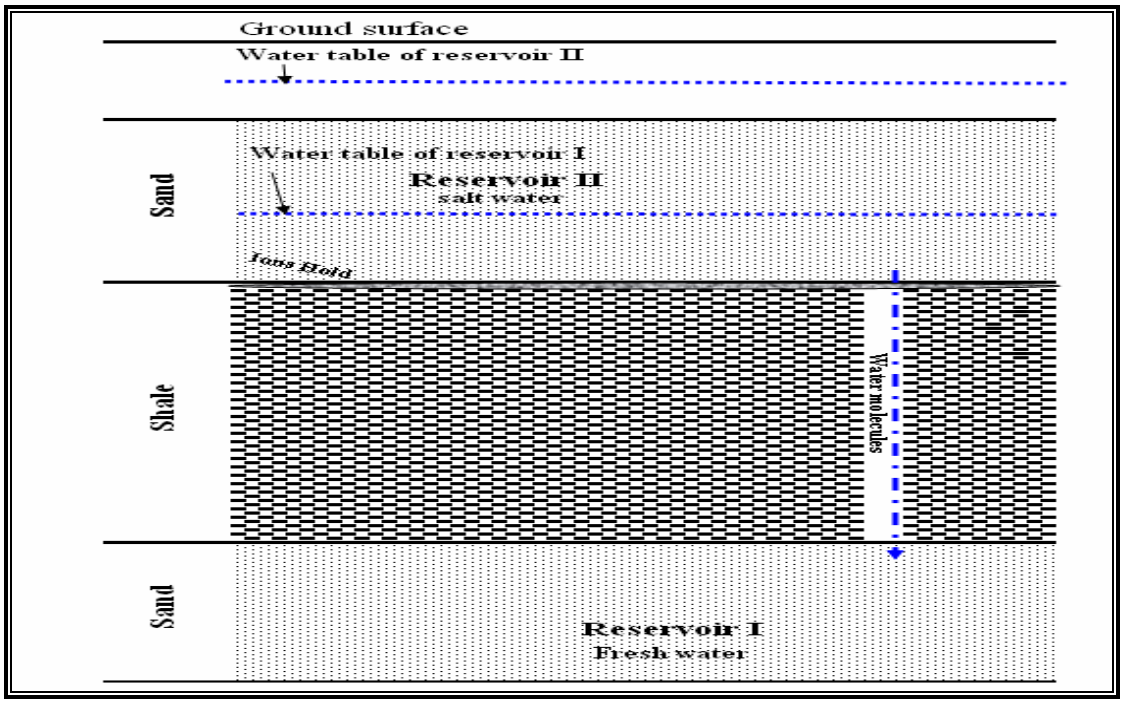

Figure (6-14): Shale works as desalination of high TDS groundwater.
The water flux from reservoir II to reservoir I but ion will be excluded by clay layers structure.

For the swelling triaxial cell, it is worth making the entire cell completely computerized to measure any change in any of the pressure and temperature outlets overtime. In addition, using servo-controlled pumps to maintain constant pore pressures and confined pressure will give the cell extra ability to measure permeability and osmotic pressure. Piezoelectric transducers can be used to increasing the ability of this cell for monitoring what is happen inside the sample (equisetic emission) especially the cell has a spaces for that.

Chapter 7

Impact of Pore Fluid Chemistry on Time Dependent Clay Mineralogy and Grain Structure

7.1. General overview

This chapter is essentially designed to study the impact of different solutions on clay minerals and the grain-size distribution of Pierre Shale for different curing times (up to one year). To simulate different geological and environmental conditions, the samples were studied under a wide range of pressure and temperature conditions, from room temperature and normal pressure (ground surface condition) up to 150 °C and 3000 psi pore pressure (≈ 6,000 feet deep condition).

From the literature review, the short- and long-term stability of clays, especially smectite, is poorly documented under relevant sedimentary basin conditions. In fact, most experiments dealing with the smectite to illite transformation were carried out under hydrothermal conditions and less attention has been paid to low temperature conditions because of the long experimental times necessary to produce observable changes. However, the understanding of illitization under low temperature conditions using solution chemistries of natural ground waters and other geochemical fluids is useful in different ways. Smectite transformation may take place in a wide range of natural environmental conditions, other than during diagenetic processes, related to its industrial applications (Cuadros and Linares, 1995). For example, the breakdown of concrete in natural environments releases Ca, Na and K into the groundwater, producing suitable conditions for clay mineral transformation (Andersson et al., 1989; Lunden and Andersson, 1989). Bentonite uses

as seals in monitoring well construction and as liners are considered best management practices in the environmental industry. In addition, clay and clay-rich rocks have been selected as potential buffer materials for nuclear waste disposal purposes because of their ability to fill the space between waste canisters and host rock, and to ensure an efficient permeability barrier against infiltrating groundwater. Smectite (bentonite) is characterized by good adsorption and fixation capacities, which are essential for preventing migration of radionuclides (Pusch, 1973; Bird, 1979; Bird and Cameron, 1982). If the fluids that have Ca, Na and K and other cations encounter clay barriers they could significantly effect the clay's composition, especially smectite, leading to a reduction in its radionuclide holding capacity. Also, the fluids that are used in hydrofracturing shale rocks in order to increase near-wellbore permeability for oil and gas production such as in Barnett Shale, Texas, USA, could significantly effect the clay composition and structure overtime.

Moreover, most studies of the illitization of smectite are carried out on mono-mineral samples, such as smectite samples, which neglect the influence of the whole-rock's mineral composition (illite, kaolinite, chlorite, quartz, feldspars pyrite and other minerals) as it exists in nature. Despite its difficulty, the study of the whole rock will give a real idea about what happens in different geological environments. Thus, the current study is dealing with natural shale rocks.

It is recognized that shales possess a "fundamental grain-size" affects pore size and shape, and other poromechanical shale properties (<4 μm for smectite and <2 μm for illite (Eberl et al., 1993). The effect of chemical fluids on the grain-size distribution has not been studied thoroughly because of the limited availability of the

technology required. The classic methods of studying grain-size (dry and wet) are limited to fine and very fine sediments (silt and clay size) and generally measure properties of clay aggregates or agglomerates. One of the most relevant studies on shale and clay grain-size distributions was done by Eberl et al., (1993). They studied the effect of illitization on fundamental grain-size using the USGS MudMaster Software, which only works with mono-mineral samples. The modern techniques, such as Laser Grain Size Analyzer technique are able to study distribution properties of fine grain materials down to nanometer scale. This technology was used during the current study, detailed in Chapter 4, to evaluate the impact of chemical fluids on the grain-size structure of the Pierre Shale.

7.2. Literature review of smectite-illite transformation

It widely accepted that illite-smectite (I-S) mixed layer, which is the most abundant mineral class by volume in sedimentary rocks (Land, et al., 1997), is intermediate product of smectite-illite transformation. In addition, the illitization of smectite has been proposed as a major source of cements (quartz) in associated formations (Hower et al., 1976; Boles and Franks, 1979). Thus, smectite-illite transition has been thought to influence shale poromechanical properties, shale consolidation, pore water solution chemistry, source of pore-filling cements and degree of cementation, redox conditions, development of secondary porosity, and development and maintenance of abnormal pressures (Perry and Hower, 1970; Nadeau, et al., 2002). Sedimentary basin temperature increase upon burial has thought to be the main agent affecting change in I-S, such that is has been proposed as a paleo-temperature indicator; a few studies have shown the importance of

nonhydrostatic stress on the illite-smectite phase changes (Colten, 1985; Coulten-Bradley, 1987). From the geochemical point of view, workers have debated whether I-S represents a true phase in the thermodynamic sense or a kinetic intermediary in the approach to an equilibrium mineral assemblage during weathering and diagenesis. Many studies have been done on smectite to illite transformation under natural or experimental conditions to describe the processes that control the nature of clays during diagenesis, weathering, or anthropogenic activities. Most of these studies focused on the mechanism of the transformation and the final product obtained under different experimental conditions with an emphasis on the geochemical effects of transformation (such as pH, byproducts formed, rate of reaction under varying temperature conditions, etc).

Illitization of smectite, as related to increasing burial depth and temperature, has been studied in sedimentary basins by many authors such as Perry and Hower (1970), Weaver and Beck (1971), Hower et al., (1976), Boles and Franks (1979), Hoffman and Hower (1979), Nadeau and Reynolds (1981), and Horseman et al. (1996). Studies that are more recent have shown that the illitization process is more complex than previously described. Laboratory studies demonstrated that several chemical and physical factors, such as temperature, effective stress, kinetics, reacting fluid compositions, the nature of smectite interlayer cations, and the rock-water ratio, affect the illitization processes (Hoffman and Hower, 1979; Roberson and Lahann, 1981; Inoue, 1983; Howard and Roy, 1985; Inoue et al., 1988; Colten-Bradley, 1988; Whitney and Northrop, 1988; Whitney 1990; Whitney, 1992; Huang et al., 1993; Cuadros and Linares, 1995; Mosser-Ruck et al., 1999; Srodan, 1999).

7.2.1. Smectite-illite transformation mechanisms

Smectite-illite transformation mechanisms have been over the last 30 years some of the most debatable questions in clay mineralogy and environmental sciences from several standpoints. Most of the progresses in characterizing such mechanisms have been made in their application to burial diagenesis. In general, there are two questions that need to be answered for any smectite illitization mechanism to be understood (Srodan, 1999). The first question is how the illitization happens chemically (the source of the chemicals consumed during the illitization and where are the final products). The second question is how do illite crystals form from smectite crystals? Thus, the answer for the illitization of smectite questions can be divided into two aspects as the following paragraphs and according to Srodan (1999),

The chemical aspect

The first aspect of smectite illitization is a question of mass balance. Hower et al. (1976) wrote the illitization reaction as:

$$K + Al + Smectite \rightarrow Illite + Na + Ca + Fe + Mg + Si + H_2O$$

This reaction is nearly mass conservative (approximately the same amount of elements lost are and as are gained) and would lower the pH of the pore fluid.

Boles and Franks (1979) introduced another reaction for smectite to illite transformation:

$$K + Smectite \rightarrow Illite + Na + Ca + Fe + Mg + Si + OH + H_2O$$

This reaction decreases the mass of clay by more than 30%, produces large amounts of quartz, and raises the pH. Many authors argued in favor of one or the other mechanism, but an unambiguous conclusion has not yet been reached. Another open

debated question in illitization of smectite is the source of potassium, whether it comes from the shale formation (close system) or it migrates into shale from the surrounding formations (open system) (Weaver and Beck, 1971). Lynch et al. (1997) did one of the most relevant studies in this trend. They concluded that burial diagenesis of Frio Formation shales, Gulf of Mexico, was an open process that required addition of K_2O and Al_2O_3 and resulted in loss of silica from shale, which was sufficient to be the source of quartz overgrowth cements in a nearby sandstone formation.

The physicochemical aspect

The second aspect of illitization of smectite is the physicochemical, which tries to explain how illite crystals form from smectite crystals.

The first answer for this question was proposed by Hower et al. (1976). They introduced a solid-state, layer-by-layer mechanism. This mechanism can be summarized as the Al substitution in the neighboring tetrahedral layer leads to an increase in the smectite interlayer charge. This charge attracts potassium ions to the smectite interlayers, leading to smectite converting to illite. However, the effects of this polarization do not change the adjacent interlayers. The result is a R1 structure (I-S-I-S) formation. A R1 structure can be changed directly into a R3 structure (I-I-I-S) if the remaining smectite interlayers collapse after the R1 is completely formed. A R2 (I-I-S) structure cannot be formed by this mechanism.

The second, and hotly debated mechanism is the dissolution and crystallization mechanism introduced by many authors, such as Nadeau et al. (1985), Eberl and Srodon (1988), and Inoue et al. (1988). In this mechanism, two processes

occur: first is the dissolution of the starting smectite, and the second is the resulting crystallization of the interstratified illite-smectite mineral. The first step consists of the partial dissolution and hydrolysis of several smectite layers. This first step is necessary for chemical equilibrium between the smectite and a K-rich solution. The long duration leads to disappearance of the initial smectite interlayers, and lack of any evidence of fully smectite layers indicate that the starting smectite tends to dissolve to form the new I-S. Eberl and Srodon (1988), and Inoue et al. (1988) suggested that Ostwald ripening mechanism drives that illitization. But, Eberl et al. (1990) found that the distribution shapes of the new illite crystals are different from the known shapes resulting from Ostwald ripening. Srodon et al. (2000) found that distribution shapes of fundamental particle thickness follow a unique pattern like the coarsening produced from illitization.

Many researchers such as Berkgaut et al. (1994) and Righi et al. (1995), introduced a wetting and drying cycle mechanism to explain their shallow surface environmental data. However, until now, no widely accepted evidence has been offered and the impact of this mechanism on the mineral composition of soil remains to be evaluated.

7.3. Experimental protocols

In this chapter, the impact of pore fluid chemistry on clay minerals transformation and grain-size distribution is presented with results on two sets of parallel experiments at different pressure and temperature conditions. The first set is the room temperature conditions (RT). The second set of experiments was conducted

at high temperature-high pressure conditions (HTHP) (Fig. 7-1). The description for these two conditions will be given in the next few paragraphs.

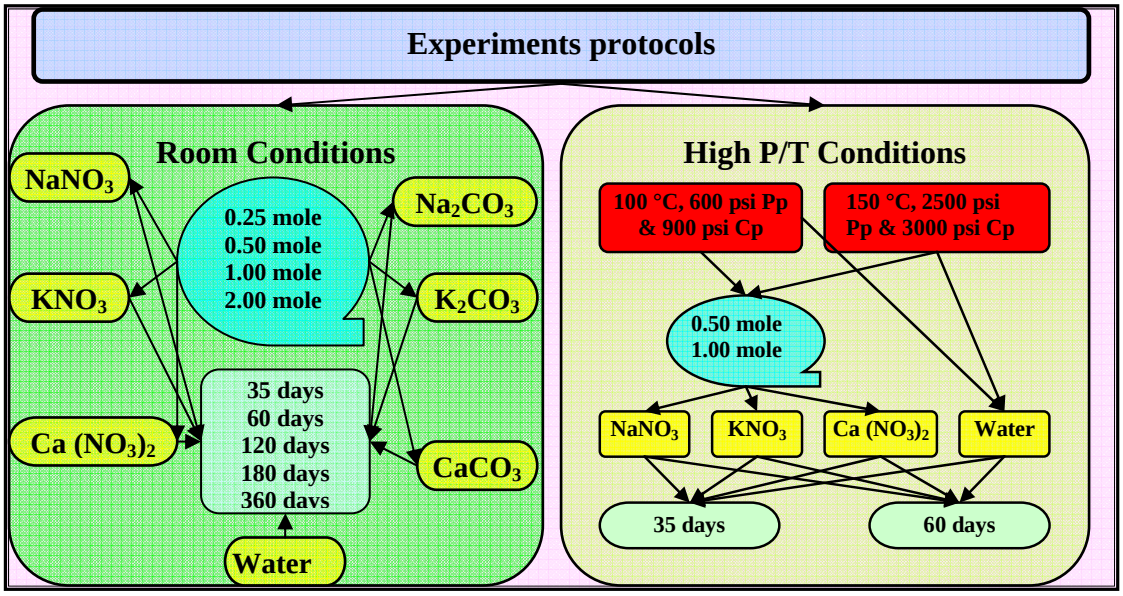

Figure (7-1): Flow diagram of the test conditions performed for smectite-illite transformation.

7.3.1. Room temperature conditions (RT)

To simulate ground surface conditions, a large shale sample is divided into parts (around 100 gm for each part). Each part is placed in a heavy-duty plastic vial with a sufficient amount of fluid (150 ml). The vials are labelled for each fluid and the lids are tightened to prevent any leaks. These are then left under ambient room conditions for the planned curing times (Fig. 7-1).

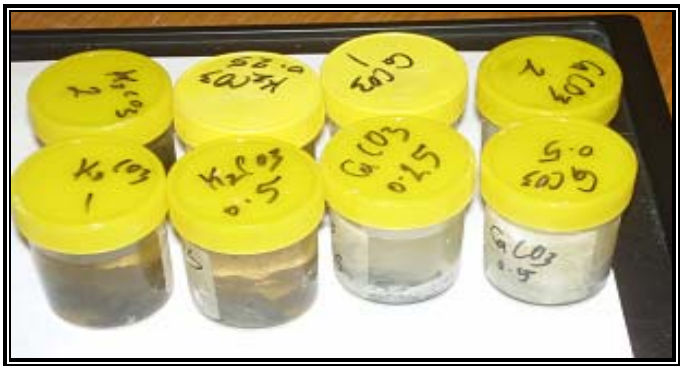

Figure (7-2): Shale samples (~ 100 gm) together with a sufficient amount of chemical solutions on heavy-duty plastic plugs at a lab temperature.

Because these experiments were not limited by having only one cell as in the HTHP conditions studies, distilled water, three nitrate fluids and three carbonate fluids ($NaNO_3$, KNO_3, Ca $(NO_3)_2$, Na_2CO_3, K_2CO_3, and $CaCO_3$) were used. Four different concentrations (0.25, 0.50, 1.00 and 2.00 molal) of each cation were cured for 35, 60,120, 180 and 366 days (Fig. 7-1). Because the solubility of $CaCO_3$ is very low, the preparation of $CaCO_3$ solutions with a specific concentration was difficult. Calcium carbonate fluids (water-calcium carbonate mixture) were prepared by adding the calculated amount of $CaCO_3$ powder to one liter of distilled water, and then the mixtures were added to the samples in the same way as with other chemical fluids.

The samples were left in these fluids for one year. After each curing time, a small sample was taken from each plug to be tested using XRD, Coulter Grain-Sizer Analyzer, and occasionally with SEM as described in Chapter 4.

7.3.2. High temperature high pressure conditions (HTHP)

In order to simulate the deep geological environmental conditions, such as in a wellbore or deep shale formations (up to 6,000 feet deep) cell no. I of HTHP Shale Apparatus was used. Figure (7-3) shows the diagrammatic sketch for the internal and external design of this cell. This cell has the ability to hold constant temperature of up to 300 °C for more than 4 months. In addition, it has the ability to hold both confining pressure and pore pressure up to 10,000 psi. Cylindrical disk samples (25 mm diameter and 3 mm thick) were prepared from Pierre Shale in the manner described in Chapter 5. The sample was placed between the two porous frits. The two frits and the sample are sandwiched by two Pyromet™ end pieces with the same diameter. Each end pieces has two fluid access ports to allow communication

between the flowing test fluids and the porous frit, which allows the fluid to contact with the sample surface. This system is jacketed using heat-shrink Teflon jackets. Two compression rings, serve to seal the sample and pore fluid from the confining fluid. During the tightening processes the system is exposed to 10 psi unconfined uniaxial compressive stress in order to not allow any space between the sample and the frits or frits and end pieces. Then, the upstream end piece is connected to two upstream pressure capillary tubes via cone-in-cone compression fittings, and by the same way, the downstream is connected to two downstream pressure capillary tubes. The tubes lead to the pore pressure pumping system including a backpressure regulator and ELDEX fluid metering pump.

To prevent any confining pressure leaking, after the system was placed in the pressure cell, the cell head closure was screwed on and tightened by 8 bolts using the procedure described in Chapter 5. After that, the cell wasplaced inside the furnace (Fig. 7-3). Next, the confining pressure and both upstream and downstream pore pressure inlets were connected to their pumps and to the pressure data acquisition system. The furnace was also connected to a temperature controller and an internal thermocouple was connected to the temperature data acquisition system. After that, gradually both confining pressure and pore pressures were increased (50 psi for each step) using mineral oil for confining pressure and distilled water for pore pressure fluid. To prevent leakage through the jacket, a 100 psi difference was kept between the confining pressure and the pore pressure. When the pressures reach the planned conditions, all valves are closed and the sample was left for 24 hours to insure complete saturation by distilled water. After the 24 hours, water was flushed from

both upstream and downstream and was replaced by a chemical solution under isopressure conditions. At this point, temperature of the cell was increased, with readjustments being made to the pressures using combined HPLC pump/back pressure regulators or ISCO pumps, depending on availability. When pressure and temperature conditions reach the planned conditions, the sample was left at this condition for up to four months.

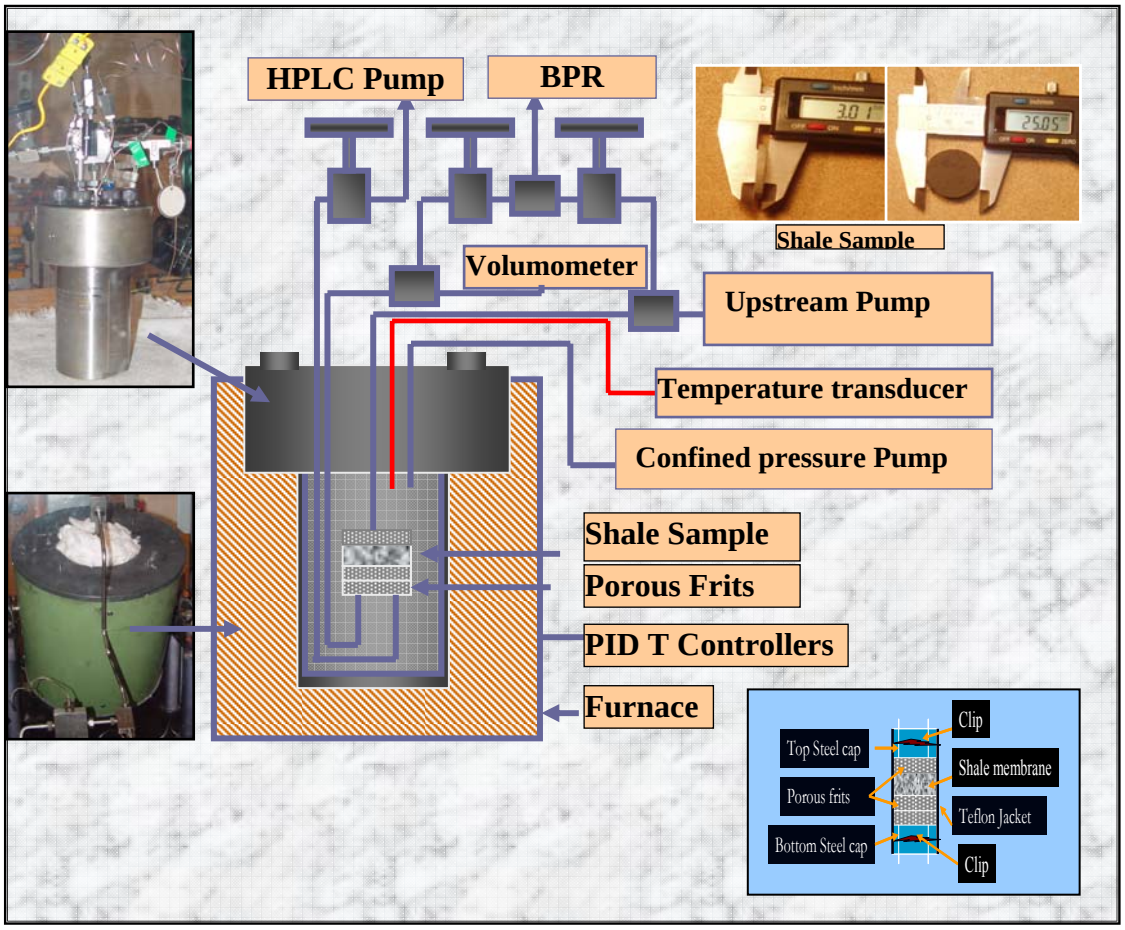

Figure (7-3): Initial HTHP cell no. I schematic design.

The experiments were performed under two different conditions:

1. 100 °C temperature, 600 psi pore pressure and 900 psi confining pressure, and
2. 150 °C temperature, 2500 psi pore pressure and 3000 psi confining pressure.

$NaNO_3$, KNO_3 and $Ca(NO_3)_2$ were used by 0.5 mole and 1 mole concentration for the two conditions (Fig. 7-1).

After the designated curing time the sample is removed from the HTHP hydrostatic cell (cell no. I) and tested by XRD, grain-size analyzer and sometimes by SEM to study the impact of these conditions on mineral transformations and changes in the grain-size distribution. The following paragraphs will discuss the results of these studies, depending on conditions.

7.4. Results and discussion

7.4.1. Room-temperature conditions

All the room conditions treated samples were subject to XRD and grain size analysis. Fifteen samples were selected for testing by SEM. Discussions and interpretations for the results will be given in the following sections based on the techniques that were used.

7.4.1.1 XRD studies

In the XRD analysis, focus is placed on the first fifteen 2θ of the XRD diffractograms as changes in clay mineralogy is of interest. In general, the high concentration fluids (1 mole and above) effect negatively the clay minerals, leading to a reduction or sometimes the disappearance of clay mineral peaks. With time, these diminishing peaks appear again as a result of the recrystallization of these minerals. On the other hand, the low concentration fluids (less than 1 mole) lead to intensifying clay mineral peaks because of clay mineral transformation or clay structural changes. However, this effect decreases and the peak intensity is found to decline over the time. Clay mineral transformations were recorded as smectite transforms to smectite-

illite mixed layer or to illite directly in the presence of K ions (KNO_3 or K_2CO_3). Smectite structural change was recorded with water and both Na and Ca ions ($NaNO_3$, Na_2CO_3, $Ca(NO_3)_2$ and $CaCO_3$). The effect of these fluids as compared with the natural sample or the water treated samples will be discussed separately.

7.4.1.1.1. Nitrate fluids

Sodium nitrate ($NaNO_3$)

Smectite is the clay mineral most affected by sodium nitrate. Mostly, $NaNO_3$ had an effect of increasing smectite peaks. Smectite peak intensity only decreased with 2 mole $NaNO_3$. The other concentrations (0.25, 0.5 and 1 mole) showed an increase in smectite intensity with some variation over time (Fig. 7-4). The most interesting concentration is one mole, since smectite intensity reaches the maximum after 35 days and then starts to decrease with time. Meanwhile, the peak moves towards higher 2θ, but does not approach a smectite-illite mixed layer. The 0.5 mole samples showed some increase in smectite peak intensity at 60 days curing time; after that, it starts decrease again overtime. The behaviors of clay mineral crystallinity indices in the presence of $NaNO_3$ fluids with time were represented in Figure (7-10). Kaolinite crystallinity indices seem unaffected by the presence of $NaNO_3$ fluids most of the time. While smectite crystallinity indices (CI's) show a general decrease with increasing concentration and time, except in the first 2 months the CI's show an increase with low concentration (with the maximum CI recorded as 20 for 0.25 moles after two months). Illite showed an irregular pattern, since it increases or decreases with different concentrations or different times (Fig. 7-10).

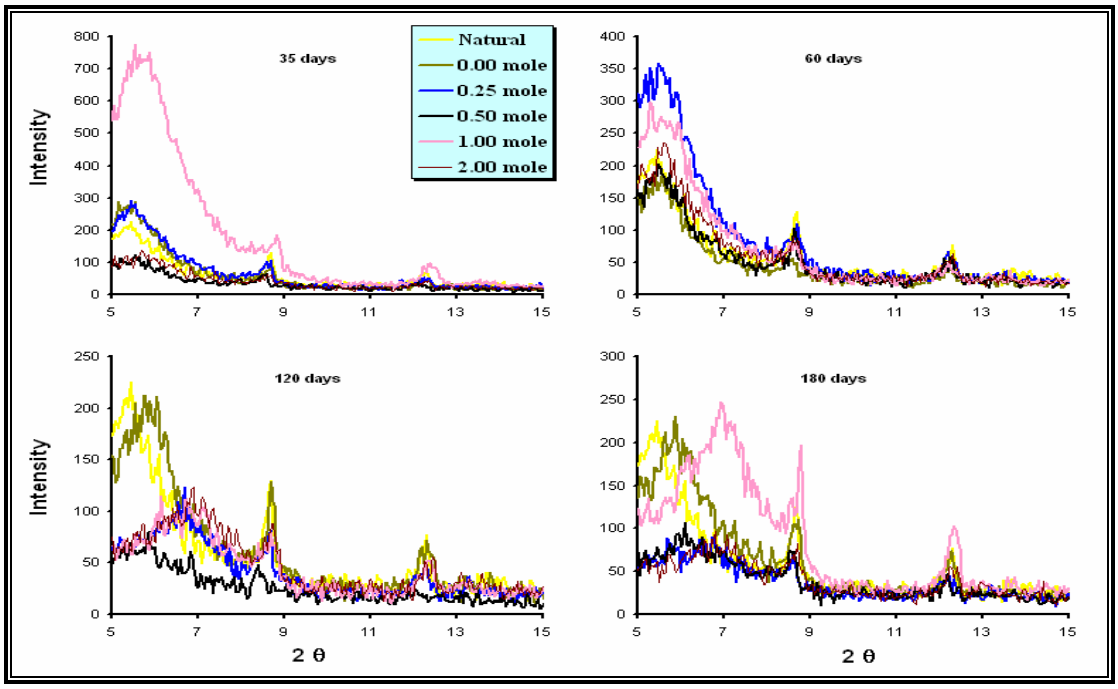

Figure (7-4): XRD diffractograms for sodium nitrates at room conditions and different time.

Calcium nitrate ($Ca(NO_3)_2$)

Calcium nitrate has negative effect on all clay minerals by decreasing clay mineral peak intensities (Fig. 7-5). This effect increases with increasing calcium nitrate concentration, except for the 0.5 mole concentration, which showed its maximum negative effect within the first 60 days, and then it follows the above behavior. This negative effect decreased over the time, meaning the destroyed mineral crystal structure may start to recrystallize. One mole concentration showed some isolation behavior over the time; hence, it showed an increase in smectite peak intensity in the 60 day samples, decreasing to the lowest peak intensity in the four month samples, and increasing to the highest peak intensity with the six month samples (Fig. 7-5). One-year samples showed the disappearance of clay minerals which might be due to the masking of these minerals by an overgrowth of amorphous materials, such as amorphous or gelatinous $CaCO_3$, which can be formed as a result

of calcium-organic matter reactions. Since these materials are amorphous, they can not be detected by XRD. The CI's in Figure (7-10) showed this negative effect clearly, especially with smectite. Illite showed some improvement in its crystallinity in the presence of $Ca(NO_3)_2$ especially with the 180 day samples which recorded a maximum CIs as 25 for 0.25 mole. As usual, kaolinite behaves as the most stable clay mineral, generally unaffected by exposure to the different solutions over time It showed only a slight negative effect by $Ca(NO_3)_2$ with all different concentrations and curing times.

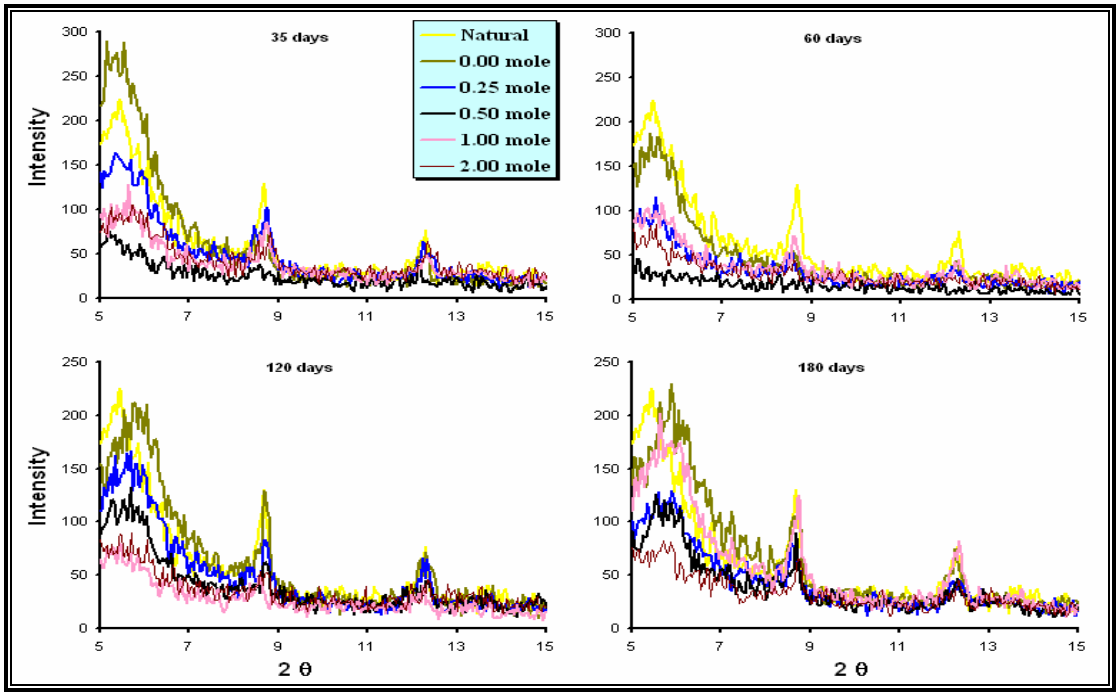

Figure (7-5): XRD diffractograms for calcium nitrates at room conditions and different time.

Potassium nitrate (KNO_3)

In the presence of potassium nitrate fluids, smectite showed a decrease in its peak intensity and shifted to a higher 2θ depending on KNO_3 concentration and curing time. Smectite peak intensity decreased with increasing concentration within the first 60 days. However, with four-month samples, smectite nearly disappeared in

all concentrations. Six-month samples showed some smectite peaks again. These new smectite peaks showed the same phenomena as the old ones; hence, their intensities decrease with increasing concentrations, except 0.5 mole samples, which showed the lowest smectite intensity. In addition, the position of these peaks shifted to higher 2θ compared to the old peaks, possibly indicating a new smectite phase. The movement of these new smectite peaks seems not to be effected by additional reaction time. They moved towards the smectite-illite mixed layer peak with all concentrations and all times. Illite peaks showed an increase in intensities when exposed to potassic solutions. 0.5 mole KNO_3 fluids showed the maximum illite peak intensity within the first 35 days then 0.25 mole solutions showed the maximum intensity for all the rest of the curing times (Fig. 7-6). These increases in illite peak intensities are likely due to the recrystallization of the destroyed smectite, forming a new illite phase. Kaolinite showed some negative effects. These effects may be due to the masking of the kaolinite by the new amorphous materials, which cannot detect by XRD.

Crystallinity indices for the clay minerals that are treated by KNO_3 showed the maximum negative effect on smectite and the maximum positive effect on illite as compared with samples that are treated by $NaNO_3$ and $Ca(NO_3)_2$ (Fig. 7-10).

These changes lead to the conclusion that KNO_3 solutions force smectite crystals to transform to illite crystals even at room temperature. The lower concentrations (0.25 and 0.5 mole) are better than the higher concentrations (1 and 2 mole) possibly, because the illite and smectite structures are weak enough to be destroyed by high concentration solutions. That is, in general high ionic strength solutions destroy clay mineral structure as indicated by XRD.

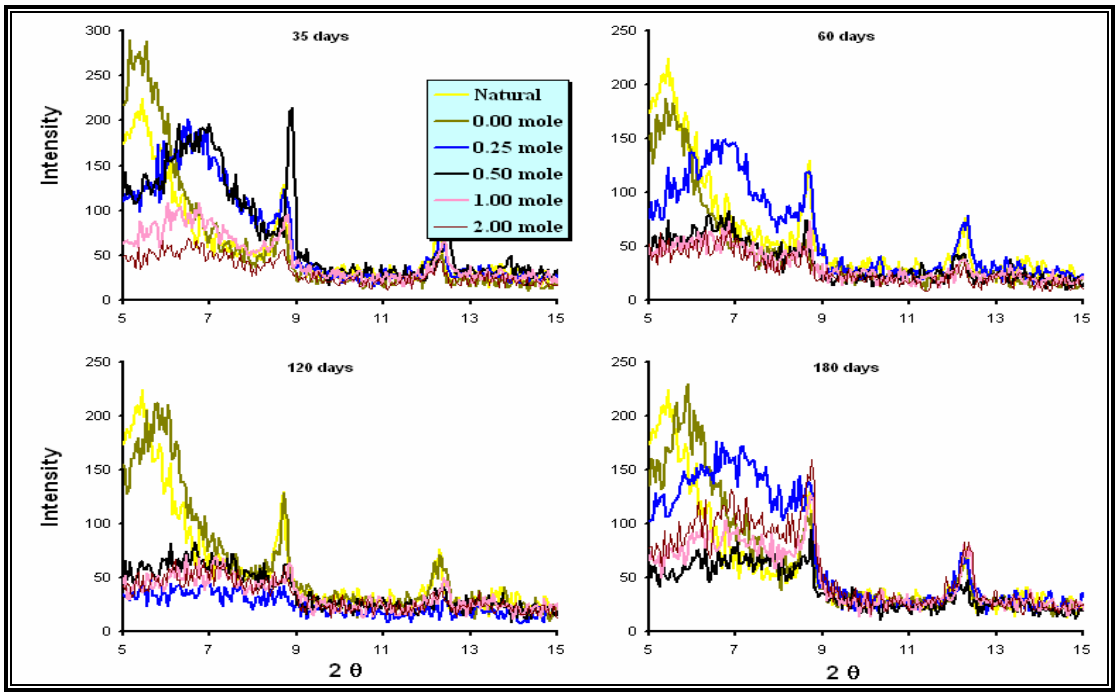

Figure (7-6): XRD diffractograms for potassium nitrates at room conditions and different time.

7.4.2.1.2 Carbonate fluids

Sodium carbonate (Na_2CO_3)

The effect of sodium carbonate is clearly shown with smectite peak intensity. 0.25, 0.5 and 1 mole sodium carbonate samples showed smectite peak intensities higher than natural (initial) and water-treated samples. Within those three concentrations, the smectite peak intensity decreases with increasing concentration, except within 35 days when the 1 mole sample showed maximum smectite peak intensity. This effect decreased with increasing time (Fig. 7-7). The sample that was exposed to 2 mole sodium carbonate showed decreases in smectite peaks with different curing times. This is likely due to distortion of the smectite lattice structure. Sodium carbonate solutions produced no change in smectite peak position within the first 60 days, but with increasing time the position start to shift toward higher 2θ but without increasing all the way to the smectite/illite mixed layer peak position. Sodium

carbonate solutions had a minimum effect on the other two clay minerals as compared to the other chemical fluids used in the current study.

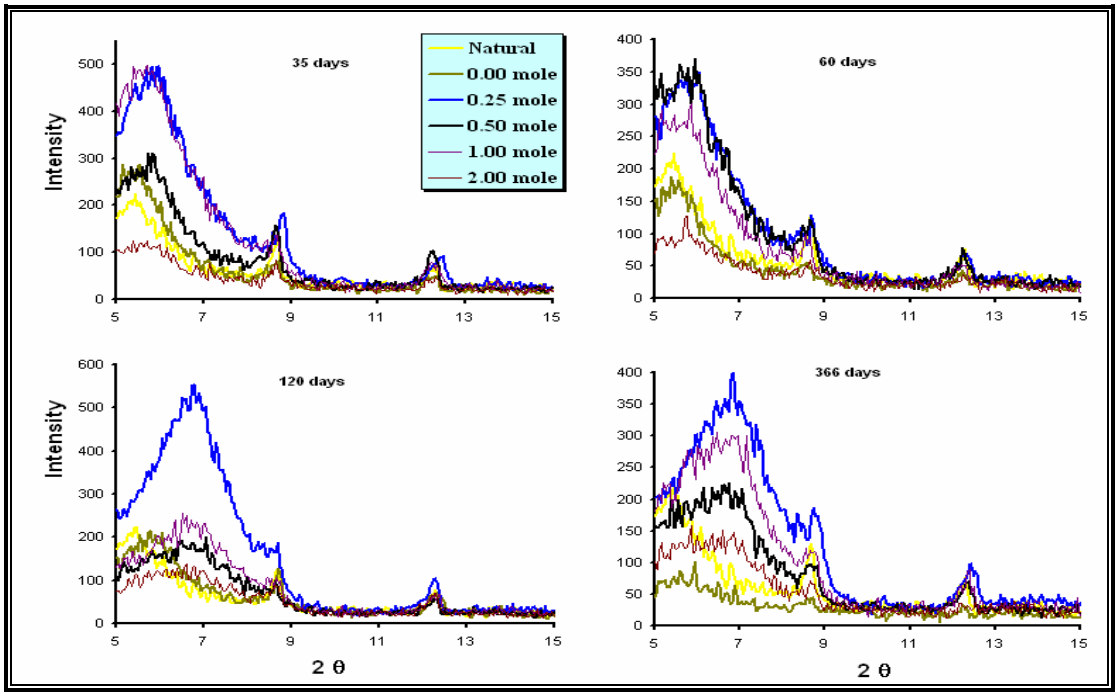

Figure (7-7): XRD diffractograms for sodium carbonates at room conditions with different time.

Effects of Na_2CO_3 on different clay minerals can also be seen from the crystallinity indices (Table 7-1 and Fig. 7-10). It is easily seen that illite and kaolinite crystallinity are not affected by Na_2CO_3 solutions while smectite crystallinity is positively affected.

Calcium carbonate ($CaCO_3$)

Most of clay mineral peaks of the samples that were treated with calcium carbonate/water mixture showed negative effects with increasing concentration (ionic strength) and time. Smectite peaks show some increase as compared to the natural sample within the first 35 days for 0.5 mole and 2 mole solutions and within 60 days. The samples at 2 mole and 0.25 mole also showed smectite peak intensity increases (Fig. 7-8). After that, all solutions showed a decrease in all clay minerals peak

intensities as compared to the natural sample. Within 240 days, sample peaks for clay minerals start to grow again. This means the destroyed mineral crystals may be starting to re-crystallize within this time. One-year samples show a complete disappearance of clay minerals that may be due to the masking of these minerals by overgrowth of calcium rich materials.

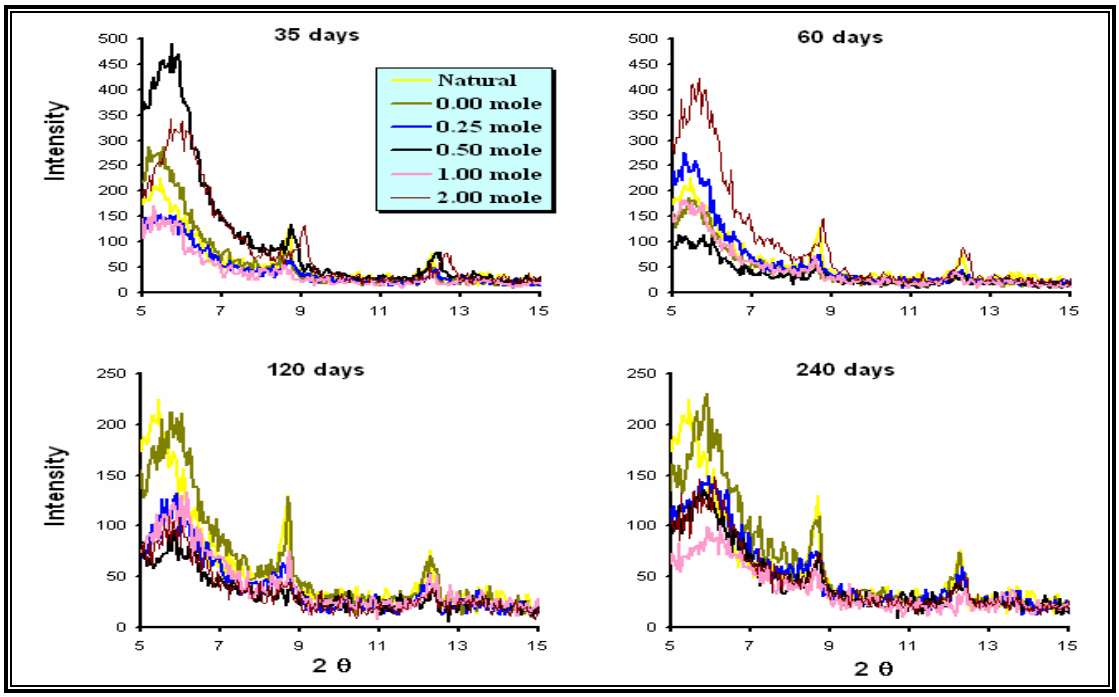

Figure (7-8): XRD diffractograms for calcium carbonates/water mixture at room conditions with different time.

The clay mineral crystallinity index table for $CaCO_3$ fluids shows that $CaCO_3$ had the most negative effect on the all clay minerals, especially illite, as compared with the other fluid used in the current study. In general smectite CI's decrease with increasing time until 120 days curing time and decrease with increasing concentration. After that, the higher concentration showed an increase of CI's as compared with natural and water treated samples. CaCO3 also affects illite and

kaolinite more negatively than any other solutions, especially within the first 60 days. Then, this negative effect decreased with increasing time (Table (7-1), and Fig. 7-10).

Potassium carbonate (K_2CO_3)

The effect of potassium carbonate on clay minerals is dependent on its concentration and curing time. 2 mole concentration solutions show that the entire clay mineral primary peaks have nearly disappeared by the sampling time. This may be because potassium carbonate activity (or ionic strength) is high enough to destroy the clay mineral structure or because newly formed potassium materials mask clay minerals. For 60 and 120 days samples (Fig. 7-13), one-mole samples showed changes in smectite peaks to smectite/illite mixed layer and illite. Both 0.25 and 0.5 mole solutions showed a positive effect on illite and this effect increased overtime. Meanwhile, these concentrations showed negative effects on smectite by two ways: by decreasing its peak intensity and shifts towards the smectite/illite mixed layer peak position.

The crystallinity index (Table (7-1) and Fig. 7-10) shows that K_2CO_3 solutions have the second most negative influence on smectite, after KNO_3 solutions. On other hand, K_2CO_3 had the most positive effect on both illite and kaolinite as compared to other solutions. Recorded CI's were the maximum for the 120 and 180 days samples for illite, and 120 days samples for kaolinite. These effects lead to the conclusion that both K_2CO_3 and KNO_3 showed illitization of smectite at room temperature.

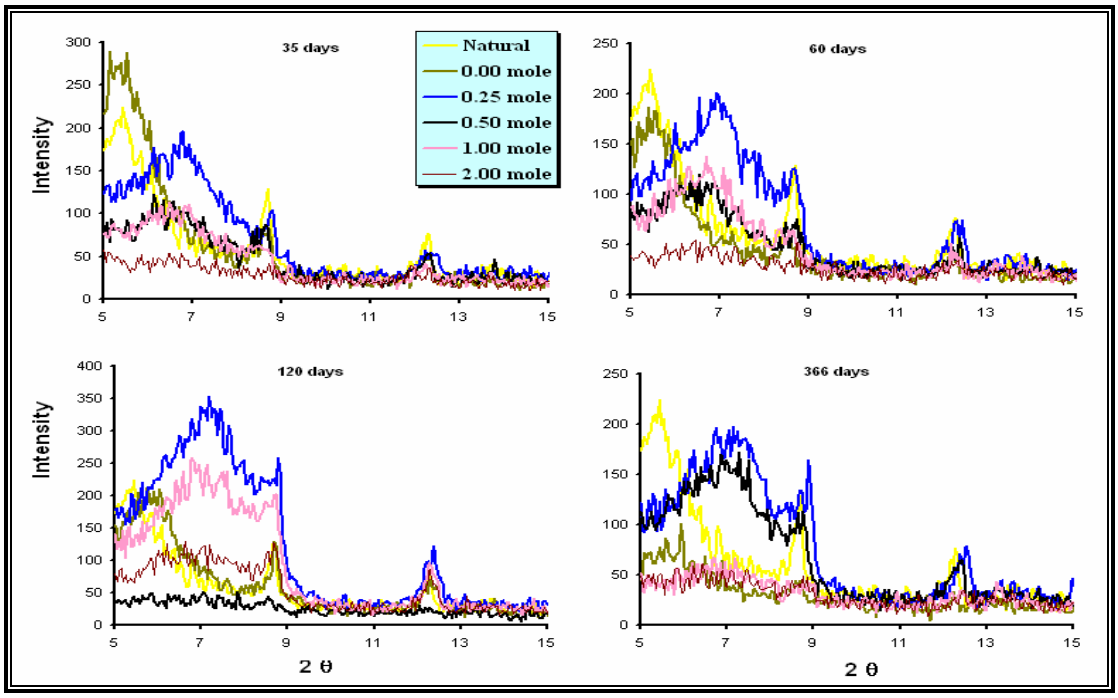

Figure (7-9): XRD diffractograms for potassium carbonates at room conditions with different times.

In general, XRD studies for Pierre Shale samples treated by different chemical fluids at room temperature conditions indicate that:

1- Clay minerals are very sensitive and easily influenced by changes in solution chemistry even at room temperature. These effects are controlled by type and the activity of the fluids.

2- Smectite is the most easily influenced clay mineral since its crystallinity is negatively impacted by most of the fluids used in the current study.

3- Kaolinite is the most stable since it did not show any effect by the fluids that are used in the current study.

4- Na-fluids had the lowest effect on clay minerals. They positively influenced smectite crystallinity, especially with low concentration and early curing times.

5- Ca-fluids behave in between that of Na and K fluids.

Table (7-1): Crystalinity indices of samples treated at room conditions.

Fluid		Smectite					Illite					Kaolinite				
	Time (days)	**35**	**60**	**120**	**180**	**366**	**35**	**60**	**120**	**180**	**366**	**35**	**60**	**120**	**180**	**366**
Water	**0.00 mole**	17.667	12.667	8.75	12.667	8.000	-	-	9.000	7.330	5.000	-	-	8.000	9.000	10.000
$NaNO_3$	**0.25 mole**	17.000	17.714	5.667	5.400	2.400	-	-	7.200	15.000	4.667	-	-	6.667	7.3333	15.000
	0.50 mole	14.667	13.667	7.500	6.000	3.000	8.667	-	12.000	12.000	6.000	10.000	5.000	4.000	8.000	4.667
	1.00 mole	16.400	12.000	4.333	8.167	3.857	-	-	5.667	13.333	12.000	-	-	7.692	9.269	11.000
	2.00 mole	10.250	14.000	3.142	2.428	3.500	8.000	4.000	7.000	7.500	7.000	3.000	8.000	5.333	10.000	9.000
$Ca(NO_3)_2$	**0.25 mole**	6.000	8.500	8.750	3.600	1.692	13.000	12.000	16.000	9.000	5.000	18.000	5.000	20.000	3.077	10.000
	0.50 mole	5.667	6.500	5.750	6.000	2.400	4.000	10.000	10.00	25.714	7.000	13.571	5.882	7.143	10.714	6.000
	1.00 mole	6.000	4.667	4.000	5.600	3.428	16.250	11.250	7.000	16.000	8.000	7.500	7.142	10.500	11.000	12.000
	2.00 mole	3.400	7.667	3.500	2.750	2.400	12.222	14.000	5.000	11.250	4.000	10.000	6.000	6.500	7.143	4.500
KNO_3	**0.25 mole**	8.285	4.375	2.714	3.300	1.176	30.000	19.333	11.333	13.500	8.500	20.000	21.500	11.000	12.000	6.500
	0.50 mole	4.500	2.439	1.454	1.764	1.500	22.00	30.000	11.000	11.111	4.667	18.571	7.692	6.250	6.667	11.000
	1.00 mole	3.846	1.889	1.500	1.600	1.750	14.667	21.000	5.200	13.333	10.000	14.000	4.667	8.333	16.000	8.000
	2.00 mole	1.5882	2.500	1.667	2.727	1.700	10.000	13.500	10.000	22.000	11.000	9.000	10.000	3.500	20.000	9.000
Na_2CO_3	**0.25 mole**	18.000	13.500	25.833	13.500	11.250	8.000	-	9.167	8.000	14.000	-	-	11.500	8.8809	18.000
	0.50 mole	16.125	15.875	6.571	9.500	4.375	20.000	-	25.000	18.846	4.000	16.000	-	10.000	17.3070	13.000
	1.00 mole	18.000	14.444	8.000	7.667	8.500	-	-	13.000	7.000	6.000	-	-	11.250	12.500	15.000
	2.00 mole	6.750	8.667	5.000	4.785	2.625	19.000	7.500	9.5	21.000	5.000	8.000	4.000	18.000	14.000	5.000
$CaCO_3$	**0.25 mole**	18.667	8.500	5.000	6.000	2.000	-	10.000	5.833	7.000	5.000	-	12.000	9.000	10.000	18.667
	0.50 mole	7.000	3.500	7.125	5.000	-	-	8.000	6.000	6.000	-	7.000	11.4257	2.333	6.500	7.000
	1.00 mole	14.667	6.571	3.8	3.333	-	-	14.285	10.000	12.000	-	-	7.000	9.000	8.000	14.667
	2.00 mole	22.571	7.500	7.75	11.714	11.333	5.000	2.000	9.000	10.000	8.750	5.000	14.000	7.000	8.000	22.573
K_2NO_3	**0.25 mole**	7.181	6.000	11.750	1.375	2.350	14.000	16.333	31.944	8.000	10.750	5.000	15.000	27.000	7.000	8.000
	0.50 mole	3.272	4.923	1.555	2.250	3.100	12.000	10.000	4.000	33.000	12.667	6.5000	13.500	10.000	7.000	6.3333
	1.00 mole	4.142	4.428	7.444	3.666	1.500	4.500	5.294	26.750	9.500	4.000	5.000	10.000	21.500	4.000	11.000
	2.00 mole	2.000	2.250	3.364	1.916	1.388	11.00.	24.285	21.000	14.411	9.000	20.000	8.000	26.500	14.000	10.000

- *can not determine*

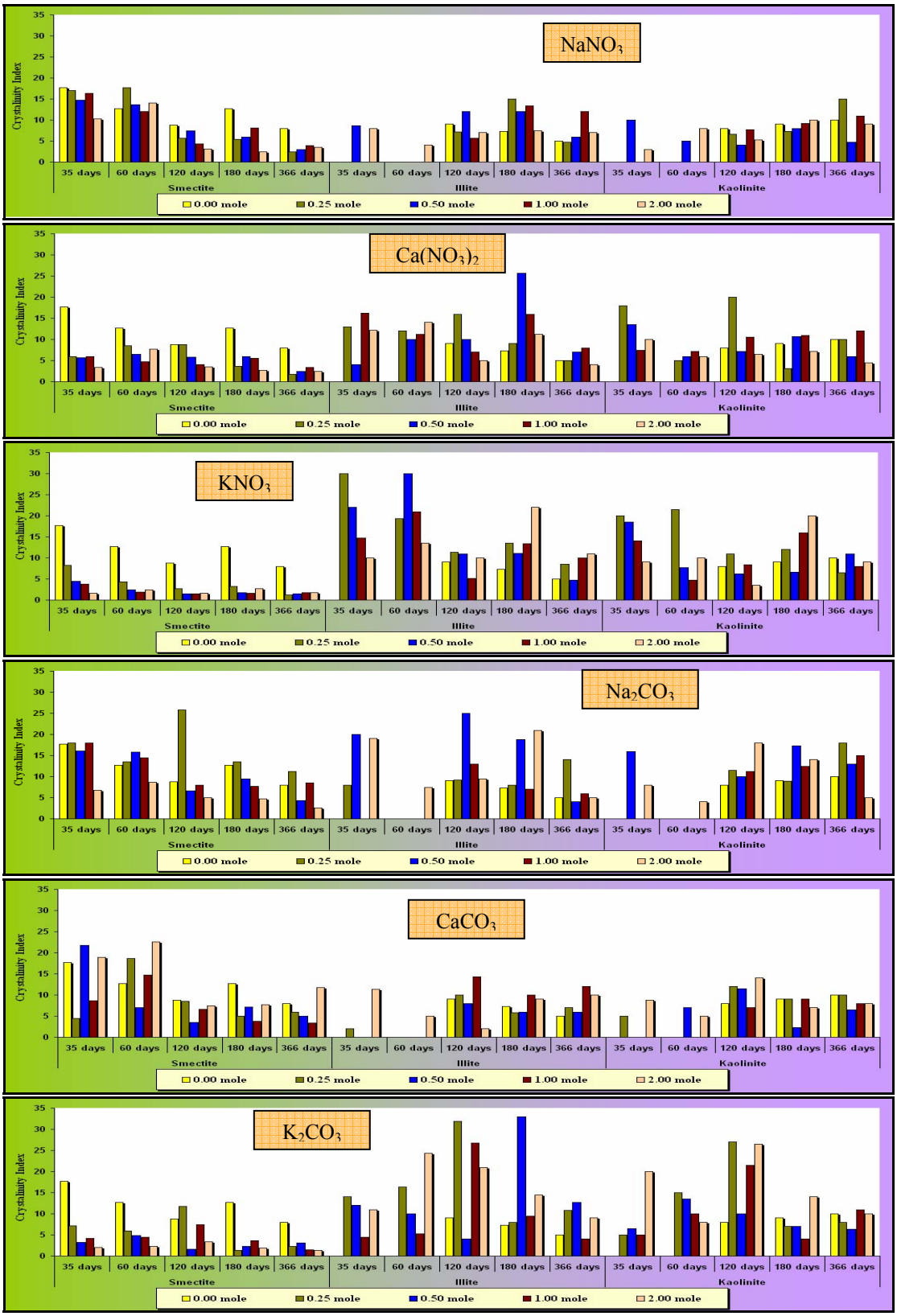

Figure (7-10): Clay minerals crystalinity indices for different chemical fluids at room temperature for different curing times.

6- K-fluids had the maximum effects on the clay minerals. They negatively affected smectite at all concentrations and at all curing times. But they positively affected illite. That means K-fluids attacked smectite crystals to form a new illite phase, even at low temperatures. This leads one to favor the non-isochemical transformation models of smectite-to-illite. Illitization of smectite appears to require an external source of potassium ions. During burial diagnesis, this could accompany the "albitization" of potassium feldspars in adjacent sandstones, as suggested by several authors such as Lynch et al., (1997).

7- Carbonate fluids had more effect on clay minerals than nitrate solutions. This is likely because of the higher ionic strength of carbonate solutions at similar concentrations.

8- Impacts of solution chemistry used in the current study on Pierre Shale clay mineralogy are dependent on the solutions ionic strength. These impacts increase with increasing fluid ionic strength.

7.4.1.2. SEM and EDX Studies

From all the room temperature samples, fifteen samples were chosen to run under the SEM-EDX system. Some of SEM images and EDX charts are represented on figures from 7-11 to 7-17. Detailed studies of these images and EDX analyses reflect the following:

1- There is a reduction in porosity because of the swelling of smectite as a result of its reaction with water, $NaNO_3$, $Ca(NO_3)_2$, Na_2CO_3 and $CaCO_3$ (Figs. 7-11, 7-12, 7-13, 7-15 and 7-16). Chapter 5 discussed the reduction in permeability with high concentrations of these nitrates fluids within only three days. One disclaimer on

this observation is the affect of drying and exposure to vacuum during sample preparation for the SEM. Nonetheless, there are clear differences in the clay mineral structures between the initial and reacted samples viewed with SEM.

2- A new phase of clay mineral formed because of fluid-clay mineral reactions. This new phase may be illite when KNO_3 and K_2CO_3 are used (Figs. 7-14 and -17), or smectite when $NaNO_3$ and Na_2CO_3 are used (Figs. 7-11 and- 15).

3- The reaction of smectite with KNO_3 and K_2CO_3 produces a new illite phase. This new illite phase looks like spots over the smectite platelets (Fig. 7-14 and 17). The growth of this new phase continues with time (Fig. 7-27).

4- Both new phases of illite and of smectite start with K for illite or Na for smectite but require Si, Al and Ca from the surrounding minerals.

5- $CaCO_3$ particles precipitate as syntaxial overgrowths on different shale components including quartz. They form new cementing material and infill the pore spaces in the shale, which decreases porosity and permeability (Fig. 7-16).

6- At room temperature $CaCO_3$ solutions were the only chemical fluids that seem to attack some of quartz crystals (Fig. 7-16). Pyrite framboid crystals are easily reacted with all of the chemical fluids including water (Fig. 7-11 and -14). These reactions introduce free Fe and S ions in the media. Redox conditions were not controlled during these experiments thus the extent of the influence of pyrite and oxidation of organic matter on the experimental results is not known.

7- Smectite-illite transformation at room temperature seems to follow dissolution and crystallization mechanism that introduced by many authors such as Eberl and Sordon (1988).

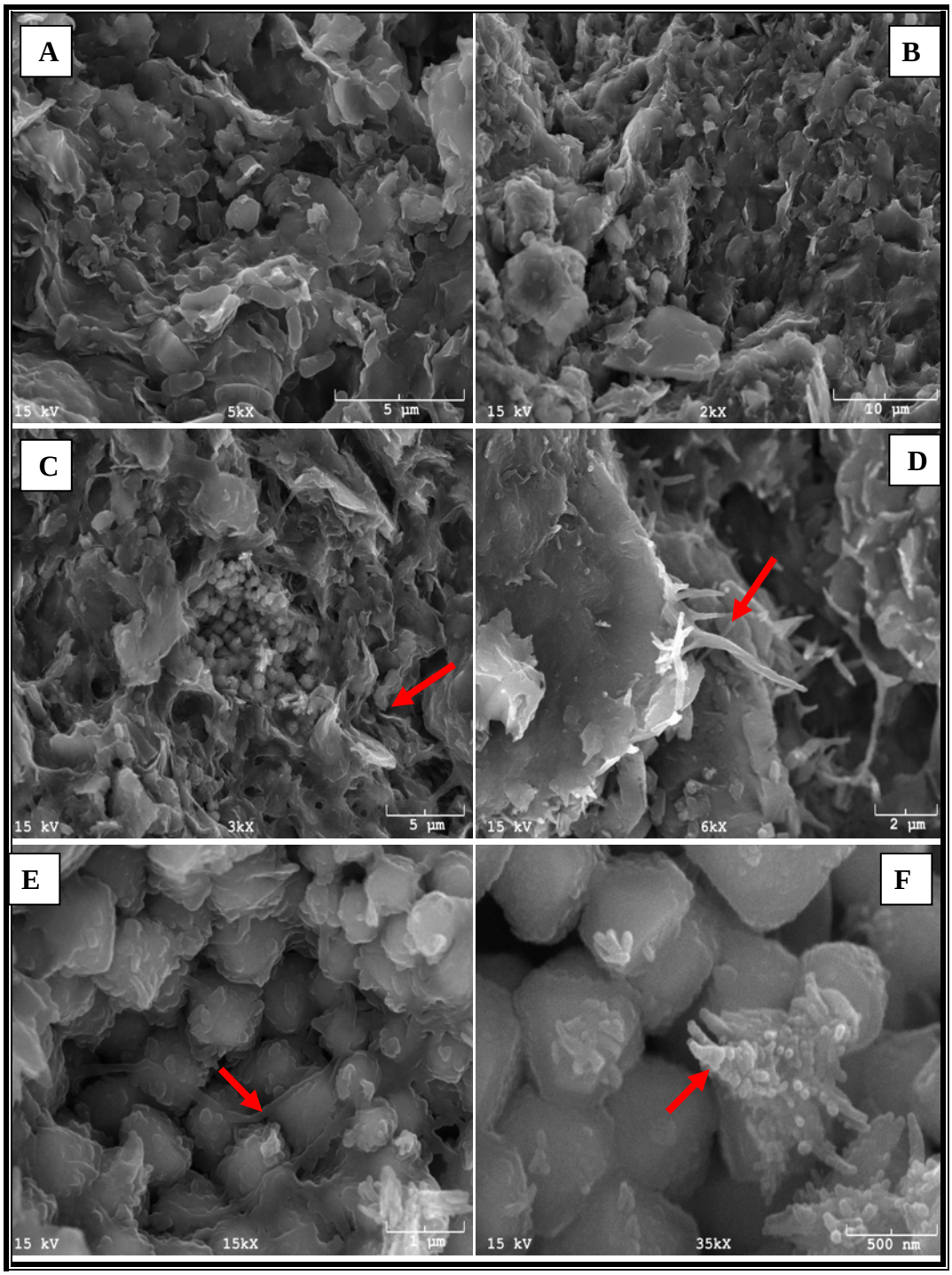

Figure (7-11): SEM photographs show the results of water reaction with Pierre Shale at room temperature.

A& B) Porosity reduction due to swelling of smectite clay mineral

C& D) Growth of new materials on clay minerals and their edge, D iron materials

E& F) Pyrite crystals covered by Fe-rich clay (E) and Iron sticks (F)

Left column for sample treated for 6 months and right column for sample treated for 12 months

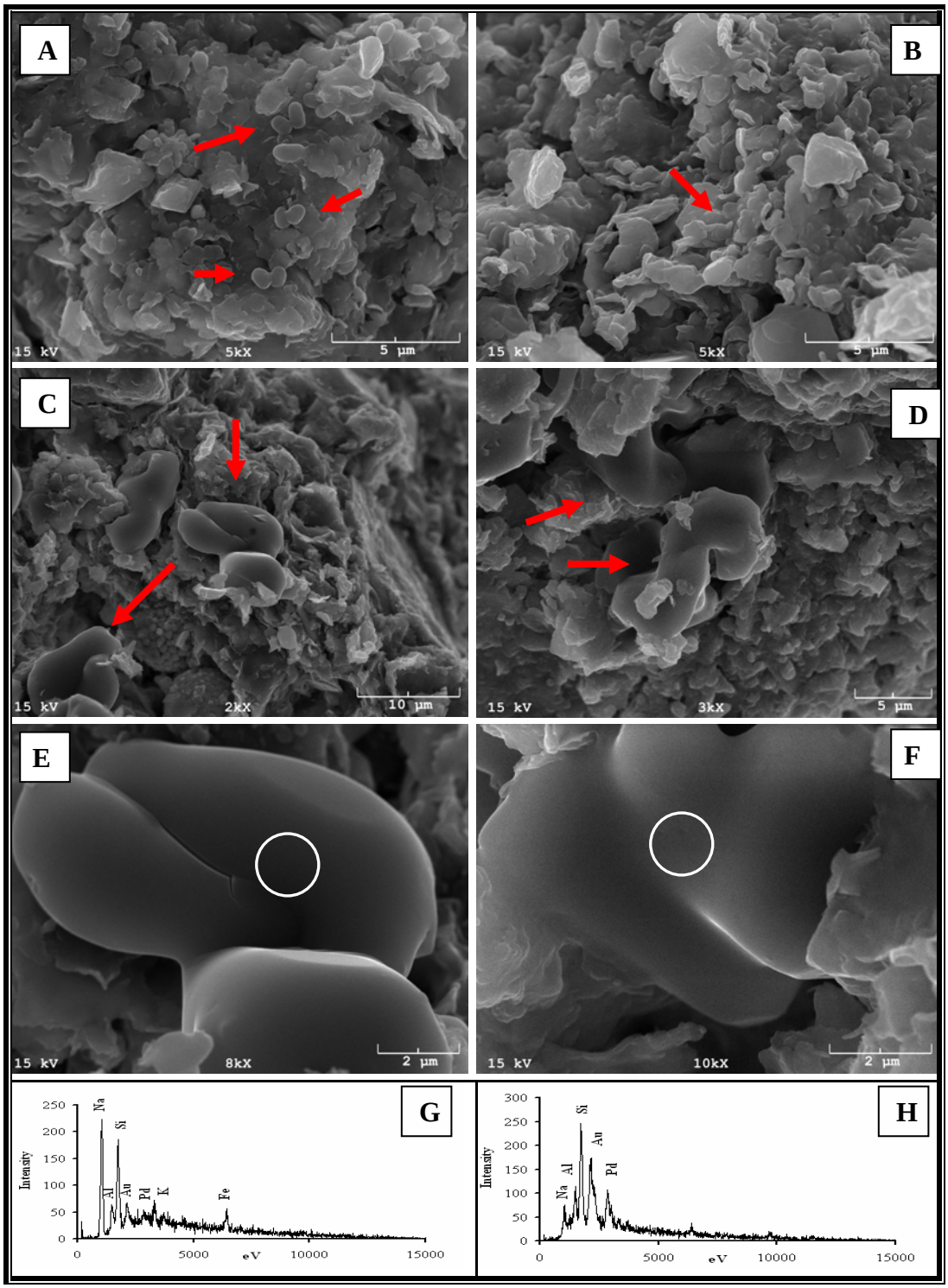

Figure (7-12): SEM photographs show the formation of a new clay phase because of $NaNO_3$ reactions with clay minerals at RT.
A& B) new Na-rich "bodies" attached to smectite platelets
C, D, E& F) shape of the new bodies
G& H) EDX analyses for the Na-rich bodies

Left column for sample treated for 6 months (1 mole) and right column for sample treated for 12 months (0.5 mole).

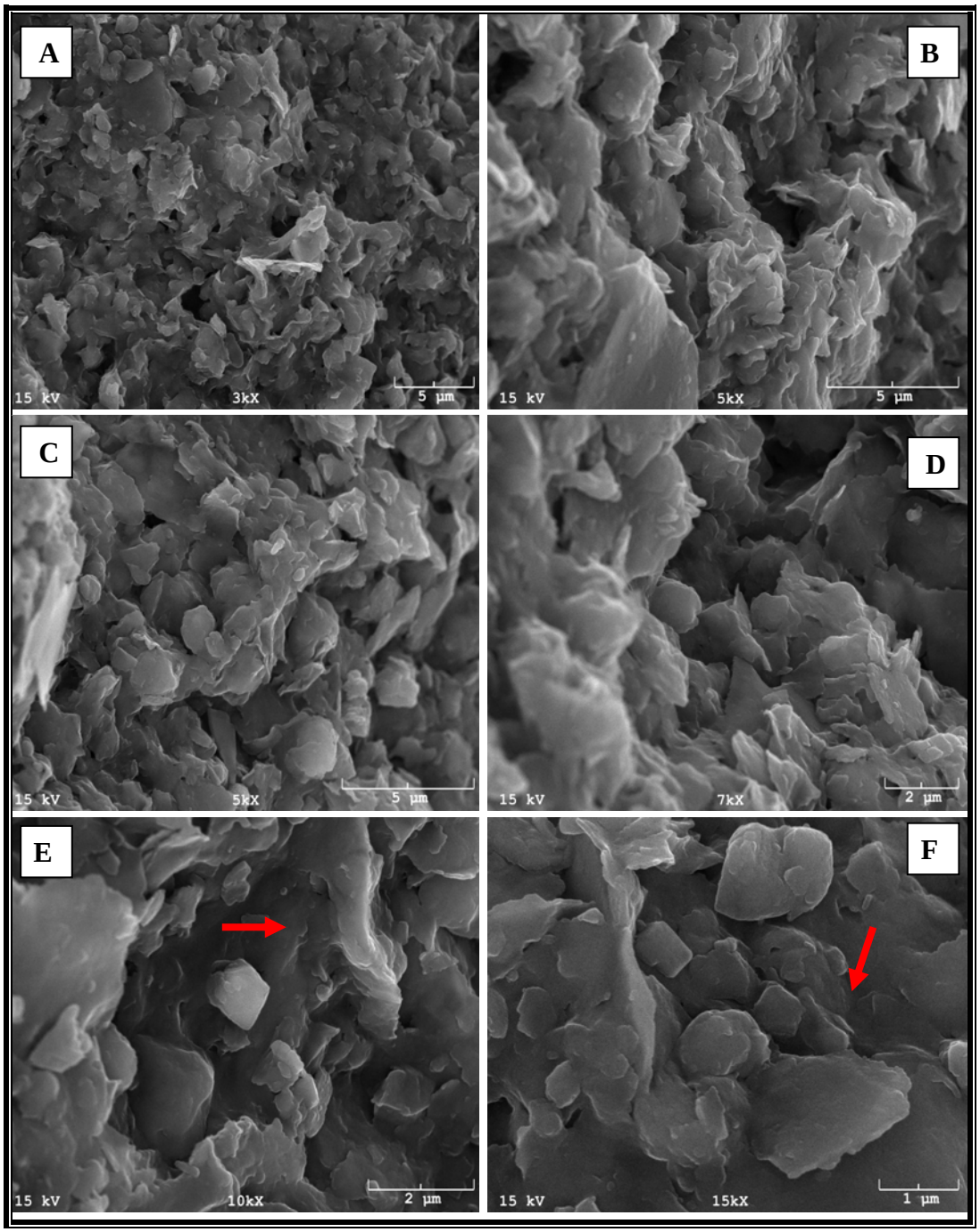

Figure (7-13): SEM photographs show the changes smectite platelets as a result of I mole $Ca(NO_3)_2$ effect on clay minerals after 12 months at RT.
A& B) Porosity reduction because of smectite swelling and formation of new cement
C& D) A new cement material covers pores and clay size particles
E& F) A new Ca-Si-Al rich material covers the pre-existing clay platelets like cement

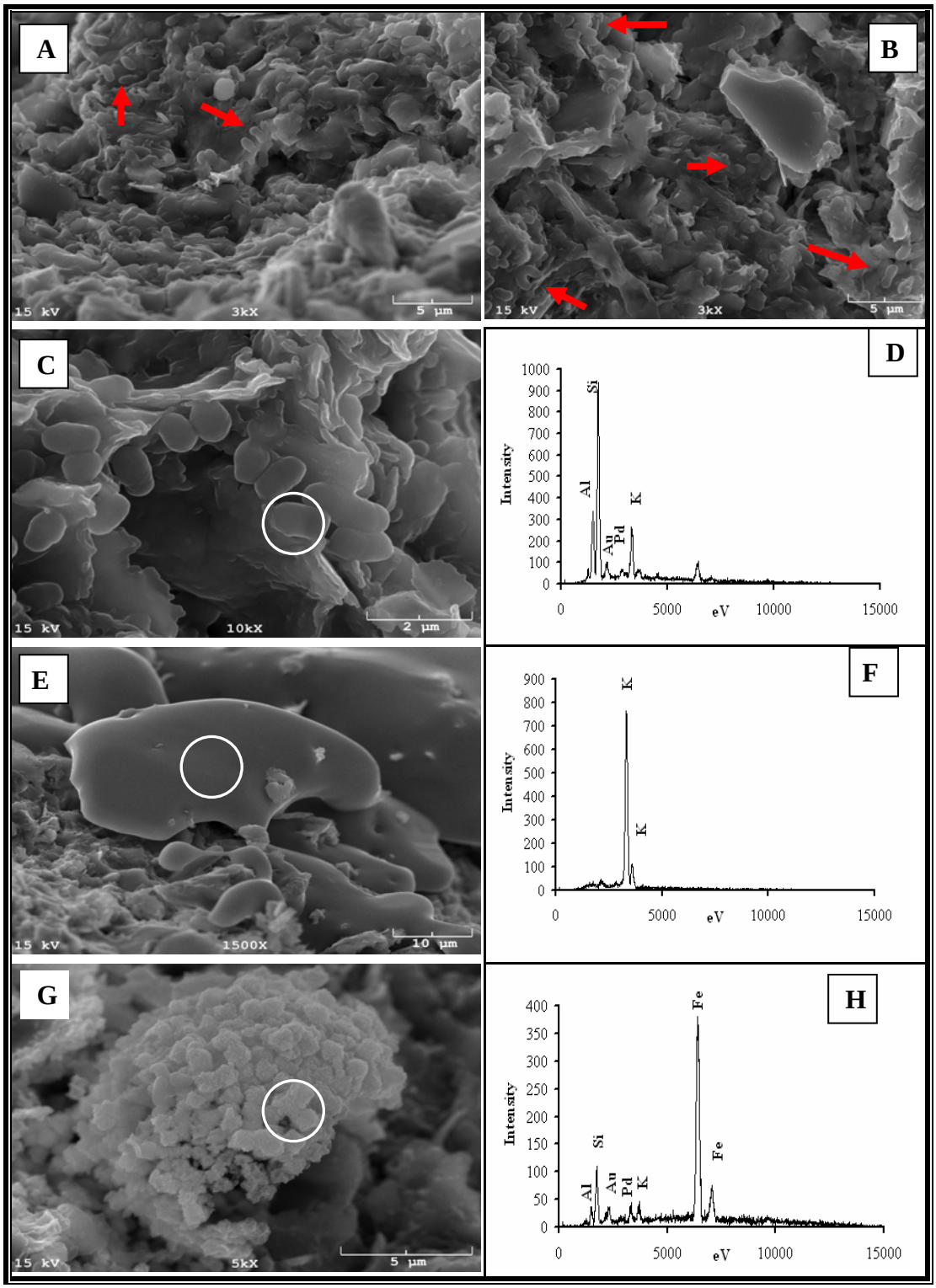

Figure (7-14): SEM photographs show the effect of 1 mole KNO_3 on shale component after 6 months at RT.
A& B) New K-Al-Si bodies formed over smectite platelets.
C& D) Shape of K-rich bodies, D) EDX analysis for these bodies
E& F) Another shape of K-rich bodies, F) EDX analysis for these bodies
G& H) Pyrite alterations produce Fe-rich material.

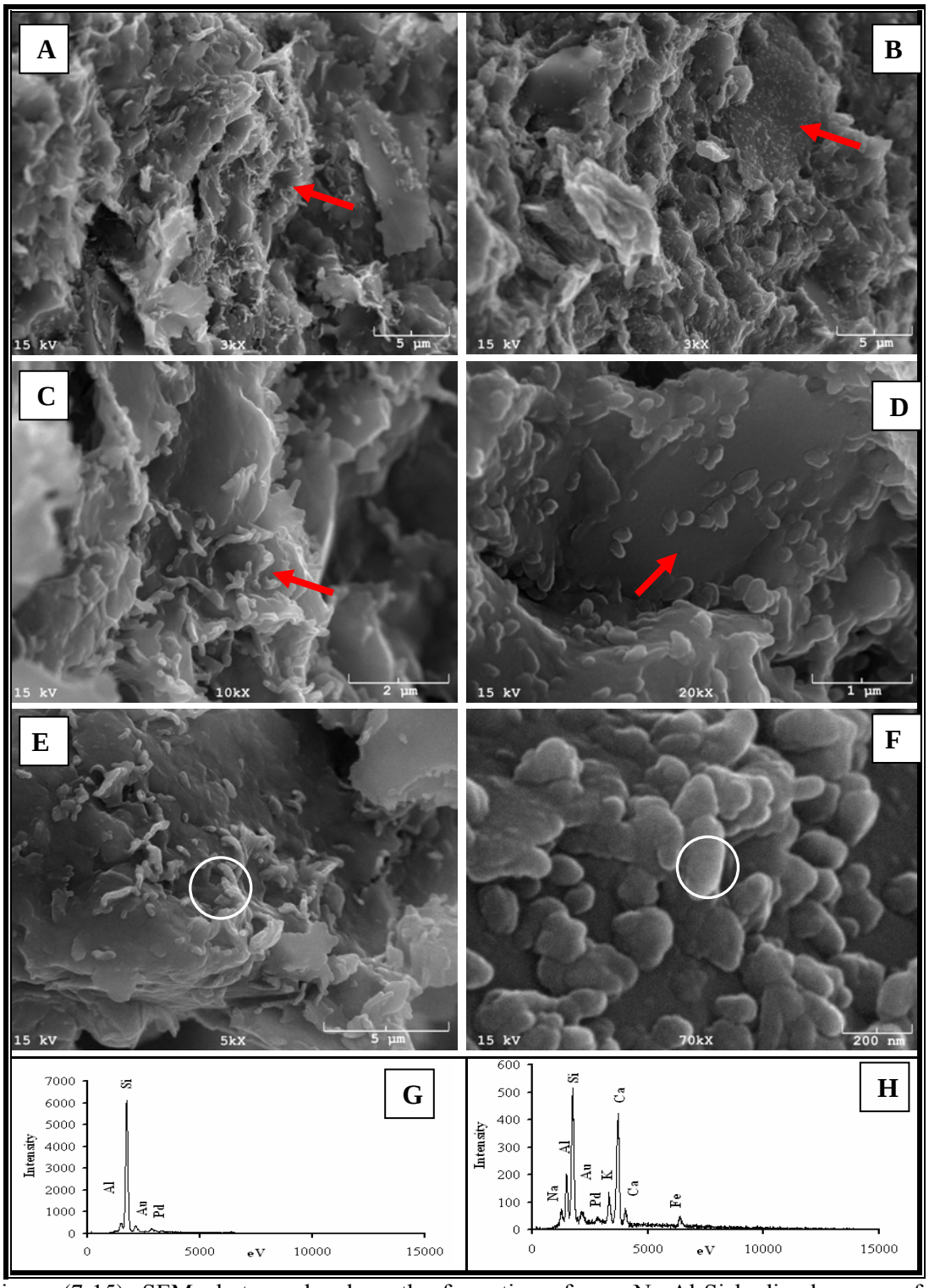

Figure (7-15): SEM photographs show the formation of new Na-Al-Si bodies because of $NaCO_3$ reaction with clay minerals at RT.
A,C, E& G) New elongated Na-Si-Al bodies formed after 6 months and 0.5 mole, G) EDX analysis.
B, D, F& H) New spherical Na-Al-Si bodies formed after 12 months and 1 mole, H) EDX analysis.

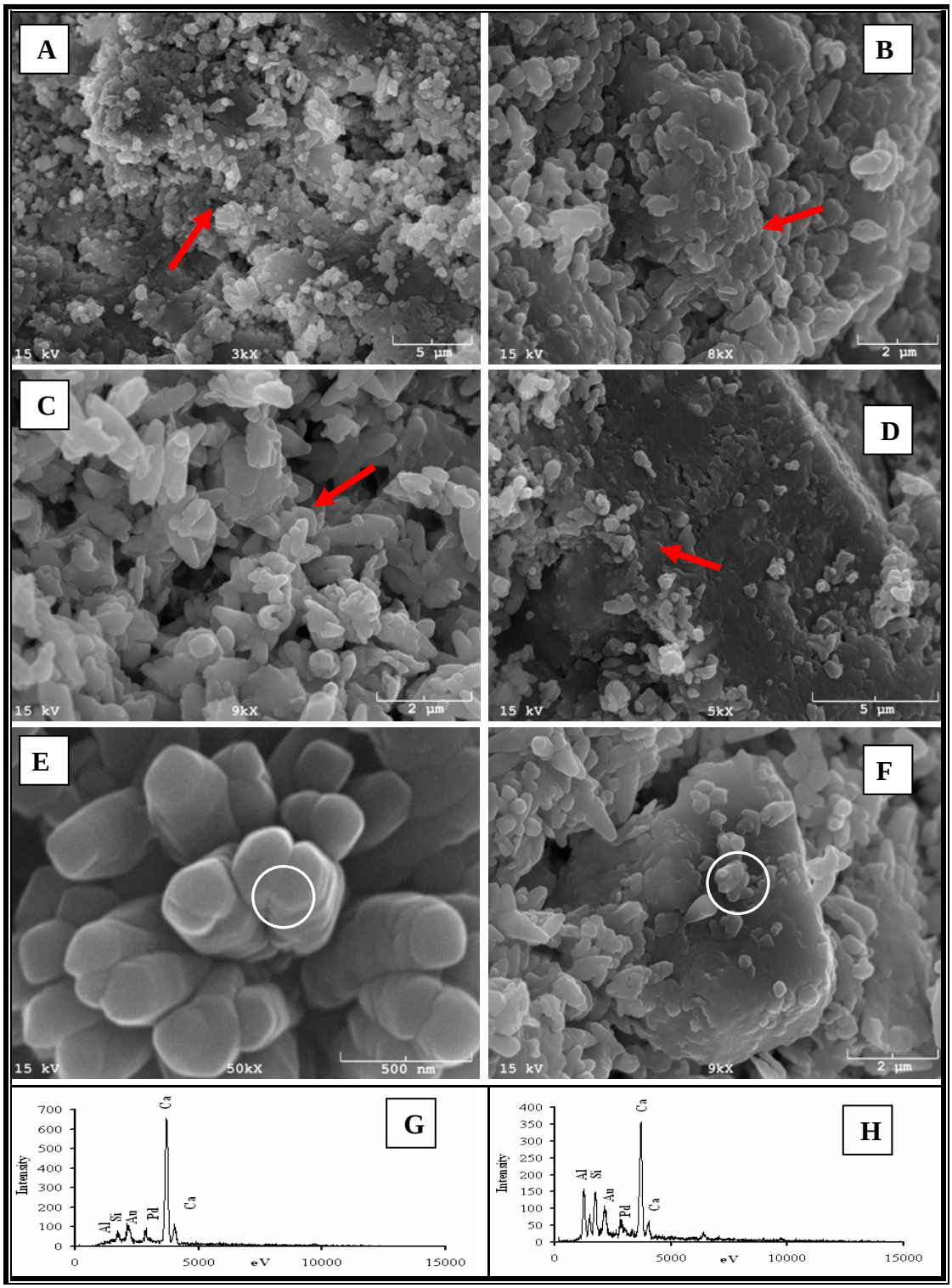

Figure (7-16): SEM photographs show the reaction of 1 mole $CaCO_3$ with shale components after 4 months at RT.

A, C, E& G) $CaCO_3$ original crystals located in pores space causing porosity reduction

B, D, F& H) $CaCO_3$ attack shale components including quartz (D) and form Ca-Al-Si rich materials covering the original components.

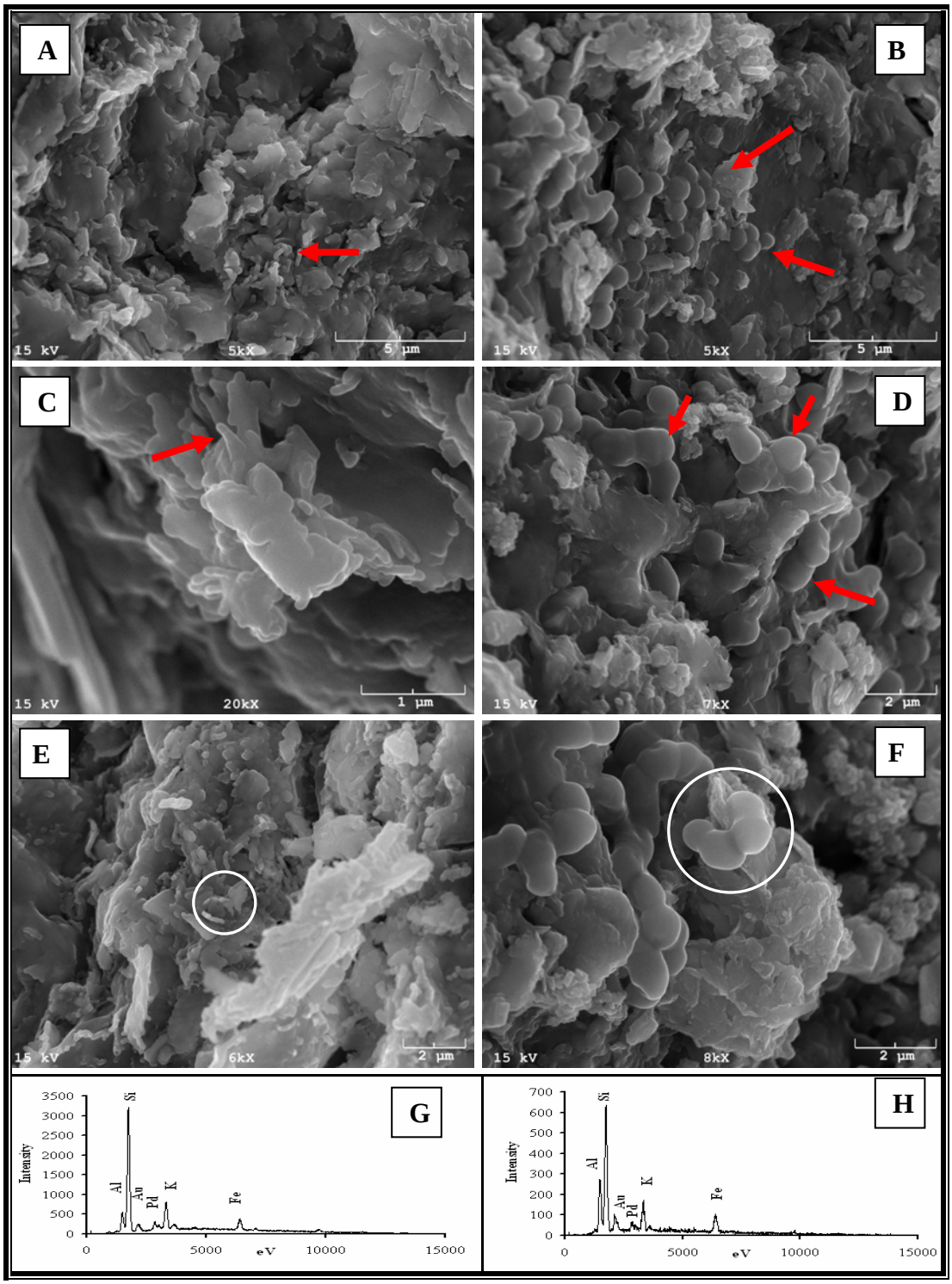

Figure (7-17): SEM photographs show the growth of K-Ca-Al-Si bodies (likely discrete illite crystals) with time due to reaction of K_2CO_3 with clay minerals at RT.
A, C, E&G) a small K-rich bodies located on smectite platelets
B, D, F&H) relatively large K-Ca-rich bodies located on smectite platelets
Note Ca Na enrichment (smectite transformation to illite)

Left column for sample treated for 4 months (2 mole) and right column for sample treated for 12 months (1 mole)

7.4.1.3. Grain-size distribution studies

For all curing times, samples treated by different fluids were studied for grain-size distribution using the Beckman-Coulter Laser Grain Analyzer as discussed in Chapter 4. The data obtained was graphed for different fluids (Figs 7-18 to 7-23). Careful studies of these data and figures indicate that the impact of fluids used in the current study of the grain-size distribution of Pierre Shale was very limited at room temperature conditions. The main recorded changes were within the 1-4 μm grain-size range. These changes were recorded with all the fluids and at different curing times. Changes in grain size distribution below 1 μm or above 4 μm were also observed with samples that tested after 6 and 12 months curing time. These changes occurred because most of the changes were for smectite and illite clay minerals as recorded by XRD and SEM studies, both of which are in these grain-size ranges. In most cases, there was an increase by about 0.5 % in each weight percentage within 1 μm or 4 μm range. This percent increased to 1.5 % with lower concentrations (0.25 and 0.5 mole) more or less in accord with the changes observed in the clay mineralogy. In addition, one can note a small increase of this percentage overtime, especially with the lower concentrations. One disclaimer on this observation is the effect of sample non-homogeneity and the error of the experiment, which is very small because all the samples run under the same conditions and Coulter running time.

This increase in one and four μm grain-size fractions is due to growth of new phases of clay minerals attached to the original one and counted as one grain or grain cluster by the Laser technique. The increase in the weight percent of this fine portion

will lead to a decrease in the weight percent of the coarse portion (Figs. 7-18 to 7-23). Using the software that is provided with the Coulter LS 230, the grain- size statistics parameter such as mean grain-size, median and the standard deviation were obtained for each sample and graphed on figure (7-24). The main observed change was for the standard deviation where Na had the lowest effect and K had the highest effect. The mean and median of grain-size showed almost no changes with different types of fluid and different curing times. Similar to what happen with clay minerals, sodium fluids had the least effect on the 1-4 μm range; potassium fluids had the greatest effect (Figs 7-18 to 7-23). Calcium fluids behaved in between sodium and potassium fluids. In addition, and similar to what happened with clay minerals, carbonate fluids had slightly more effect on grain-size distribution than nitrate fluids.

The magnitude of the effect of Na, Ca and K fluids on clay minerals and grain-size distribution does not follow the activity order of these fluids (Fig. 4-11, Chapter 4). Ca should be greater effective than Na, which should be greater effective than K. Instead the magnitude of the effect follows the order of atomic volume which is 23.7 cm^3/mole for sodium, 29.9 cm^3/mole for calcium and 45.46 cm^3/mole for potassium (atomic radius for, Na = 1.44 A°, Ca = 2.33 A° and K = 2.77A°). That means the effect of fluid on clay minerals increases with increases in the atomic volume, which leads to the formation of more stable components because of ionic exchange that takes place between the induced fluids and clay interlayers.

In general and for different curing times, grain-size distribution of the studied samples showed fewer effects than clay minerals with different chemical solutions.

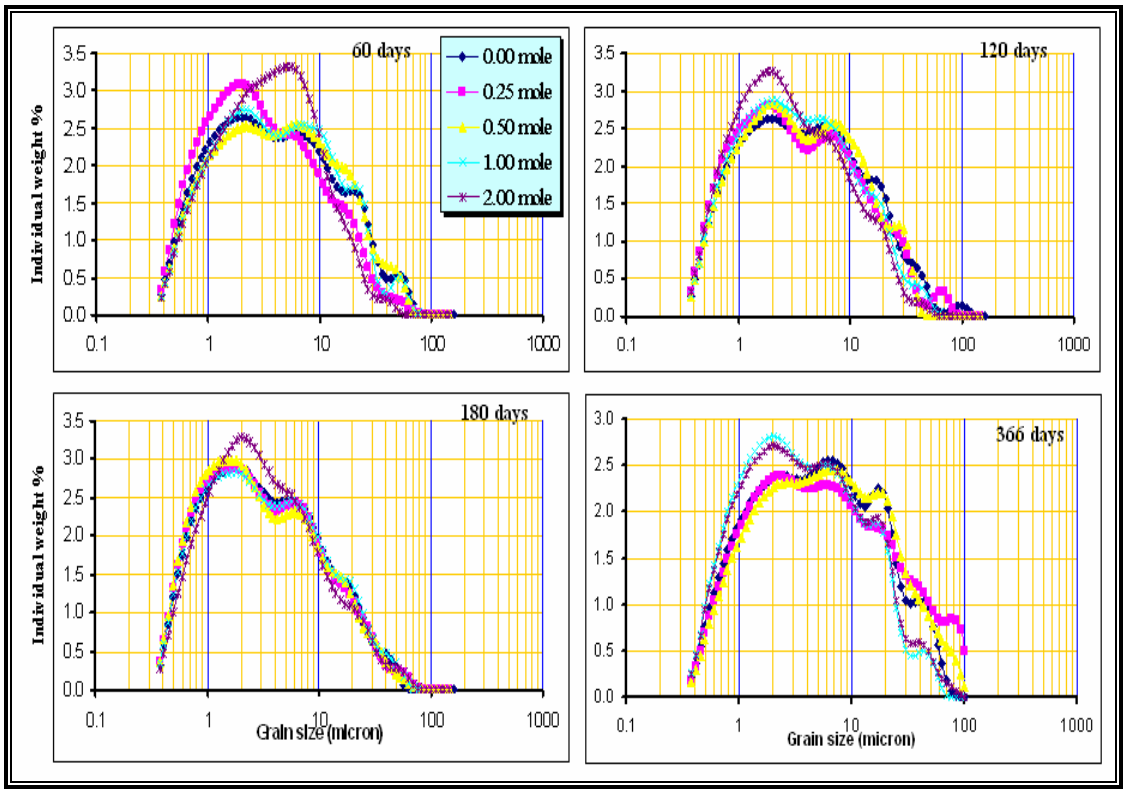

Figure (7-18): Grain-size distribution curves for sodium nitrate at room temperature for different curing times.

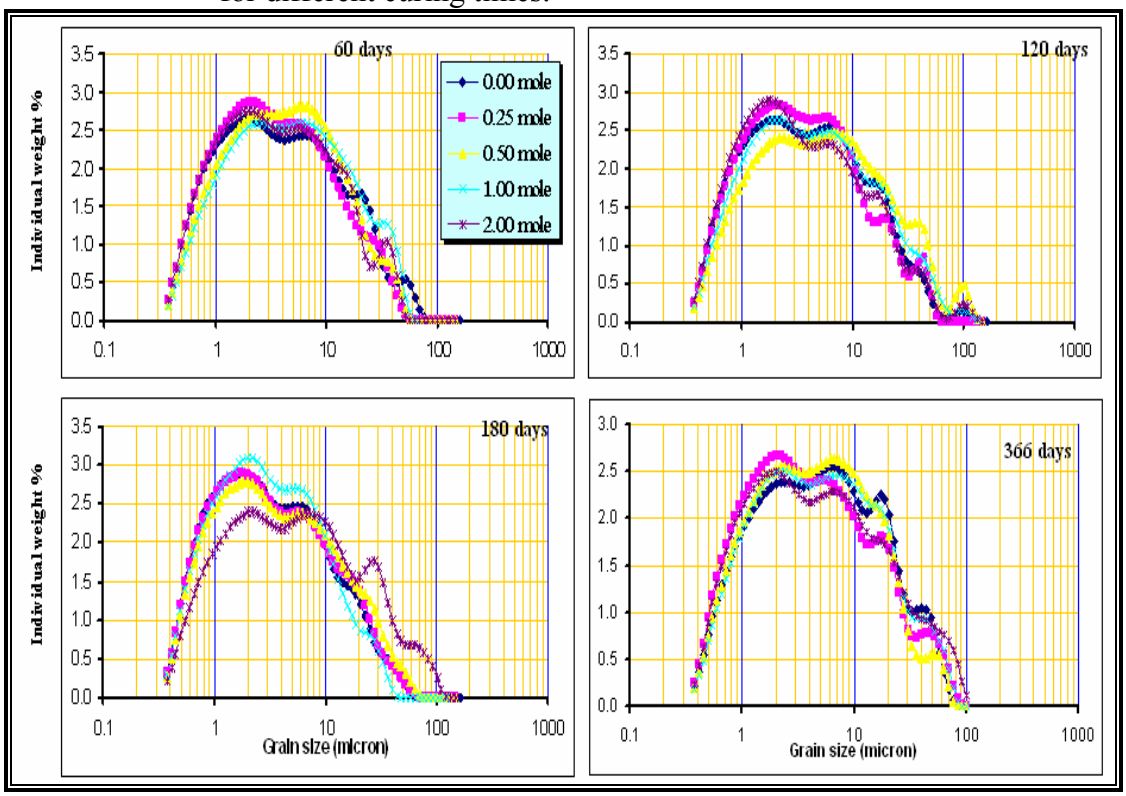

Figure (7-19): Grain-size distribution curves for calcium nitrate at room temperature for different curing times.

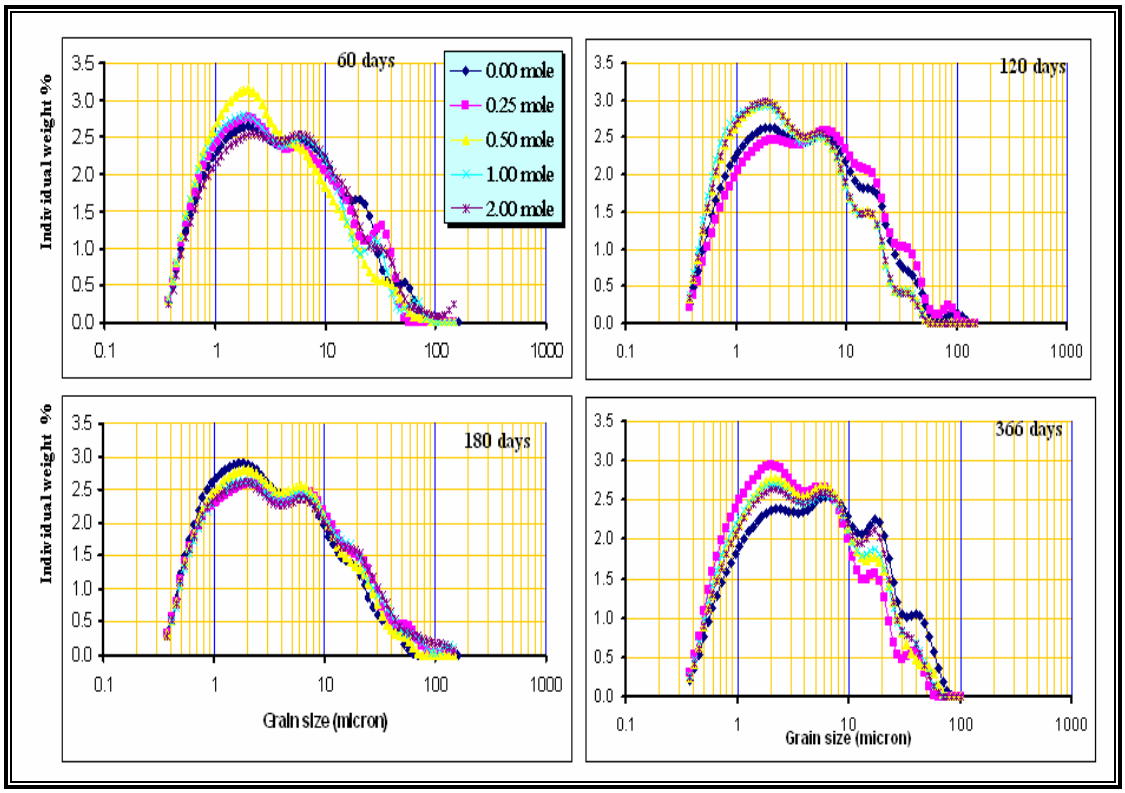

Figure (7-20): Grain-size distribution curves for potassium nitrate at room temperature for different curing times.

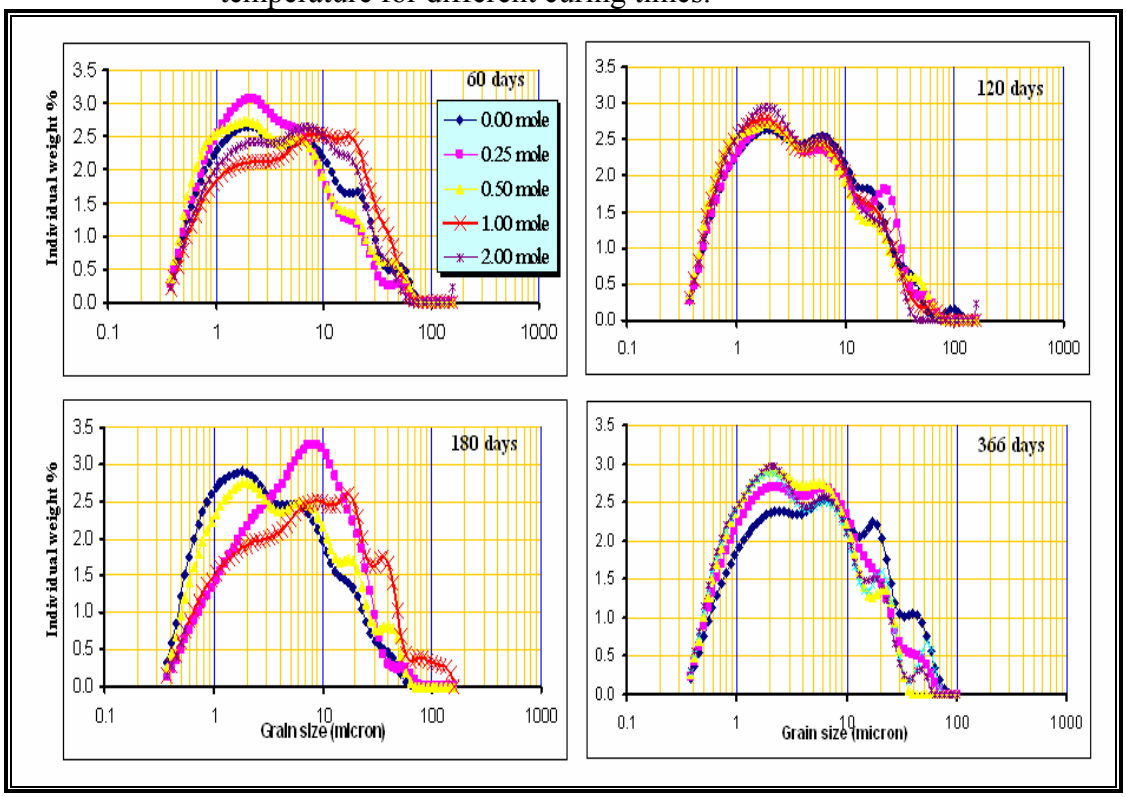

Figure (7-21): Grain-size distribution curves for sodium carbonate at room temperature for different curing times.

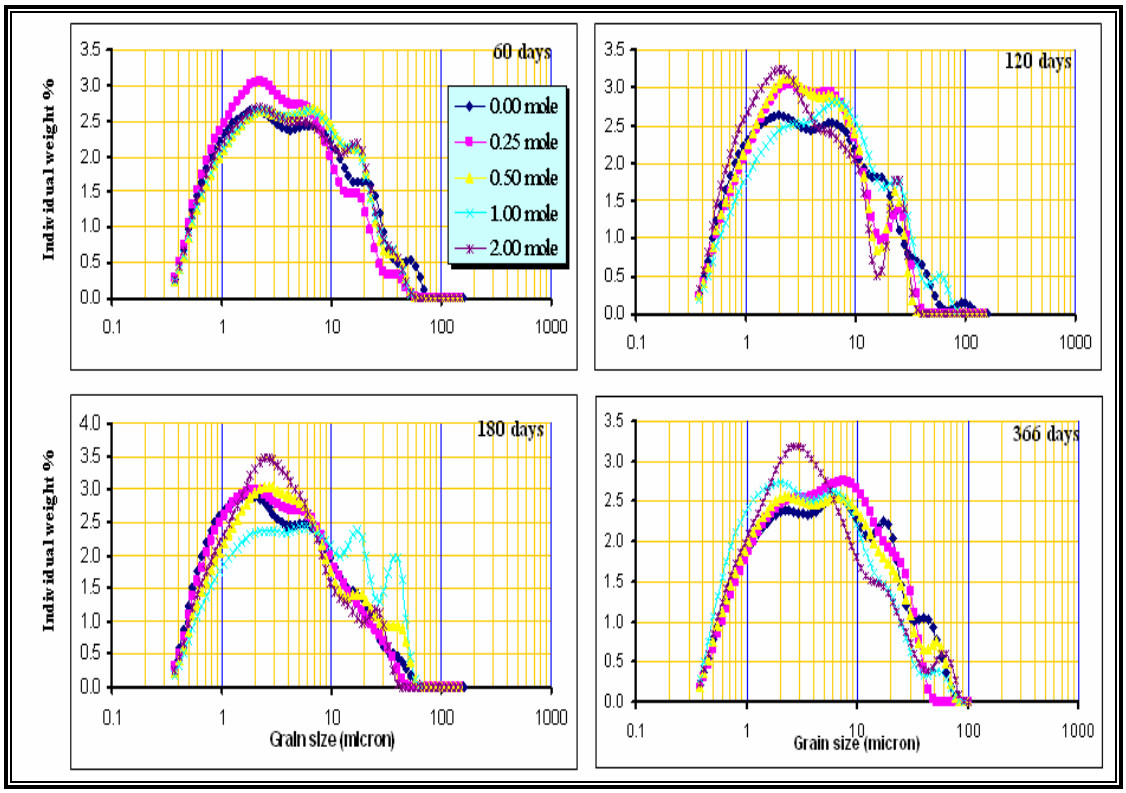

Figure (7-22): Grain-size distribution curves for calcium carbonate at room temperature for different curing times.

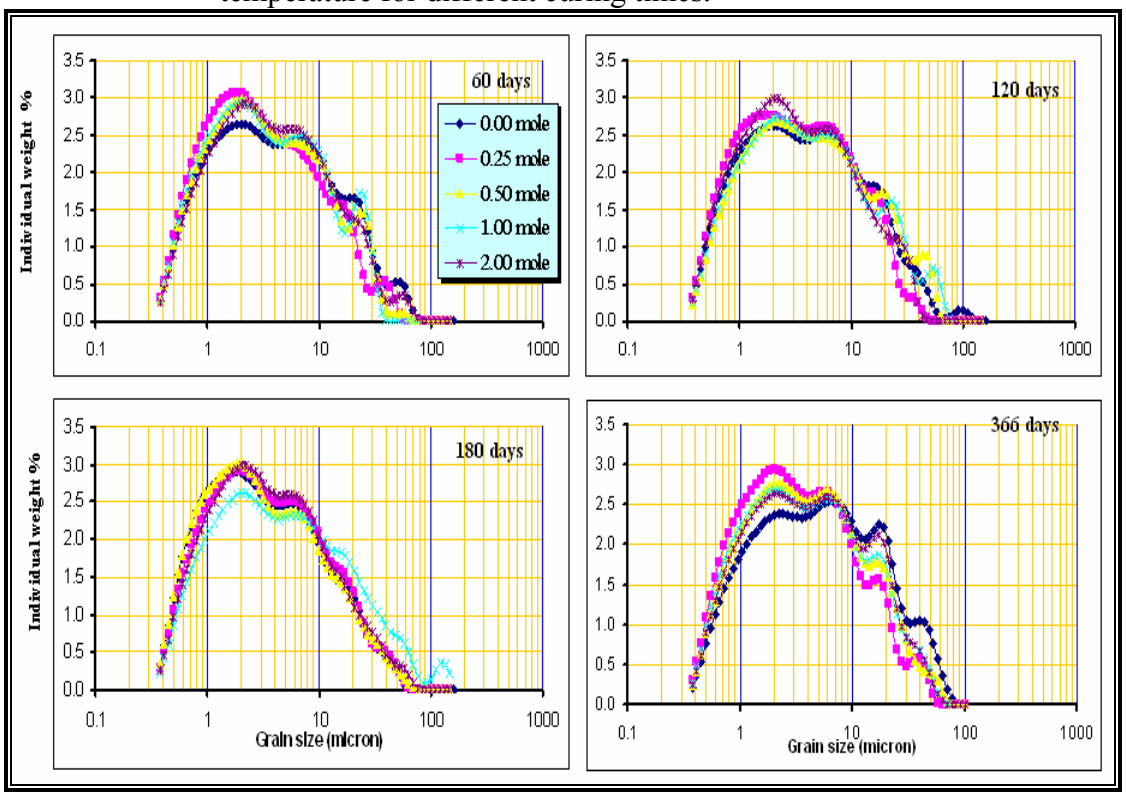

Figure (7-23): Grain-size distribution curves for potassium carbonate at room temperature for different curing times.

Table (7-2): Grain-size statistics for samples treated by different chemicals at room temperature for different curing time.

Fluid		Mean					Median					Stander division				
	Time (days)	**35**	**60**	**120**	**180**	**366**	**35**	**60**	**120**	**180**	**366**	**35**	**60**	**120**	**180**	**366**
Water	**0.00 mole**	9.689	8.337	8.291	6.447	10.15	4.246	3.824	3.829	3.042	4.993	13.17	11.24	12.32	8.532	12.83
$NaNO_3$	**0.25 mole**	6.642	6.179	7.603	6.487	13.92	3.34	2.917	3.31	2.928	5.317	8.967	8.42	11.18	9.067	20.62
	0.50 mole	11.36	8.602	6.941	6.283	12.11	6.536	4.259	3.593	2.768	5.666	12.71	10.99	8.056	8.711	16.29
	1.00 mole	11.43	8.075	6.689	6.774	7.323	6.746	4.008	3.371	3.102	3.569	12.39	10.43	8.563	9.203	9.52
	2.00 mole	7.121	5.847	5.515	6.379	8.047	4.288	3.682	2.762	2.995	3.812	8.109	6.27	7.031	9.077	10.97
$Ca(NO_3)_2$	**0.25 mole**	9.591	6.903	7.355	6.647	8.047	4.762	3.443	3.558	3.097	3.812	11.99	8.634	9.782	8.679	10.97
	0.50 mole	9.591	7.644	12.1	7.564	8.972	4.762	4.2	5.256	3.448	4.605	11.99	9.091	18.07	9.996	11.54
	1.00 mole	9.196	9.09	9.649	5.579	10.4	4.369	4.682	4.258	3.01	4.92	12.2	10.83	14.13	6.603	13.69
	2.00 mole	7.363	7.338	8.356	12.22	11.37	3.288	3.625	3.338	5.063	4.469	10.16	9.192	14.04	17.76	16.88
KNO_3	**0.25 mole**	6.891	7.61	9.435	8.39	6.506	3.343	3.479	4.55	3.742	3.237	9.523	9.71	13.1	11.95	8.419
	0.50 mole	7.424	6.468	5.903	7.002	7.786	3.049	2.89	2.915	3.334	3.86	11.1	9.557	7.607	9.322	10.04
	1.00 mole	7.362	7.435	5.769	9.08	7.799	3.269	3.22	2.795	3.738	3.798	10.82	10.82	7.498	15.7	9.919
	2.00 mole	6.651	11.41	5.787	9.612	8.02	2.945	4.18	2.889	3.73	4.094	9.972	14.83	7.325	16.44	9.788
Na_2CO_3	**0.25 mole**	18.17	6.351	8.231	9.033	7.466	11.68	3.114	3.711	5.89	3.704	18.23	8.704	10.77	9.602	10.04
	0.50 mole	7.535	7.352	3.936	7.987	5.953	4.226	3.186	2.456	3.72	3.303	8.768	10.63	3.696	10.45	6.65
	1.00 mole	16.31	10.15	7.095	14.61	7.421	10.72	5.668	3.292	7.123	3.321	16.13	11.41	9.53	20.9	10.66
	2.00 mole	9.258	8.316	6.276	13.63	6.349	6.315	4.581	3.169	5.511	3.167	9.38	9.557	7.415	22.51	8.069
$CaCO_3$	**0.25 mole**	5.982	6.373	5.996	8.291	3.009	3.176	3.603	3.107	4.83	7.935	7.339	7.251	7.332	8.834	10.97
	0.50 mole	7.643	9.41	7.791	9.491	5.156	4.169	4.887	3.631	4.569	10.69	8.869	12.13	10.41	12.49	11.54
	1.00 mole	7.609	5.996	10.57	7.325	3.613	4.12	3.44	5.197	3.495	8.746	8.78	6.63	12.4	10.31	13.69
	2.00 mole	7.622	5.736	5.825	8.295	4.015	3.91	2.842	3.133	3.604	9.344	8.951	7.028	7.046	12.74	16.88
K_2NO_3	**0.25 mole**	9.454	6.201	6.068	6.821	8.389	5.361	2.942	3.27	3.288	4.132	10.94	8.166	7.018	8.909	11.23
	0.50 mole	9.291	6.732	8.653	6.502	9.612	4.749	3.307	4.011	2.92	4.389	11.27	8.58	11.27	9.016	12.67
	1.00 mole	5.648	6.438	8.851	7.54	7.422	3.138	3.274	3.94	4.313	3.662	6.416	7.41	12.22	10.2	9.293
	2.00 mole	6.065	7.476	6.464	7.134	7.675	3.455	3.622	3.282	3.391	3.458	6.802	10.09	7.787	9.81	10.3

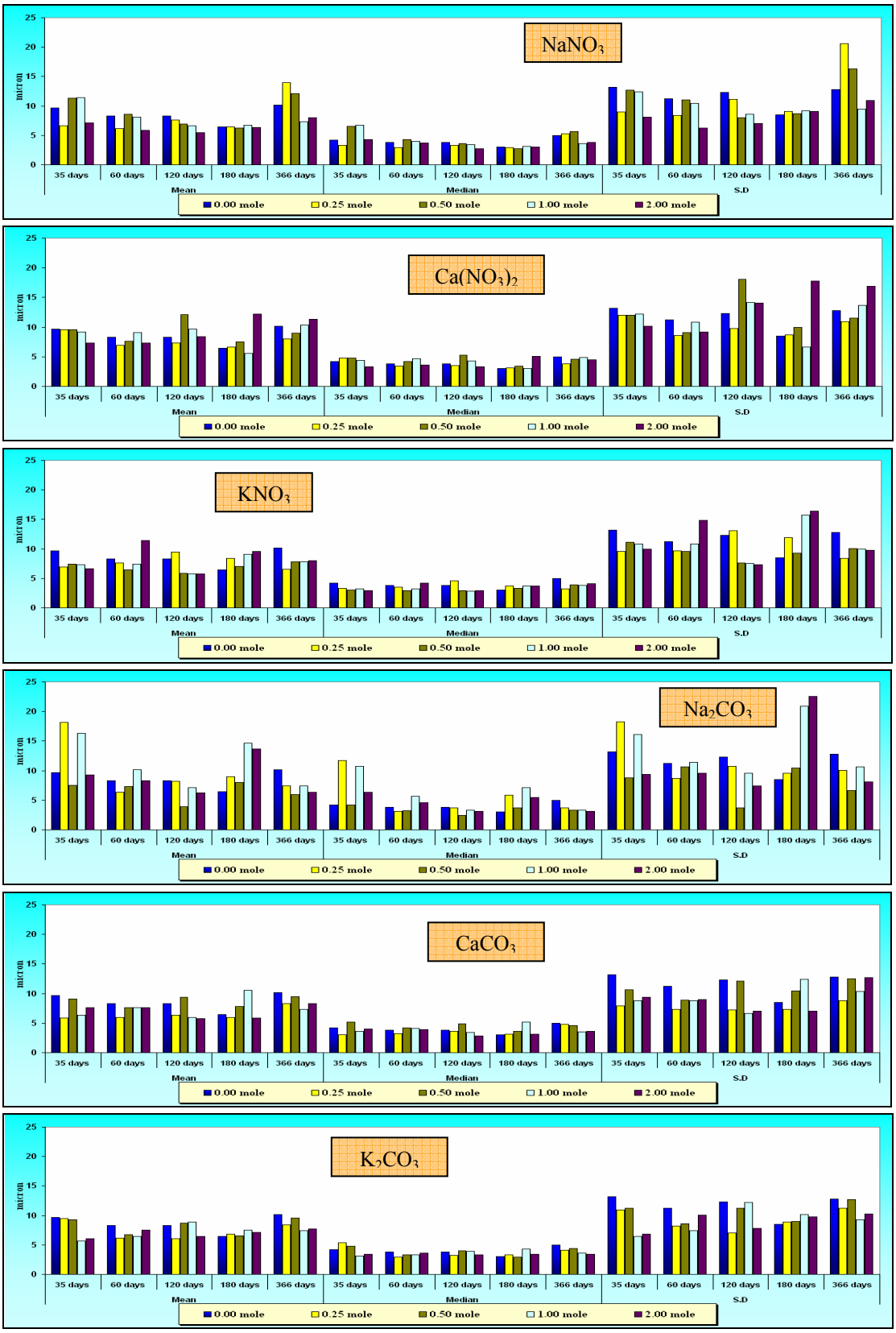

Figure (7-24): Grain-size statistics for different chemical fluids at room temperate for different curing times.

7.4.2. HTHP conditions

Figure (7-1) shows the effects on Pierre Shale samples exposed to 0.5 and 1 mole of three different nitrate solutions and distilled water under two sets of temperature/pressure conditions were studied. These conditions were applied for both 35 and 60 days separately. Only one sample was cured for four months at 1 mole KNO_3, 150 °C, and 2,500 psi Pp and 3,000 psi Pc condition. The impact of all of these conditions on clay minerals and grain-size distribution will be discussed in the subsequent section.

7.4.1.1. XRD studies

Careful study of the first fifteen 2θ of the XRD diffractograms (Fig. 7-25 a & b) indicates the clay mineral transformations in these experiments. Using nitrate solutions under the HTHP conditions, three major changes are shown by clay mineral peaks:

1- Change in mineral peak position, especially the smectite peaks (5 to 8 2θ), which reflect changes in the mineral structure,

2- Change in clay mineral peak intensities, which reflect change in mineral amounts,

3- Change in peak sharpness, which reflects changes in crystallinity and crystal structure.

These changes are directly related to type and concentration of the nitrate solution chemistry, temperature and pressure conditions, and curing time used in the experiments.

Smectite

Smectite was the clay mineral most affected by fluid composition and/or temperature/pressure conditions. Changes in smectite peak position, intensity and sharpness can be easily noticed on figure (7-25 a and b). The natural Pierre Shale sample has the sharpest smectite peak and its position is located between five and seven 2θ. The chemicals and T/P conditions changes the positions and sharpness of the peaks. Smectite peak intensity decreases with increasing temperature, because temperature destroys the smectite crystals (Fig. 7-25 a and b). The smectite peak intensity decreases similarly in the presence of water, $Ca(NO_3)_2$ and $NaNO_3$. By increasing temperature from 100 °C to 150 °C, the smectite peak intensity has nearly disappeared for these three fluids. Of these three, $NaNO_3$ has the least effect on smectite destruction because it has the opposite effect on recrystallization of the smectite. The recrystallization of smectite with the presence of $NaNO_3$ appeared clearly with room temperature studies, as shown in the last section.

KNO_3 changed the smectite peak position to a high 2θ (7-8) smectite/illite mixed-layer position. This peak intensity is the higher than the intensity produced by other fluids at the same conditions. This is because the KNO_3 starts to push the smectite towards a smectite/illite mixed layer, and eventually toward illite by re-crystallizing the smectite crystals destroyed under the effect of temperature. For a 150 °C samples, the formation of smectite/illite mixed layer seems to be greater than the formation of a discrete illite phase. In the experiment where the sample was treated for four months at 1 mole KNO_3 and 150 °C, smectite almost disappeared (Fig. 7-26).

Illite

The effect of 100 °C decreases the illite peak in the presence of $Ca(NO_3)_2$ and water, because there were no cations to help in the recrystallization of the destroyed smectite. At this temperature condition in the presence of $NaNO_3$, the effect of temperature on illite is minimal. On the other hand, KNO_3 seems to be able to recrystallize the destroyed smectite and mixed layer smectite/illite or discrete illite crystals to form a new phase of illite. This is indicated by the increase of the illite peak intensity and "sharpening" of the peak (Fig. 7-25 a). At 150 °C, most of the illite is destroyed in the presence of water, $NaNO_3$ and $Ca(NO_3)_2$. At this temperature and in the presence of KNO_3, the illite peak's intensity does not show the same rapid increase as in the 100 °C conditions. This may be because the rate of illitization of the destroyed smectite is less than the rate of destruction of the initial illite itself. This clearly appears when the time for the same condition is increased to four months the illite and smectite peaks disappear while the quartz peak sharply increases, most probably because of the formation of α- quartz new phase (Fig. 7-26). The disappearance of illite may be partially because masking of the new silica phase.

Kaolinite

Kaolinite is the clay mineral least affected by the study conditions. Temperature less than 150 °C has no effect on kaolinite which starts to break down at 550 °C. The nitrate fluids that are used in the current study had no effect on kaolinite because of the great stability of its structure that is not influenced by changes in cation chemistry of pore fluid (Fig. 7-25). The only effect observed for kaolinite is a

slight shift in kaolinite peak position towards the high 2θ at 150 °C for the 4 months sample (Fig. 7-26), possibly indicating a slight Ostwald ripening of kaolinite crystals.

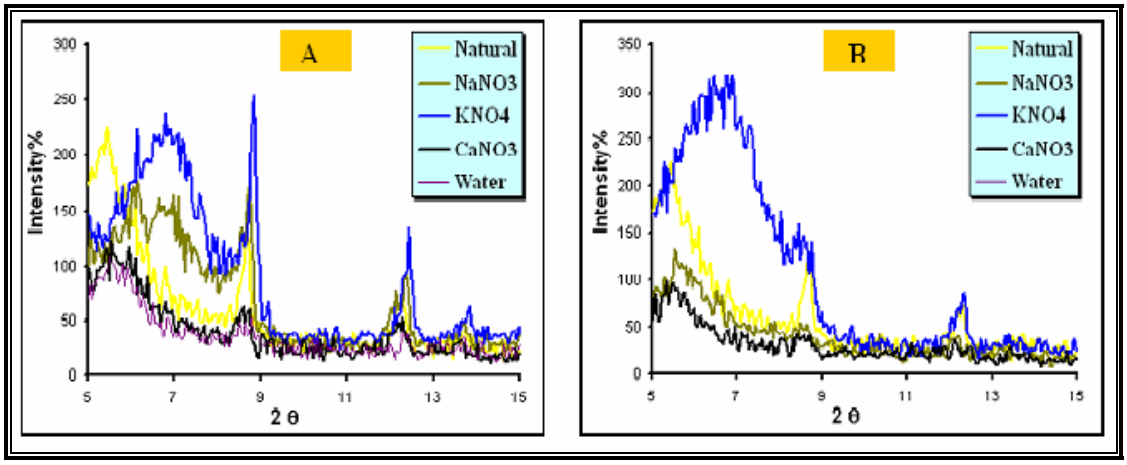

Figure (7-25): XRD chart diagrams for samples treated by 1 mole nitrate fluids for 35 days.
A) 100 °C temperature, 600 psi Pp and 900 psi Cp
B) 150 °C temperature, 2,500 psi Pp and 3,000 psi Cp

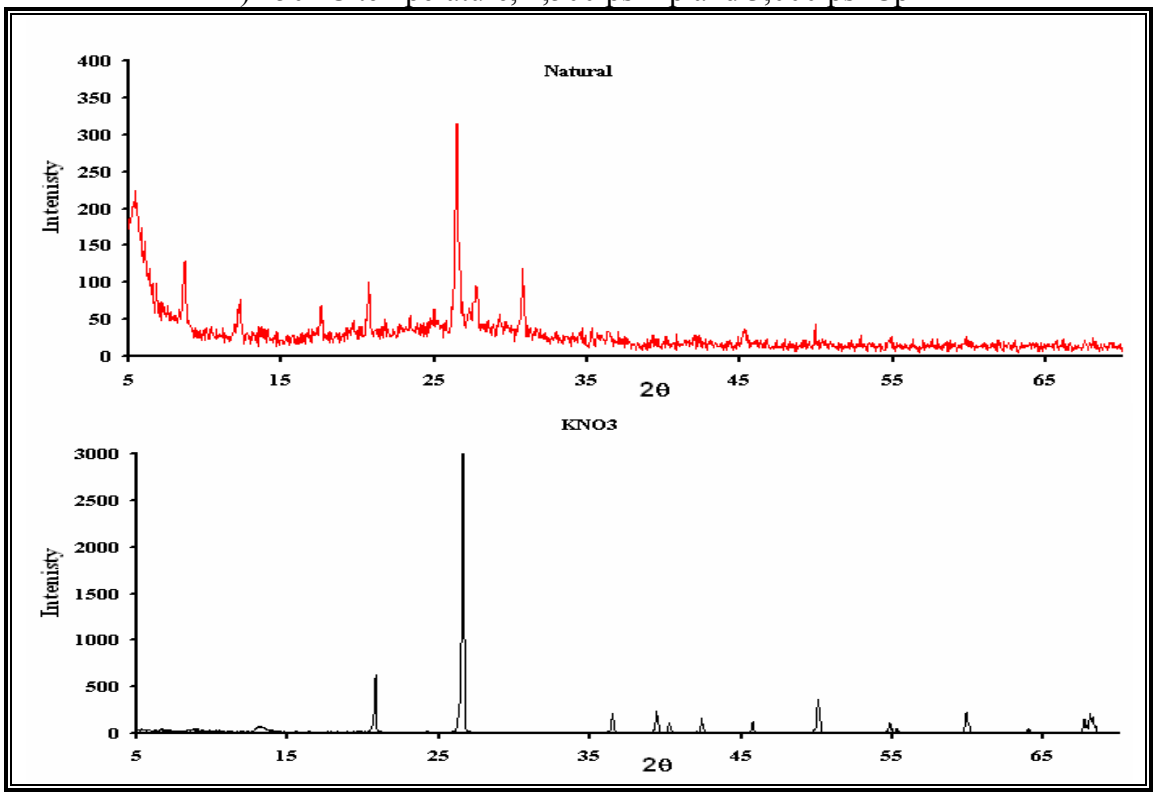

Figure (7-26): XRD chart diagram for natural Pierre Shale and 1 mole KNO_3 treated sample at 150 °C temperature, 2500 psi Pp and 3000 psi Pc for four months. Note different scales for intensities. This different does not affect the quantitative analysis.

Crystallinity Index

Another aspect from the XRD study is the crystalinity index (CI), represented by dividing the peak high by the high-peak width (Table 7-2), for smectite at 6.46 2θ, illite at 8.61 2θ, and kaolinite at 12.32 2θ. The crystalinity index increases with increasing mineral crystallinity and visa versa (Biscaye, 1965).

Table (7-2) and Figure (7-6) represent the clay mineral crystalinity indices of the studied samples at HTHP conditions. They show that at 100 °C, the temperature has negative effects on the smectite and illite crystallinity index, except with presence of KNO_3 where the illite start to recrystallize from destroyed smectite or illite. By increasing temperature up to 150 °C, smectite and illite crystallinity decreased, even with KNO_3. The kaolinite crystalinity was also affected negatively with an increase in temperature. That leads to say 100 °C in the presence of the KNO_3 maximizes illitization of smectite within a short time period (one or two months) as compared to other conditions that were used in the current study. In natural geological conditions, chemical, temperature and pressure conditions, as well as time play an important role in the recrystallization of illite from the destroyed smectite and or illite crystals and in the presence of K ions.

Table (7-3): Crystalinity indices samples treated under HTHP treated using one mole for 35 days.

Sample	100 ^{0}C conditions			150 ^{0}C conditions		
	Smectite	Illite	Kaolinite	Smectite	Illite	Kaolinite
Natural	7.25	22.33	26.00	7.25	22.33	26.00
Water	4.00	3.50	5.33	4.00	3.50	5.33
NaNO3	7.00	7.67	6.00	14.33	6.00	14.00
Ca(NO3)2	5.20	6.00	11.00	11.50	3.00	6.00
KNO3	4.00	35.33	20.00	7.50	12.50	12.00

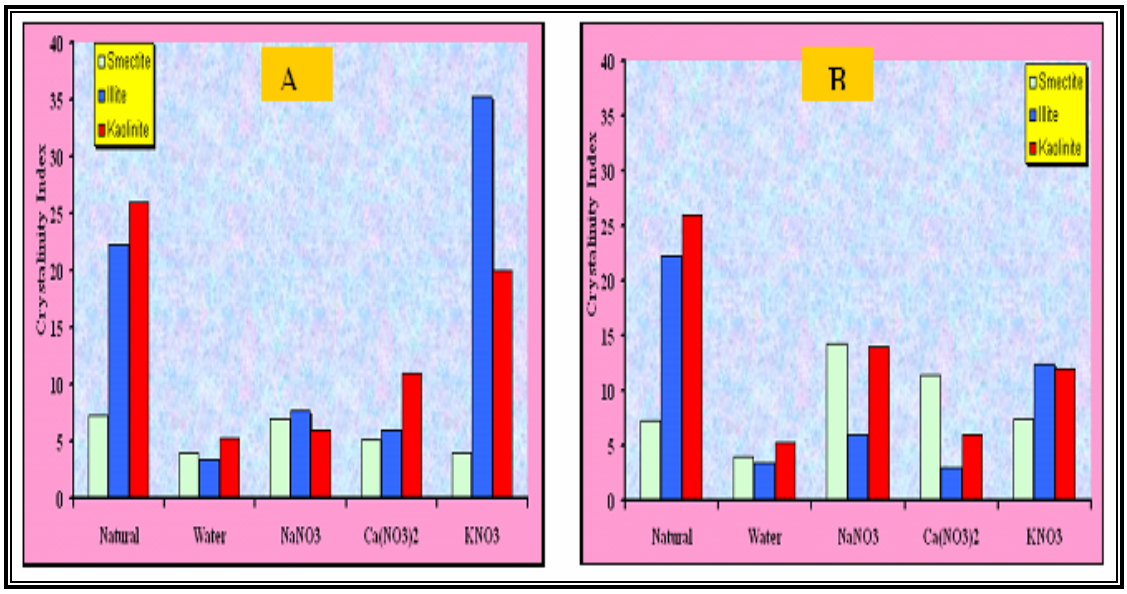

Figure (7-27): Crystalinity indices for 1 mole nitrate fluids for 35 days curing time.
A) 100 °C temperature, 600 psi Pp and 900 psi Cp
B) 150 °C temperature, 2,500 psi Pp and 3,000 psi Cp

7.4.2.2. SEM and EDX studies

Five samples were studied using SEM and EDX after treatment by different nitrate solutions under high temperature/high pressure conditions. Four of them were treated for 35 days and the fifth one was treated for four months (Figs 4-28 to 4-32). The formation of new material phases especially those of silica oxides, smectite, and illite are recorded under these conditions.

SEM and EDX studies show a clear illitization of smectite to form a new phase of illite dustlines on smectite platelets when the samples are treated by KNO_3 at 100°C or 150°C for one or two months, but these effects diminish with 150°C conditions at four months. Instead, silicification of clay minerals was recorded. This supports the previous XRD studies. This silicification of clay minerals is sensitive to the type of chemical fluid. $NaNO_3$ showed minimum silicification, KNO_3 showed the

maximum at the same conditions. Behavior with $Ca(NO_3)_2$ is usually in between that observed for KNO_3 and $NaNO_3$. $NaNO_3$ and $Ca(NO_3)_2$ showed a new phase of smectite forming over the existing one. In both solutions, these new phases usually composed of Ca, Al and silica with little Na content. This compositional change may explain increase in the 2θ position of smectite on XRD diffractograms. The newly formed materials cover the pre-existing component and migrate to deposit in micro-pores. These effects will increase the rock strength and reduce its porosity and permeability.

Pyrite framboids also showed extensive effects caused by these conditions, because of the oxidating conditions the samples were subjected to during the experiments. The euhedral crystals change to anhedral ones (Fig. 7-30b), and crystal edges dissolve to form an iron-silica phase covering the original crystals (Fig. 7-30b and 7-31b). Figure (7-31b) shows a reduction in pore size between the pyrite crystals as a result of the new cementation. The cement material composition is recorded by EDX as a Fe-Ca-silicate, suggesting mass transfer of Ca and silica from adjacent materials as a result of the destruction of the clay minerals under the influence of the chemical solution chemistry and elevated temperature conditions.

These lead one to conclude that temperature is not only enhance illitization of smectite but also accelerates shale silicification.

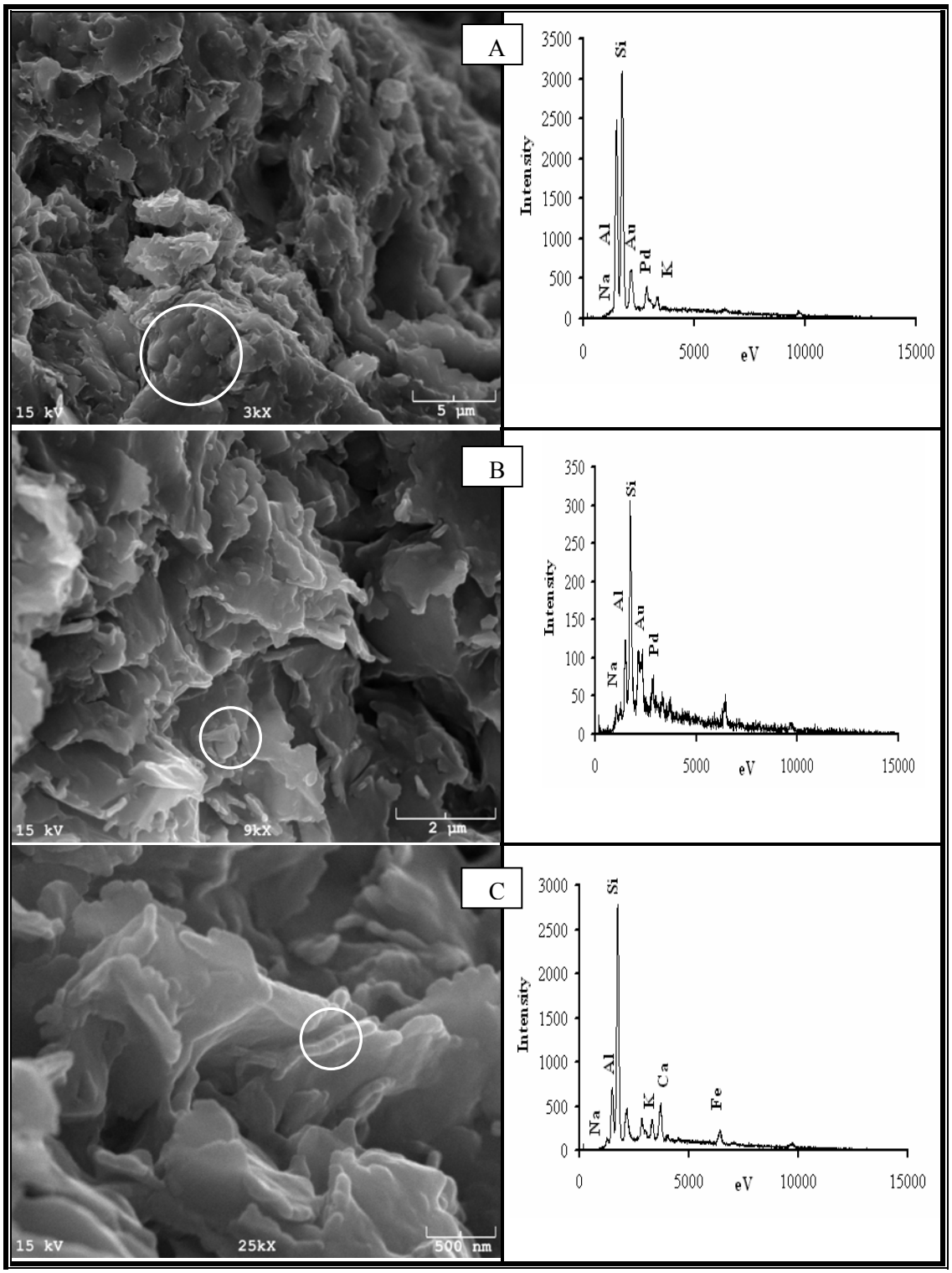

Figure (7-28): SEM images and the EDX analysis (1 molal $NaNO_3$ treated sample at 150 °C for 35 days).
A, B and C show the growth of new Na-smectite form over the existing one

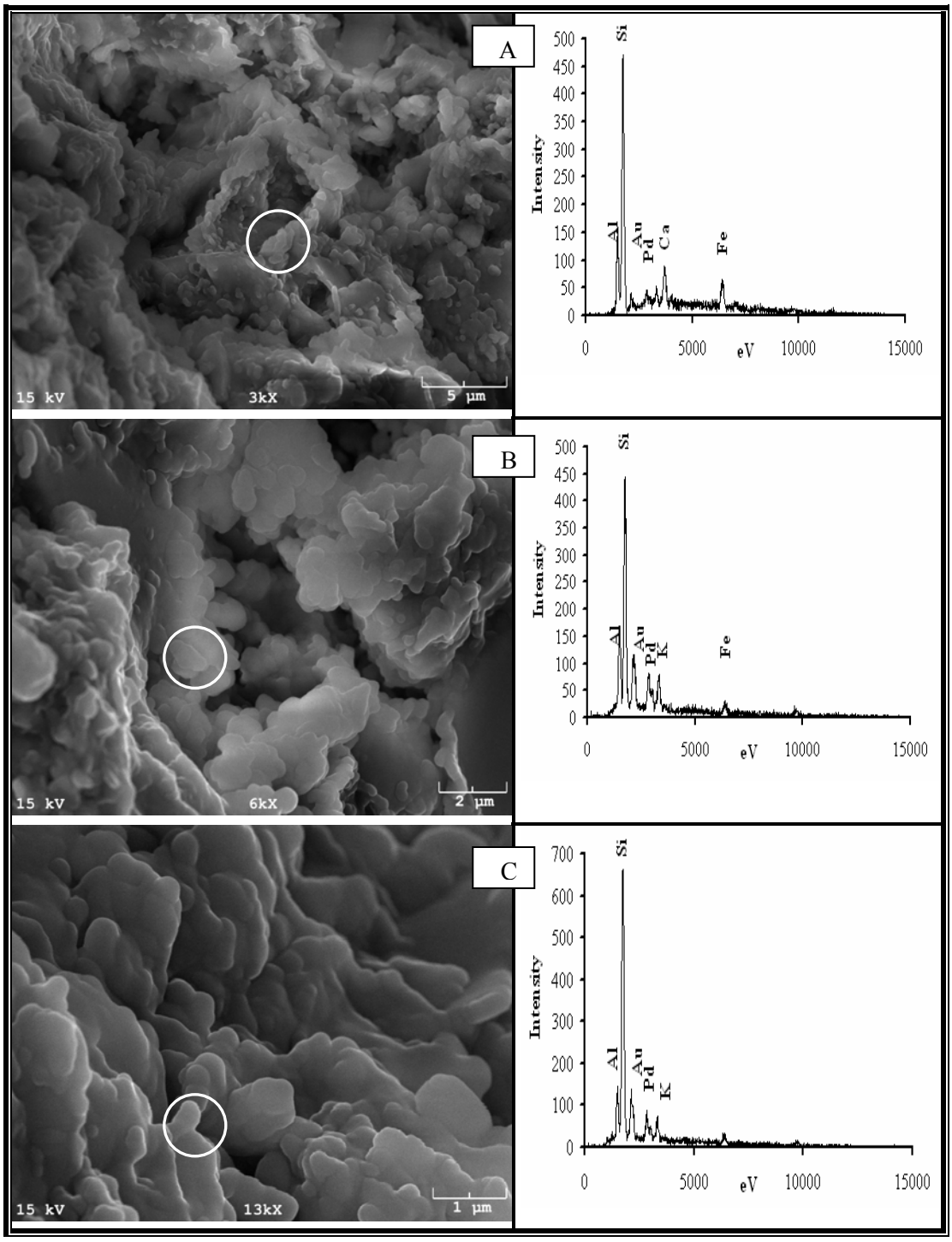

Figure (7-29): SEM images and the EDX analysis (1 molal Ca $(NO_3)_2$ treated sample at 150 °C for 35 days).
A) Growth of new Ca-smectite forms over the existing ones,
B & C) Silica covers the clay particles.
Note pores can be still be recognized

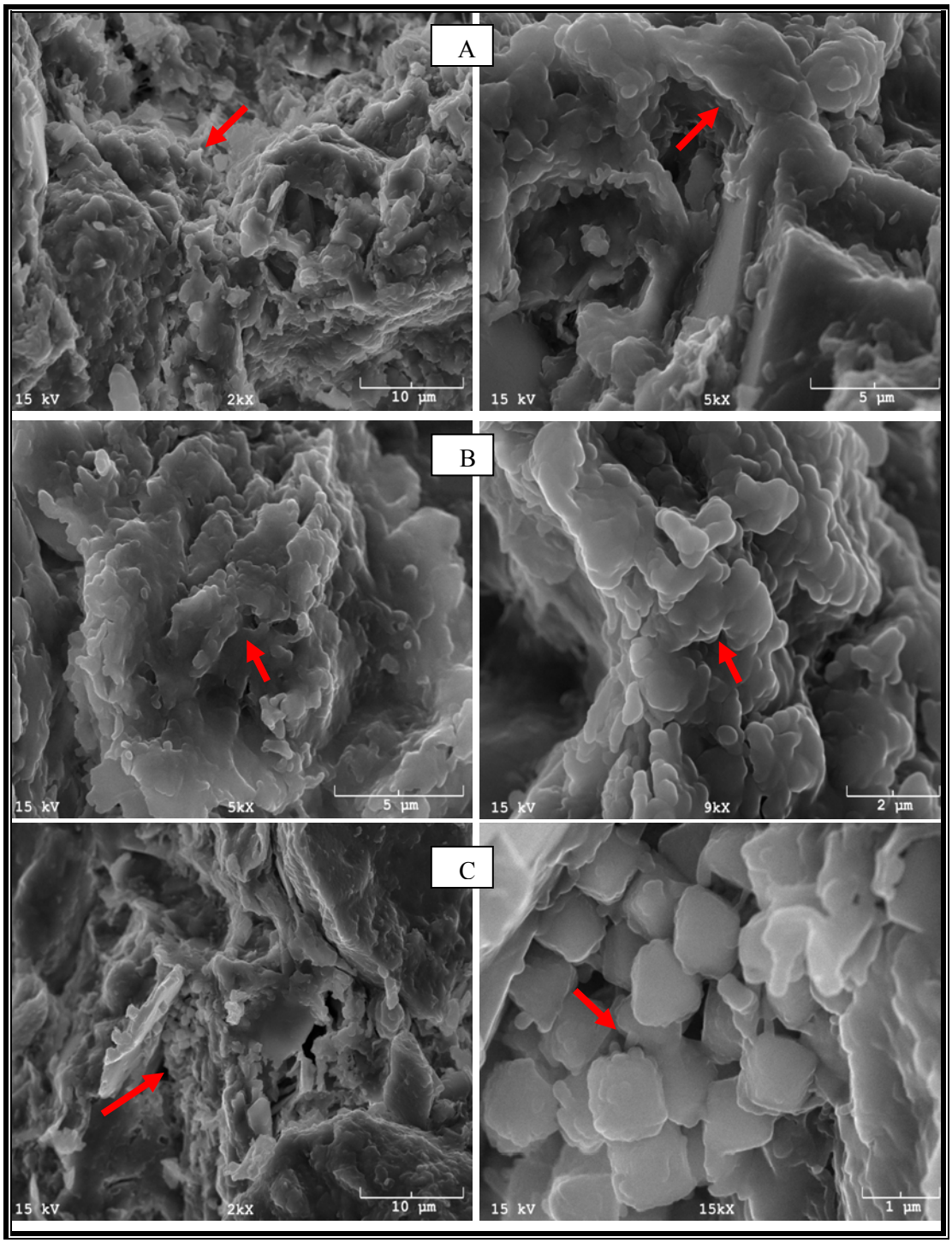

Figure (7-30): SEM images for 1 molal KNO_3 treated sample at 150 °C for 35 days).
A) Silica covers quartz grains
B) Silica and a new illite form a cover on the clay particles
C) The euhedral pyrite crystals change to anhedral and silica-iron cement starting to form.
Note pores can be still be recognized

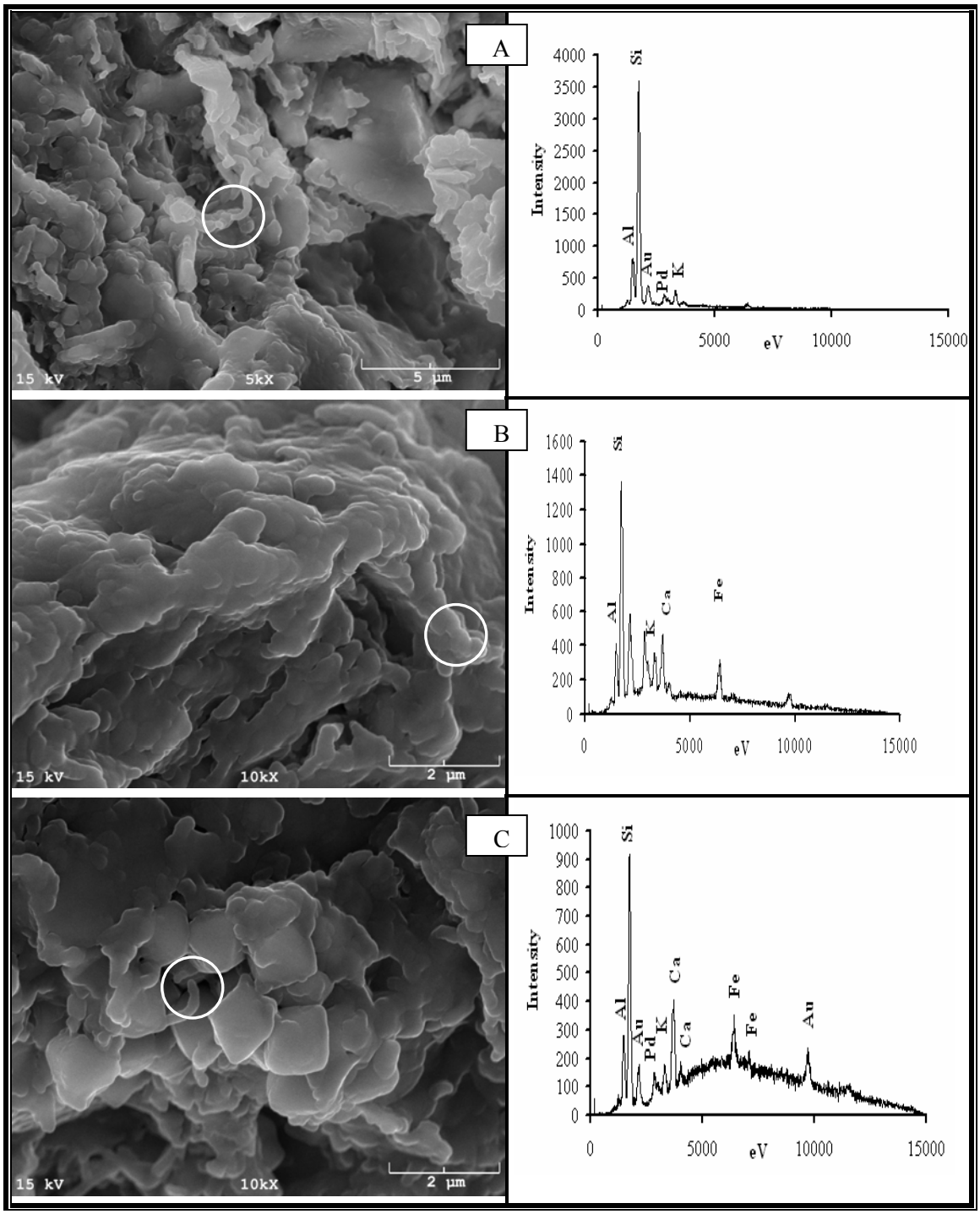

Figure (7-31): SEM images and EDX analysis (1 molal KNO_3 treated sample at 150 °C for 4 months).

A) Silica-Al-Ca-K rich (illite) overgrowing quartz and clay particles

B) Silicification in the shale components

C) The euhedral pyrite crystals change to anhedral and silica-Ca cement deposited on pore space.

Note pores almost disappear leading to reduction in both porosity and permeability

7.4.2.3. Grain-size distribution studies

Grain-size distribution for the HTHP treated samples were studied using the Beckman-Coulter Laser Grain Size Analyzer discussed in Chapter 4. There is no big change in grain-size distribution due to the use of the nitrate fluids under the HTHP condition based on analyses of the grain-size distribution charts (Fig 7-32). The only change that can be seen from these charts is a slight increase in 1-7 μm range with all the nitrate fluids under the same two temperature conditions (100 and 150 °C). The only disclaimer on this observation and as mentioned in room temperature conditions come from the samples heterogeneity. $Ca(NO_3)_2$ shows the maximum increase in this size range and $NaNO_3$ shows the minimum. This change is enhanced with increasing temperature. The reason for no big change in grain-size being recorded may be due to the newly formed materials being too small (see SEM images) to be recorded by the current technique. Alternatively, because the grain-size analyzer may record both of the small newly formed materials and the pre-existing components as grain aggregates or agglomerates since the new silica cement (SEM images) attaches them to each other. This may be the cause of the small increase in the 1-7 μm portions. The sand-silt-clay percentages or the grain size static parameters show no change at all (Fig. 7-33). The coarsening of 1-4 μm grain-size that recorded during room temperature condition to be 1-7 μm recorded change in HTHP is suggested. The changes in grain-size distribution during room conditions and HTHP condition are in agreement with Eberl et al. (1993) studies that concluded the main change in grain-size due to illitization of smectite will be within the fundamental grain-sizes (4 μm for smectite and 2 μm for illite).

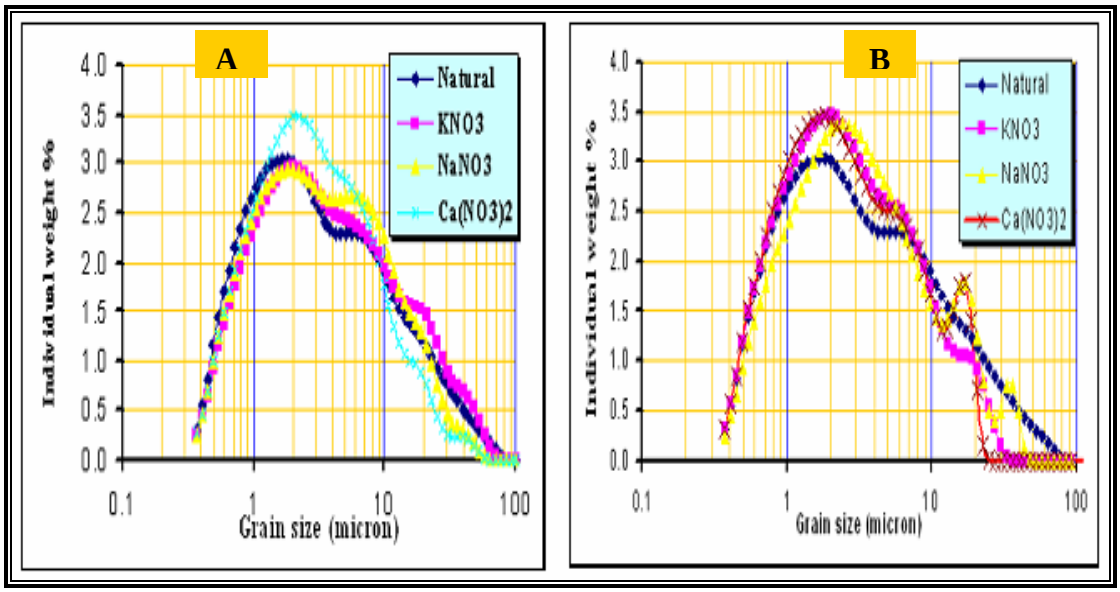

Figure (7-32): Grain-size distribution curves for sample treated by 1 mole nitrate for 35 days curing time.
A) 100 °C temperature, 600 psi Pp and 900 psi Pc
B) 150 °C temperature, 2,800 psi Pp and 3,000 psi Pc.

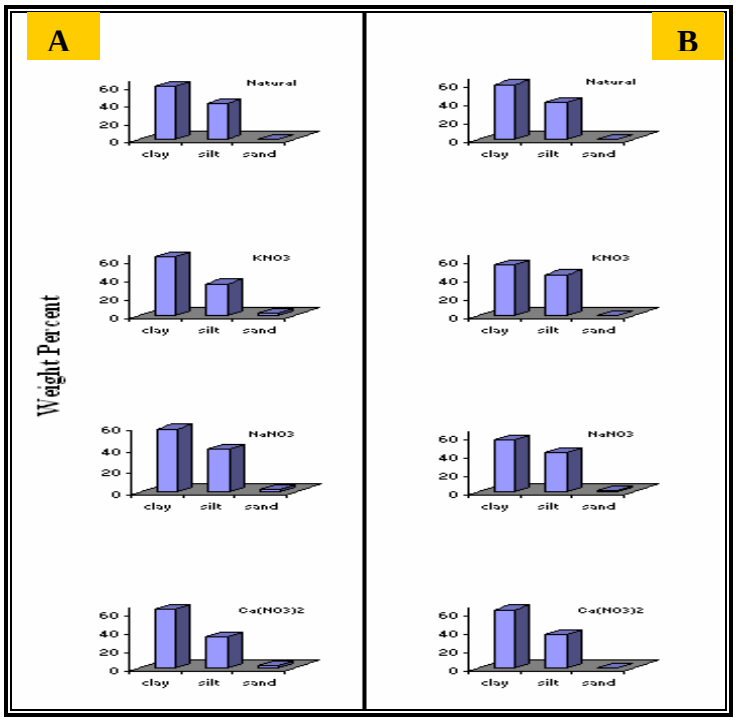

Figure (8-33): Clay-silt-sand content for 1 mole nitrate treated samples for 35 days curing time at:
A) 100 °C temperature, 600 psi Pp and 900 psi Pc
B) 150 °C temperature, 2,500 psi Pp and 3,000 psi Pc.

7.5. Conclusions

- The composition and structure of clay minerals are very sensitive and are easily influenced by pore fluid chemistry even at normal temperature conditions.
- Pore fluid changes produce a new phase of clay minerals at room temperature and up to 150 °C. Na, Ca-bearing solutions showed a new smectite phase but K-bearing solutions showed a new illite phase.
- In the presence of K ions smectite minerals showed progressive transformation to smectite/illite mixed layer and/or illite at room temperature and up to 150 °C. This transformation is controlled by the concentration of K, temperature and curing time.
- High temperature (up to 150 °C) was able to destroy smectite and illite structures and form Si instead, most probably α–quartz (silicification). The rate of mineral dissolution and precipitation is temperature and time dependent. That means temperature not only accelerates smectite/illite transformation but also accelerates shale silicification.
- Na and Ca ions enhance smectite crystallinity at room temperature, depending on the concentrations of these elements and the exposure time. However, this effect may be diminishing with increasing temperature especially at or above 150 °C. This effect leads to an increase in smectite swelling ability, which leads to porosity and permeability reduction under certain conditions.
- Na has the least effect on clay minerals and grain-size distribution; K has the highest effect. Ca behaves in between. These behaviors follow the order of atomic radius.

-Smectite-illite transformation seems to follow dissolution and crystallization mechanism.

- Clay mineral transformations during the experiments produced a 0.5 to 1.5 % increase within 1-4 μm grain-size fractions for room temperature condition samples and within 1-7 μm grain-size fractions for HTHP condition samples.

7.6. Recommendations

The current study did not study the effect of chemical fluids on the organic matter, which is a part of the shale component. Changes in the order and the color of the fluids that were used in the current study were noted, especially Ca-fluids ($CaCO_3$ and $Ca(NO_3)_2$ (Fig. 7-34). these changes inferred to be the reaction of these fluids with organic matter. Therefore, further study on this issue is recommended.

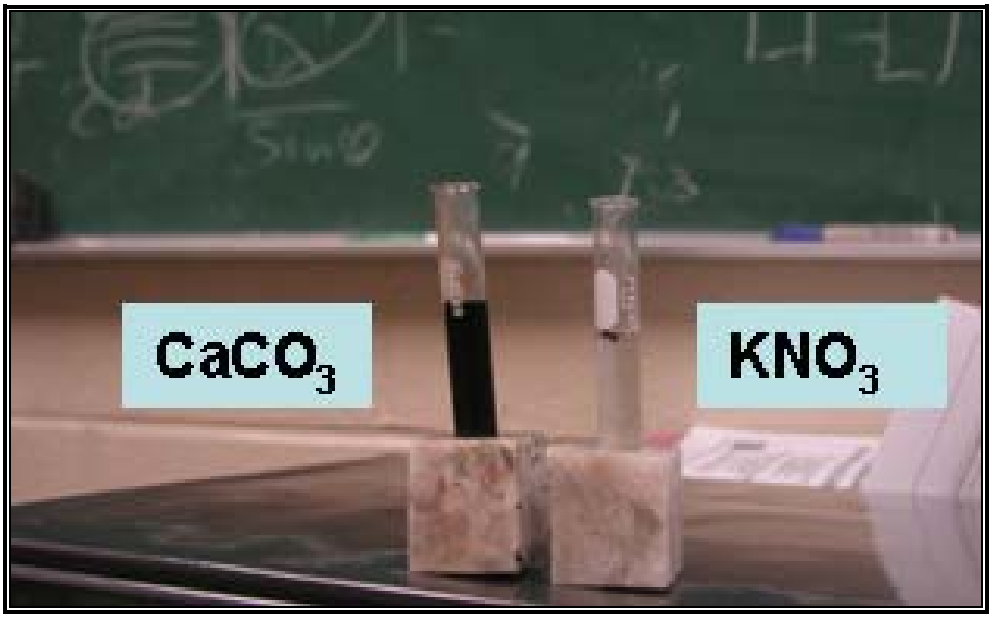

Figure (7-34): Change of fluid color especially with calcium inferred to the reaction of these fluid with the organic matter.

Grain-size studies showed little or no changes. Theoretically, the percent of grain-size less than 1 μm should change significantly. Instead, the increased within 1-

7 μm because most of the new small particles were attached to the original one (SEM images) that might be recorded as one particle. The running time for Coulter Grain Sized analyzer should be increased from 1 minute to 30 minutes to separate new particles from the original ones.

Chapter 8

Summary and Conclusions

Dehydration of shale is a key feature in mediating shale related problems such as wellbore stability, landslides, and soil stability problems created by swelling. Chemical osmotic behaviors of shale have been studied as a means of dehydration/dewatering of shale when exposed to pore fluid chemical potential gradients. New laboratory studies using Pierre Shale are presented for osmotic membrane efficiency, solute diffusion, swelling pressure, permeability mineralogical and textural changes with time as functions of temperature, effective pressure, and pore fluid chemistry. Experiments several months in duration were run with up to 2 molal calcium, sodium, and potassium nitrate salt solutions, at temperature up to 150 degrees Celsius and up to 3,000 psi effective pressure. The competing effects that increase or decrease membrane efficiency with time are highly dependent on the dominant cation in the solutions. Membrane efficiency increases progressively with consolidation and swelling; it decreases with chemical diffusion and continued illitization of smectite. These effects were captured in a mathematical model for membrane efficiency and by numerical solutions for coupled solute and water reaction-transport equations.

Using Van't Hoff's (1887) equation, irreversible thermodynamics (e.g. Fritz, 1965 and 1986) and mass conservation relations, two mathematical models were derived for the coupled fluid and ionic flux in shales.

The study of this model reveals that, the flux of solute through the semi-permeable membrane and the shale pore fluid's activities will be reduced over the

time leading to a reduction in the membrane properties of shales and clay sediments. Given enough time, chemical and hydraulic differences across the membrane will decrease leading to a diminishing of the fluid osmotic flow. This model can help in correlating and representing clay materials semi-permeable membrane behavior, and enhance understanding of the relevant processes.

Laboratory study of Pierre Shale osmotic flow and the permeability evolution studies using three different nitrate solutions indicated that:

1-Pierre Shale is a very low permeable rock 871 nDarcy on average.

2-Pierre Shale acts as a non-ideal semi-permeable membrane with membrane efficiency of 13 % for 0.25 mole $NaNO_3$ and decrease to 1 % for 2 mole $Ca(NO_3)_2$.

3-Membrane efficiency decreases with an increase in nitrate fluid concentration; this decrease is more dramatic for the calcium nitrate solutions.

4-Osmotic pressure changes with time in the experiments because of diffusion that reduces the concentration difference across shale sample or by reducing the Na-smectite mineral content by K-Na ionic exchange leading to illitization.

5-Low concentration solutions yielded increases in permeability. High concentrations reduce it, except with KNO_3 solutions.

6-Sodium nitrate solutions developed the lowest permeability values; potassium nitrate solutions developed the highest values.

7- 0.5 and 1 mole calcium nitrate solutions developed high permeability values compared to the same concentrations of other nitrate fluids. Also the osmotic

pressure that was produced from those two $Ca(NO_3)_2$ concentrations exhibited a heretofore unobserved oscillatory transient behavior.

8-There is inverse relationship between osmotic pressure and the developed permeability.

Study of the diffusion and swelling behaviors of Pierre Shale within one-month curing time indicated that;

1- There is good inverse relationship between swelling and diffusion and permeability. a direct relationship exists between osmotic pressure and swelling. The swelling reduces the ability of both fluid and cations to move through shale leading to the development of high osmotic pressure.

2- Many ions were excluded by clay mineral structure during the diffusion test which makes shale suitable for possible use in water purification.

3- Moderate concentration (activity) gradients can induce fluid fluxes (Darcy velocities) of up to 1 cm/day.

4- Swelling of Pierre Shale depends on chemical type and time.

5- KNO_3 solutions produced very low swelling stress shown but $NaNO_3$ solution produce the maximum swelling stress.

6- Swelling stress over a long period showed oscillatory phenomena with all nitrate fluids. Intensity and frequency of this phenomenon depends on the type and concentration of the fluid. This phenomenon may lead to an increase in shale permeability. This phenomenon may be the result of cyclic tensile fracturing or pore space increases that accompanying from swelling leading to pore pressure increases.

The impacts of different fluids on clay minerals and grain-size distribution in Pierre Shale were performed at room temperature conditions using three different nitrate solutions and three different carbonate solutions. In addition, behaviors of Pierre Shale clay minerals were studied under high-pressure temperature conditions using three nitrate solutions. From these studies, the following conclusions are obtained:

1- Clay minerals are sensitive and easy affected by changes of pore fluid chemistry at normal temperature conditions and engineering time-scales. Geologic time and/or increases in temperature are not necessary. This has important consequences for use of clays in monitor well construction, containment of wastes by clay liners, and other engineering uses of clay materials.

2- Because of pore fluid changes, new phases of clay minerals were formed from room temperature up to 150 °C. Na, Ca fluids induced changes in smectite while K fluids induced growth of a new discrete illite phase.

3- In the presence of K ions, clay minerals showed progressive transformation from smectite to illite at different temperature conditions, from room temperature up to 150 °C. This transformation is directly related to concentration of the K, temperature and the duration of the experiments.

4- High temperatures (up to 150 °C) destroy smectite and illite structures to form silica new phase, probably alpha-quartz. The rate of destruction and formation of the new phases is temperature and time dependent. That means temperature not only accelerates smectite-illite transformation but also accelerate shale silicification.

5- Na and Ca-bearing solutions increase smectite crystallinity at room temperature depending on concentrations of these elements and the exposed time. However, this effect may be diminished with increasing temperature, especially approaching to 150 °C. This effect leads to increasing smectite swelling ability, which leads to porosity and permeability reduction.

6- Na has the lowest effect on clay minerals and grain size distribution; K has the highest effect. Ca behaves in between.

7-Smectite-illite transformation seems to follow dissolution and crystallization mechanism.

8- Clay mineral transformations during the experiments produced a 0.5 to 1.5 % increase within 1-4 μm grain-size fractions for room temperature condition samples and 1-7 μm grain-size fractions for HTHP condition samples.

References

Al-Bazali, T. M., 2005. Experimental Study of the Membrane Behavior of Shale During Interaction with Water-Based and Oil-Based Muds: Austin, USA, University of Taxes.

Alexander, J., 1990. A Review of Osmotic Processes in Sedimentary Basin, *in* Survey, B.G., ed.: Nottingham, UK.

Andersson, K., Allard, B., Bengtsson, M. and Magnusson, B., 1989. Chemical Composition of Cement Pore Waters. Cement and Concrete Research, 19: 327-332.

ASTM-D422, 1990. Standerd Test Methods for Perticles Size Analysis of Soils, Annual Books of ASTM Standards.

Bailey, S.W., 1980. Structures of Layer Silicates. , *in* Brindley, G. W., and Brown, G., eds., Crystal Structures of Clay Minerals and their X-ray Identification: London, Mineralogical Society p. 6-28.

Bailey, S.W., and Robinson, K., 1951. The Chlorite Minerals, *in* W., B.G., and Brown, G., eds., Crystal Structures of Clay Minerals and their X-Ray Identification London, Mineralogical Society, p. 125-195.

Barbour, S. L. and Fredlund, D. G., 1989. Mechanisms of Osmotic Flow and Volume Change in Clay Soils. Canadian Geotechnical Journal 26(4): 551-562.

Bates, R.L., and Jackson, J.A., 1987. Glossary of Geology. American Geological Institute, Fall Church. 788 p.

Berkgaut, V., Singer, A. and Stahr, K., 1994. Palagonite Reconsidered: Paracrystalline Illite-Smectites from Regoliths on Basic Pyroclastics. Clays and Clay Minerals, 42: 582-592.

Berner, R. A., 1969. The Synthesis of Framboidal Pyrite: Econ. Geology, v. 64, p. 383-384.

Berry, F. A., 1969. Relative Factors Influencing Membrane Filtration Effects in Geological Environments: Chemical Geology, v. 4, p. 295-301.

Bilir, M. E., Muftuoglu, Y. V. and Sari, D., 2004. A Computer-Controlled Triaxial Swelling test Apparatus. Turkish J. Eng. Env. Sci, 28: 269-280.

Bird, G.W., 1979. Possible Buffer Materials for Use in a Nuclear Waste Vault. Atomic Energy of Canada Limited Technical Record, TR-72.

Bird, G.W. and Cameron, D. J., 1982. Fault Sealing Research for the Canadian Nuclear Fuel Waste Management Program. . Atomic Energy of Canada Limited Technical Record, TR-145.

Biscaye, P. E., 1965. Mineralogy and Sedimentation of Recent Deep Sea Clay in the Atlantic Ocean and Adjacent Seas and Oceans. Geol. Soc. Am. Bull, 76: 803 - 831.

Boggs, S. Jr., 1995. Principles of Sedimentology and Stratigraphy. 2nd edition. Prentice-Hall , Inc. New Jersey, 774 pp.

Boles, J. R. and Franks, S.G., 1979. Clay Diagenesis in Wilcox Sandstones of Southwest Texas: Implication of Smectite Diagenesis on Sandstone Cementation. J. Sed. Pet, 49: 55-70.

Bolt, G. H., 1956. Physico-Chemical Analysis of the Compressibility of Pure Clays. Geotechnique, 6(2): 86-93.

—, 1970. Sedimentary Pyrite Formation: American Journal of Science, v. 268, p. 1-23.

Bowles, J. E., 1992. Engineering Properties of Soil and their Measurements: New York, McGeaw-Hill, 241 p.

Brace, W. F., Walsh, J. B. and Frangos, W.T., 1968. Permeability of Granite Under High Pressure J. Geophys. Res, 73 2225-2236.

Bradley, W. F., 1945. Molecular Associations between Montmorillonite and Some Polyfunctional Organic Liquids: Journal. Am. Chem. Soc., v. 67, p. 975-981.

Brindley, G.W., and Brown, G., 1980. Crystal Structures of Clay Minerals and their X-Ray Identification Monographs No. 5, Mineralogical Society, p. 249-303.

Brunton, G., 1955. Vapour Pressure Glycolation of Oriented Clay Minerals: Am. Mineral. , v. 40, p. 124-126.

Canfield, D. E., and Berner, R. A., 1987. Dissolution and Pyritization of Magnetite in Anoxic Marine Sediments: Geochimica et Cosmochimica Acta, v. 51, p. 645-659.

Carminati, S., Brignoli, M., Di Marco, A. and Santarelli, F.J., 1997. The Activity Concept Applied to Shale: Consequences for Oil, Tunneling and Civil Engineering Operations. . International Journal of Rock Mechanics and Mining Division, 34(3-4): No. 038.

Cey, B. D., Barbour, S. L., and Hendry, M. J., 2001. Osmotic Flow through a Cretaceous Clay in Southern Saskatchewan, Canada: Can. Geotech. J/Rev. Can. Geotech, v. 35, p. 1025-1033.

Chamley, H., 1989. Clay Sedimentology: Berlin, Springer-Verlag, 623 p.

Chapman, D. L., 1913. A Contribution to the Theory of Electrocapillarity: Philosoph. Magaz., v. 25, p. 475–481.

Chenevert, M. E., 1970. Shale Alteration by Water Adsorption: Journal of Petroleum Technology, p. 1141-1148.

Chenevert, M. E., 1990. Diffusion of Water and Ions into Shales. Rock at Great Depth, 3: 1177-1184.

Colten, V. A., 1985. Experimental Determination of Smectite Hydration States under Simulated Diagenetic Conditions. University of Illinois at Urbana-Champaign, 1985, 154 pages; AAT 8511598

Coulten-Bradley, V. A., 1987. Role of Pressure in Smectite Dehydration-Effect on Geopressure and Smectite-to-Illite Transformation. AAPG Bulletin, 71 (11), 1414-1427

Cuadros, J. and Linares, J., 1995. Experimental Kinetic Study of the Smectite-to-Illite Transformation. Geochim. Cosmochim. Acta, 60(3): 439-453.

DeGroot, S. R., and Mazur, P., 1962. Non Equilibrium Thermodynamics, North Holland Publishing Company, North Holland, Amsterdam, 510 p.

Demir, I., 1988. Studies of Smectite Membrane Behavior: Electrokinetic, Osmotic, and Istopic Fractionation: Geochimica et Cosmochimica Acta, v. 52, p. 727-737.

Diek, A., Santos, H., and Varela, A., 1996. Determinants of Shale and Clay Fabric Features: Structure and Properties (a Critical Review): University of Oklahoma, Norman, Rock Mechanics Institute Report (RMC-96-05).

Dixon, J.B., 1990. Kaolin and Serpentine Group Minerals. , *in* Dixon, J.B., and Weed, S.B., eds., Minerals in Soil Environments, Soil Science Society of America, p. 467 - 511.

Dhowain. A. W., Erol, A.O. and Youssef, A., 1990. Evaluation of Expansive Soils and Foundation Methodology in the Kingdom of Saudi Arabia.

Dzialowski, A., Hale, A. and Mahajan, S., 1993. Lubricity and Wear of Shale: Effects of Drilling Fluids and Mechanical Parameters. In: SPE/IADC25730 (Editor), SPE/IADC Drilling Conference Amsterdam.

Eberl, D. and Hower, J., 1976. Kinetics of Illite Formation. Geol. Soc. Am. Bull, 87: 1326-1330.

Eberl, D. and Srodon, J., 1988. Ostwald Ripening and Interparticle Diffraction Effects for Illite Crystals. Am. mineral., 73: 1335-1345.

Eberl, D., Srodon, J., Kralik, M., Yaylor, R. and Peterman, Z., 1990. Ostwald Ripening of Clays and Metamorphic Minerals. Science, 248: 474-477.

Eberl, D., Velde, B. and McCormick, T., 1993. Synthesis of Illite-Smectite from Smectite at Earth Surface Temperatures and High pH. Clay Minerals, 28: 49–60.

Ebrahim, S., and Abdel-Jawad, M., 1994. Economics of Seawater Desalination by Reverse Osmosis: Desalination, v. 99, p. 39-55.

El-Guendouzi, M., and Marouani, M., 2003. Water Activities and Osmotic and Activity Coefficients of Aqueous Solutions of Nitrates at 25 ^{0}C by Hygrometric Method: Journal of Solution Chemistry, v. 32, p. 535-546.

El-Swaify, S. A. and Henderson, D. W., 1967. Water Retention by Osmotic Swelling of Certain Colloidal Clays with Varying Ionic Composition. Journal of Soil Science, 18(1): 118-124.

Everhart, T. E. and Hayes, T. L., (1972). The Scanning Electron Microscope: Sci. Am., v. 226, p 55-69.

Ewy, R.T. and Stankovich, R. J., 2000. Pore Pressure Change due to Shale-Fluid interactions: Measurements under Simulated Wellbore Conditions. In: P.P. Rocks (Editor), 4th North American Rock Mechanics Symposium. Belkema, Rotterdam, Seattle, pp. 147-154.

Farrand, M., 1970. Framboidal Sulphids Precipitated Synthetically: Mineral Depos. , v. 5, p. 237-247.

Fetter, C. W., 1994. Applied Hydrogeology: New York, Macmillan College Publishing Co., 691 p.

Folk, R. L., 1974. Petrology of Sedimentary Rocks. Hemphill, Austin, Tex, 182 pp.

Forsans, T. M. and Schmitt, L., 1994. Capillary Forces; the Neglected Factor in Shale Instability Studies. Eurock 94,BelKema, Rotterdam.

Fritz, S. J., 1986. Ideality of Clay Membranes in Osmotic Processes: A Review: Clays and Clay Minerals, v. 34, p. 214-223.

Gouy, D.L., 1910. Sur la constitution de la charge électrique a la surface d‘un électrolyte: Ann. Phys, v. 9, p. 457-468.

Graf, D.L., 1983. Chemical Osmosis, reverse Chemical Osmosis and the Origin of Subsurface Brines: Geochimica et Cosmochimica Acta, v. 46, p. 1431-1448.

Griffith, A. A., 1920. Phenomena of Rupture and Flow in Solids. Philosophical Transactions of the Royal Society of London, A221: 163-198.

Grim, R.E., 1953. Clay Mineralogy: New York, McGraw-Hill Book Co., 596 p.

—, 1962. Applied Clay Mineralogy: New York, McGraw-Hill Book Co. , 422 p.

—, 1968. Clay Mineralogy: New York, McGraw-Hill Book Co., 596 p.

Groenevelt, P. H., and Bolt, G. H., 1969. Non-equilibrium Thermodynamics of the Soil-water System: Journal of Hydrology, v. 7, p. 358-388.

Hanshaw, B. B., and Hill, G. A., 1969. Geochemistry and Hydrodynamics of the Paradox Basin Region Utah, Colorado and New Mexico: Chemical Geology, v. 4, p. 263-294.

Hanshaw, B. B., and Zen, E. A., 1965. Osmotic Equilibrium and Overthrust Faulting.: Bulletin of the Geological Society of America, v. 76, p. 1379-1386.

Hillel, D., 1980. Fundamentals of Soil Physics: New York, Academic Press, 413 p.

Hoffman, J. and Hower, J., 1979. Clay Mineral Assemblages as Low Grade Metamorphic Geothermometers: Application to the Thrust Faulted Distributed Belt of Montana, USA. . Soc. Econ. Pal. Spec., 26: 55-79.

Horseman, S.T., Higgo, J. J. W., Alexander, J. and Harrington, J. F., 1996. Water, Gas and Solute Movement Through Argillaceous Media, Paris.

Howard, J. J. and Roy, D. M., 1985. Development of Layer Charge and Kinetics of Experimental Smectite Alteration. Clays and Clay Minerals, 33: 81-88.

Hower, J., Eslinger, E.V., Hower, M.E. and Perry, E.A., 1976. Mechanism of Burial Metamorphism of Argillaceous Sediments: Mineralogical and Chemical Evidence. . Geol. Soc. Am. Bull, 87: 725-737.

Huang, W. H., Longo, J. M. and Peaver, D. R., 1993. An Experimental Derived Kinetic Model for the Smectite-to-Illite Conversion and its Use as a Geothermometer. Clays and Clay Minerals, 41: 162-177.

Inoue, A., 1983. Potassium Fixation by Clay Minerals During Hydrothermal Treatment. Clays and Clay Minerals, 31: 81-91.

Inoue, A., Koyama, N., Kitagawa, R. and Watanabe, T., 1988. Chemical and Morphological Evidence for the Conversion of Smectite to Illite. Clays and Clay Minerals, 352(2): 111-120.

Ishiguro, M., Matsuuro, T., and Detellier, C., 1995. Reverse Osmosis Seperation for a Montmorillonite Membrane: Journal of Membrane Science, v. 107, p. 87-92.

Jaeger, J. C. and Cook, N.G.W., 1979. Fundamentals of Rock Mechanics. Chapman and Hall, London, 593 pp.

Kalliokoski, J., and Cathles, L., 1969. Morphology, Mode of Formation, and Diagenetic Changes in Framboid: Bulletin of the Geological Society of Finland, v. 41, p. 125-133.

Kastelan-Kunst, L., Kosutic, K., Dananic, V., and Kunst, B., 1997. FT30 Membranes of Characterized Porosities in the Reverse Osmotic Organics Removal from Aqueous solutions Water Research, v. 31, p. 2878-2884.

Kedem, O., and Katchalsky, A., 1958. Thermodynamic Analysis of the Permeability of Biological Membranes to Non-electrolytes. Biochim. Biophys. Acta , 27: 229-246.

Keijer, T. J .S., 2000. Chemical Osmosis in Natural Clayey Materials, Universiteit Utrecht.

Kemper, W. D. and Rollis, J. D., 1966. Osmotic Efficiency Coefficients across Compacted Clays Soil Science Society of America Proceedings, 30(5): 529-534.

Kemper, W. D. and Van Schaik, J. C., 1966. Diffusion of Salts in Clay-Water Systems. Soil Science Society of America Proceedings, 30(5): 534-540.

Land, S. L., Mack, L. E., Milliken K. L., and Lynch, F. L., 1997. Burial Diagenesis of Argillaceous Sediment, South Texas Gulf of Mexico Sedimentary Basin: A Reexamination: Geological Society of America, Bulletin, v. 103, p. 2–15.

Loch, J. P., and Keijzer, T.J., 1996. Chemical Osmosis in Contaminated Clayey Materials: Heidelberg, V.M. Goldschmidt Conference, 367 p.

Loma, R. F., Chenevert, M. E. and Sharma, M. M., 2000. The Ion-selective Membrane Behavior of Native Shales. Journal of Petroleum Science and Engineering: 9-23.

Love, L. G., and Amstutz, G. C., 1966. Review of Microscopic Pyrite from the Devonian Chattanooga Shale and Rammelasberg Banderz: Fortschr Miner, v. 43, p. 273-309.

Low, P.E., 1961. Physical Chemistry of Clay-Water Interaction: Advances in Agronomy, v. 13, p. 269-327.

Lunden, I. and Andersson, K., 1989. Modeling the Mixing of Cement Pore Water and Groundwater Using the PHREEQE Code. . Materials Research Society Symposium Proceedings, 127: 949–956

Lynch, F. L., Mack, L. E., Milliken K. L., and Land, S. L. 1997. Burial Diagenesis of Illite/Smectite in Shales and Origins of Authigenic Quartz and Secondary Porosity in Sandstone. Geochimica et Cosmochimica acta, v. 61 (10), p. 1995–2006.

MacEwan, D. M. C., and Ruiz-Amil, A., 1975. Interstratified Clay Minerals, *in* Gieseking, J.E., ed., Inorganic components, Soil Components, Volume 2: New York, Springer-Verlag, p. 265-334.

Mackenzie, R. C., 1959. The Classification and Nomenclature of Clay Minerals: Clay Minerals Bull., v. 4, p. 52-66.

Manohar, L., 1999. Drilling Fluid Interaction and Shale Strength. In: S. 54356 (Editor), SPE Latin American and Caribbean Petroleum Engineering Conference, Caracas, Venezuelan.

Marine, I. W., and Fritz, S. J., 1981, Osmotic Model to Explain Anomalous Hydraulic Heads: Water Resources Research, v. 17, p. 73-81.

Menon, K. K., 1967. Origin of Diagenetic Pyrite in the Quilon Limestone, Kerala, India.: Nature, v. 213, p. 1219-1220.

Merten, U., 1966. Desalination by Reverse Osmotic: London, MIT Press, 289 p.

Millot, C., 1970. Geology of Clays: Berlin, Springer-Verlag, 499 p.

Mitchell, J. K., 1993. Fundamentals of Soil Behavior. New York, Jon Wiley & Sons, 456 p.

Mitchell, J. K., Greenberg, J. A. and Witherspoon, P. A., 1973. Chemico-Osmotic Effects in Fine-Grained Soils. Journal of soil Mechanics and foundations Division, A.S.C.E, 99(SM4): 307-322.

Mody, F. K., and Hale, A. H., 1993. A Borehole Stability Model to Couple the Mechanics and Chemistry of Drilling Fluid Shale Interaction. SPE/IADC25728, SPE/IADC Drilling Confrance: Amstrerdam.

Morgenstern, N. R. and Balasubramonian, B. I., 1980. Effects of Pore Fluid on the Swelling of Clay Shale. 4th International Conference on Expansive Soils, Denver, Colorado, pp. 190-205.

Mosser-Ruck, R., Cathelineau, M., Baronnet, A. and Trouiller , A., 1999. Hydrothermal Reactivity of K-smectite at 300oC and 100 Bar: Dissolution-Crystallization Process and non-Expandable Dehydrated Smectite Formation. Clay Minerals, 34: 275-290.

Nadeau, P. H. and Reynolds, R. C., 1981. Burial and Contact Metamorphism in the Mancos Shale. Clays and Clay Minerals, 29: 249-259.

Nadeau, P. H., Peacor, D. R., Yan, J., and Hillier, S., 2002. I-S Precipitation in Pore Space as the Cause of Geopressureing in Mesozoic Mudstones, Egresund Basin, Norwegian Continental Shelf. American Mineralogist. v. 87, p 1580-1589.

Nadeau, P. H., Wilson, M. J., McHardy, W. J. and Tiat, J. M., 1985. The Conversion of Smectite to Illite during Diagenesis: Evidence from Some Illitic Clays from Bentonites and Sandstones. Mineral. Mag., 49(393-400).

Neuzil, C. E., 1998. Is Osmosis Important in the Subsurface? Evidence fro an In-situ Experiment.: Abstracts with Programs, v. 30, p. 173.

Neuzil, C. E., 2000. Osmotic Generation of Anomalous Fluid Pressures in Geological Environments: Nature, v. 403, p. 182-184.

O'Brien, N. R. and Slatt, R. M., 1990. Argillaceous Rock Atlas. Springer-Verlag, New York, 141 pp.

Olson, R. E. and Mesri, G., 1970. Mechanisms Controlling Compressibility of Clays. Journal of soil Mechanics and Foundations Division, A.S.C.E, 96(SM6): 1863-1878.

Osisanya, S. O. and Chenevert, M. E., 1996. Physico-Chemical Modelling of Wellbore Stability in Shale Formations. The Journal of Canadian Petroleum Technology, 35(2): 53-63.

Perry, E. A. and Hower, J., 1970. Burial Diagenesis in Gulf Coast Pelitic Sediments. Clays and Clay Minerals, 18: 165-177.

Pierce, J.W., and Siegel, F.R., 1969. Quantification in clay mineral studies of sediments and sedimentary rock: Journal of Sed. Petrol, v. 9, p. 187-193.

Potter, P. E., Maynard, J. B. and Pryor, W.A., 1980. Sedimentology of Shale. Springer-Verlag, New York, 553 pp.

Pusch, R., 1973. Highly Compacted Na Bentonite as Buffer Substance, Sweden.

Reynolds, R. C., 1980. Interstratified Clay minerals, *in* W., B.G., and Brown, G., eds., Crystal Structures of Clay Minerals and their X-Ray Identification, : London, Mineralogical Society, p. 249-303.

—, 1988. Mixed layer Chlorite Minerals, *in* Bailey, S.W., ed., Hydrous Phyllosilicates (exclusive of micas): Reviews in Mineralogy Volume 19, Mineralogical Society of America, p. 601-629.

Reynolds, R. C., and Hower, J., 1970. The Nature of Interlayering in Mixed-Layer Illite-Montmorillonite: Clays and Clay Minerals, v. 18, p. 25-36.

Righi, D., Velde, B. and Meunier, A., 1995. Clay Stability in Clay-Dominated Soil Systems. Clay Minerals, 30: 45-54.

Roberson, H. E. and Lahann, R.W., 1981. Smectite to Illite Conversion Rates: Effects of Solution Chemistry. Clays and Clay Minerals, 29: 129-135.

Robinson, R. A., and Stokes, R. H., 1959. Electrolyte Solutions: London, Butterworths-Heinemann 559 p.

Ruwaih I. A., 1987. Experiences with Expansive Soils in Saudi Arabia. 6th International Conference on Expansive Soils, New Delhi, India, pp. 317-322.

Sawlowicz, Z., 1992. Primary Sulphide Mineralization in Cu-Fe-S Zones of Kupferschiefer, Fore-Sudetic Monocline, Poland.: Trans Instn Min Metall (sec. B: Appl Earth Sci),, v. 101, p. B1-B8.

Sherwood, J. D., 1995. Ionic Transport in Swelling Shale. Advances in Colloid and Interface Science, 61: 51-64.

Srodon, J., 1999. Nature of Mixed-Layer Clays and Mechanisms of their Formation and Alteration: Annu. Rev. Earth Plant. Sci, v. 27, p. 19-53.

Srodon, J., Eberl, D., and Drits, V., 2000. Evolution of Fundamental-Particle Size During Illitization of Smectite and Implications for Reaction Mechanism: Clays and Clay Minerals, v. 48, p. 446-458.

Steiger, R. P., 1993. Advanced Triaxial Swelling Tests on Preserved Shale Cores. International Journal of Rock Mechanics and Mining Science, 30: 681-685.

Sunagawa, I., Endo, Y., and Nakai, N., 1971. Hydrothermal Synthesis of Framboids Pyrite: Soc Min Geol Jp Spec Issue, v. 2, p. 10-14.

Terzaghi, K., 1943. Theoretical Soil Mechanics. John Wiley, New York, 210 pp.

Tourtelot, H. A., 1960. Origin and Use of the Word Shale. Am. Jour.Sci., 258-A: 335-343.

Vallentyne, J. R., 1963. Isolation of Pyrite Spherules from Recent Sediments: Limnol Oceanogr, v. 8, p. 16-30.

Van der Pluijm, B.A., and Marshak, S., 1997, Earth Structure: An Introduction to Structural Geology and Tectonics: New York, McGraw-Hill, 495 p.

Van't Hoff, J. H., 1887. The Role of Osmotic Pressure in the Analogy between Solutions and Gases Zeitschrift fur Physikalische Chemie, v. 1, p. 481-508.

Van Oort, E., 2003. On the Physical and Chemical Stability of Shale: Journal of Petroleum Science & Engineering, v. 38, p. 213-235.

Van Oort, E., Hale, A. H., and Mody, F. K., 1996. Transport in Shales and the Design of Improved Water-based Shale Drilling Fluids SPE Drilling and Completion 11, Volume 3, p. 137-146.

Van Oort, E., Ripley, D., Ward, I., Chapman, J. W., Wiliamson, R., and Aston, M., 1996. Silicate-Based Drilling Fluids: Competent, Cost-Effective and Benign Solutions to Wellbore Stability Problems. : SPE 35059.

Velde, B., 1995. Composition and Mineralogy of Clay Minerals *in* Velde, B., ed., Origin and Mineralogy of Clays: Clays and the Environment New York, Springer-Verlag, p. 8-42.

Walsh, J. B., 1965. The Effect of Cracks on the Compressibility of Rock: J. Geophys. Res, v. 70, p. 381-389.

Warkentin, B. P. and Bozozuk, M., 1961. Shrinking and Swelling Properties of Two Canadian Clays, Fifth International Conference on Soil Mechanics and Foundation Engineering, pp. 851-855.

Weaver C. E., 1989. Clays, Muds and Shales: Amsterdam, Elsevier, 890 p.

Weaver, C. E. and Beck, K. C., 1971. Clay-Water Diagenesis During Burial: How Mud Becomes Gneiss. . Geol. Soc. Am. Spec. , 134(96).

Welton, J. E., 1984. SEM Petrology Atlas: Methods in Exploration Series: Tulsa, Oklahoma, American Association of Petroleum Geologists, 237 p.

Whitney, G., 1990. Role of Water in the Smectite-to-Illite Reaction. Clays and Clay Minerals, 38: 343-350.

Whitney, G., 1992. Dioctahedral Smectite Reactions at Elevated Temperatures: Effects of K-Availability, Na/K Ratio and Ionic Strength. Appl. Clay Sci., 7: 97-112.

Whitney, G. and Northrop, H.R., 1988. Experimental Investigation of the Smectite to Illite Reaction: Dual Reaction Mechanisms and Oxygen-Isotope Systematics. Am. Mineral., 73: 77-90.

Whitworth, T. M., 1993. Hyper filtration-Induced Isotopic Fractionation: Mechanisms and Role in the Subsurface [Ph. D thesis]: Purdue, Purdue University.

Whitworth, T. M., and Fritz, S. J., 1994. Electrolyte-Induced Solute Permeability Effects in Compacted Smectite Membranes. : Appl. Geochem, v. 9, p. 533–546.

Wilson, M. J., 1987. X-ray Powder Diffraction Methods, *in* Wilson, M.J., ed., A handbook of determinative methods in clay mineralogy New York, Chapman and Hall, p. 26-98.

Wood, W.W., 1976. A Hypothesis of Ion Filtration in a Potable-Water Aquifer System: Ground water, v. 14, p. 233-244.

Yeung, A.T., and Mitchell, J. K., 1993. Coupled Fluid, Electrical and Chemical Flows in Soil: Journal of Geotechnique v. 43, p. 121-134.

Yu, M., Sharma, M. M., and Chenevert, M.E., 2003. Chemical-Mechanical Wellbore Instability Model in Shales Accounting for Solute Diffusion: Journal of Petroleum Science and Engineering, v. 38, p. 131-143.

Zhang, J., Chenevert, M. E., Al-Bazali, T. and Sharma, M. M., 2004. A New Gravimetric-Swelling Test for Evaluating Water and Ion Uptake in Shales. In: S.P. 89831 (Editor), SPE Annual Technical Conference and Exhibition, Houston, Texas.

Appendix A:

Numerical Solutions for Osmotic Flow and Ions' Flux Models Using Mathematica™

Off [General:: "spell1"]

Off [General:: "spell"]

Clear [solution, c, p, p_{up}, x, t, σ, q, f_1, f_2, f_3]

(*Parameters*)

$\kappa = 25 \text{ X } 10^{-21}$ $m.sec^{-1}$

$p_{zero} = 7$ Mpa

$a = 3.14 (0.5 \text{ X } 10^{-2})^2$ m^2

$x_{max} = 3 \text{ X } 10^{-3}$ m

$\phi = .01$ unitless

$t_{max} = 4 \text{ X } 3600$ sec

$c_{max} = 1000.0$ $mol.m^{-3}$

$D = 1.0 \text{ X } 10^{-12}$ m^2s^{-1}

$\beta = 4.59 \text{ X } 10^{-4}$ MPa^{-1}

$\vartheta = 0.8$ unitless

$\eta = 1.0 \text{ X} 10^{-9}$ MPa^{-5}

$vol = 1.0 \text{ X } 10^{-6}$ m^3

bb = 0.00005

aa =1.0

(*Functions*)

q [t_, x_]: = - $(\kappa/\eta)\ \delta_x$ p[t, x] + σ [t, x]$(\vartheta\ \kappa\ \eta)\delta_x$ c [t, x]

f_1 [t_, x_] := D - (1 - σ [t, x]) σ [t, x] $\kappa \vartheta$ c[t, x]/(ϕ η)

f_2 [t_, x_] := (1 - σ [t, x]) κ c[t, x]/(ϕ η)

f_3 [t_, x_] := (1 - σ [t, x]) q [t, x]/ ϕ

(*Model Solution*)

Solution= NDSolve [{

δ_t c [t, x] == f_1 [t, x] $\delta_{x,x}$ c[t, x] - f_3 [t, x] $\delta_{x,}$ c[t, x] + f_2 [t, x] $\delta_{x,x}$ p [t, x],

δ_t p [t, x] == (κ/(β η ϕ)) $\delta_{x,x}$ p [t, x] - (σ [t, x] ϑ κ/(β η ϕ))$\delta_{x,x}$ c[t, x],

δ_t p_{up} [t, x]== - a/(vol β) q[t, x],

(*Boundary Conditions*)

c [0, x] == 0,

p [0, x] == p_{zero},

p_{up}[0, x] == p_{zero},

p_{up}[t, x_{max}] == p_{zero},

c [t, 0] == c_{max} (1 - Exp[-100 t],

p [t, 0] == p_{up}[t, 0],

c [t, x_{max}] == 0,

p [t, x_{max}] == p_{zero}},

{c, p, p_{up}}, {x, 0, x_{max}}, {t, 0, t_{max}}, AccuracyGoal→1];

(*Plots*)

Plot3D[Evaluate[p [t, x]/.First[solution]],{t, 0, t_{max}},{x, 0, x_{max}}, AxesLabel→

{"time, s", "length, m", "pressure" }, PlotRange →{{0, t_{max}}, {0, x_{max}},

{7,12}}, ViewPoint→{-1,-1,1}]

Plot3D[Evaluate[c [t, x]/.First[solution]],{t, 0, t_{max}},{x, 0, x_{max}}, AxesLabel →
{"time, s", "length, m", "conc, m mol/m^3" }, PlotRange → {{0, t_{max}}, {0, x_{max}},
{0,1000}}, ViewPoint→{-1, 0, 1}]

Plot3D[Evaluate[q [t, x]/.First[solution]],{t, 0, t_{max}},{x, 0, x_{max}}, AxesLabel →
{"time, s", "length, m", "vol flux, m/sec" }, PlotRange → {{0, t_{max}}, {0, x_{max}},
Automatic}, ViewPoint→{-1,-1,1}]

Plot[Evaluate[p[t,0]/.First[solution]],{t,0,tmax},AxesLabel → {"time,s","pressure,
mpa" }, PlotRange → All]

Table[Evaluate[c[t,x]/.First[solution]],{t,0,tmax},{x,0,xmax}]

Run

Appendix B:

Permeability

Many geologic processes, mining, construction projects and other geo-engineering projects are affected by not only the mechanical properties of solid rock but also the characteristics of pore fluid and how easily this fluid can move in and out of the rock. Permeability is a measurement of the rate of fluid flow through a porous material under a hydraulic gradient. Permeability κ is usually determined by measuring the flow rate through a sample under a constant pressure gradient using Darcy's law

$$k = -\frac{Q}{A}\frac{\mu}{\rho g}\left(\frac{\delta h}{\delta x}\right)^{-1}$$

where Q is the volume of fluid discharge per unit time,

A is the cross-section area,

μ is the fluid viscosity,

ρ is the fluid density,

g is acceleration due to gravity, and

$\frac{\delta h}{\delta x}$ is the hydraulic gradient in the flow direction x.

It is generally not practical to determine the permeability of low permeability rocks using steady state methods. These rocks require longer times to establish steady state flow. Brace et al., (1968) used transient methods to measure the permeability of granite under high pressure. This method depends on measuring the decay of in pressure imposed at one end of the sample instead of measuring the flow rate or velocity of fluid through the sample. Brace et al., (1968) assumed that Darcy's law

was valid and from the pressure decay characteristics, they calculated the permeability. To achieve that, they used a mathematic model that will be described in the following paragraphs.

From Darcy's law the rate (q) at which fluid flows in the presence of a pressure gradient ($\frac{\delta P}{\delta x}$) is

$$q = -\frac{kA}{\mu}\frac{\delta P}{\delta x}$$

The net increase in flow dq across a differential volume element dx in length is $\frac{\delta q}{\delta x}dx$ or

$$dq = -\frac{kA}{\mu}(\frac{\delta^2 P}{\delta x^2})dx$$

The net storage of fluid inside the pores during a time increment dt is

$$\frac{\delta}{\delta t}(\frac{V_p dx}{L})dt + (\frac{V_p dx}{L})\beta(\frac{\delta P}{\delta t})dt$$

where V_p is the total pore volume in a sample of length L,

$\frac{\delta}{\delta t}(\frac{V_p dx}{L})dt$ represents the storage of fluid due to compression of the solid matrix, and

$(\frac{V_p dx}{L})\beta(\frac{\delta P}{\delta t})dt$ represents the storage due to compression of the fluid (β).

The net storage of fluid inside the pores must equal the net increase in flow during the same time increment. So

$$\frac{kA}{\mu}(\frac{\delta^2 P}{\delta x^2})dxdt = \frac{\delta}{\delta t}(\frac{V_p dx}{L})dt + (\frac{V_p dx}{L})\beta(\frac{\delta P}{\delta t})dt$$

$$(\frac{\delta^2 P}{\delta x^2}) = \frac{\mu}{k}\frac{\delta}{\delta t}(\frac{V_p}{AL}) + \frac{\mu}{k}(\frac{V_p}{AL})\beta(\frac{\delta P}{\delta t})$$

Or $$\frac{\delta^2 P}{\delta x^2} = \frac{\mu}{k}[\frac{\delta \phi}{\delta t} + \beta\phi(\frac{\delta P}{\delta t})]$$

Where ϕ is the porosity $= \frac{V_p}{AL}$

If the change in porosity is due only to the change in the pore fluid pressure then the change in porosity due to an increase in internal pressure is

$$d\phi = (-\phi\beta_s dP - d\phi_e)$$

where β_s is the compressibility of the solid matrix, and

ϕ_e is the change in porosity due to change in external pressure as in Walsh (1965)

$$d\phi_e = (\beta_s - \beta_{eff})dP$$

where β_{eff} is the effective compressibility of the rock.

The following equations is obtained after substitution:

$$\delta^2 P / \delta x^2 = (\mu\beta / k)\left[\frac{(\beta_{eff} - \beta_s)}{\beta} + \phi(1 - \beta_s / \beta)\right](\delta p / \delta t)$$

They assume both β_{eff} and β_s are very small as compared with β and that the porosity is very small. So the value of $\left[\frac{(\beta_{eff} - \beta_s)}{\beta} + \phi(1 - \beta_s / \beta)\right]$ approaches zero, which means that the pressure distribution along the sample is equal to

$$\delta^2 P / \delta x^2 = 0$$

$$\delta P / \delta x = f(t)$$

Thus, the pressure gradient in the sample is constant along its length, although it will vary with time.

If there is a system like that in the next figure,

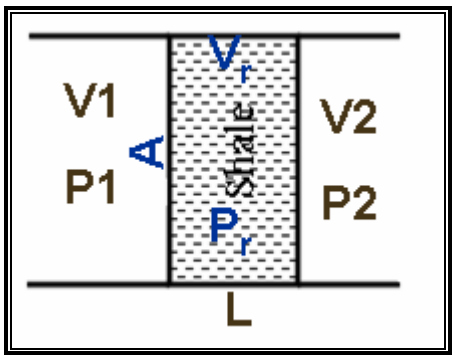

Figure (B-1): Sample sandwiched between to different pore pressure reservoirs.

the pressure P_1 at reservoir 1, P_2 at reservoir 2 and P_r in the pore space V_p function on time and can be related to each other by three differential equations

$$\frac{\delta P_1}{\delta t} = -(P_1 - P_r)\left(\frac{k}{\beta\mu L^2} 2\frac{V_r}{V_1}\right)$$

$$\frac{\delta P_2}{\delta t} = -(P_2 - P_r)\left(\frac{k}{\beta\mu L^2} 2\frac{V_r}{V_2}\right)$$

$$\frac{\delta P_r}{\delta t} = (P_1 + P_2 - 2P_r)\left(\frac{k}{\beta\mu L^2} 2\frac{V_r}{V_p}\right)$$

At time 0,

$P_1 = P_i$, $P_r = P_0$ and $P_2 = P_0$.

Brace et al. (1968) took Laplace transformation for these three pressures equations and they got

$$dP_t = \Delta P[(V_2 / V_1) + V_2]e^{-\alpha t}$$

$$dP_t = P_l - P_{final} \text{ and } \Delta P = P_{final} - P_0$$

$$\alpha = -\frac{kA}{\mu\beta L}\left[\frac{V_2 + V_1}{V_1 V_2}\right]$$

When both V_2 and P_2 are kept to be constant overtime, only two differential pressures equations for P_1 and P_r are obtained. Al-Bazali (2005) used Laplace transformation to solve these two equations, finding:

$$\frac{P(L,t) - P_0}{P_u - P_0} = 1 - e^{\left(\frac{-Akt}{\mu\beta VL}\right)}$$

where dP_t *is* $P(L,t) - P_0$ *and* dP_0 *is* $P_u - P_0$

By taking the natural logarithm

$$Ln\frac{P(L,t) - P_0}{P_u - P_0} = \alpha t$$

$$\alpha = \frac{-Ak}{\mu\beta VL}$$

These two models are used to determine sample permeability from the decay of pressure overtime with different experimental configurations during the current study.

Appendix C:

Nomenclature and Units Conversion Factors

Nomenclature

J_s = flux of solute (mol.m^{-2}.s^{-1}) with time

I = hydraulic pressure gradient

V_w = mean partial molar volume of water

J_v = volume flux of solution (m.s^{-1})

m = concentration of solute in molality (mol kg^{-1})

L_{ii} = conductivity coefficient of this flux

X_i = driving forces i for flux i

J_i = flux of the fluid (f) or solutes (s)

Q_h = flux of water (mL/sec)

g = gravitational constant (9.8066 m.s^{-2})

K_h = hydraulic conductivity

L_p = hydraulic permeability coefficient in (m^3.N^{-1}.s^{-1})

ν = number of ions in which the electrolyte dissociates

a = activity of the water.

C = cohesion

c = solute concentration across the membrane (mol.m^{-3})

D = diffusion coefficient (m^{2}s^{-1})

h = overburden thickness (m)

h_w = water column thickness

k = permeability (m^2 or darcys)

K_h = hydraulic conductivity ($m.s^{-1}$)

P_{pore} = pore pressure (MPa)

R = gas constant

T = temperature (K or ^oC as indicated)

x = thickness of the membrane (m)

ρ = fluid density ($kg.\ m^{-3}$)

ρ_w = saturated water density ($kg.\ m^{-3}$)

β = compressibility of the water (MPa^{-1})

σ = reflection coefficient (membrane efficiency)

σ_i = vertical stress (MPa)

η = fluid viscosity (Pa-s)

ω = solute "permeability" coefficient ($mol.N^{-1}.s^{-1}$)

ϕ = active porosity

μ_w = chemical potential of water

ϑ = constant = $\dfrac{RT}{V_w a_w}\ 0.017\nu$

ξ = tortuosity of the membrane

θ = friction angle

τ = shear stress

Δ = gradient

∇ = differential

ΔP = hydraulic pressure gradient (MPa)

$\Delta \pi$ = chemical osmotic pressure gradient (MPa)

$\Delta \pi_0$ = osmotic pressure in the equilibrium solution

TDS = total dissolved solids (mg/L)

CI = crystallinity index

Pp = pore pressure (MPa)

Pc = confining pressure (MPa)

CEC = cation exchange capacity (meg/100g)

M.C = moisture content (%)

BD =black density (g/cc)

Mole = no. of moles of solutes per one liter of solution

Molal = no. of moles of solutes per one kilogram of solution

Unit Conversion

Unit	Conversion	
cm	0.3937	**Inch**
cm	0.0328	**Feet**
cm	10	**mm**
mm	10^3	**μm**
μm	10^3	**nm**
nm	10	**A°**
Darcy	10^9	**nDarcy**
(at 25 °C) Darcy	~ 1.1 X 10^{-4}	**cm/sec**
MPa	145.038	**psi**
psi	0.6895	**Dyne/cm^2**

Appendix D:

CD-ROM Contains Raw-Data for HTHP Tests, Swelling, Diffusion, XRD and Coulter Grain-Sizer Analyses